HUMBOLDT-UNIVERSITÄT ZU BERLIN

Oxidative intramolecular crosslinking in sequence-controlled polymers: Approaches toward more complex designs and folding analysis

Dissertation

zur Erlangung des akademischen Grades
doctor rerum naturalium (Dr. rer. nat.)
im Fach Chemie
eingereicht an der Mathematisch-Naturwissenschaftlichen Fakultät
der Humboldt-Universität zu Berlin

von **Emmanuelle Schué**

Präsidentin der Humboldt-Universität zu Berlin
Prof. Dr.-Ing. Dr. Sabine Kunst

Dekan der Mathematisch-Naturwissenschaftlichen Fakultät

Prof. Dr. Elmar Kulke

Gutachter : 1. Prof. Hans G. Börner
2. Dr. Jean-François Lutz
3. Prof. Matthias Ballauf

Tag der mündlichen Prüfung : 16.06.2020

We are here for this – to make mistakes and correct ourselves, to stand the blow and hand them out. We must never feel disarmed: nature is immense and complex, but it is not impermeable to the intelligence; we must circle around it, pierce and probe it, look for the opening or make it.

Primo Levi, The Periodic Table.

ABSTRACT

The field of material science has evolved drastically over the last century. Progress in synthetic polymers primarily focuses on efforts to design synthetic materials at a molecular level to reach promising properties and functions at a macroscopic level. Hence, improving material synthesis, as well as increasing the complexity of macromolecular design have become a major research focus. Cyclic polymers are a simple class of topological polymers, but already exhibit considerably different physical and chemical properties compared to their linear analogues. Remarkable synthetic strategies have been developed toward the elaboration of sequence-defined oligomers, in which the precise microstructure can allow subsequent folding into controlled and precise cyclic or multi-cyclic origamis. However, current synthetic routes toward precision polymers with high molecular weight remain statistical to some degree, which reflects a loss of structural control. Thus, designing large synthetic macromolecules that can fold into precise and uniform cyclic-shape structures remains difficult to reach. Moreover, parallel progress in characterization of large cyclic and multi-cyclic macromolecular designs are highly demanded since most of the current techniques are only capable of providing circumstantial evidence of structural organization. Indeed, a combination of complementary analysis are required to fully characterize advanced macromolecular structures.

Macromolecules with dynamic intramolecular crosslinks have become relevant due to their ability to potentially reach equilibrium structures in response to external stimuli. In this study, controlled synthetic route and morphology characterization of dynamic cyclic polymers are investigated. The synthetic concept is based on the preparation of sequence-controlled macromolecules to guide the insertion of reactive selenol or thiol groups at desired positions within a polymer chain. Controlled oxidative dimerization of the functional groups leads to diselenide or disulfide bridges respectively and induces intramolecular crosslinking to generate dynamic single chain cyclization. To gain insight into the molecular level to reveal the degree of structural control, a synthetic strategy is developed to access an additional analytic tool and enable direct visualization of the obtained polymer conformations. The cyclic polymers are transformed into cyclic molecular brushes that are known to be visualizable as single molecule by Atomic Force Microscopy. The synthetic concept was first established with intermediate molecular weight macromolecules and was subsequently transferred to large polymer chains, with the aim to improve folding analysis and move forward the structural complexity.

Keywords: sequence-controlled macromolecules, diselenide bridge, disulfide bridge, cyclic polymers, cyclic brush polymers, Atomic Force Microscopy.

KURZZUSAMMENFASSUNG

Der Bereich der Materialwissenschaften hat sich im Laufe des letzten Jahrhunderts stark weiterentwickelt. Die Fortschritte bei synthetischen Polymeren konzentrieren sich in erster Linie auf die Bemühungen, Kunststoffe auf molekularer Ebene zu entwickeln, um vielversprechende Eigenschaften und Funktionen auf makroskopischer Ebene zu erreichen. Daher sind die Verbesserung der Materialsynthese sowie die Zunahme der Komplexität des makromolekularen Designs zu einem wichtigen Forschungsschwerpunkt geworden. Zyklische Polymere sind eine einfache Klasse von topologischen Polymeren, weisen aber bereits deutlich andere physikalische und chemische Eigenschaften auf als ihre linearen Analoga. Es wurden bemerkenswerte synthetische Strategien zur Entwicklung von sequenzgesteuerten Oligomeren entwickelt, die durch eine präzise Mikrostruktur eine anschließende Faltung zu kontrollierten und präzisen zyklischen oder multizyklischen Origamis ermöglichten. Allerdings bleiben die derzeitigen synthetischen Methoden für die Herstellung von Präzisionspolymeren mit hohem Molekulargewicht bis zu einem gewissen Grad statistisch, was mit einem Verlust an struktureller Kontrolle einhergeht. Daher ist es nach wie vor schwierig, große synthetische Makromoleküle zu entwerfen, die sich zu präzisen und einheitlichen zyklischen Strukturen zusammenfügen können. Darüber hinaus sind parallele Fortschritte bei der Charakterisierung von großen zyklischen und multizyklischen makromolekularen Strukturen sehr gefragt, da die meisten der derzeitigen Techniken nur in der Lage sind, Indizien für die Strukturorganisation zu liefern. Tatsächlich ist eine Kombination aus komplementären Analysen erforderlich, um fortgeschrittene makromolekulare Strukturen vollständig charakterisieren zu können.

Makromoleküle mit dynamischen intramolekularen Querverbindungen sind von Interesse, da sie als Reaktion auf externe Stimuli die gewünschte Struktur als Gleichgewicht erreichen können. Die vorliegende Arbeit untersucht dabei die Synthese und die Morphologie von dynamischen und kontrollierten zyklischen Polymeren. Das synthetische Konzept basiert auf der Herstellung von sequenzgesteuerten Makromolekülen mittels regulierten Einbaus von reaktiven Selenol- oder Thiolgruppen an gewünschten Positionen innerhalb einer Polymerkette. Die kontrollierte oxidative Dimerisierung der funktionellen Gruppen führt zu Diselenid- bzw. Disulfidbrücken und bewirkt eine intramolekulare Vernetzung zur Erzeugung einer dynamischen einkettigen Zyklisierung. Um Einblicke auf molekularer Ebene zu gewinnen und den Grad an struktureller Kontrolle aufzuzeigen, wird eine synthetische Strategie entwickelt, die eine direkte Visualisierung der erhaltenen Polymerkonformation ermöglicht. Die zyklischen Polymere werden in zyklische Molekülbürsten umgewandelt, die

bekanntermaßen durch Rasterkraftmikroskopie (AFM) als einzelne Molekülstrukturen visualisiert werden können. Das Gesamtsynthesekonzept wurde in erster Linie mit Zwischenmolekülen etabliert und anschließend auf hochmolekulare Polymerketten übertragen, mit dem Ziel, die Konformationsanalyse zu verbessern und die strukturelle Komplexität voranzutreiben.

Schlüsselwörter: sequenzgesteuerte Makromoleküle, Diselenidbrücke, Disulfidbrücke, zyklische Polymere, zyklische Molekülbürsten, Rasterkraftmikroskopie.

1. MOTIVATION AND AIMS

Natural polymers such as proteins, deoxyribonucleic acid (DNA) and saccharides have continuously inspired polymer chemists in the last decades. Arising from absolute sequence control, proteins adopt in solution highly complex and uniform conformations. Their delicate three-dimensional (3D) structures, as well as their self-adaptive behaviour in response to environmental changes, endow proteins with advanced biological functions, such as catalysis or molecular recognition.[1] Stimulated by this delicate structure-function relationship displayed by biomacromolecules, an increasing interest has been shown toward the development of synthetic materials mimicking features of biopolymer classes.[2] Yet, the preparation of macromolecular designs with such degree of structural complexity remains a fascinating challenge. Currently in material science, elegant synthetic strategies toward the design of various topologies such as cyclic or multi-cyclic polymers were developed with the emergence of the powerful controlled living polymerizations, often combined with functionalization of chain-end to induce intramolecular crosslinking.[3] A broad toolbox of chemical coupling reactions, from irreversible permanent bonds to dynamic covalent bonds and supramolecular interactions, have been thoroughly explored to elaborate compacted synthetic materials nano-objects.[4] In the last years, advanced approaches have tailored polymer compositions, such as, block, multi-block copolymers, or even copolymers with random monomer sequence to incorporate one or several intramolecular bridges and induce single macromolecular folding capable of exhibiting simple functions.[5] However, the complexity, as well as the folding control in these synthetic methods, remained limited since the intramolecular crosslinking bonds were, in most of the cases, formed at random positions within the macromolecules.[6]

Following Nature's example, it seems very plausible to achieve a new class of highly organized materials using sequence-ordered polymers.[7] The control of primary structure plays a crucial role in biology, since it strongly influences their subsequent 3D structures and properties.[8,9] Hence, the regulation of the monomer sequence in synthetic polymers would allow the control of single polymer chain folding and provide the opportunity to mimic closer biopolymer functions such as molecular recognition and catalysis, or improve the control over macroscopic material properties.[10] Sequence-regulation in synthetic polymers is an impressive on-going material science field, in which advanced synthetic concepts toward precision polymers have already proved efficiency.[7] Current methodologies, such as the powerful iterative methods, allow the synthesis of well-defined oligomers essentially, capable of folding into precise conformation in a controlled manner, such as foldamers.[11,12] However, the

preparation of sequence-defined synthetic macromolecules with higher molecular weight, comparable to those of natural polymers, remains tedious. Although synthetic strategies based on chain growth polymerizations exhibit monomer regulation to some extent for the elaboration of high molecular weight polymers,[13] it is believed that further progress in precision polymers could give access to a next-generation synthetic polymers with unprecedented properties and functions.[14] Besides, parallel improvements in characterization of large cyclic and multi-cyclic macromolecular designs are highly demanded since most of the current techniques are only capable of providing circumstantial evidence of structural organization.

Macromolecules with dynamic intramolecular crosslinks have become relevant due to their self-adaptive characteristics in response to external stimuli.[3] In this study, controlled synthetic route and morphology characterization of dynamic cyclic polymers are investigated. Controlled single polymer chain cyclization of fully synthetic polymers is studied by using oxidative dynamic covalent bond such as disulfide or diselenide bridges.[15] Sequence-regulated polymerization is exploited to control the position of the intramolecular crosslinking bond within the polymer chain bond and therefore command single polymer chain cyclization. Different sequence-controlled polymers exhibiting either thiols or selenols, are synthesized and oxidation into disulfide or diselenide bonds, respectively, triggers single chain collapse. Furthermore, a synthetic strategy is developed in the aim to access additional analytic tool and reveal the degree of structural control. The cyclic polymers are transformed into folded molecular brushes to enable direct visualization of the resulting macromolecular conformation by AFM (**Figure 1**).[16] Monocyclic macromolecular topologies are targeted in the aim to primarily study the efficiency of the developed synthetic concept.

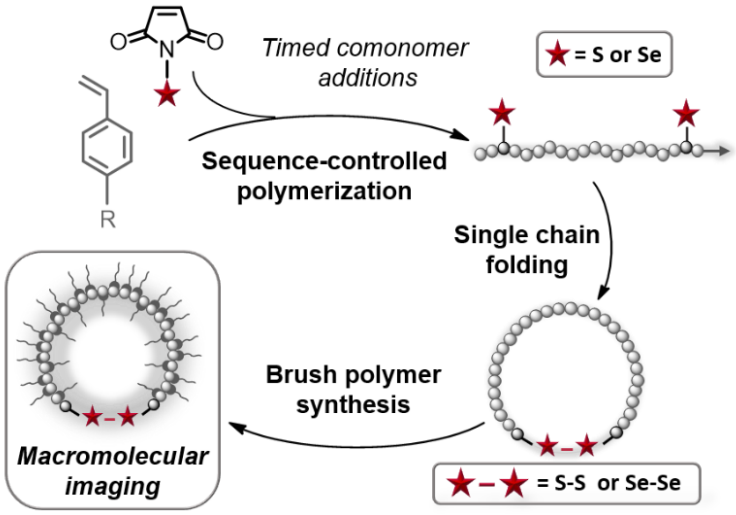

Figure 1. General synthetic strategy for controlled oxidative single polymer chain folding and conformation analysis by AFM. (Adapted from reference 15)

2. THEORETICAL BACKGROUND

2.1. Advanced macromolecular engineering

In the last decades, the field of material science has been revolutionized. Tailoring polymeric material design has become a major goal for polymer chemists since material's properties are inherently dependent on its molecular structure. In the field of synthetic polymer chemistry, the topology of macromolecules has long been restricted to linear or a randomly branched macromolecules. However, over the past decades, a large variety of macromolecular architectures has been reached along with the developments of advanced synthetic concepts.

Step-growth and chain growth polymerizations are the two standard synthetic techniques for the preparation of synthetic polymers and are extensively exploited in the industry field. In step-growth process, bifunctional or multi-functional monomers react with another in a high yield to generate dimer, trimer, longer oligomers and eventually macromolecules with significant molecular weight. Chain growth polymerization relies on the sequential addition of monomer units by reaction with an active species of the growing polymer chain, such as free radical, cation and anion. This polymerization method generally involves three steps called initiation, propagation and termination. These both techniques lead to the synthesis of statistical polymers with high molecular weight and can be exploited for a broad range of synthetic monomers. However, the main limitations of these standard methods are the poor control over molecular weight, polydispersity, monomer composition, chain architecture, and site-specific functionalities. In the 1990s–2000s, the emergence of various living/controlled polymerization methods, based on the chain-growth process, offered a noteworthy development of powerful synthetic approaches to engineer complex macromolecular materials with advanced structural control.[17,18]

2.1.1. Controlled/Living polymerization techniques

In contrast with traditional chain growth polymerizations, living chain growth polymerization is a technique composed only of the initiation and propagation steps. The suppression of transfer and termination reactions provides the "livingness" of the polymerization, maintaining a constant concentration of active growing chains, and therefore allows a control over the molecular weight and a low dispersity.[19] Living polymerization concept was firstly introduced for the anionic polymerization of polystyrene with low molecular weight distribution and quantitative chain-end functionality.[20] This concept was subsequently exploited for various other anionic and cationic polymerization methods.[21,22]

However, while ionic polymerizations require stringent reaction conditions and are extremely sensitive to chemical functionalities, limiting the variety of suitable monomers, radical polymerization process offers the advantage of being applicable to a large library of vinylic building blocks and are relatively easy to implement.[23] Hence, researchers have been aspired to combine the advantages of conventional radical polymerization and living polymerization. As a result, controlled radical polymerization (CRP), also named reversible deactivation radical polymerization (RDRP), was primarily introduced in the 1980's.[24] Currently, the three main controlled radical polymerization methods are Nitroxide Mediated radical Polymerization (NMP),[25] Atom Transfer Radical Polymerization (ATRP)[26] and Reversible Addition Fragmentation chain Transfer (RAFT) polymerization.[27] Each method relies on establishing a dynamic equilibrium between a low concentration of active propagating chains and a predominant amount of dormant chains that are unable to propagate or terminate (**Scheme 1**).[28] This reversible equilibrium enables the synthesis of synthetic polymers with controlled molecular weight and low chain length distributions. Although this three techniques are the most used and exploited, several different controlled radical polymerization methods have been developed[24] and CRP has become an industrial reality during the 21st century.[29]

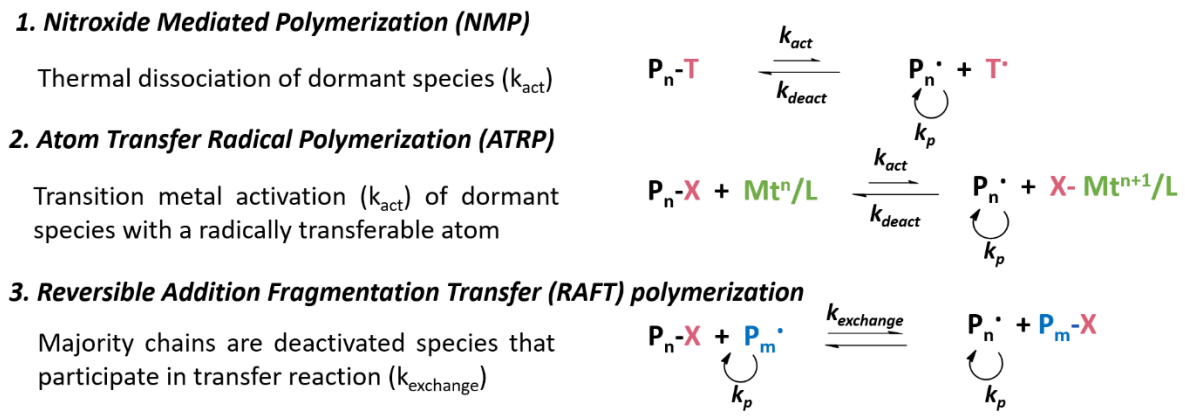

Scheme 1. Schematic representation of the three main dynamic equilibrium mechanisms exploited in controlled radical polymerizations.

2.1.2. Development of complex macromolecular designs

With the emergence of living/controlled polymerizations, the field of macromolecular chemistry has made noteworthy breakthrough in the preparation of polymers with controlled molecular weight, length distribution and end-chain functionalities.[30] More importantly, these techniques offered the construction of various and unprecedented macromolecular designs (**Figure 2**).[28,31] Monomer composition in a polymer chain could be modulated and allowed the synthesis of block, statistical, alternating and gradient copolymers.[32-34] By exploiting end-

group functionalities and functional initiators, new topological polymers have been reached such as cyclic, multi-cyclic polymers and branched polymers.[35-37] Grafted, stars and brush polymers have been synthesized by exploiting macroinitiators and multi-functional initiators.[38,39] The development of this remarkable polymer designs allowed the preparation of synthetic macromolecules with interesting properties (optical, mechanical, thermal, etc.) and applications especially in the fields of thermoplastics and drug delivery.[24,40-42]

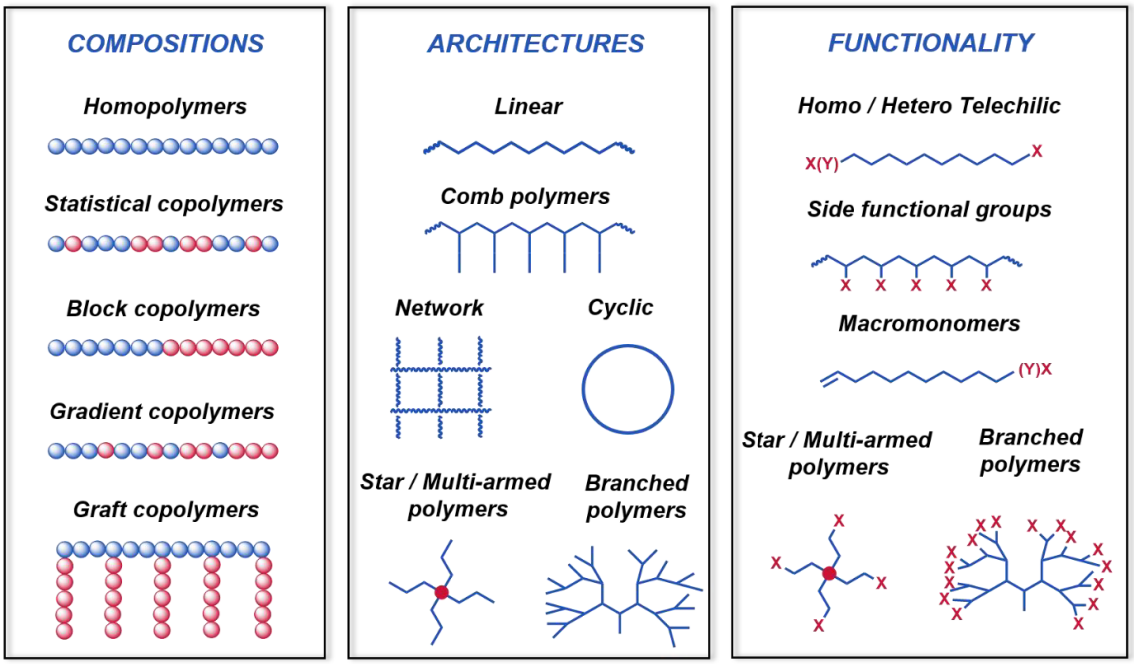

Figure 2. Examples of macromolecular designs developed by living/controlled polymerizations (Adapted from reference 28).

Copolymers prepared via living/controlled polymerizations commonly exhibit simple monomer sequence, such as random, alternative or block monomer distribution. In the more general case, it is only possible to control the sequence at the block or segment level. For example, living/controlled polymerizations enable the preparation of sequence-regulated multiblock copolymers, which exhibit a microstructure regulation to some degree.[34] The synthesis of sequence-controlled multiblock polymers can be performed by sequential polymerizations, in one-pot if the targeted copolymers are composed of monomers exhibiting similar reactivities. In such case, the monomer reactivities (i.e. the monomer cross-propagation rates) determine the order of monomer additions to ensure efficient block switches.[43] This synthetic approach was first described for the synthesis of diblock copolymers by living anionic polymerization.[44] This concept was later expanded for the preparation of multiblocks by anionic polymerization,[45] ring opening polymerization[46] and especially by controlled radical polymerizations.[47-49] Among the pioneers, Perrier and co-workers described a simple and

scalable method for the one-pot synthesis of twenty-blocks copolymers (**Scheme 2**).[50] Sequential polymerization of acrylamide derivatives was performed by RAFT radical polymerization. For each building block addition, the monomer conversion reached over 99%, thereby avoiding purification steps and leading potentially to scalability. Sequence-control at the block level offers opportunities for designing large nanostructured materials with, for example, potential used in the field of drug delivery where amphiphilic block copolymers can form self-organized structures in solution and act as drug nanocarriers.[51]

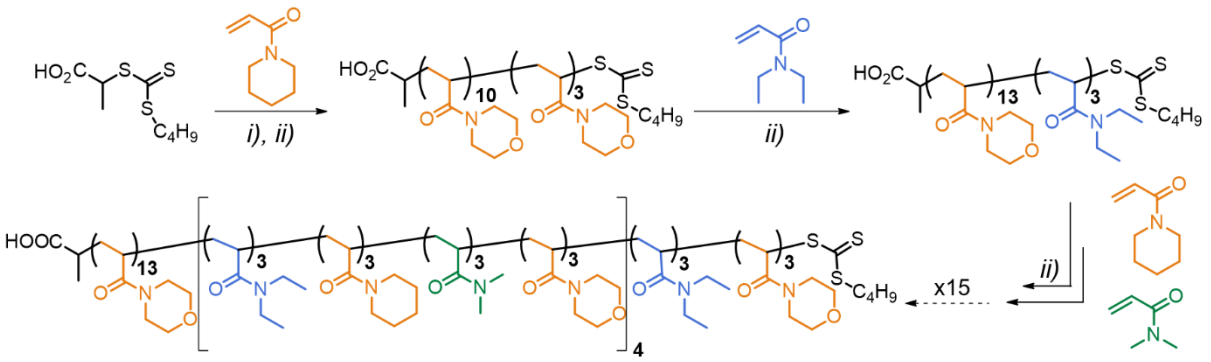

Scheme 2. Schematic representation of the synthesis of the multiblock copolymers by RAFT with i) azo-initiator, H_2O-Dioxane (80/20), 70°C, 2 h and ii) azo-initiator, H_2O, 70°C, 2 h.

However, the degree of sequence control remains rather low in conventional controlled polymerization techniques due to the statistical nature of the propagation step. Yet, synthetic macromolecules with ordered monomer sequences could potentially be of significant importance in the development of material science.[2] Indeed, the defined microstructure found in biopolymers plays a crucial role in biology, since their monomer arrangement is in large part responsible for the unique features of natural processes, such as self-replication and molecular recognition.[7] Thus, in the last decades, a growing research interest has emerged toward the development of specialized synthetic routes that enable regulation of the monomer sequence in synthetic material. It is envisioned that controlling the monomer order would allow higher level of control over structural and physicochemical properties.[7] Synthetic concepts enabling the elaboration of uniform macromolecules with defined microstructure are believed to access synthetic material with next-generation performance and unprecedented functions.[52]

2.2. Precision polymers

Biomacromolecules such as protein and DNA fold in solution into complex and well-defined three-dimensional structures that enable various biological functions.[53] For example, in molecular biology, the key processes are well executed by proteins and DNA, with

remarkable functions such as catalysis, molecular recognition, and molecular storage of information.[1] The biopolymer primary sequence, which is the specific order of monomer units within the polymer chain (amino acids in the case of peptide/protein), is governing the folding process.[8,9] Over the last decades, this property control through molecular design displayed by these information-rich biomacromolecules, have become an intense source of inspiration for macromolecular science.[7] While efficient methods are available for the synthesis and characterization of natural precision polymers[54] such as DNA, ribonucleic acid (RNA), and proteins, the development of synthetic routs and analysis of man-made polymers with monomer sequence-control is a much more recent research field.[13,54] During the last years, significant attention has been devoted to prepare sequence-controlled polymers, targeting ultimately similar degree of monomer sequence control as natural polymers. The term "sequence-controlled polymers" refers to architecturally advanced macromolecules with sequential and precise arrangement of the monomer units along the polymer chain.[11] Achieving the perfection of biopolymer composition, length and distribution in synthetic macromolecules, would give access to synthetic materials exhibiting unprecedented opportunities, especially in the field of data storage and biomimetic materials.[7] Therefore, there is a high demand for specialized synthetic approaches that allow to achieve similar monomer regulation in synthetic polymers.

In nature, the defined primary sequence is achieved by efficient biocatalytic reactions.[2] For example, biological polymerization processes such as DNA replication, transcription and translation, are remarkable examples of sequence-controlled polymerizations.[1,55] In the last decades, two main strategies have emerged toward the preparation of synthetic macromolecules with defined primary sequence. The first and obvious trend consists in exploiting natural concepts that have been designed by nature itself for controlling monomer sequence. For instance, DNA templates,[56] enzyme[57] and ribosomal machinery[58] have been used to prepare sequence-defined polymers. Such biological polymerization methods can offer outstanding sequence control but are limited to biologically compatible monomers in terms of structural diversity.[7] Meanwhile, some chemical approaches have been described for regulating monomer sequence based on step-growth polymerization, iterative synthesis, chain growth and molecular machines.[59] An overview of well-established sequence-controlled polymerizations based on chemical approaches is discussed in the following sections.

2.2.1. Sequence-control in step-growth polymerization

Standard step-growth polymerization is a well-established method in which multi-functional monomers react with another to form dimer, trimer, polymer chain and afford linear, cyclic, or crosslinked macromolecular architectures. Due to the simple polymerization concept, this technique exhibits major limitations, such as low control over the microstructure and broad chain length distribution. Nevertheless, synthetic routes based on step-growth polymerization have been described for the synthesis of alternating high molecular weight polymers.[60] More interestingly, sequence-controlled polymers exhibiting periodic microstructures have been developed. The general strategy consists in the polymerization of building blocks containing two distinct terminal reactive groups, spaced by a defined molecular segment. A given functional moiety or oligomer segment can be included periodically in a polymer chain. For example, the synthesis of protein-mimic polymers has been reported by using building blocks bearing azide/alkyne terminal groups spaced by a defined peptide sequence that was able to form either α-helix or β-sheet, respectively (**Scheme 3**).[61,62] These monomers were polymerized by performing copper-catalysed azide-alkyne cycloaddition (CuAAC) reaction and the resulting polymers exhibited defined secondary structures, induced by the peptide sequence inherited from the monomer. Such strategy provides an efficient approach to access a broad range of high molecular weight protein-mimic polymers for biomaterials applications.

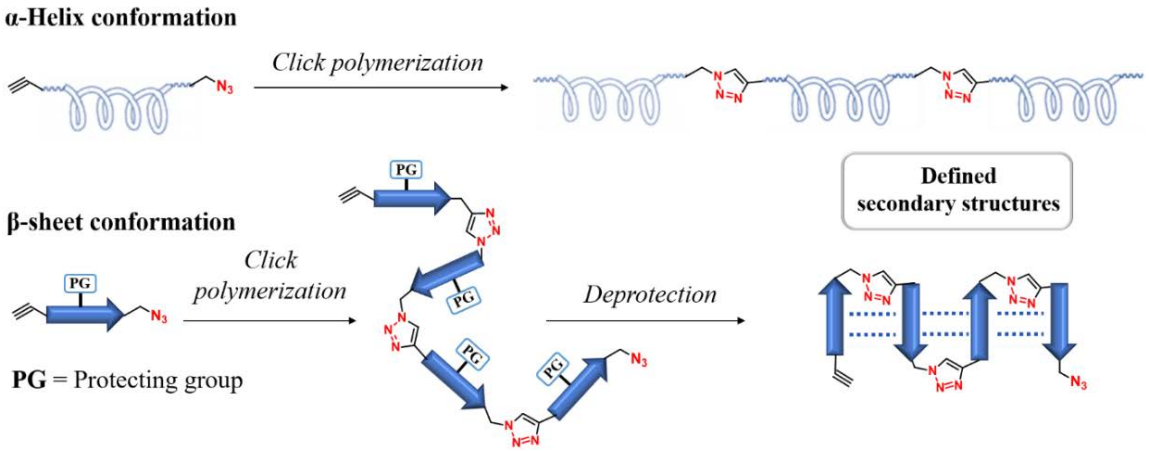

Scheme 3. Synthesis of multiblocks polypeptides by step-growth polymerization (Adapted from references 61 and 62).

Acyclic diene metathesis (ADMET) and click reactions such as CuAAC and thiol-ene, have been also extensively used as coupling reaction in step-growth process for the synthesis of sequence-controlled polymers.[63-65] These reactions are highly efficient and required standard and mild conditions. Furthermore, comparable approach was described for the preparation of

periodic biodegradable polymers, such as poly(lactic-*co*-glycolic acid), by exploiting condensation reaction.[66] Step-growth polymerization is a versatile and interesting technique for the preparation of periodic macromolecules with significant molecular weight. However, the preparation of more complex and aperiodic polymer microstructure remains challenging with this polymerization mechanism. More importantly, this approach has no control on the chain length distribution and consequently the resulting macromolecules are not uniform. Thus, step-growth polymerization exhibits major limitations toward the preparation of uniform sequence-controlled polymers. Current development in controlled-living step-growth process could be a promising alternative for the synthesis of sequence-controlled polymers.[67]

2.2.2. Sequence-control in multi-step growth polymerization

Multi-step growth polymerization is currently a powerful pathway for monomer regulation in both biopolymer and synthetic macromolecule synthesis. The iterative strategies enable the preparation of uniform macromolecules (Đ=1) by performing stepwise chemical reactions. A general scheme of iterative solid phase synthesis is presented in **Scheme 4**. The nascent polymers are connected, via a cleavable bond, to an insoluble cross link polymer bead swollen by a solvent. Bifunctional monomers (XY) are coupled one by one to the growing chain by reaction between the reactive end group (X) of the monomer and functional groups of the support (Y). The functionality (Y) of the monomer is protected in order to avoid side reactions and oligomerization in solution. After monomer coupling, the protecting group is removed to generate the reactive function (Y) on the growing oligomer.

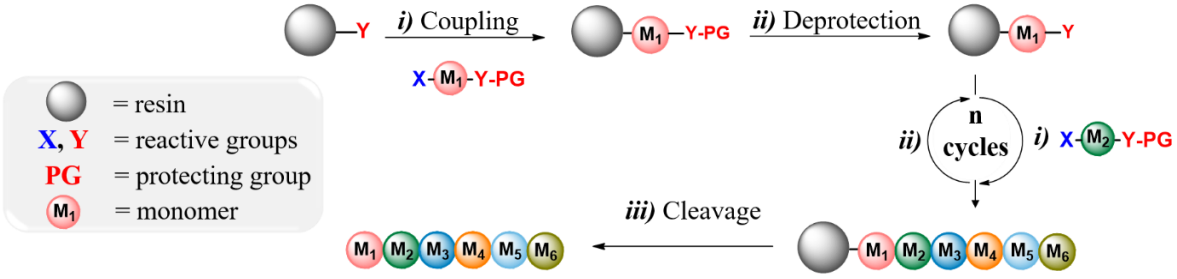

Scheme 4. General approach for iterative incorporation of monomers.

Hence, successive stepwise coupling/deprotection cycles enable the addition of monomers in a predetermined order on the growing chain. The final step is the cleavage of the resulting polymer chain from the solid support. The main advantages of this method are the perfect control of the macromolecule primary structure, but also the easy purification after each monomer incorporation by filtration. However, the accessibility of the chain reactive group

remains difficult on polymeric solid support. Hence, coupling reaction rate and reaction yields are decreased. For this purpose, this conceptual approach was slightly modified by replacing insoluble cross-linked resins with soluble polymer supports.[68] Such macromolecular system combines the advantages of solid-phase strategy (facile isolation) and chemical reaction in solution (accessibility).[14] The development of solid phase synthesis has been a significant breakthrough in the field of sequence-defined natural and synthetic polymers. This synthetic approach was introduced by Merrifield and co-workers for the synthesis of peptides.[69] The subsequent development of automated peptide synthesizers assisted with microwave allowed faster polypeptide preparation and significant progress toward the synthesis of higher molecular weight peptides.[70] In the last years, this synthetic method has been replicated for the synthesis of a broad range of sequence-regulated natural polymers such as polysaccharides[71], DNA[72] and bioconjugates,[73] but also for the preparation of non-natural materials.[74,75] A large library of functional monomers, protecting groups and chemical reactions were used to access new types of sequence-defined polymers with promising properties and applications, especially in the field of data storage.[76]

In the last decades, several alternative approaches have been developed to bypass the use of protecting groups in solid phase synthesis.[76] Indeed, protected building blocks requires a mandatory deprotection step for each cycle, which is not convenient for the synthesis of larger polymers and lead to long synthesis time. Different strategies have been described toward the synthesis of sequence-defined polymers based on protecting-group free procedures,[77,78] latent protecting group[79] and multi-components strategies.[80,81] Moreover, a submonomer approach was introduced for the preparation of polypeptoids, a class of peptidomimetics, based on a two-step monomer addition to avoid the use of protecting groups.[82] This iterative submonomer solid phase route is composed of two steps (**Scheme 5**). The first one consists in an acylation of a resin-bound secondary amine with a bromoacetic acid. Afterwards, the resulting α-bromo acetamide reacts with a primary amine bearing the side chain group by nucleophilic displacement of the halogen, forming the secondary amine fragment involved in the first step. This cycle is repeated to incorporate various building blocks, allowing precise monomer regulation of the primary structure and uniform molecular weight distribution. Since this synthetic approach requires mild conditions, polypeptoid preparation has been successfully transferred to an automated solid support synthesizer which significantly reduced polypeptoid preparation time. Such sequence-defined macromolecules have emerged as a class of

peptidomimetic materials that are particularly interesting due to their chemical diversity, ability to form secondary structures in solution and biological relevance.[83]

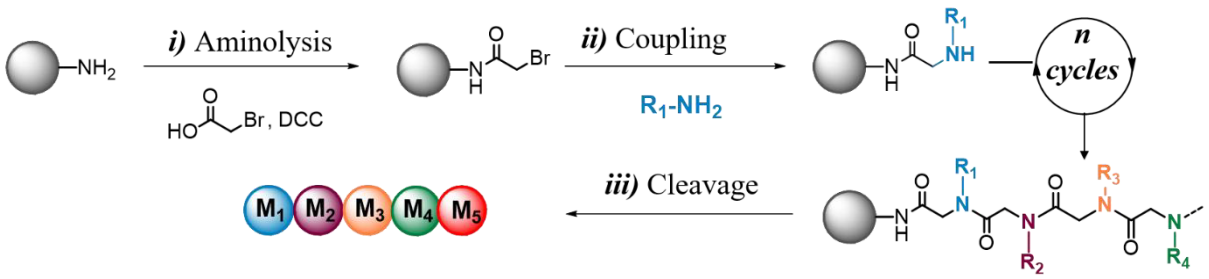

Scheme 5. Polypeptoid synthetic strategy. (i) Amidification with haloacetic acid, DCC, DMF; (ii) Nucleophilic displacement with amine in DMF; (iii) Cleavage with H^+ (Adapted from reference 82).

Recently, an innovative synthesis route based on thiolactone chemistry have been reported for the preparation of sequence-defined oligomers via a two-step orthogonal iterative method (**Scheme 6**).[84] Such synthetic strategy enables the preparation of oligomers (up to decamers) containing highly functional sequences, with the additional possibility to translate the method to an automated protocol.[85] In the first step of the synthetic cycle, a thiolactone group connected to the resin is selectively opened by the primary amine of an amino alcohol reagent. The released thiol reacts subsequently with a functional acrylate or acrylamide through a nucleophilic thiol-ene reaction. The second step is the chain extension, allowing the reintroduction of the thiolactone group by reaction of the remaining hydroxy moiety from the amino alcohol with α-isocyanato-γ-thiolactone. A series of multifunctional sequence-defined oligomers were synthesized, and an interesting investigation focused on their potential use to store digitally encoded information was explored.[86]

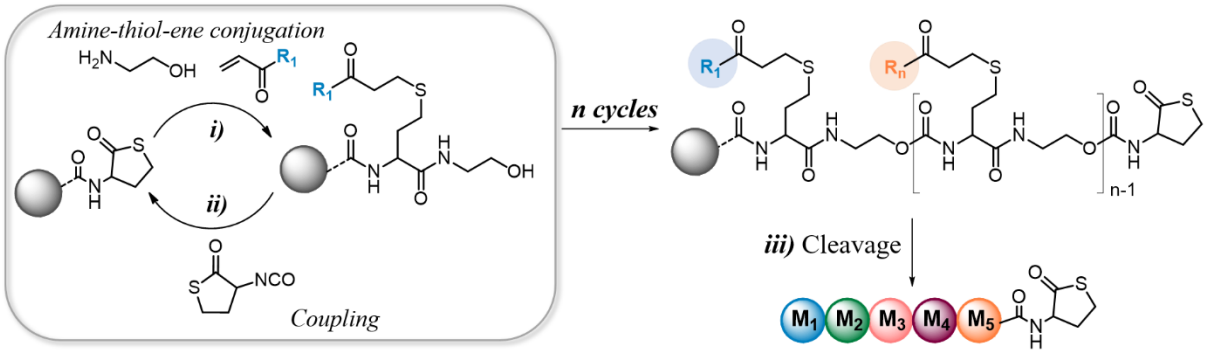

Scheme 6. Synthetic strategy of sequence-defined polymers based on thiolactone chemistry. (i) One-pot aminolysis / chain functionalization in $CHCl_3$, 15 min. (ii) Chain extension: $CHCl_3$, dibutyltin dilaurate; (iii) Cleavage: TFA (Adapted from reference 84).

Currently, multi-step growth polymerization is certainly the most powerful and versatile tool for the synthesis of highly uniform and sequence-defined macromolecules.

Unprecedented types of synthetic sequence-regulated oligomers have been synthesized and are promising materials, particularly in the field of data storage and self-assembly. However, this iterative synthetic approach presents some limitations and weakness. As illustrated in this section, this method is highly efficient and precise for the preparation of oligomers or small polymers. Conversely, the preparation of high molecular weight polymeric materials with such precise monomer sequence remains tedious and not yet suitable with this synthetic approach. High coupling yields are crucial parameters to avoid sequence defects and target the synthesis of polymers with significant molecular weight. Fast coupling step reactions are also required, since monomer units are added one per one. The building blocks should be commercial or easily prepared due to their use in excess in several iterative strategies to ensure nearly quantitative yields. For instance, it appears that this strategy requires some optimizations to generate sequence-defined high molecular weight macromolecules. Thus, research interest have grown toward the development of synthetic routs capable of regulating monomer sequence in large polymers. Alternative synthetic approaches have been explored in chain growth polymerization, since the synthesis of higher molecular weight polymers with narrow length distribution became accessible and straightforward with the emergence of controlled/living polymerizations.

2.2.3. Sequence-control in chain growth polymerization

Chain growth polymerization is a powerful and versatile technique due to its standard implementation and suitability for a broad range of functional monomers. Moreover, this process is the most convenient and efficient pathway for the preparation of high molecular weight polymers with low chain length distribution. However, the chain-growth mechanism leads generally to random monomer sequence due to the statistical nature of the propagation step which relies on highly reactive species (free radical or ions).[87] Although controlling monomer insertions in a chain-growth process is theoretically much more challenging than in an iterative process, several interesting polymerization methods have been described in the last decades toward the preparation of sequence-regulated polymers based on chain-growth mechanism.[13] In this section, an overview of different techniques is discussed and particularly focused on advanced concepts based on controlled radical polymerizations.

- **Single monomer insertion**

Similarly to iterative solid phase approach, single monomer insertion strategy has also been investigated in living controlled polymerizations to regulate monomer sequence.[88] In such case,

the chain-growth polymerization is decomposed into a multi-step growth process. This concept was first described in living cationic copolymerization of vinyl ethers.[89] Later, such approach has been transferred to controlled radical polymerizations, although limited so far to small number of monomer insertions.[90,91] Interestingly, successive and defined single monomer unit insertion (SUMI) in a growing chain was achieved by combining controlled radical polymerization and automated purification techniques.[92] In this study, successive monomer incorporations of distinct acrylates was performed by RAFT polymerization, followed by purification with automated recycling size-exclusion chromatography (SEC) after each single monomer unit incorporation. Such strategy could enable the precise and uniform insertion of a larger amount of monomers in growing chain due to the implementation of an in-line purification protocol, that enables the separation of the desired sequence-defined oligomers from polydisperse mixtures. Nevertheless, this synthetic pathway remains limited to the fabrication of oligomers, since the isolation of polymers by recycling SEC chromatography is more tedious with increasing molecular weight.

- **Template polymerization**

In biological polymerization processes, such as DNA synthesis, the defined primary structure of biopolymers is regulated via a templated mechanism.[55,93] Template polymerization is a powerful natural process in which selective interactions, between a preformed macromolecule (template) and a specific monomer, are directing its insertion in a growing chain and thus controlling the monomer sequence. A growing interest has been developed toward the preparation of sequence-controlled polymers, based on synthetic macromolecular system which could mimic this sophisticated natural template systems.[94] With the emergence of living/controlled polymerizations, interesting synthetic approaches have been developed by exploiting templated mechanisms, such as template initiator and template monomer strategies. While template initiators have been limited so far to low molecular weight models,[95,96] template monomer approach enables sequence regulation from moderate, to high molecular weight macromolecules in some cases.[97] This approach, also called cyclopolymerization, relies on the polymerization of monomers bearing two or more monomeric units linked together.[97] Such strategy offers the opportunity to build alternating or periodic polymers with monomers exhibiting similar reactivity. Indeed, alternating structures are generally possible only in very specific cases, in which the monomers, due to their electronic properties or peculiar structure, possess a very low homopolymerization rate of reaction, but a high cross-propagation rate with the selected comonomers.[23] Sawamato and co-workers have reported the preparation of a

monomer containing an acrylic and a methacrylic units linked covalently together via a naphthalene fragment (**Scheme 7A**).[98] Under diluted conditions, these building blocks polymerized via CRP process without crosslinking. This work demonstrated that the growing chain reacts preferentially with the more reactive vinylic unit (methacrylate) of the building block and intramolecular propagation step proceeds with the intramolecular acrylate unit. Subsequent removal of naphthalene template afforded alternating copolymers composed of methacrylic acid and acrylic acid. Following a likewise strategy, the same group reported the cyclopolymerization of three vinylic styrene-derivatives linked to each other in the presence of a palladium-templated precursor, yielding in repetitive ABA sequences (**Scheme 7**B).[99,100] Crucial in the polymerization were π–π-stacking interactions between aromatic side groups to position the three vinyl groups. Removal of the template led to sequence-regulated copolymers. Such approach enabled the preparation of strictly periodic -ABA- copolymers.

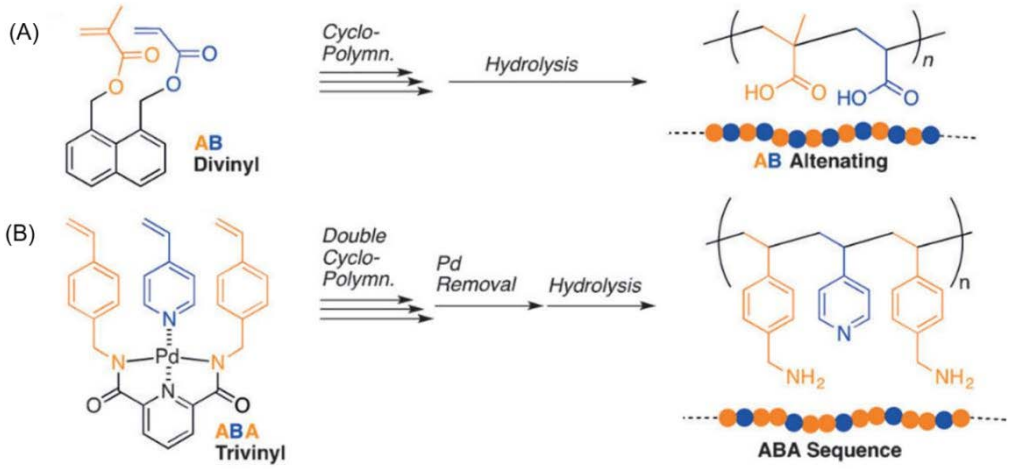

Scheme 7. Cyclopolymerizations to control the alternating sequence. a) Cyclopolymerization of AB-type divinyl monomer with naphthalene spacer, b) double-cyclopolymerization of ABA-type tri-vinyl monomer based on a palladium complex (Adapted from reference 100).

During the last years, cyclopolymerization methods have been largely extended for the preparation of alternating polymers, by exploiting template monomer systems based on other covalent groups[100] and supramolecular motives.[101] Such chain-growth polymerization approach give access to the fabrication of complex periodic monomer sequences which are hardly synthesized by conventional polymerization. Although this synthetic approach enables the construction of large sequence-regulated macromolecules, the degree of sequence complexity remains limited to periodic copolymers.

- **Kinetically controlled polymerization**

The introduction of living/controlled chain polymerizations enabled at early stages the preparation of alternating copolymers, which is the simplest sequence-defined polymer microstructure. Alternated sequences have been described for various monomer pairs by ring opening metathesis,[102] living ionic[103] and controlled radical polymerizations (CRP).[104] In the latter one, the exploitation of electron-donor and electron-acceptor monomer pairs is a powerful strategy to obtain alternating copolymers.[105] Indeed, in stoichiometric CRP copolymerization of donor monomer with acceptor comonomer, the cross-propagation (the reaction of one monomer with the adjacent other) is highly promoted compared to homopolymerization due to the electronic effects of each monomer.[106] For example, maleic anhydride, *N*-substituted maleimides and pentafluorostyrene are strong electron-acceptor monomers whereas styrene derivatives, vinyl ethers and isobutylene are electron-donor monomers. In 2000, a synthetic concept based on non-stoichiometric CRP copolymerization of styrene with maleic anhydride has been investigated.[107] It has been shown that when an excess of styrene was copolymerized with a small amount of maleic anhydride, a diblock copolymer was obtained, composed of a homo-poly(styrene) block and a narrow copolymer block of styrene/maleic anhydride.[107] Inspired by this methodology, Lutz and co-workers have developed an elegant kinetic strategy for the insertion of functional building blocks at precise locations among a polymer chain.[108] In this work, styrene and functionalized *N*-substituted maleimides were used as donor/acceptor monomer pair (**Figure 3**). Small amounts of *N*-substituted maleimides were added at desired times during the homopolymerization of styrene. The maleimides are directly and locally incorporated in the growing chain due to two crucial aspects: 1) the cross-propagation rate is significantly higher than the homo-propagation rate. 2) the formed polymer chains are growing simultaneously because of the CRP process. Thanks to these both features, the consumption of the acceptor comonomer is kinetically favoured and introduced simultaneously at similar positions within the growing chains. This strategy enables the incorporation of functional group in narrow regions within the macromolecules. A large library of *N*-functionalized maleimides has been developed to enable local insertions of functionalities within a polymer chain.[109] It must be pointed that the obtained macromolecules are not strictly sequence defined. After each monomer injection, the copolymerization remains to some degree statistical because of the variation in concentrations between styrene and added maleimides.[108,110] Later, the precision of monomer insertion along the polymer chain has been interestingly improved by performing the sequential maleimide additions in a monomer-starved polymerization conditions.[111]

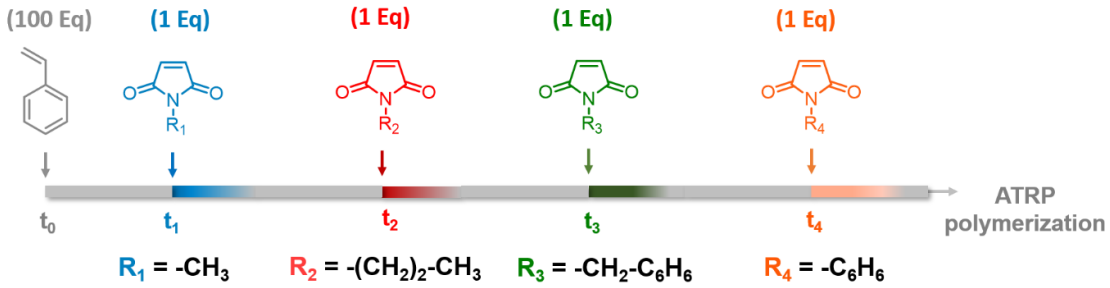

Figure 3. Synthetic concept of the sequential ATRP copolymerization of styrene and various *N*-substituted maleimides (Reproduction from reference 108).

A similar kinetic control approach based on ring-opening metathesis polymerization (ROMP) of exo- and endo-norbornenes has been described.[112] This approach relies on the different kinetics of the two isomers endo- and exo-norbornenes with the metal-complex catalytic center of polymerization. It has been previously demonstrated that the exo-norbornene isomer undergoes much faster ROMP in the presence of ruthenium-based catalysts than the endo-isomer due to steric interactions between the growing polymer chain and the incoming monomer.[113,114] Therefore, time-controlled additions of functionalized exo-norbornene derivatives during the ROMP polymerization of endo-norbornene enabled the preparation of polymers exhibiting functional groups in narrow regions among the polymer chain.

Kinetically controlled polymerization approach is a straightforward and versatile method for functionalizing "on demand" synthetic macromolecules. This concept of pulse-injection functionalization was exploited to prepare sequence-controlled macromolecules with complex microstructures and new types of polymer topologies became accessible.[115,116] Furthermore, this approach enables a sequence-regulation to a certain degree in higher molecular polymeric materials compared to the synthetic strategies discussed so far. Due to the statistical nature of the propagation step, small variations in polymer chain length and defaults in monomer composition can be expected and, therefore chain growth polymerization remains a challenging method for the preparation of sequence-defined polymers.

The field of synthetic sequence-controlled polymers has made considerable progress in the last years and has become a major research interest in polymer chemistry. Interestingly, challenges remain in achieving the precise sequence definition and high efficiency synthesis of natural polymers for the preparation of synthetic materials. As illustrated in this section, the preparation of large synthetic macromolecules exhibiting highly defined primary sequence as biopolymers, remains still difficult to reach. Although this field is relatively young, it is already demonstrated that precision polymer synthesis gives access to unprecedented sophisticated

materials and are already promising materials in different fields.[11] Controlling the microstructure of synthetic macromolecules offers the opportunity to tune bulk material properties such as optical, mechanical and thermal properties or biocompatibility, etc...[7,13] More interestingly, sequence-defined polymers are excellent candidates for digital data storage. Indeed, digital information is a binary sequence of bits (0 and 1), which can be encoded in a copolymer exhibiting a sequence of two monomer units arbitrarily defined as 0 and 1 bits.[13] Thus, sequence-defined macromolecules are promising materials for data storage systems and were already examined utilizing natural (DNA) and also non-natural sequence-defined polymers.[117,118] Moreover, sequence-controlled macromolecules are an attractive platform for generating unprecedented structural complexity such as self-assembly into nanostructures, folding, and catalytic sites.[7] The control of primary structure is a keystone for biomacromolecules, since it strongly influences their subsequent 3D structures and functions.[8,9] Hence, the regulation of the monomer sequence in synthetic polymers would provide the opportunity to mimic closer biopolymer properties such as molecular recognition and catalysis. An overview of the field of single polymer chain folding is discussed in the next section.

2.3. Single chain folding of synthetic macromolecules

The functions of biopolymers such as enzymatic catalysis, transport, and recognition are closely correlated to their highly ordered and complex 3D architectures.[119] Biomacromolecules such as peptides and nucleotides, are high molecular weight natural polymers which are uniform with well-defined monomer sequence.[8,9] Driven by a specific sequence of amino acids, polypeptides fold via the formation of secondary structures such as single-chain helices, double helices and sheets.[120,121] The formation of specific 3D structures, as well as the self-adaptive character in response to changes of environment, are in most case responsible for their unique biological features.[122] For example, enzymes are the most efficient catalysts known for biochemical reactions that take place in water.[119] Arising from a finely selected sequence of building blocks, the macromolecular chains arrange dynamically into secondary and tertiary structures. In general, deep within the 3D structure is located an hydrophobic cavity, from which originate the exceptional catalytic activity, specificity and selectivity.[119] This sophisticated structure–function relationships observed in natural polymers has been a fascinating source of inspiration in the field of material science. Within the past decades, intense research efforts were dedicated to mimic closer the features of biopolymer classes with synthetic macromolecular folding.[5,123] Synthetic macromolecules are typically composed of a random sequence of monomers and fold, in most cases, into amorphous random coil nano-

objects. Nevertheless, it has been shown that a single polymer chain can be structured and hold into a compact conformation by generating intramolecular crosslinks within a polymer chain.[124] Inspired by this concept, the field of single polymer chain folding has drastically evolved, so rapidly and to such an extent, that several compacted polymer chains started to be promising and versatile nano-objects with potential applications in many fields, from catalysis to nanomedicine.[125] Progress in the synthesis of functional polymers through CRP processes, post-functionalization methods and efficient intramolecular coupling reactions have paved the way to the reliable fabrication of complex folded macromolecules.[5] In the last years, advanced synthetic concepts have been developed for the preparation of larger folded macromolecules by forming one or more intramolecular crosslinks, *via* irreversible covalent bond or dynamic bonds.[5] An overview of synthetic approaches toward folded polymer chains is discussed In the next section,.

2.3.1. Single chain compaction by intramolecular covalent crosslinks

Many types of conventional organic reactions and clicks reactions have been exploited to induce single polymer chain compaction, such as Cu-mediated azide-alkyne cycloaddition,[126,127] thiol-ene coupling,[128] cross-metathesis,[129,130] urea formation,[131] lactone ROP,[132] ect.[4] It must be noticed that covalent fixation of the macromolecules removes the dynamic nature of the macromolecular folding in solution and prevent unfolding process, conversely to natural polymers. However, the use of covalent fixation generates static and permanent folded macromolecules which endow them with increased stability against thermal degradation at high temperatures.[5] Moreover, non-dynamic compacted polymers have also shown to be attractive for drug delivery applications, where biodegradable crosslinks are exploited to ensure controlled release of the molecule of interest.[133] In such strategy, peptides of interest were not directly attached to the transporter molecule but rather to a nanoparticle scaffold over cleavable disulfide linkers, where also the molecular transporter units are directly conjugated to the nanoparticle backbone. This system demonstrated that higher drug load of macromolecular therapeutics could be achieved than a direct conjugation to the molecular transporter molecule.[133]

2.3.2. Single chain compaction by intramolecular dynamic crosslinks

Dynamic folded macromolecules can be achieved by using supramolecular bonds or dynamic covalent bonds. Conversely to covalently folded macromolecules, exploiting intramolecular dynamic bonds generates compacted single chain nano-objects that are adaptive

to the environment and can respond to an external trigger, such as pH, solvent, light, heat, oxidation or metals. This responsiveness to external stimuli induces reversible transformation of the polymer random coil into a compact nano-object, which is an attractive feature since folding/unfolding of proteins is often directly associated with their functioning. [134,135]

- Supramolecular bond

Within the last decades, supramolecular chemistry has been widely explored to induce single polymer chain folding. Several synthetic methods have been reported for the preparation of single chain compaction by using non-covalent bonds such as hydrogen bond (H-bond), metal ligation,[136-138] host-guest interactions[139,140] and hydrophobic interactions.[4,141] Elegant synthetic approaches have been developed toward the preparation of synthetic folded macromolecules via H-bond interactions by using various motifs such as diamides,[142] BTA bipyridines,[143] thymine-diaminopyridine,[144] six-point cyanuric acid-Hamilton wedge interactions.[145] Meijer and co-workers have reported an extremely mild method to induce single chain collapse by exploiting protected 2-ureidopyrimidinone (UPy) as H-bond motifs (**Figure 4**).[146] Controlled Cu-mediated radical polymerization was performed to synthesize alkyne-functionalized methacrylate-based polymers. Azide functionalized UPy motives were incorporated on the alkyne methacrylate units by azide-alkyne 1,3-dipolar cycloaddition. The UPy motifs were protected with o-nitro benzyl ether photolabile protecting groups. The photolabile protecting groups were removed by photoirradiation, which triggered the folding process. Subsequently the UPy motifs could dimerize intramolecularly in highly diluted conditions, resulting in the formation of folded macromolecules. In a following work, it has been showed that the chiral hydrogen bond motif benzene- 1,3,5-tricarboxamides (BTAs) can be exploited to induce chain compaction and dimerize intramolecularly into helical stacks.[147]

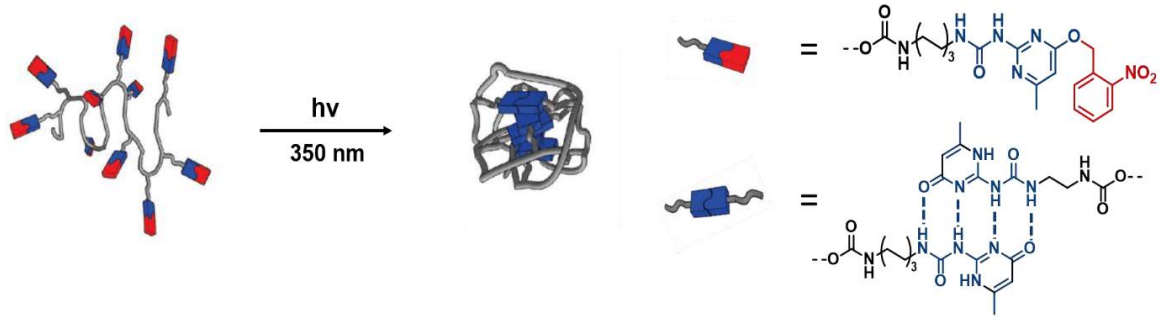

Figure 4. Single polymer chain compaction induced by UV irradiation via supramolecular cross-linking of UPy-motifs (Adapted from reference 146).

- Dynamic covalent bond

Although supramolecular crosslinking bonds have been widely investigated for the preparation of folded macromolecules, the exploration via dynamic covalent bond has only emerged in the last years. Recently, polymers with intramolecular dynamic crosslinking bonds have become an important research focus due to their ability to reversibly assemble or disassemble in response to external environmental changes.[148,149] For example, the dynamic nature allows the incorporation and release of desired molecules inside the folded macromolecules and therefore, these polymeric materials are widely exploited for drug delivery systems involving the controlled loading and release of drug molecules.[150] Various types of dynamic covalent bonds have been successfully applied to generate intramolecular crosslinking, such as disulfides,[151] reversible cycloadditions,[152] acyl hydrazones,[153,154] or enamines.[155,156] Disulfides are a dynamic covalent bond of interest due to their crucial role in protein folding and sensitivity to redox chemistry. Following Nature's systems, an interesting approach has exploited the formation of several disulfide bridges to induce reversible single-chain collapse.[157] In this work, oxidation of thiol groups by iron chloride ($FeCl_3$) into disulfide bonds led to polymer chain compaction while subsequent reduction of disulfide bonds with dithiothreitol (DTT) resulted in the corresponding thiols and the random coil precursor was regenerated.

- Diselenide bond

Among the several types of dynamic covalent bonds, diselenide bridges have been less exploited in general in polymer science.[158]Although organic selenium chemistry has been rising very fast, the introduction of selenium groups in macromolecular chemistry has only emerged recently. The development of selenium-based polymers was underexposed for mainly two reasons.[159] Firstly, the synthesized selenium-containing polymers often demonstrate poor solubility in common organic solvent, thus limiting their uses and applications. Secondly, macromolecules containing selenium group are not, in general, very stable due to the high reactivity of this element. However, for the last decade, diselenide-containing polymers has attracted considerable attention due to the unprecedented characteristic of diselenide bond. The selenium element (Se) is part of the chalcogen group in the periodic table of elements, like sulfur (S) and exhibits similar properties as its analogue. Indeed, selenium and sulfur display similar characteristics, such as electronegativity, atom size and accessible oxidation states. In contrast to the disulfide bond, the diselenide bond has a lower bond energy (Se-Se: 172 $kJ.mol^{-1}$) than disulfide bond (S-S: 240 $kJ.mol^{-1}$). Due to this inherent feature, the

diselenide bond are less stable and consequently more dynamic and responsive in mild conditions.[160,161] Diselenide containing polymers are sensitive to extremely mild external stimuli such as light, reducing agent (phosphine, DTT) or oxidizing agents (H_2O_2) and this property makes them promising biomaterials for synthetic enzyme mimics and drug delivery.[158,159,162] Indeed, dynamic material containing diselenides are already established polymer class in the fields of drug delivery and self-healing materials. Recently, amphiphilic triblock copolymer containing an internal diselenide bond in the main chain could self-assemble into spherical micelles in water.[163] The self-organized structure showed very mild sensitive redox responsive property and disassembled under treatment of only 0.01% of oxidizing agent. Such unique property endows diselenide-containing polymers as promising candidates for smart drug delivery vehicles, which release the loading drug molecules in response to redox stimuli in the tumor microenvironment.[159] Besides the redox responsiveness, another exceptional feature displayed by diselenide-containing polymers is the responsiveness to light. Diselenide can undergo metathesis reaction under visible light, while disulfide bond undergo metathesis reaction under UV-light, which is more energy consuming and may cause unnecessary damage to the macromolecular system.[159] An elegant study have taken the advantage of the relatively mild diselenide metathesis reaction to fabricate self-healing materials.[164]

Interestingly, the use of diselenide chemistry in the field of single chain folding has not been thoroughly explored and is still at his infancy. For instance, some studies have been focused on the preparation of simple topological polymers such as linear block copolymers,[163] cyclic,[165] and dendritic[166] polymers by exploiting diselenide bonds. Recently, a synthetic strategy based on the use of selenolactone as building block, has been reported for the straightforward and mild synthesis of branched, cyclic, and cross-linked polymers containing several diselenide moieties.[165] Moreover, a study provided an alternative approach to modulate topological transformation of macromolecules, by exploiting multiple diselenide groups in cyclic polymers (**Scheme 8**).[167] In this work, CRP of styrene was mediated by using a novel bifunctional diselenocarbonate chain transfer reagent, resulting in a linear polystyrene chain with protected selenols at both chain extremities. Then, diselenocarbonate groups were transformed into free selenols by aminolysis, followed by spontaneous oxidation by air of selenols into diselenide bridges. By tuning the concentration of α, ω-telechelic polystyrene for the one pot aminolysis/oxidation reaction, monoblock or multiblock cyclic copolymer linked by one or several diselenide bonds were obtained. Interestingly, the cyclic copolymers could

be then converted to each other under UV irradiation by adjusting the concentration. Besides, the reduction or oxidation of diselenide bonds both enable the conversion from cyclic to linear polymers. This work shows a straightforward approach for the preparation of cyclic polymers and evidences the unique stimuli-responsiveness behaviour of diselenide bond, which can be exploited to induce topological transformation under very mild conditions.

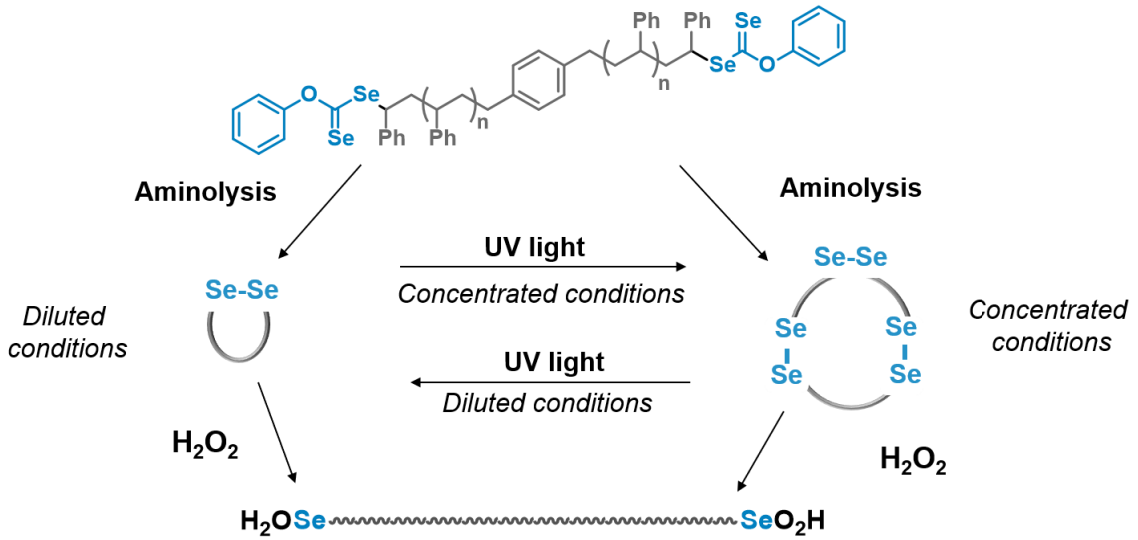

Scheme 8. Schematic illustration of the one-pot synthetic approach for the preparation of cyclic polymer by aminolysis of the linear RAFT polymer, the metathesis reaction for shuffling diselenide bonds, and ring-chain opening by hydrogen peroxide (Adapted from reference 167).

2.3.3. Next generation of folded single polymer chains

Currently, a large chemical toolbox for intramolecular crosslink formations has been developed.[4] However, such intramolecular bridges are mostly introduced randomly into the polymer chain and generate random single chain compaction.[168] Conversely in natural polymers, the primary sequence is the key parameter for controlling the formation of their complex and uniform 3D structures, which subsequently display biological functions. Thus, research focus is currently shifting to the preparation of folded macromolecules with complex and uniform structures which could mimic closer the complexity exhibited only by natural polymers.[169] Within the last years, different trends have emerged toward the preparation of more complex 3D structures or controlled folded macromolecules.[169] For example, multiple orthogonal crosslinking motifs have been exploited to generate complex synthetic polymers folding.[170,171] An elegant synthetic route has been described by using two orthogonal hydrogen-bond motifs to induce a stepwise folding process and access complex structural self-organization.[172] An ABA triblock copolymer bearing chiral BTA motifs in the middle block (B) and UPy motifs in both end blocks (A) has been synthesized and exploited to induce a

stepwise orthogonal folding process (**Figure 5a**). Protected functionalized monomers such as propargyl methacrylate (PMA), hydroxyethyl methacrylate (HEMA), and isobornyl methacrylate (IBMA) were copolymerized by ATRP to form a triblock copolymer poly(IBMA-*co*-HEMA)-*b*-poly(IBMA-*co*-PMA)-*b*-poly(IBMA-*co*-HEMA). Subsequently, the alkyne groups were functionalized with BTA motifs via azide-alkyne cycloaddition, while hydroxyl side groups were post-modified by isocyanate conjugation reactions to introduce protected UPy motifs. Such synthesis enabled the elaboration of a ABA-type triblock copolymers, with the middle-block-containing BTAs and the two outer blocks o-nitrobenzyl protected UPy groups (**Figure 5b**). These complex copolymers were folded in an orthogonal stepwise manner. The ABA block copolymers could fold by thermal treatment through intramolecular H-bond of the BTAs motifs to generate helical stacks (**Figure 5c**). Then, the photolabile protecting groups of UPy moieties were removed by photoirradiation and intramolecular UPy motifs could dimerize (**Figure 5d**). This second reaction induced a further folding step to yield into more compact and stabilized conformation. An additional study showed that when the order of block was inverted, the BAB-type triblock copolymers were found to fold into a slightly less compacted nanoparticle than the ABA-type copolymers. These examples illustrate how the complexity and specificity of the internal structure of folded macromolecule can be tuned by using multiple orthogonal intrachain bonds.

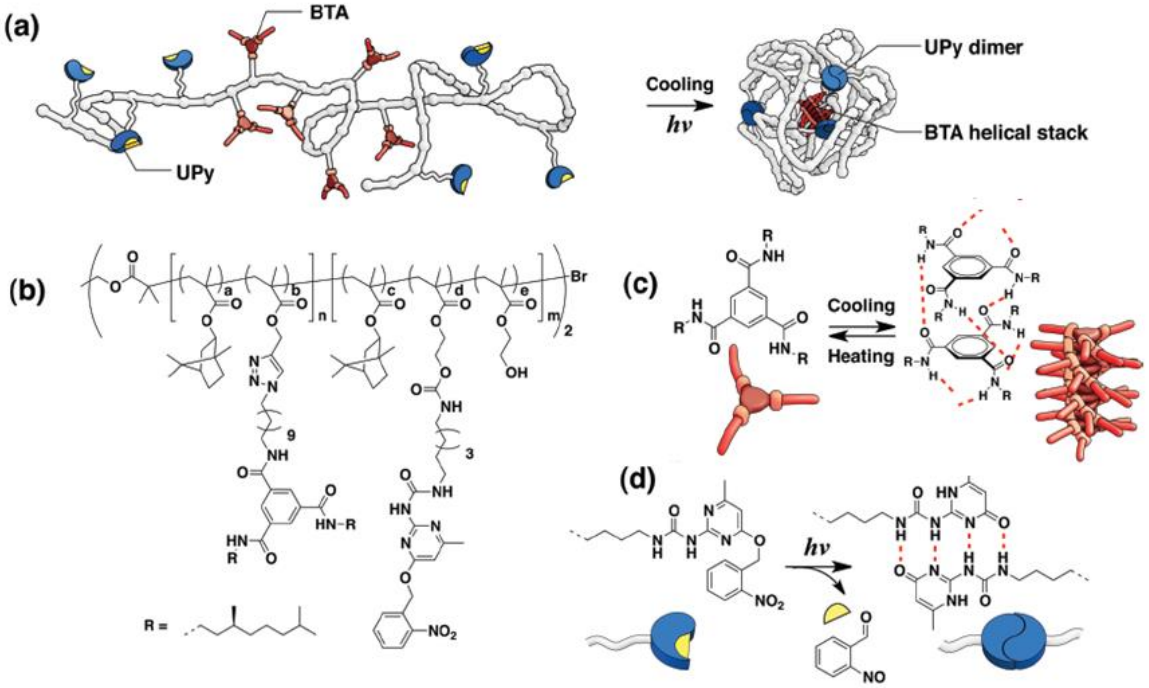

Figure 5. (a) Triblock copolymer with BTA and UPy motifs that folds via orthogonal self-assembly. (b) Chemical structure of the copolymers. (c) Helical self-assembly of chiral BTAs via H-bond. (d) Photoinduced dimerization of protected UPys via H-bond (Adapted from reference 172).

Besides, arising from their well-defined primary structures, biopolymers are capable to undergo guided folding in solution to complex structures.[123,173] Thus, research interest has grown toward the use of sequence-controlled polymers to induce single chain folding in a controlled manner and toward complex architectures. For instance, foldamers, which are synthetic sequence-defined oligomers, were extensively investigated to adopt well defined secondary structures.[174] In the contrary, progress in controlled folded macromolecules with high-molecular weight is less advanced compared to oligomers. Interestingly, an elegant method to generate controlled single polymer chain folding into a precise origami has been reported by exploiting sequence-controlled polymerization (**Figure 6**).[175] In this study, sequence-regulated polymerization based on the styrene/ maleimide platform with timed monomer additions was performed to form at desired position an intramolecular bridge within the macromolecule. Linear polymer precursors were synthesized by ATRP copolymerization of an excess of styrene with one equivalent of *N*-substituted maleimides bearing a protected alkyne group. The donor monomer is the main constituent of the chain, while the maleimide unit was precisely positioned within the polymer chain via timed injection during the polymerization. The bromine terminal group inherited from the ATRP process was exploited and transformed into azide group. After deprotection of the alkyne reactive groups located on the maleimide, copper-catalysed azide-alkyne "click" reaction was performed between the alkyne group and the azide terminal group to induce a controlled intramolecular cross linking.

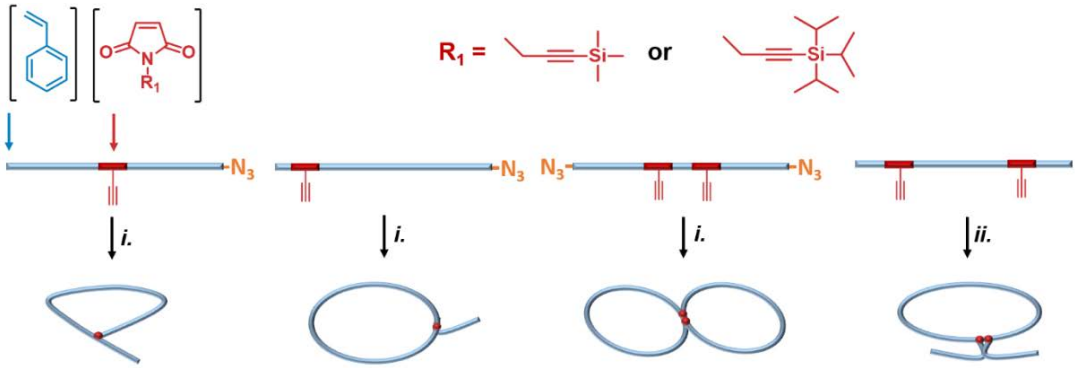

Figure 6. Schematic illustration of the controlled shapes obtained by click reaction: tadpole (P-shaped), pseudocyclic (Q-shaped), bicyclic (8-shaped) and knotted (α-shaped). Experimental conditions: i) azide–alkyne 1,3-dipolar cycloaddition: CuBr, 2,2′-bipyridine, dimethylformamide, 80 °C. ii) Glaser coupling: CuBr,2,2′-bipyridine, O_2, dimethylformamide, 80 °C (Adapted from reference 175).

This approach leads to a variety of tuneable cyclic shapes, commanded by the position maleimide units bearing the reactive groups. Inspired by this work, Lutz and co-workers have also described the fabrication of controlled folded macromolecules by forming one positional dynamic disulfide bridge.[176] The use of sequence-controlled multiblock copolymers has also been employed to induce controlled single polymer chain compartmentalization.[177-179]

Exploiting such sequence-regulation techniques could potentially enable new designs of tailored polymer microstructures, in which the amount and positioning of cross-linking sites can be precisely controlled.[169] Hence, it is reasonable to assume that the use of sequence-controlled polymerizations is a major step to move forward the complexity and uniformity of folded macromolecules. Such current progress highly requires parallelly the development of analytic tools capable of characterizing this emerging class of synthetic of folded macromolecules. An overview of the typical analytic tools is discussed in the next section.

2.3.4. Characterization methods

In terms of characterization, a significant number of analytical techniques has been used to characterize folded macromolecules. However, most of them can provide only circumstantial evidence of compacted nano-object characteristics. A combination of different characterization techniques is generally required to fully characterize folded macromolecules. The main analytic tools used to either evidence the compaction process or characterize the resulting morphology are reported in this section.

Size Exclusion Chromatography (SEC) remains one of the crucial analytic tools to prove the formation of compacted macromolecules. First, this characterization method allows to gain insight into the formation of intramolecular vs. intermolecular crosslinking bond formations. Furthermore, upon compaction, an increase in retention time from the polymer precursor to folded polymer can be observed, indicating a decrease in apparent molecular weight.[180] This shift in elution volume is typical of a hydrodynamic volume reduction caused by intramolecular crosslinking bond formations.[181] However, while this technique demonstrates a reduction in hydrodynamic volume, the quantification of this change is impossible with standard SEC measurements alone. Quantitative information can be obtained by coupling SEC chromatography with multiple in-line detectors, such as Multi-Angles Light Scattering (MALS).[182] Often, the analytical data obtained by SEC can be verified by Dynamic Light Scattering (DLS).[183,184] Proton NMR spectroscopy is also an important analytic tool, since this characterization enables to monitor the appearance or disappearance of signals corresponding to the formed crosslinking bonds. However, this technique does not differentiate the formation of intramolecular and intermolecular bond. Nevertheless, others NMR spectroscopies such as Diffusion Ordered Spectroscopy (DOSY) can indicate a decrease in hydrodynamic volume. DOSY experiments reveal the diffusion coefficient of a macromolecule in solution, which is inversely proportional to the hydrodynamic volume.[127] The formation of folded nanoparticles

should lead to an increase of the diffusion coefficient, as evidence of the formation of single chain compaction. Regarding complex macromolecular folding obtained by formation of several crosslinks, one challenging aspect of characterization is accurately deciphering their compact morphology, which is in some cases dependant on solvent and concentration.[168] Characterization of the morphology can be achieved by using solution-free microscopy techniques, such as Atomic Force Microscopy (AFM) and Transmission Electron Microscopy (TEM), to gain insight into the size and shape of folded macromolecules. These microscopies are powerful methods since both allow the direct visualization of the folded nano-objects. However, the absence of solvent can potentially modify the initial morphology. Also, interactions with the analytical substrate can occur and even yield in misleading images.[185] Hence, characterization of single chain compaction in solution is also achieved using small-angle neutron scattering (SANS) and small-angle X-ray scattering (SAXS) by measuring essentially the radius of gyration.

The synthesis and characterization of folded macromolecules represents an important initial step toward advanced nano-architectures that are capable of mimicking the complexity found in natural systems.[169] Such compacted systems are believed to make major contributions to a wide range of fields, from nanomedicine to sensing, catalysis, and other diverse uses.[5] Already some proof-of-concept applications of single-chain folded macromolecules are reported in literature, as synthetic materials capable of exhibiting functions.[6,125,186] Compacted nano-objects can be used as enzyme-mimic systems: such synthetic collapsed polymers are exhibiting an internal cavity, which can be used as nanoreactor and/or in which catalysis can take place. For example, an impressive study showed that an amphiphilic grafted triblock copolymer can fold in water via intramolecular hydrogen bonds, leading to the formation of an internal compartment. The resulting hydrophobic cavity proved to efficiently catalyse the transfer hydrogenation reaction of ketones.[187] Similar copolymers were also able to facilitate the oxidation of secondary alcohols into their corresponding ketones.[188] Modelling enzymes with synthetic polymers offers the opportunity to improve the catalysis efficiency by controlling polymer solubility or even increasing catalytic site accessibilities.[168] Moreover, some folded macromolecules have been reported as effective molecular sensors for metal ions. In a recent study, linear copolymers exhibiting pendant bipyridine-BTA units were synthesized by ring opening metathesis polymerisation and used to detect copper ions.[143] The polymers fold intramolecularly *via* π–π interactions into fluorescent, compartmentalised particles in a mixture of organic solvents. The fluorescence intensity was found to depend on the bipyridine content in

the polymer precursor.[143] Quenching of fluorescence was observed in the presence of metal ions, such as copper, since copper exhibits high affinity toward the bipyridine units and thus were encapsulated in the macromolecules. Such characteristic endows these nanoparticles as promising materials in sensor applications to detect the presence of metal ions.

Although remarkable progress has been made for the fabrication of folded polymers with promising functions, current synthetic strategies remains limited in terms of sophisticated design, folding control and unique characterization techniques.[169] Another impediment seen in most syntheses is the requirement of dilute polymer solutions, which complicate the practicality of scalable or industrial production of folded macromolecules. It is certainly clear, despite some obstacles, that folded macromolecules are a firmly established research topic in modern polymer science and the field of single-chain technology will undoubtedly continue to evolve and access synthetic materials with unprecedented properties.

3. RESULTS AND DISCUSSION

3.1. Controlled oxidative single-chain cyclization and conformation analysis

Synthetic macromolecules with sophisticated microstructure and complex structural organization are attracting artificial nano-objects for mimic biological functions such as enzyme activities or self-recognition.[125] As discussed in the previous section, while well-defined oligomer and short polymer can fold into precise and controlled 3D organization such as helical and sheet conformations,[12] compaction of larger synthetic single polymer chain into precise conformation (DP_n > 50 units) remains challenging. Nevertheless, macromolecular folding is continuously investigated by forming intramolecular crosslinks to induce a macromolecular collapsed state. Monocyclic polymers are the simplest class of polymer chain folding since their formation arises from the use of one single intramolecular crosslink. Due to the absence of polymer extremities, this class of macromolecules have already shown different physical and chemical properties compared to linear polymer chain, such as smaller hydrodynamic volume and radius of gyration, higher glass transition temperature, lower intrinsic viscosity, etc.[189] Two main trends have merged toward the preparation of cyclic polymers. The first approach is ring-chain expansion polymerization, which relies on successive incorporations of monomers unit into an activated cyclic initiator to expand the ring.[190] This method provides a unique and powerful synthetic strategy to produce high molecular weight cyclic polymers, without linear polymer counterparts, but enables limited control over the molecular weight and distribution.[189,191-196] The second method is the ring chain closure approach and relies on the cyclization of a linear polymer precursor.[190] With the emergence of controlled/living polymerizations, end-chain groups were easily exploited to introduce reactive functional moieties at both sides of linear polymer chain and induce subsequent polymer cyclization.[197-201] Furthermore, this approach allows advantageously the preparation of cyclic polymers with a wide range of chemical structures and topologies.[202] It must be pointed out that, during the intramolecular cyclization process, the increased distance between the reactive groups compromised ring-closing efficiency.[189] Cyclic polymers are generally characterized and distinguished from their linear polymer analogues by SEC chromatography, SEC-viscometer apparatus, MALDI-TOF MS, and NMR.[190] Few studies have investigated the visualization of cyclic polymers by Atomic Force Microscopy (AFM) and Transmission Electron Microscopy (TEM).[195,203-205]

While most of the synthetic routs exploits end-chain groups to induce chain cyclization and results in an unique ring-shape,[206] the precise placement of intramolecular bridge within a polymer chain is and enables to access atypical and well-controlled cyclic macromolecules.[175,176,207] Besides, folding of biomacromolecules in nature is often dynamic and responsive to environmental changes. Inspired by this natural concept, the use of oxidative dynamic covalent bonds, such as disulfide and diselenide bridges, have shown increasing interest due to their dynamic responsiveness to soft external stimuli.[134,158] Compared to its disulfide analogue, diselenide bridge displays higher sensitivity to light, reducing and oxidizing agents.[161]

In this section, controlled synthesis and morphology analysis of cyclic polymers was explored. Sequence-controlled polymerization was exploited to prepare linear macromolecules of intermediate molecular weight (DP_n = 50) and containing protected selenols at precise positions within the polymer chain. Oxidative single chain folding was investigated by forming intramolecular diselenide bridge and induce controlled single polymer chain cyclization. This synthetic concept enables to access atypical and uniform monocyclic origamis via dynamic diselenide bridge. Moreover, a novel synthetic approach which consists to transform folded polymers into folded brush polymers, was developed to access macromolecular imaging and direct topology visualization by AFM. This study was realized in collaboration with the group of Prof. Svetlana Santer and co-workers, who contributed to the work by performing the AFM characterizations.

3.1.1. Synthesis of polymers with positioned protected selenols

Among the several specialized synthetic routes, which enable sequence-regulation in synthetic polymers, the styrene and maleimide copolymerization via timed monomer additions was selected in this study.[108] This simple kinetically-control polymerization method allows placement of reactive groups at desired positions, which can be virtually anywhere along the growing polymer chains.[175] Recently, it was reported that Nitroxide Mediated Polymerization (NMP) of electron-rich functional styrene derivatives, such as 4-methylstyrene, 4-acetoxystyrene and 4-*tert*-butoxystyrene, with a non-stoichiometric amount of maleimides allowed likewise the synthesis of copolymers with well-controlled molecular weight distribution and local insertions of maleimides.[208] In the present work, the commercially available 4-*tert*-butoxystyrene monomer **(**StyO*t*Bu**),** bearing a protected functionality on the para position of the aromatic ring was selected as electron-rich monomer. The protected alcohol

fragment located on this electron-rich monomer offers the opportunity for subsequent polymer backbone post functionalization.[208]

As acceptor monomer, a *N*-substituted maleimide bearing a protected selenol moiety was designed in the aim to introduce reactive selenol groups at desired positions within a polymer chain. To avoid interference of selenol in the polymerization process, this functionality was protected with a *p*-methoxybenzyl fragment (Mob) which is a common protecting group for selenol side group in peptide chemistry.[209] *N*-(2-*p*-methoxy-benzylselenoethyl) maleimide (MISeMob) was successfully synthesized over four steps (**Scheme 9**). A common synthetic route for the preparation of maleimide derivatives is the treatment of maleic anhydride with substituted primary amines, leading to maleamic acid, followed by a dehydration step. Thus, the first two steps of this synthesis consisted in the preparation of a compound bearing both a primary amine and the protected selenol fragment. First, elemental selenium was reduced with hydrazine monohydrate and sodium hydroxide to generate sodium diselenide (Na_2Se_2), followed by reaction with *p*-methoxybenzyl chloride.[210] To introduce the required primary amine, the resulting bis-(*p*-methoxybenzyl) diselenide was reduced with sodium borohydride ($NaBH_4$) and the released selenolates reacted with 2-bromoethylamine.[211] Then, nucleophilic attack of the primary amine on maleic anhydride lead to the formation of maleamic acid in extremely mild conditions. Dehydration of maleamic acid occurred at high temperature with an excess of sodium acetate in acetic anhydride to induce *N*-substituted maleimide cyclization.[212] The purification of the desired maleimide was performed by column chromatography and led to a yellow solid with 32% yield over the last three steps.

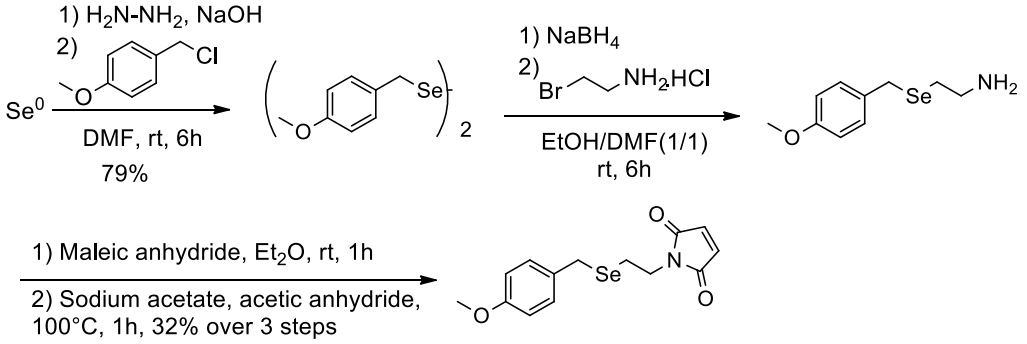

Scheme 9. Synthetic route for the preparation of *N*-(2-*p*-methoxy-benzylselenoethyl) maleimide (MISeMob).

Sequence-controlled polymerization of *4-tert*-butoxystyrene with the *N*-functionalized maleimide (MISeMob) was then investigated according to a protocol previously described in litterature.[208] The commercially available Blocbuilder MA (BB) was used to initiate the

polymerization. This initiator is composed of a SG_1 nitroxide fragment (*N*-*tert*-butyl-*N*-(1-diethylphosphono-2,2-dimethylpropyl)-*N*-oxyl, **Figure 7**), that allows controlled radical polymerization of a broad range of monomers compared to the commonly established TEMPO nitroxide (2,2,6,6-tetramethylpiperidinyl-1-oxy) and its derivatives.[213] The sequence-controlled polymerization started with the homopolymerization of StyO*t*Bu at 120°C in anisole with the ratio [StyO*t*Bu: BB] = [100: 1]. The polymerization kinetic was monitored by ^{1}H NMR spectroscopy. Injections of MISeMob maleimides were performed at different time during the homopolymerization of StyO*t*Bu (**Figure 7**). One equivalent of MISeMob was added to the polymerization at approximatively 10% of 4-*tert*-butoxystyrene conversion, and a second addition of 1 equivalent of maleimide was performed at approximately 45%. The copolymerization was stopped in the range of 53% of 4-*tert*-butoxystyrene monomer conversion. The copolymerization kinetic demonstrated the full and fast incorporation of the functional maleimide units on both sides of the formed polystyrene chains (**Figure 8A**). For both additions, the conversion of maleimides reached 100% (1 unit of maleimide was added in average in each growing chain), while StyO*t*Bu conversion gained 7% only (7 styrene units were added in average in each growing chain).

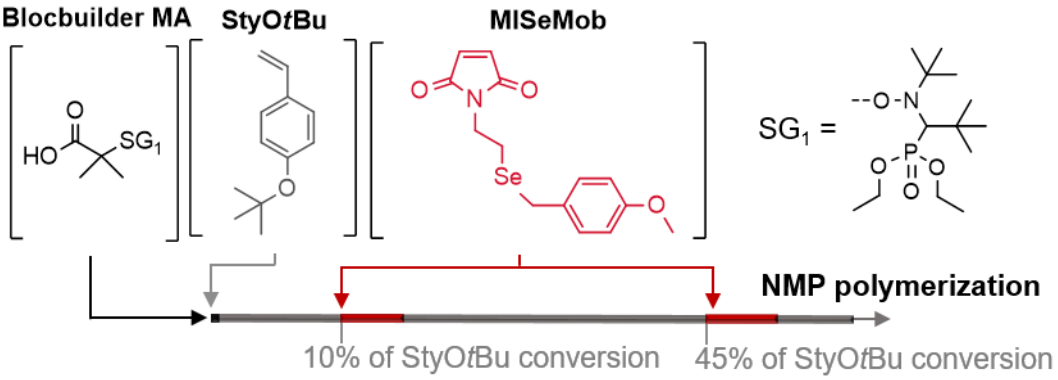

Figure 7. NMP sequence-controlled copolymerization of StyO*t*Bu with MISeMob initiated by Blocbuilder MA in anisole with the ratio [BB: StyO*t*Bu: MISeMob : anisole] = [1: 100: 2: 35% vol.] at 120°C.

The resulting copolymer was isolated to afford a linear sequence-controlled prepolymer with positioned MISeMob functionalities (poly(StyO*t*Bu-*co*-MISeMob)) and was characterized by SEC chromatography in tetrahydrofuran (THF) and ^{1}H NMR. The SEC analysis evidenced the formation of macromolecules with controlled molecular weights and narrow molecular weight distributions (SEC in THF, $M_{n,\,app}$ = 10700, Đ = 1.10), indicating that the insertion of MISeMob did not interfere in the CRP process (**Figure 8B**). The NMR spectrum confirmed the incorporation of maleimide units in the growing polymer chains.

Signals corresponding to the methoxybenzyl group of the functional maleimides could be observed at 7.17, 6.80 and 3.70 ppm (**Figure 9**). The integral intensities indicated that approximatively 2 maleimides were introduced in average in the polymer chains of $DP_n \approx 50$.

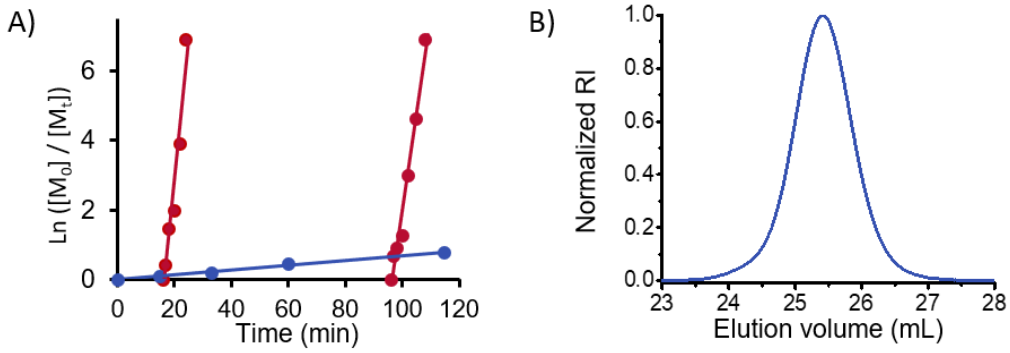

Figure 8. A) Semilogarithmic plot of monomer conversion *vs*. time of the sequence-controlled copolymerization. B) SEC trace of the isolated poly(StyO*t*Bu-*co*-MISeMob).

N-substituted maleimides bearing selenol fragments were successfully incorporated at desired positions along the polymer chain. In fact, the maleimides were introduced in narrow regions and thus the obtained copolymers were not strictly sequence defined. However, both incorporation windows were narrowed down to 7 StyO*t*Bu units in average and thus the obtained copolymers still exhibit a relatively precise chain-to-chain sequence distribution. It should be emphasized that the sequence-controlled polymerization and functionality positioning are limited in precision by the statistical radical growth process. It is reasonable to assume that a minor fraction of poly(StyO*t*Bu-*co*-MISeMob) chains could contain one or three maleimide units *per* chain.

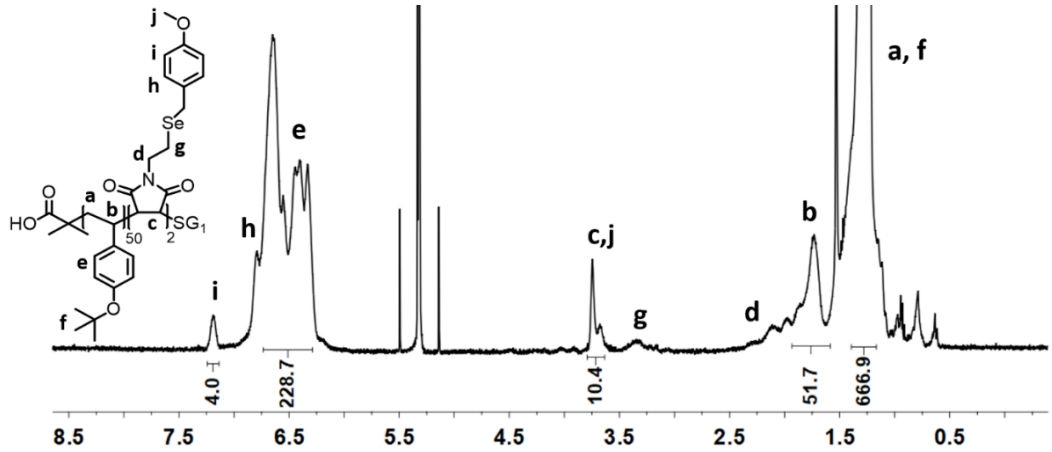

Figure 9. ^{1}H NMR spectrum in CD_2Cl_2 of the isolated copolymer poly(StyO*t*Bu-*co*-MISeMob) prepared by NMP sequence-controlled copolymerization.

3.1.2. Polymer backbone deprotection

The subsequent step consisted in the deprotection of the *tert*-butyl groups located on the backbone phenolic units. The *tert*-butyl moiety is a common acidic-labile protecting group, widely used in peptide chemistry.[214] First deprotection attempts were conducted in trifluoracetic acid (TFA) in the presence of water and triethylsilane as scavenger. However, evident re-alkylations of released *tert*-butyl fragment on phenolic units were observed and could not be constantly avoided even in the presence of scavengers. Thus, removal was successfully achieved by hydrolysis with aqueous hydrochloric acid (HCl) in dioxane at high temperature (**Scheme 10**).[208] The deprotection reaction fully occurred and yielded in the formation of a linear poly(4-hydroxystyrene) with positioned protected selenol segments (*l*-poly(StyOH-*co*-MISeMob)). The polymer modification reaction was verified by ^{1}H NMR. Disappearance of the signals assigned to the *tert*-butyl resonances at 1.0 - 1.5 ppm confirmed a quantitative deprotection of phenol units while the characteristic peaks corresponding to the Mob-protected selenol group (SeMob) remained unchanged (**Figure 10**). Moreover, the SEC chromatography in dimethylacetamide (DMAc) confirmed a clean polymer modification reaction, showing the formation of macromolecules with controlled molecular weight and narrow molecular weight distribution ($M_{n,\,app}$ = 14700, and Đ = 1.11).

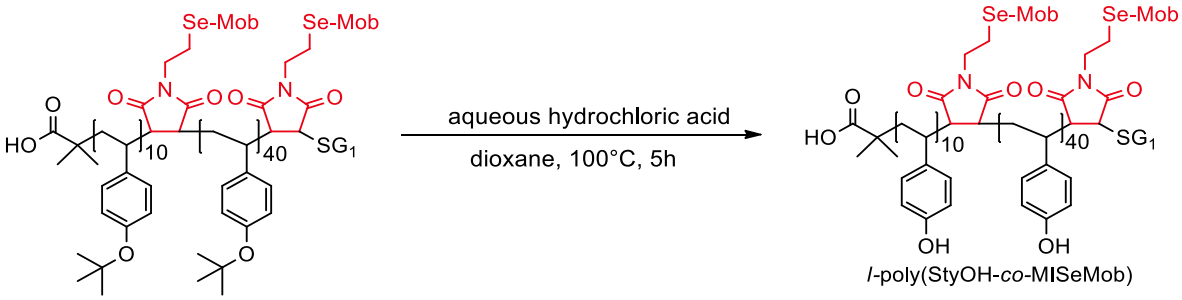

Scheme 10. *Tert*-butyl groups deprotection reaction achieved by HCl catalysed hydrolysis, resulting in the deprotected linear precursor *l*-poly(StyOH-*co*-MISeMob).

It should be pointed out that a shift of the polymer peak to higher elution volume in the SEC chromatogram was expected after removal of the *tert*-butyl fragments. However, a shift to lower elution volume was noticed, indicating a higher hydrodynamic volume. This observation reflected a potential swelling of the polymer chain due to polymer-solvent interaction via hydrogen-bond interaction in dimethylacetamide.

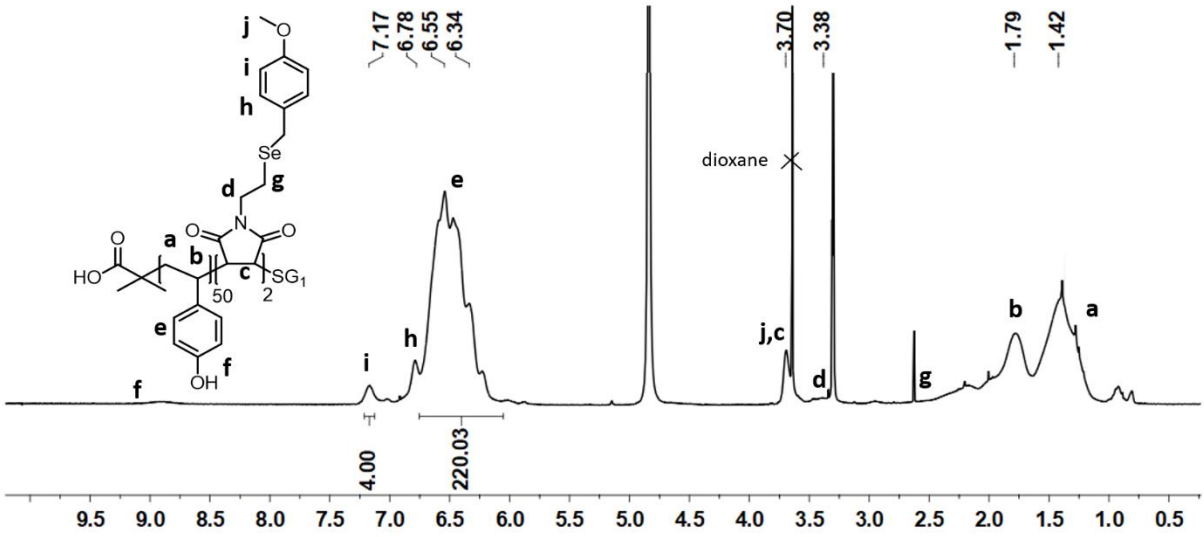

Figure 10. ^{1}H NMR spectrum in CD_3OD of the isolated copolymer *l*-poly(StyOH-*co*-MISeMob) after *tert*-butyl deprotection achieved by HCl catalysed hydrolysis.

3.1.3. Synthesis of cyclic polymers by forming intramolecular diselenide bridge

In this section, the formation of individual folded macromolecules by generating one intramolecular crosslink was studied. Oxidation of the two inserted selenol fragments into diselenide bond was explored to form an intramolecular bridge formation and lead to a chain cyclization. Since the selenols were under a protected form, removal of the blocking groups followed by oxidation of selenols was investigated.

3.1.3.1. Formation of intramolecular diselenide bridge

In peptide chemistry, *p*-methoxybenzyl selenocysteine (SecMob) protection is by far the most exploited selenol blocking protocol.[209] After incorporation of this protected amino acid derivative into desired positions of peptide chain, removal of SecMob has been implemented by using various synthetic approaches. Often, extremely harsh conditions were used for *p*-methoxybenzyl (Mob) deprotection such as treatment with trimethyl sulfonic acid (TMFSA),[215] hydrofluoric acid gas (HF),[216] and silyl-Lewis acids.[217,218] Mob-deprotection and selenols oxidation into diselenide bridge has also been described in a one-pot reaction by using molecular iodine (I_2) or DMSO.[219,220] However, the use of iodine was often problematic since it is highly reactive. Side reactions such as removal of selenol fragment or iodinated adducts were commonly occurring. The use of DMSO as an oxidative deprotection reagent provided satisfactory results and yielded in the formation of diselenide bond.[219] Recently, an even more gentle and highly efficient reaction has been described for the removal of SecMob followed by spontaneous oxidation of selenols into diselenides by treatment with 2,2'-dithiobis(5-

nitropyridine) (DTNP) in trifluoroacetic acid (TFA) as outlined in **Scheme 11**.[221] This method used DTNP to remove 4-methoxybenzyl protecting group and substitute by the 2-thio-5-nitro-pyridine group derived from DTNP fragmentation. Subsequently the released 2-thio-5-nitro-pyridine (S-Npyr) cleaved the Se–S bond of the protected selenol intermediate Se(S-Npyr), which generated free selenols and spontaneous oxidation into diselenide by exposure to air.[216]

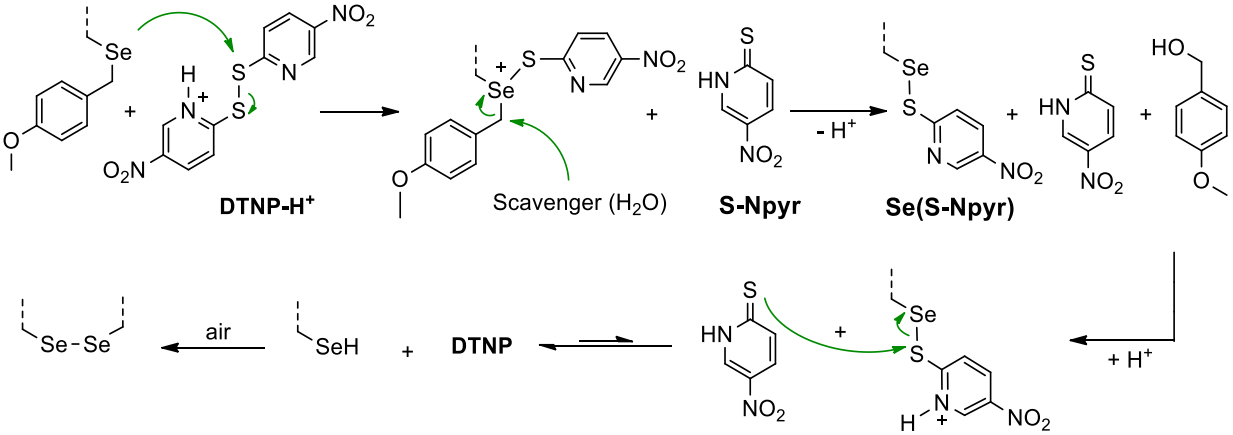

Scheme 11. Proposed mechanism for the deprotection of *p*-methoxybenzyl protecting group by using DTNP and subsequent selenol oxidation into diselenide.

Herein, one pot Mob-deprotection and selenol oxidation was performed by using DTNP in acidic conditions to generate intramolecular diselenide bridge and induce chain cyclization.[216] The reaction conditions were slightly modified from literature since poly(4-hydroxystyrene) chains are not soluble in pure TFA. A solvent mixture composed of methanol/TFA was employed to carry out the concomitant deprotection/oxidation of selenols into diselenide. The linear polymer precursor *l*-poly(StyOH-*co*-MISeMob) was used to investigate the cyclization process and various protocols were performed in the solvent mixture at room temperature to afford cyclic copolymers (*c*-poly(StyOH-*co*-MISe)$_X$). The reactions conditions and characterizations are summarized in **Table 1**. The deprotection/cyclization process was monitored by SEC in dimethylacetamide (DMAc). After reaction, a shift in the SEC chromatogram toward higher elution volume is expected due to a reduction of the polymer hydrodynamic volume caused by the formation of intramolecular crosslinking.[222] In a first attempt, one equivalent of DTNP in MeOH/TFA (80/20 %vol.) was used to induce Mob deprotection (**Table 1, Entry a**). The SEC chromatogram showed no change between the linear precursor and the resulting polymer after reaction. Additionally, proton NMR indicated that the Mob deprotection did not fully occur (see section 6.4, **Figure 69**). The integral intensity of the Mob-group signals indicated that 77% of protected selenols were recovered at the end of the reaction. Compared to the conditions described in literature, the stoichiometric amount of

DTNP was much more diluted in this system, which decreases the reaction rate and efficiency. Thus, an excess of DTNP (7 equiv) was used to perform the reaction. When the reaction was conducted in the solvent mixture methanol/TFA (80/20 %vol.) for 2 days with a concentration in the range of 10^{-4} mol/L, the deprotection reaction went to completion (**Table 1, entry b**). However, the SEC chromatogram showed a bimodal molecular weight distribution (**Figure 11A**, red curve). Mainly intermolecular crosslinks were formed, resulting in the formation of a dimer, i.e. two polymers linked together via the formation of a diselenide bridge. This result was very encouraging since the oxidation of selenols into diselenide group seemed to occur. To promote the formation of intramolecular diselenide crosslink and reduce intermolecular side reactions, deprotection/oxidation was conducted in highly diluted conditions in the solvent mixture methanol/TFA (80/20) for 4 days with a concentration in the range of 10^{-5} mol/L (**Table 1, entry d**). The SEC chromatogram showed no shift between the linear polymer precursor and the obtained polymer (**Figure 11A**, blue curve). However, an important high molecular weight shoulder was observed indicating that the formation of intermolecular diselenides was decreased but still significantly occurring. Therefore, the reaction was further optimized by performing the same deprotection/oxidation conditions with the use of a syringe pump for a slow addition of the linear polymer precursor (with a speed of 10^{-6} mol/h) in the solvent mixture containing DTNP (**Table 1, entry e**).

Table 1. Reaction conditions and characterizations of the resulting cyclic copolymers *c*-poly(StyOH-*co*-MISe)$_X$ after one pot deprotection/oxidation reactions of SeMob segments into diselenide by using DTNP.

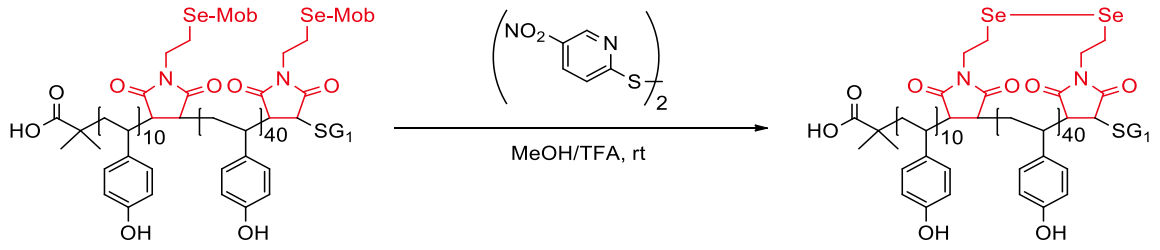

l-poly(StyOH-*co*-MISeMob) → *c*-poly(StyOH-*co*-MISe)$_X$

Entry (x)	DTNP (equiv)	MeOH/TFA (v/v)	Time (days)	Concentration (M)	$M_{n,\,app}$ [a]	Đ [a]
a	1	80/20	2	4×10^{-4}	12800[b]	1.13[b]
b	7	80/20	2	4×10^{-4}	31200	1.33
c	7	90/10	2	4×10^{-4}	16000[b]	1.17[b]
d	7	80/20	4	5×10^{-5}	16500	1.24
e	7	80/20	4	5×10^{-5} [c]	13100	1.22

[a] SEC in DMAc. [b] ^{1}H NMR indicated no full deprotection of SeMob. [c] Dropwise addition of linear precursor *l*-poly(StyOH-*co*-MISeMob) via a syringe pump.

The SEC curve of the resulting polymer shifted to lower molecular weight region (**Figure 11B**, purple curve), which is typical of the reduction of hydrodynamic volume caused by forming intramolecular crosslinking (ΔV = 0.25 mL, $M_{p,\,app}$ = 13100 and Đ = 1.22 for the cyclic polymer *c*-poly(StyOH-*co*-MISe)$_e$ *vs.* $M_{p,\,app}$ = 14700 and Đ = 1.11 for the linear precursor *l*-poly(StyOH-*co*-MISeMob)). Besides, the chromatogram showed a minor high molecular weight shoulder. Intermolecular oxidation occurred during the oxidation step but generated a limited amount of chain dimerization.

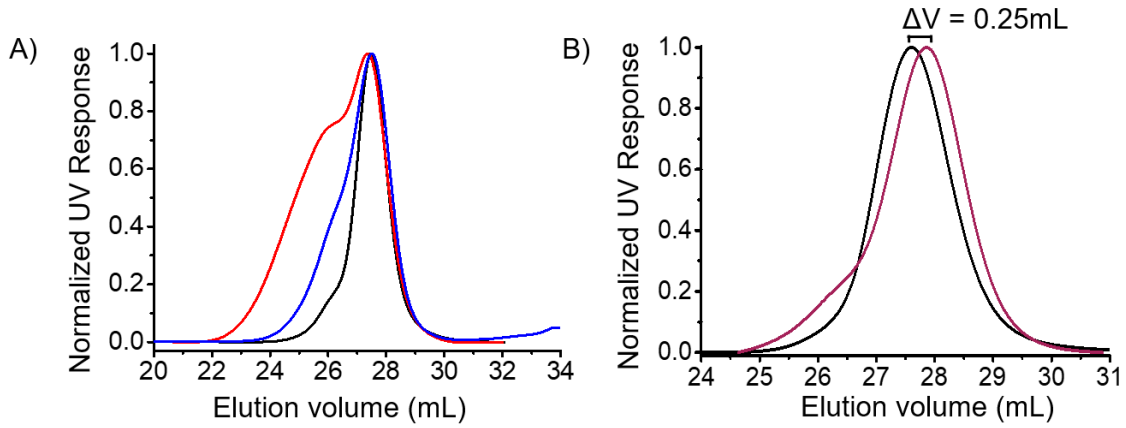

Figure 11. A) SEC traces of the linear precursor (black curve) with the resulting *c*-poly(StyOH-*co*-MISe)$_b$ (red curve) and *c*-poly(StyOH-*co*-MISe)$_d$ (blue curve) after one pot deprotection/oxidation reaction by DTNP (Table 1). B) SEC traces of the linear precursor *l*-poly(StyOH-*co*-MISeMob) (black curve) with the resulting cyclic polymer *c*-poly(StyOH-*co*-MISe)$_e$ (purple curve) after optimized deprotection/oxidation reaction by DTNP in highly diluted conditions.

2D HSQC NMR analysis of the resulting cyclic polymers indicated that the signals corresponding to *CH*$_2$-Se moiety shifted in both dimensions from 2.25/20.16 to 2.82/29.31 ppm respectively, suggesting diselenide bond formation (**Figure 12**). Proton NMR analysis indicated the full disappearance of the signals at 7.10, 6.80 and 3.70 ppm, corresponding to 4-methoxybenzyl group, and confirmed a complete selenol deprotection (see section 6.4, **Figure 68**). However, signals corresponding to the protected selenol intermediate Se(S-Npys) could be observed at 9.13, 8.32 and 7.82 ppm. The integral intensities indicated that only 14% of selenol moieties were still protected with the intermediate protecting group Se(S-Npys). It should be pointed out, that the sequence-controlled polymerization and functionality positioning is limited in precision by the statistical radical growth process. Therefore, it is plausible to assume that some chains could be mono-functionalized during the sequence-controlled copolymerization. A minor fraction of the chains could not be able to generate intramolecular diselenide bridge formation and conversion of the intermediate protected polymers into the cyclic forms could not be quantitative.

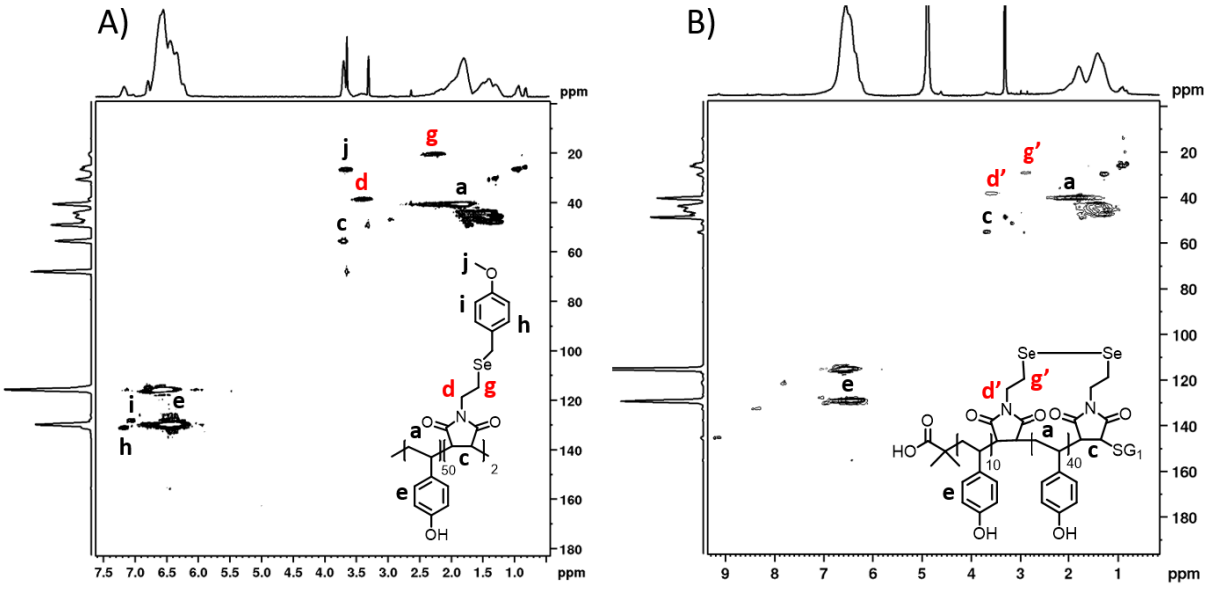

Figure 12. 2D HSQC NMR spectrums in CD_3OD of the linear precursor *l*-poly(StyOH-*co*-MISeMob) and the obtained cyclic copolymer *c*-poly(StyOH-*co*-MISe)$_e$ after optimized deprotection/oxidation reaction (Table 1, entry e).

3.1.3.2. Ring chain-opening by oxidation

The redox sensitivity of diselenide-containing polymer was exploited to confirm the cyclic topology. Oxidation or reduction of the diselenide segment could lead to a ring chain-opening. Such reverse topological transformation could be followed by SEC analysis and could indirectly evidence the successful previous cyclization step. Oxidation of intramolecular diselenide moiety into selenic acids was performed by treatment with hydrogen peroxide (H_2O_2, 37%) (**Figure 13A**).[223] The topology transformation from cyclic polymer chains to linear chains was then analysed by SEC chromatography (**Figure 13B**).

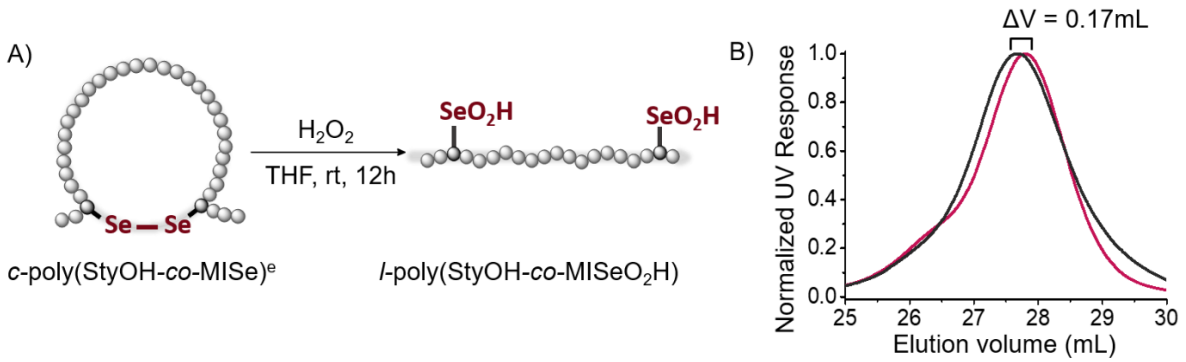

Figure 13. A) Schematic illustration of ring-chain opening induced by oxidation with H_2O_2 in THF at room temperature for 12 h. B) SEC traces of the cyclic polymer *c*-poly(StyOH-*co*-MISe)$_e$ (purple curve) and the resulting linear polymer product *l*-poly(StyOH-*co*-MISeO_2H) (black curve) after oxidation by H_2O_2.

After oxidation, the resulting linear copolymer with pendant selenic acids (*l*-poly(StyOH-*co*-MISeO$_2$H)) was detected at smaller elution volume, indicating a higher hydrodynamic volume and confirming the previous cyclization process ($M_{p,\ app}$ = 13100 for *c*-poly(StyOH-*co*-MISe)$_e$ *vs.* $M_{p,\ app}$ = 14000 for *l*-poly(StyOH-*co*-MISeO$_2$H).

3.1.4. Synthesis of cyclic brush polymers

In the aim to gain insight into the degree of structural control, visualization of the obtained cyclic macromolecules by AFM was targeted. In literature, it has been thoroughly reported that AFM enables direct and effective visualization, at the molecular level, of bottlebrush structures.[16] Bottlebrush polymers composed of poly*(n*-butyl acrylate) poly(*n*BuA) side chains are often exploited to investigate AFM microscopy.[224] Due to strong interactions of poly(*n*BuA) with mica substrates,[16] the polymers are effectively immobilized on the substrate, which facilitates the visualization of single macromolecules. In the present work, the transformation of cyclic polymers into cyclic grafted or brush macromolecules was targeted to enable conformation analysis. The phenolic units composing the cyclic backbone were used to attach poly(*n*-butyl acrylate) side chains. Either the «grafting from» approach or «grafting onto» approach could be exploited to introduce side chains since the polymer backbone was previously formed by sequence-controlled polymerization. «Grafting from» approach is an effective synthetic method for the preparation of bottlebrush polymers due to a reachable high grafting density of side chains on a polymer backbone and the easy purification of the obtained macromolecules. Hence, the use of this synthetic route was firstly chosen for the preparation of folded macromolecules.

3.1.4.1. « Grafting from » approach

The «grafting from» technique enables the preparation of grafted/brush polymers by growing polymer side chains via living/controlled polymerization on a polymeric backbone bearing pendant initiator segments.[225] So far, grafting side chains has been mainly achieved by performing ATRP process initiated by pendant α-bromoester groups on a polymer backbone.[226] ATRP polymerization conducted in the presence of diselenide-containing compounds has not been described in literature. For that reason, an initial investigation has been performed to evaluate the stability of a diselenide group during a radical polymerization process. It has been reported that ATRP polymerization of styrene is successfully conducted by using a difunctional initiator bearing an internal disulfide bridge.[227] This work demonstrated that a disulfide bond was stable during the polymerization and its presence did not interfere with the ATRP process.

This study has been reproduced here as reaction control and has been slightly adapted to investigate likewise the stability of a diselenide bridge during an ATRP polymerization.

- **ATRP polymerization initiated by disulfide-containing initiator**

As model investigation, polymers with internal disulfide bridge in the backbone was firstly performed. For this purpose, a difunctional ATRP initiator bearing an internal disulfide bridge (**1**) was preliminary designed (synthesis described in section 6.3.4). ATRP of styrene was conducted at 90 °C in anisole, by using the catalytic complex CuBr/N,N,N′,N″,N″-pentamethyl diethylenetriamine (PMDETA) and (**1**) as difunctional initiator, with a ratio of [**1**: CuBr: PMDETA: Styrene] = [1: 2: 2: 300] **(Scheme 12)**.[227] The polymerization reached 98% of conversion after 15 h and the polymer was analysed by SEC chromatography ($M_{n,\,app}$ = 48000 and Đ = 1.25). As expected, poly(styrene) containing a disulfide bridge in the middle of the chain, was successfully synthesized with narrow molecular weight distribution and confirmed no interference of the disulfide group in the radical polymerization process.

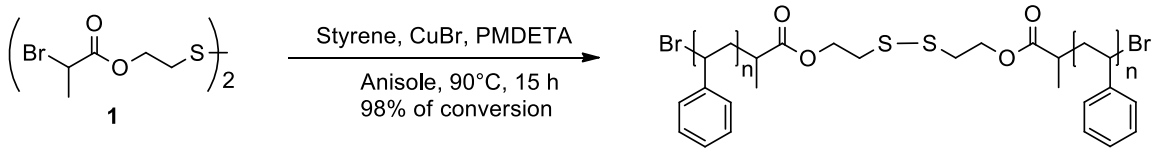

Scheme 12. ATRP polymerization of styrene in anisole at 90 °C initiated by the disulfide-containing initiator (**1**) with the ratio [**1**: CuBr: PMDETA: Styrene] = [1: 2: 2: 300], indicating the stability of disulfide group during ATRP process.

- **ATRP polymerization initiated by diselenide-containing initiator**

Similar synthetic approach was used to investigate the stability of diselenide group. A difunctional initiator bearing an internal diselenide bond has been synthesized over 2 steps (**Scheme 13A**). Elemental selenium was reduced with sodium borohydride ($NaBH_4$) to generate sodium diselenide (Na_2Se_2), which reacted subsequently with bromopropanol. The resulting bis(3-hydroxypropyl) diselenide was esterified by using 2-bromopropionyl bromide in the presence of pyridine to afford bis(3-propyl-2-bromopropanoate) diselenide (**2**) corresponding to the difunctional ATRP initiator bearing an internal diselenide group. ATRP polymerization of styrene was then performed by using the experimental conditions previously described for the polymerization initiated by the disulfide-containing initiator (**Scheme 13B**).The polymerization was conducted for 65 h and was monitored by ^{1}H NMR. However, the monomer conversion reached 5% within 15 h and 55% within 65 h.

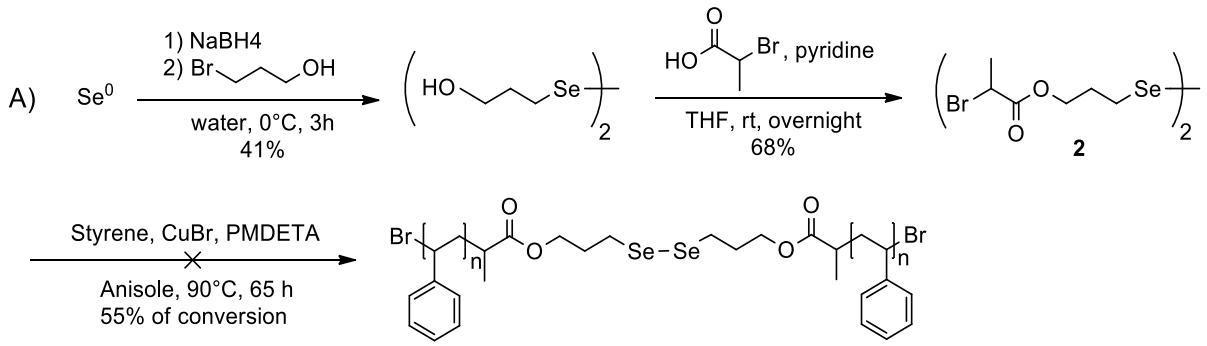

Scheme 13. A) Synthetic route for the preparation of difunctional diselenide-containing initiator (**2**), followed by the ATRP polymerization of styrene in anisole at 90 °C initiated by the diselenide-containing initiator (**2**) with the ratio [**2**: CuBr: PMDETA: Styrene] = [1: 2: 2: 300].

The semilogarithmic plot of monomer conversion *vs.* time, which evolves linearly in the case of controlled polymerizations,[228] showed a nonlinear evolution (**Figure 14A**). This kinetic curve suggested a retardation in the rate of polymerization. Furthermore, SEC chromatogram indicated a bimodal molecular weight distribution ($M_{n,\ app}$ = 58000 and Đ = 1.90) (**Figure 14B**). Both characterizations demonstrated that the polymerization was not controlled, which suggested that the diselenide group seemed to interfere in the polymerization process. It was reasonable to assume that diselenide metathesis was occurring at such high temperature. It has been reported that diselenide metathesis reactions could be observed by heating at 70 °C or higher.[229] Although the mechanism is not well established, it has been evidenced that the metathesis reaction proceeds through a radical mechanism.[229] Herein, diselenide bond could undergo homolytic cleavage while heating the polymerization mixture and result in the formation of free selenyl radicals. Then, the formation of this radical specie could either undergo radical-radical coupling or could further propagate by reaction with styrene monomer. Such metathesis side reaction could potentially explain the retardation in the rate of polymerization and the large molecular weight distribution indicated by the SEC analysis. The ATRP process using the diselenide-containing initiator was further investigated by conducting the polymerization at lower temperature. Since diselenide metathesis reaction barely occurs at 60 °C, the ATRP radical process was tested at 50 °C.[229] ATRP polymerization of *n*-butyl acrylate (*n*BuA) was studied and as control reaction, a polymerization using the common monofunctional initiator methyl bromopropionate (MBrP) was primarily conducted. ATRP of *n*BuA was performed at 50 °C in ethyl methyl ketone, by using CuBr/PMDETA and MBrP with a ratio of [MBrP: CuBr: PMDETA: *n*BuA] = [1: 1: 1: 200] (**Scheme 14A**).

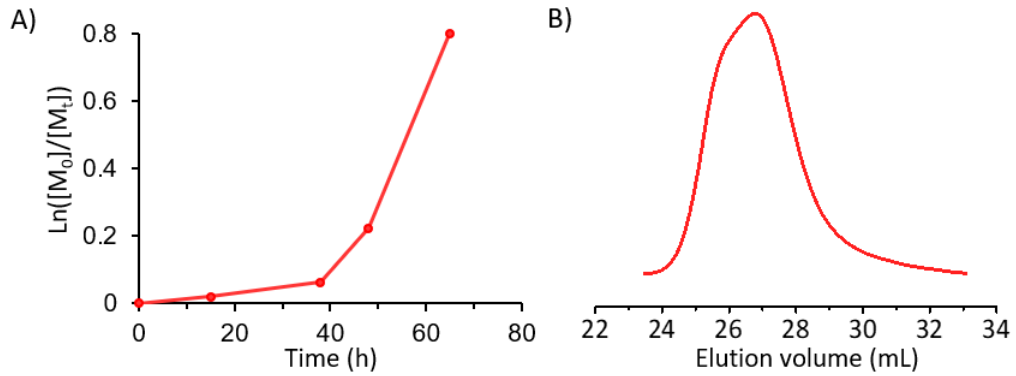

Figure 14. A) Semilogarithmic plot of monomer conversion *vs*. time of the ATRP of styrene initiated by the diselenide-containing initiator (**2**) at 90 °C in anisole. B) SEC trace in THF of the obtained poly(styrene) (UV signal). Both analysis evidenced interference of the diselenide in the ATRP process.

The polymerization reached 87% of monomer conversion within 42 h. Kinetic monitoring of the polymerization by ^{1}H NMR spectroscopy and SEC characterization both evidenced a controlled polymerization process with the obtention of a narrow molecular weight distribution (SEC in THF, $M_{n,\,app}$ = 20000 and Đ = 1.09) (see section 6.3.4). Then, similar polymerization conditions were exploited to investigate ATRP process by using the diselenide-containing initiator (**2**) at low temperature. The polymerization was performed at 50 °C in butanone, by using CuBr/PMDETA and the diselenide-containing initiator (**2**) (**Scheme 14B**). The reaction was conducted for 24 h and was monitored by ^{1}H NMR. Within 3.5 h, the polymerization reached 5% of monomer conversion and stopped afterwards. The semilogarithmic plot of monomer conversion *vs.* time showed a nonlinear evolution, which suggested a decrease of active specie concentration during the polymerization and potentially termination side reactions (**Figure 15**). Moreover, the CuBr/PMDETA catalytic complex turned generally brown when the polymerization proceeds properly.[26]

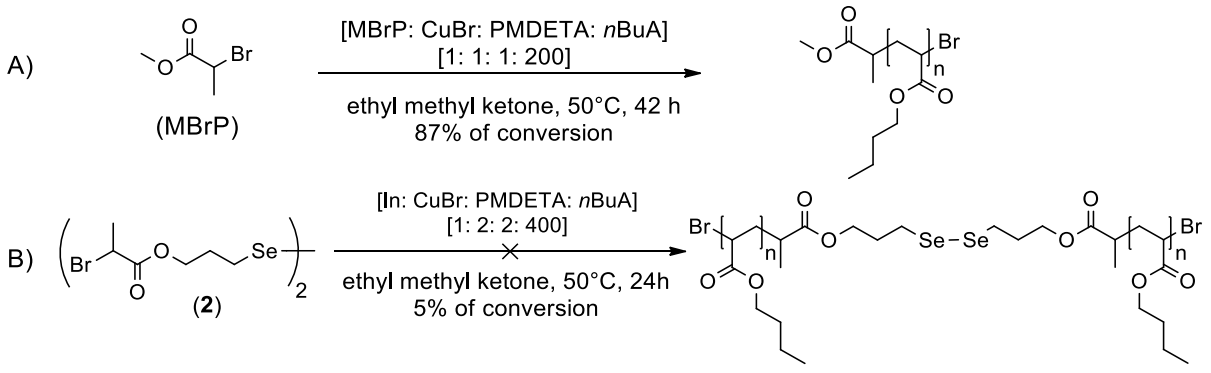

Scheme 14. A) Polymerizations of *n*-butyl acrylate at 50 °C in ethyl methyl ketone by using the CuBr/PMDETA catalytic complex and initiated by: A) methyl bromopropionate. B) the diselenide-containing initiator (**2**).

In the present case, the complex turned brown at the beginning of the ATRP process and latter, turned light green approximatively when the reaction stopped to progress. Also, it seemed that the cuprous compound was not soluble anymore in the mixture. Regarding the mechanism of an ATRP polymerization, the transition metal complex $Cu^{I}Br$/PMDETA catalyses the polymerization via a reversible one-electron redox process between Cu^{I} and Cu^{II}. The coordination of the ligand PMDETA to Cu^{I} increases the solubility of the inorganic salt and influences the redox equilibrium to promote the abstraction of the bromine atom from the dormant species and lead to the formation of active growing chains.[26,230] Due to the observed insolubility of the cuprous compound, it seems reasonable to hypothesize that the catalytic complex could be deactivated during the course of the polymerization and thus could stop the reaction. The copper metal could be coordinated with diselenide groups which could affect the redox equilibrium of the complex CuBr/PMDETA and result in an inhibition of the catalyst function.[159] This coordination could push the equilibrium to the deactivated chain species and thus inhibit the reaction.

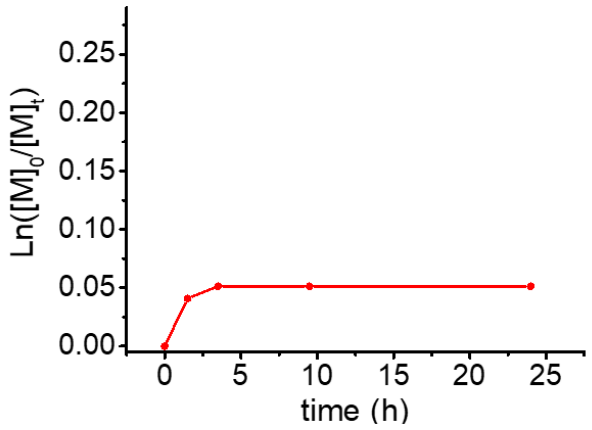

Figure 15. Semilogarithmic plot of monomer conversion *vs*. time for the ATRP polymerization of *n*-butyl acrylate initiated by diselenide-containing initiator (**2**) at 50 °C, revealing interference of the diselenide with the radical process at low temperature.

This experimental study demonstrated that an ATRP polymerization cannot be conducted on diselenide-containing polymers. Therefore, the use of the «grafting from» synthetic approach toward the transformation of cyclic polymers via diselenide bridge into folded brush macromolecules seemed to be incompatible. Other controlled radical polymerizations could be exploited to grow polymer side chains on the backbone, such as NMP and RAFT radical controlled polymerizations. However, NMP process requires high temperatures and would lead to diselenide group cleavage by metathesis reaction. RAFT polymerization involves the use of dithio compounds, which could potentially react with diselenide groups. Hence, it appeared that the «grafting from» synthetic approach was

generally not suitable for the current synthesis and the «grafting onto» approach was thus investigated.

3.1.4.2. « Grafting onto » approach

In the «grafting onto» method, the polymer backbone and the polymer side chains are synthesized independently. To graft side chains on the polymer backbone, efficient coupling reactions are performed between pendant functional groups of the backbone and reactive end-functional groups of side chains.[225] The main advantage of this synthetic strategy is that both the polymer backbone and the side chains can be prepared without affecting the synthesis of each other and by using different living/controlled polymerization techniques. However, the grafting density (GD) of bottlebrush macromolecules prepared with the «grafting onto» strategy is often limited for both kinetic and thermodynamic reasons.[226] Regarding the entropy, the free side chains adopt a random coil conformation in solution while once attached, the grafts adopt a more stretched and extended structure mainly due to steric hindrance.[225] For this reason, a high grafting density is not entropically favoured. Regarding the kinetic during the course of the coupling reaction, the diffusion of free unreacted polymer side chains to reactive pendant groups located on the backbone slows down due to an increasing steric congestion.[226] Structural parameters such as the chemical structure and length of side chains, are influencing the polymer-polymer coupling reaction. As expectable, when the linear side polymer chains have a bulky structure and/or high molecular weight, the steric hindrance and chain-end group concentration effect decrease the grafting efficiency and limit the achievable grafting densities.[231] Generally, the use of highly efficient and fast coupling reactions can promote the grafting process. Click reactions have been widely exploited for the preparation of brush polymers, such as Diels−Alder cycloaddition,[232] atom transfer nitroxide radical coupling chemistry,[233,234] thiol−expoxy,[235] and thiol−ene.[236,237] To date, the preparation of bottlebrush polymers *via* the «grafting onto» method exploiting either azide/alkyne cycloaddition[231] or Triazolinedione (TAD)−diene Diels Alder (DA)[238] reactions, are the most efficient synthetic strategies. In fact, the use of TAD−diene cycloaddition allowed to attach side chain polymers on the polymer backbone in nearly quantitative yields with a grafting densities above 90%.[238] In the present study, it has been previously discussed that copper catalyst could be potentially coordinated by diselenide groups (see section 3.1.4.1). Consequently, the use of copper-catalysed azide−alkyne cycloaddition, as coupling reaction, was not chosen for the preparation of folded brush polymers *via* the «grafting onto» method. The efficient triazolinedione−diene

Diels Alder reaction was selected. Some prior experimental studies were performed in order to verify the potential success of this synthetic strategy.

- **Chemical stability of diselenide during Triazolinedione–Diene click reaction**

TAD-Diene cycloaddition has not been reported on diselenide-containing compounds. For that reason, a short study has been investigated to verify the chemical stability of the diselenide group while a TAD-Diene Diels-Alder (DA) cycloaddition was performed. First, a conjugated diene compound bearing a diselenide group was synthesized by a three-step procedure (**Scheme 15**). Succinic anhydride was esterified with 2,4-hexadien-1-ol (HDEO) to afford 2,4-hexadien-1-yl succinic acid monoester (**3**). Elemental selenium was reduced with sodium borohydride ($NaBH_4$) to generate sodium diselenide (Na_2Se_2), which reacted subsequently in one pot with 2-bromopropanol. The resulting bis(3-hydroxypropyl) diselenide was esterified with 2,4-hexadien-1-yl succinic acid monoester (**3**) in the presence of the coupling reagent *N,N′*-dicyclohexylcarbodiimide (DCC) and 4-dimethyl aminopyridine to result in bis(2,4-hexadien-3-propyl succinic diester) diselenide (**4**). The TAD-diene Diels-Alder (DA) cycloaddition was then investigated by using the commercially available 4-phenyl-1,2,4-triazole-3,5-dione (2.1 equiv) with the diene compounds (**4**) (1.0 equiv). The reaction was conducted at room temperature for 30 min to afford the DA adduct (**5**) (**Scheme 15**).

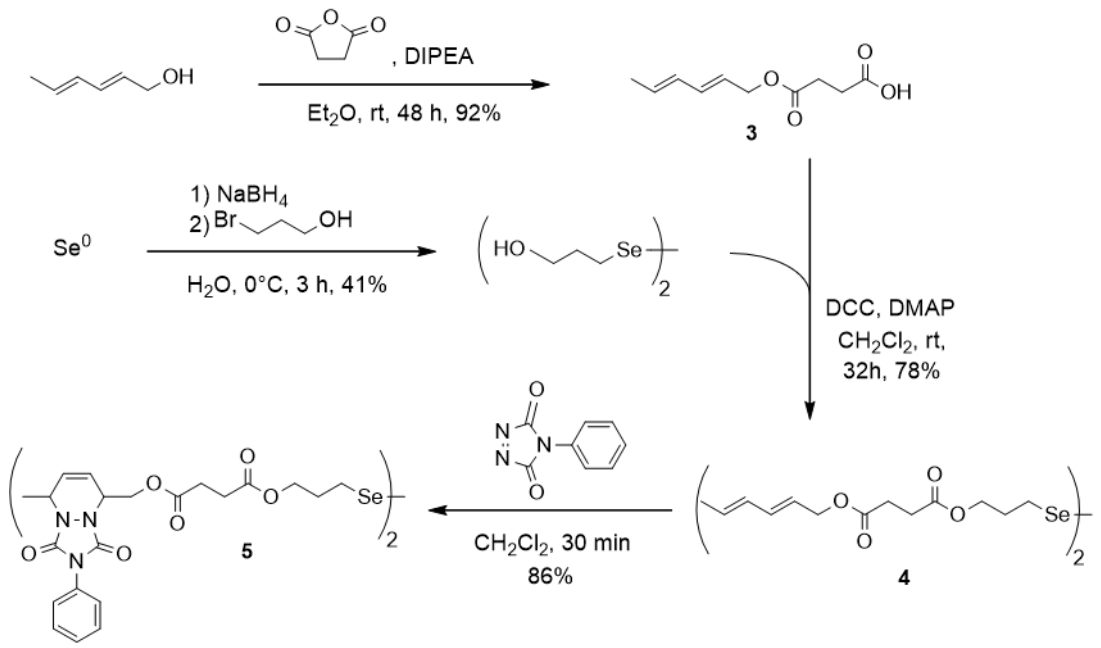

Scheme 15. Synthetic route for the investigation of TAD-diene click reaction on a diselenide-containing compound model.

The resulting mixture was analysed by UPLC-MS, ^{13}C and ^{1}H NMR analysis, all of which revealed that the reaction was nearly quantitative and the diselenide group was unchanged after the cycloaddition. This orthogonality study demonstrated the chemical stability of a diselenide group during a TAD-diene cycloaddition. Hence, this TAD-Diene click reaction could be potentially exploited as coupling reaction for the preparation of folded brush macromolecules *via* the «grafting onto» method.

- **Synthesis of linear bottlebrush polymer via « grafting onto approach »**

The metal-free « grafting onto » method exploiting TAD-diene cycloaddition has been reported for the synthesis of bottlebrush macromolecules composed of a poly(acrylate) backbone and various side chain polymers such as poly(methyl acrylate), poly(*tert*-butyl acrylate), and poly(styrene).[238] Herein, brush polymers composed of styrenic backbone and *n*-butyl acrylate side chains were targeted. Poly(*n*-butyl acrylate) are moderately bulky side chains, that could decrease the diffusion of unreactive free side chains to the backbone pendant groups and result in a limited grafting density. Therefore, the synthesis of linear bottlebrush polymer composed of a poly(4-hydroxystyrene) backbone and poly(*n*BuA) side chains was performed to verify that a high grafting density could be reached for this brush chemical structure. In this synthetic strategy, a phenolic backbone was chosen to enable the introduction of conjugated diene moieties on the backbone via post-modification of the hydroxyl group. Separately, TAD-terminated poly(*n*BuA) side chains precursors were synthesized by using controlled radical polymerization.

A poly(4-hydroxystyrene) homopolymer chain was prepared by NMP polymerization of 4-*tert*-butoxystyrene, followed by a deprotection step to remove *tert*-butyl groups (**Scheme 16**). The polymerization of StyO*t*Bu was conducted at 115 °C in anisole initiated by Blocbuilder MA with the ratio [BB: StyO*t*Bu] = [1: 900].

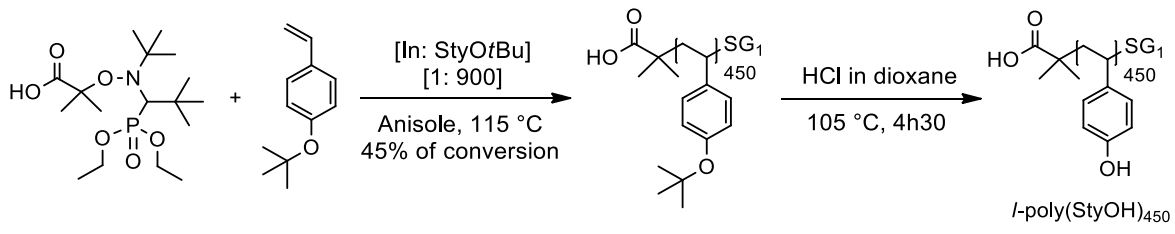

Scheme 16. NMP polymerization of 4-*tert*-butoxystyrene initiated by Blocbuilder MA, followed by the removal of *tert*-butyl groups for the preparation of linear poly(4-hydroxystyrene).

Aliquots were taken during the polymerization to monitor the radical process by ^{1}H NMR and SEC analysis. Both semilogarithmic plot of monomer conversion *vs.* time and plot of experimental M_n *vs.* monomer conversion indicated a controlled polymerization process (**Figure 16**). The isolated homopolymer poly(StyO*t*Bu)$_{450}$ was analysed by SEC analysis (DP_n = 450, $M_{n,\,app}$ = 77000 and Đ = 1.29, see section 6.3.8) and ^{1}H NMR. The following step involved the removal of *tert*-butyl groups present at the poly(4-hydroyxstyrene) backbone. The deprotection was achieved by hydrolysis with hydrochloric acid (HCl) in dioxane at 105 °C and afforded the deprotected linear precursor (*l*-poly(StyOH)$_{450}$). Quantitative deprotection was confirmed by ^{1}H NMR (see section 6.4, **Figure 79**) and SEC analysis indicated a clean polymer modification reaction ($M_{n,\,app}$ = 85000 and Đ = 1.23, see section 6.3.8).

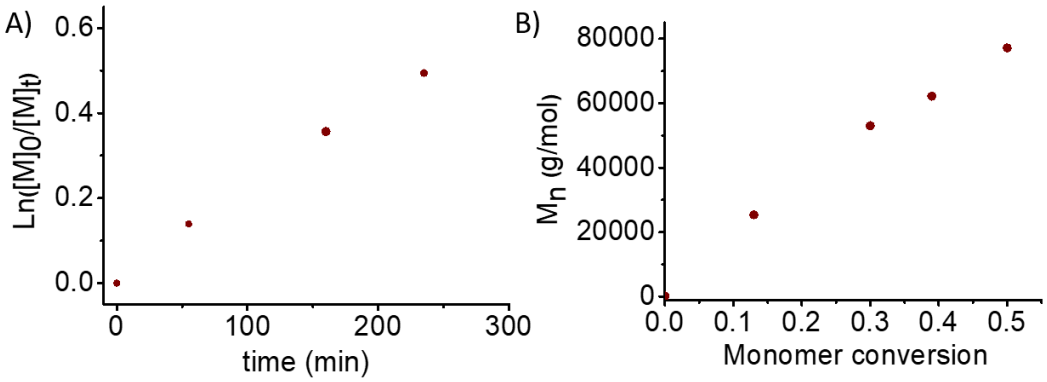

Figure 16. A) Semilogarithmic plot of monomer conversion *vs.* time of the homopolymerization of 4-*tert*-butoxystyrene. B) Plots of experimental M_n *vs.* monomer conversion for the same experiment. Both polymerization characteristics indicated a controlled NMP process.

The pendant phenol groups were esterified to introduce conjugated diene moieties on the backbone which are necessary for the TAD−diene coupling reaction toward the brush polymer synthesis. For this purpose, a symmetric anhydride of 2,4-hexadien-1-yl succinic acid monoester was synthesized in a two-step procedure (see section 6.3.5). Then, the hydroxyl functionalities of the linear poly(4-hydroxystyrene) precursor were esterified by treatment with the symmetric anhydride in the presence of DMAP to yield the poly(styrene) backbone bearing conjugated diene segments (*l*-poly(Sty-diene)$_{450}$, **Scheme 17**). The resulting polymer was characterized by ^{1}H NMR and SEC analysis. The ^{1}H NMR spectrum showed the appearance of a series of new resonances (from 5.60 to 6.30 ppm) corresponding to the introduced conjugated diene side groups (see section 6.4, **Figure 80**). SEC characterization demonstrated a shift to higher molecular weight region compared to the phenolic backbone precursor and indicated $M_{n,\,app}$ = 92000 with Đ = 1.24 (SEC trace in **Figure 17**).

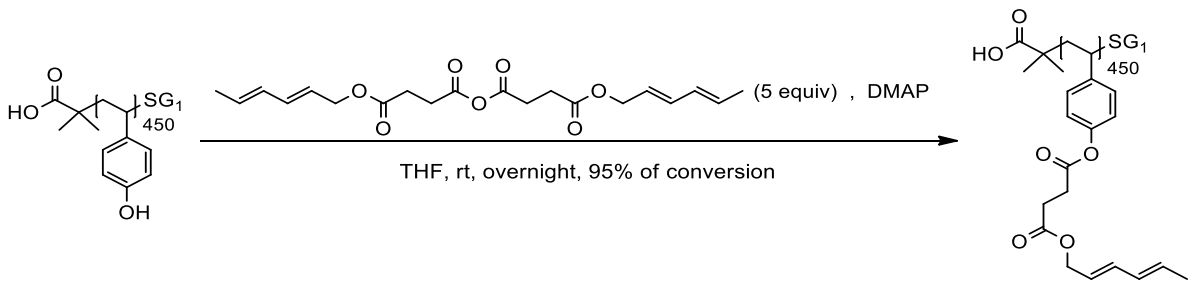

Scheme 17. Esterification of poly(4-hydroxystyrene) with the symmetric anhydride of 2,4-hexadien-1-yl succinic acid monoester in presence of DMAP to introduce conjugated diene groups on the polymer backbone.

Separately, poly(*n*-butyl acrylate) homopolymer containing a clickable TAD end group was synthesized by controlled radical polymerization. The synthesis was previously described by Du Prez et al. and was prepared as reported.[239] First, an urazole-containing initiator (**6**) was synthesized in a four-step procedure for Cu-mediated radical polymerization (synthesis in section 6.3.7). Then, *n*-butyl acrylate polymerization was performed in dimethylformamide at 25°C by using the complex $CuBr_2$/Me_6TREN, the urazole-containing initiator and Cu^0 with the following ratio [In: *n*BuA: $CuBr_2$: Me_6TREN]=[1: 80: 0.5: 0.15] (**Scheme 18A**). The polymerization afforded the formation of poly(*n*-butyl acrylate) polymer chains containing an urazole end-group (Ur-poly(*n*BuA)$_{60}$), with a degree of polymerization of 60 units. The urazole end-group was then converted into TAD moiety to afford TAD-terminated poly(*n*BuA) side chains. Several reactions have been reported in literature for the oxidation of urazole group into its corresponding TAD group, such as nitrogen oxide-based, halogen-mediated and electrochemical oxidations.[240] In the present work, subsequent heterogeneous oxidation of the urazole-terminated polymer chains was achieved by halogen-mediated reaction with the use of a tetrameric complex of 1,4-diazabicyclo[2.2.2]octane with bromine (DABCO-Br) **(Scheme 18B**).[239] The oxidation was conducted in dry dichloromethane under inert atmosphere for 3 h, leading to the formation of a brightly coloured TAD end-functionalized polymers (TAD-poly(*n*BuA)$_{60}$). The advantage of using the complex DABCO-Br is the easy and simple purification of the resulting TAD-terminated polymers by filtration. The highly reactive azo compounds TAD-poly(*n*BuA)$_{60}$, was directly used without any further purification step.

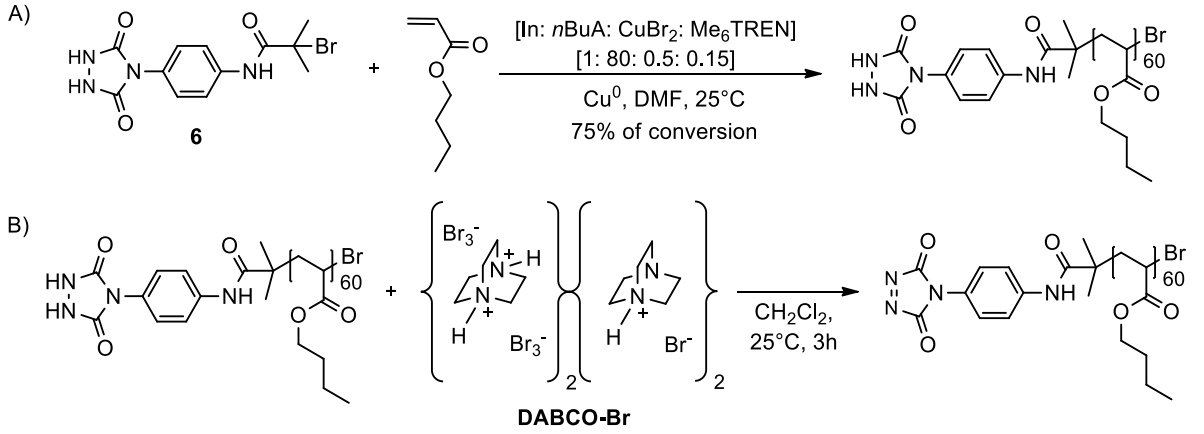

Scheme 18. A) Cu^0-mediated radical polymerization of *n*-butyl acrylate initiated by the urazole-containing initiator for the preparation of urazole-terminated poly(*n*-butyl acrylate) chains. B) Oxidation of urazole-terminated poly(*n*-butyl acrylate) chains into the corresponding TAD-terminated poly(*n*-butyl acrylate) by the DABCO-Br complex.

Linear bottlebrush polymers were synthesized by grafting TAD-end group polymer side chains TAD-poly(nBuA)$_{60}$ onto the diene-functionalized poly(styrene) backbone by performing TAD-Diene Diel-Alder cycloaddition. According to the literature, a slight excess (1.1 equiv) of TAD-terminated side chains was required to reach nearly quantitative grafting density.[238] Furthermore, reactions were conducted in concentrated conditions to force more the diffusion of free TAD-side chains toward the pendant conjugated diene groups of the backbone. In a first attempt, a molar ratio of 1.1/1 (TAD/diene groups of poly(Sty-diene)$_{450}$) was used and the coupling reaction was conducted in dry dichloromethane under inert atmosphere for 14 h. The resulting mixture was characterized by ^{1}H NMR and SEC analysis (**Table 2**, *l*-poly(Sty)$_{450}$-*g*-[poly(nBuA)$_{60}$]$^{0.7}$). SEC characterization of the crude polymer clearly demonstrated a shift to smaller elution volume, indicating that the molecular weight increased. ^{1}H NMR showed that the signals corresponding to the diene group significantly decreased and new signals appeared at 5.85 and 5.73 ppm, corresponding to the formed alkene protons (see section 6.4, **Figure 81**). The grafting density (GD) was calculated from proton NMR and resulted in only 70% of attached poly(nBuA)$_{60}$ side chains onto the polymer backbone poly(Sty-diene)$_{450}$. It must be noticed that two aliquot samples were taken after 14 h and 24 h of reaction. The reaction did not progress over time between the two taken samples, meaning that the grafting process was over. As expected, the steric load and the osmotic pressure restricted the incorporation of linear chains into the grafted copolymers and reduced the achievable GD. Thus, to ensure a high GD, TAD-poly(nBuA)$_{60}$ was used in excess over diene groups with a

molar ratio of 2.0/1 (**Table 2**, *l*-poly(Sty)$_{450}$-*g*-[poly(*n*BuA)$_{60}$]$^{1.0}$). The grafting density of the obtained brush polymer was determined by ^{1}H NMR spectroscopy.

Table 2. Reaction Conditions of molecular linear bottlebrush polymers synthesis and characterization.

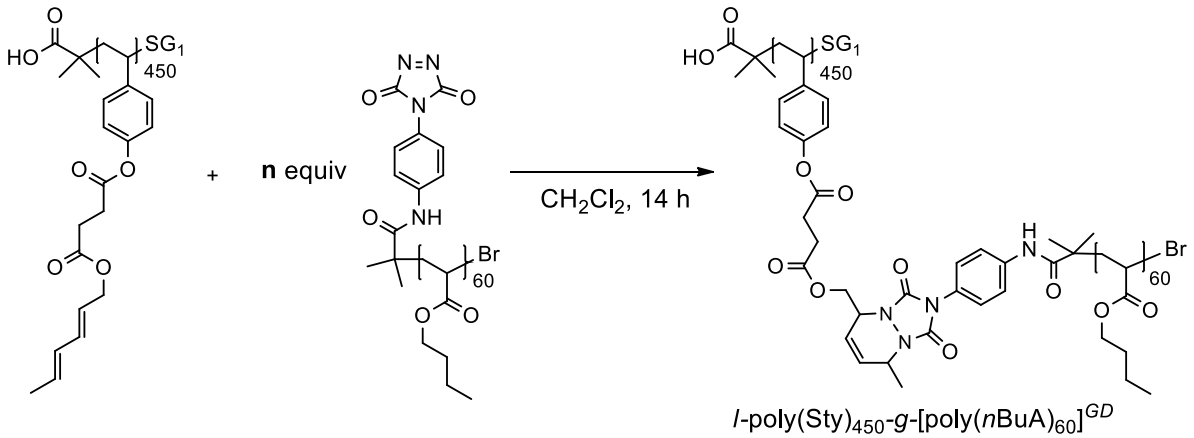

Brush polymers	Grafting onto: molar ratio TAD/diene [a]	GD [b] (%)	M_n [c] (g/mol)	$M_{n,sec}$ [d] (g/mol)	Đ [d]
***l*-poly(Sty)$_{450}$-*g*-[poly(*n*BuA)$_{60}$]$^{0.7}$**	1.1/1	70	1.8×10^6	440000	1.4
***l*-poly(Sty)$_{450}$-*g*-[poly(*n*BuA)$_{60}$]$^{1.0}$**	2.0/1	100	2.6×10^6	415000	1.3

[a] Coupling reaction of poly(Sty-diene)$_{450}$ with TAD-poly(*n*BuA)$_{60}$ in CH_2Cl_2 for 14 h at room temperature. [b] GD calculated from ^{1}H NMR in $CDCl_3$. by using the equation GD = (1 – [Diene]$_t$ /[Diene]$_{initial}$) × 100. [c] Calculated from ^{1}H NMR analysis by using the equation $M_n = M_n$ (poly(Sty-diene)$_{450}$) + $GD_{NMR} \times DP_{Backbone} \times$ Mn (poly(*n*BuA)$_{60}$). [d] Determined by SEC in DMAc based on polystyrene calibration.

The grafting process resulted in approximatively 100% of GD since the peaks corresponding to the diene resonance had disappeared and the signal attributed to the formed alkene appeared at 5.89 and 5.79 ppm (see section 6.4, **Figure 82**). The SEC curve showed a monomodal peak shape and rather narrow molecular weight distribution was preserved in the obtained bottlebrush polymer (**Figure 17**). In both resulting brush polymers, a small amount of free side chains was not attached to the polystyrene backbone and could not be successfully removed after purification by precipitation. It must be mentioned that the aim of this synthetic strategy was to allow the visualization of single chain morphology by AFM. The obtained crude polymers were not purified, in order to analyse by AFM, the overall samples and evaluate the visualization of bottlebrush polymers even in the presence of free side chains.

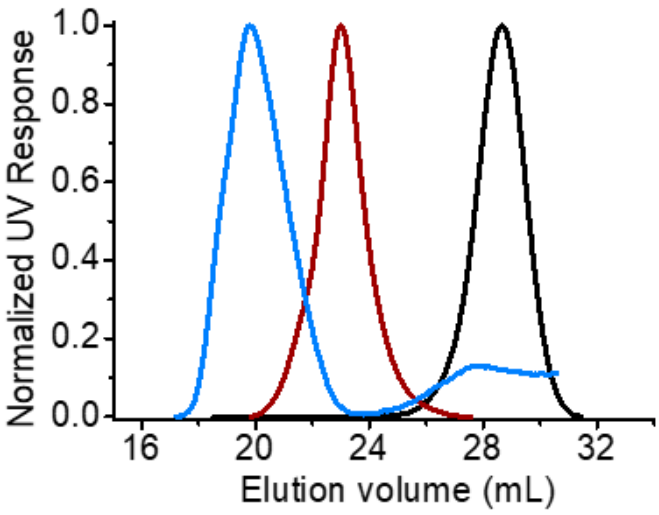

Figure 17. SEC traces of free TAD-poly(nBuA)$_{60}$ side chain (black curve), macroinitiator poly(Sty-diene)$_{450}$ (red curve) and the resulting bottlebrush polymer *l*-poly(Sty)$_{450}$-*g*-[poly(nBuA)$_{60}$]$^{1.0}$ (blue curve).

AFM microscopy was used to characterize the molecular morphology of the resulting bottlebrush polymer *l*-poly(Sty)$_{450}$-*g*-[poly(nBuA)$_{60}$]$^{1.0}$. For AFM studies, the sample was prepared by spin-coating a dilute solution of crude polymer in chloroform (ca. 0.01 mg/mL) on a freshly cleaved mica substrate to obtain a monomolecular film.

Figure 18 shows the obtained height and amplitude images. In both micrographs, bottlebrush polymers were clearly observed and exhibited worm-like molecular morphologies. Indeed, due to steric hinderance of the attached side chains, bottlebrush polymers typically do not exhibit a random coil morphology but rather have a high tendency to adapt an extended chain structure such as worm-like morphology.[16] To further demonstrate the successful preparation of bottlebrush macromolecules, the backbone contraction was evaluated. Statistical molecular dimensions were determined by direct measurement of a significant ensemble of fifty bottlebrush macromolecules from the AFM micrograph. The average contour length, width and height were estimated in the range of 104.2 ± 30 nm, 25.1 ± 5 nm, and 0.8 ± 0.1 nm, respectively. This experimental average length meet the range of the maximal length l_{max} = 108 nm estimated for a polymer backbone of DP_n = 450 with fully extended all-trans repeated unit bond conformation ($l_{unit,\ max}$ = 0.24 nm). Thus, it appeared that the bottlebrush morphology was nearly exhibiting a fully extended conformation (104.2 *vs* 108 nm), which indirectly suggested the high grafting density of poly(*n*-butyl acrylate) side chains on the styrenic backbone.

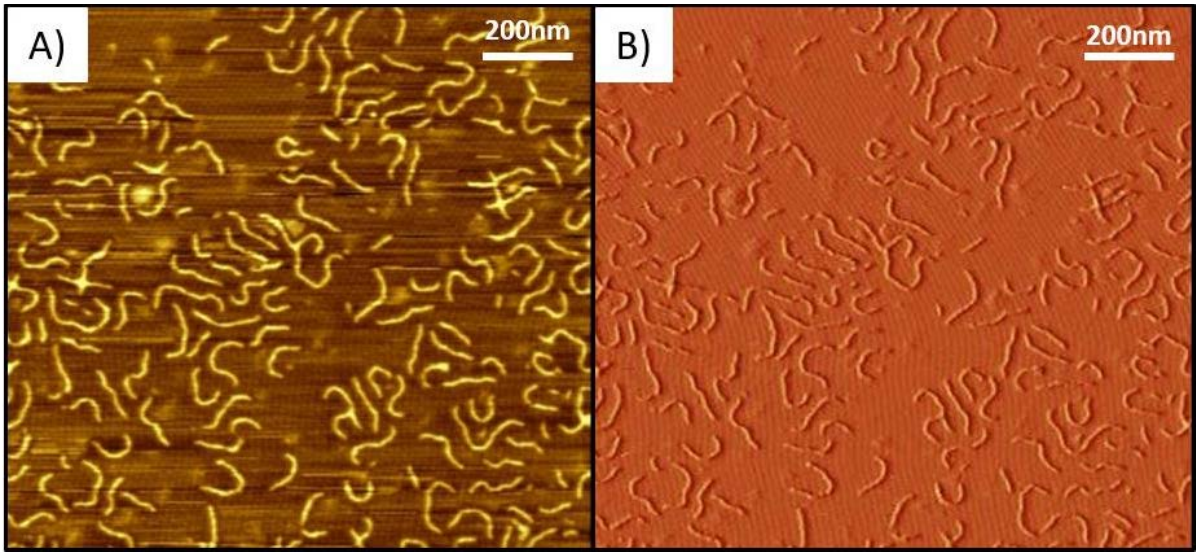

Figure 18. AFM micrographs of the linear bottlebrush polymer *l*-poly(Sty)$_{450}$-*g*-[poly(*n*BuA)$_{60}$]$^{1.0}$. A) Height image. B) Amplitude image.

Linear bottlebrush polymers composed of a poly(styrene) backbone and poly(*n*-butyl acrylate) side chains were successfully synthesized by using the « grafting onto » approach. High grafting densities of side chains on the polymer backbone were achieved by exploiting the efficient TAD-diene cycloaddition as coupling reaction. In the previous section, it has been evidenced that TAD-diene cycloaddition does not interfere with diselenide groups. Therefore, this « grafting onto » synthetic strategy seemed to be a promising pathway to transform cyclic polymers (previously cyclized by intramolecular diselenide bridge), into cyclic brush polymers.

3.1.4.3. Synthesis of cyclic brush polymers

Previously, cyclic macromolecules have been synthesized by generating an intramolecular crosslink via a diselenide bridge formation (see section 3.1.3.1). In the aim to allow direct visualization by AFM of the resulting single chain compaction, cyclic macromolecules were transformed into cyclic brush polymers. The « grafting onto » approach was used by exploiting triazolinedione (TAD)−diene cycloaddition click reaction to graft poly(*n*-butyl acrylate) side chain polymers on the cyclic poly(4-hydroxystyrene) backbone. The synthetic route described in the previous section for the preparation of linear bottlebrush polymers was similarly reproduced for the synthesis of cyclic brush polymers. Herein, a set of brush polymers with different grafting densities (GD) was synthesized to study the potential visualization by AFM of folded single polymer chains. The cyclic polymer *c*-poly(StyOH-*co*-MISe)$_e$ was taken as polymer precursor. Conjugated diene segments were introduced on the cyclic polymer by esterification of the 4-hydroxystyrene repeated units with the symmetric

anhydride of 2,4-hexadien-1-yl succinic acid monoester to afford a cyclic poly(styrene) backbone with pendant diene groups (*c*-poly(Sty-diene-*co*-MISe), **Scheme 19**). The ^{1}H NMR spectrum of the resulting polymer showed the appearance of a series of new signals (from 5.61 to 6.24 ppm) corresponding to the attached diene groups on the polymer backbone and proved a nearly quantitative reaction with 99% of conversion (See section 6.4, **Figure 85**). SEC characterization demonstrated a shift to higher molecular weight region compared to the cyclic polymer precursor and suggested a clean polymer modification reaction ($M_{n,\,app}$ = 14400 and Đ = 1.22, SEC trace in **Figure 19**). TAD-terminated poly(*n*-butyl acrylate) synthesis was previously described and was prepared as reported[239] (See section 3.1.4.2). Well-defined urazole-terminated side chain precursors with DP_n = 40, were successfully synthesized and characterized by ^{1}H NMR and SEC in THF (Ur-poly(*n*BuA)$_{40}$, $M_{n,\,app}$ = 5500, Đ = 1.20). Subsequently, the urazole-terminated polymer was oxidized by using the complex DABCO-Bromide (DABCO-Br) and lead to the corresponding TAD-terminated polymers TAD-poly(*n*BuA)$_{40}$.

After the preparation of *c*-poly(Sty-diene-*co*-MISe) and TAD-poly(*n*BuA)$_{40}$, cyclic grafted/brush polymers were obtained by performing TAD-Diene ultrafast Diels-Alder cycloaddition as coupling reaction (**Scheme 19**). A set of folded grafted polymers was prepared and summarized in **Table 3**. With this approach, the side chain grafting density (GD) on the polymer backbone could be adjusted with the molar ratio of TAD groups to diene groups and characterized by ^{1}H NMR spectroscopy. The coupling reaction was performed in dry dichloromethane at room temperature for 14 h. When a ratio of 0.7/1.0 (TAD/diene groups of *c*-poly(Sty-diene-*co*-MISe)) was used, the grafting density reached 27% (**Table 3**, *c*-poly(Sty)$_{50}$-*g*-[poly(*n*BuA)$_{40}$]$^{0.27}$). The use of TAD-poly(*n*BuA)$_{40}$ with a ratio of 1.0/1.0 resulted in 65% of grafted side chains (**Table 3**, *c*-poly(Sty)$_{50}$-*g*-[poly(*n*BuA)$_{40}$]$^{0.65}$). In both cases, ^{1}H NMR spectroscopy indicated that the intensity of signals corresponding to the conjugated diene resonances significantly decreased and new signals appeared at 5.87 and 5.78 ppm, which correspond to the formed alkene protons after TAD-diene cycloaddition (see section 6.4, **Figure 86** and **Figure 87**). A significant amount of free side chains was not attached to the polystyrene backbone, which is consistent with the observations described previously for the preparation of linear bottlebrush polymers (section 3.1.4.2). Although the cycloaddition proved to proceed fast and to reach high yields, the steric load and the diffusion of free side chains to pendant diene groups of the polymer backbone reduced, in the present case, both ligation rates and achievable conversions. Finally, to ensure a high grafting density, a large excess of TAD-poly(*n*BuA)$_{40}$ over diene groups with a molar ratio of 2.0/1.0. The

coupling reaction resulted in the formation of brush polymers with a GD of approximatively 100% (**Table 3**, *c*-poly(Sty)$_{50}$-*g*-[poly(*n*BuA)$_{40}$]$^{1.0}$). In this case, ^{1}H NMR spectroscopy showed that the peaks corresponding to conjugated diene resonances had fully disappeared and the resonances related to the formed alkene appeared at 5.83 and 5.74 ppm (see section 6.4, **Figure 88**).

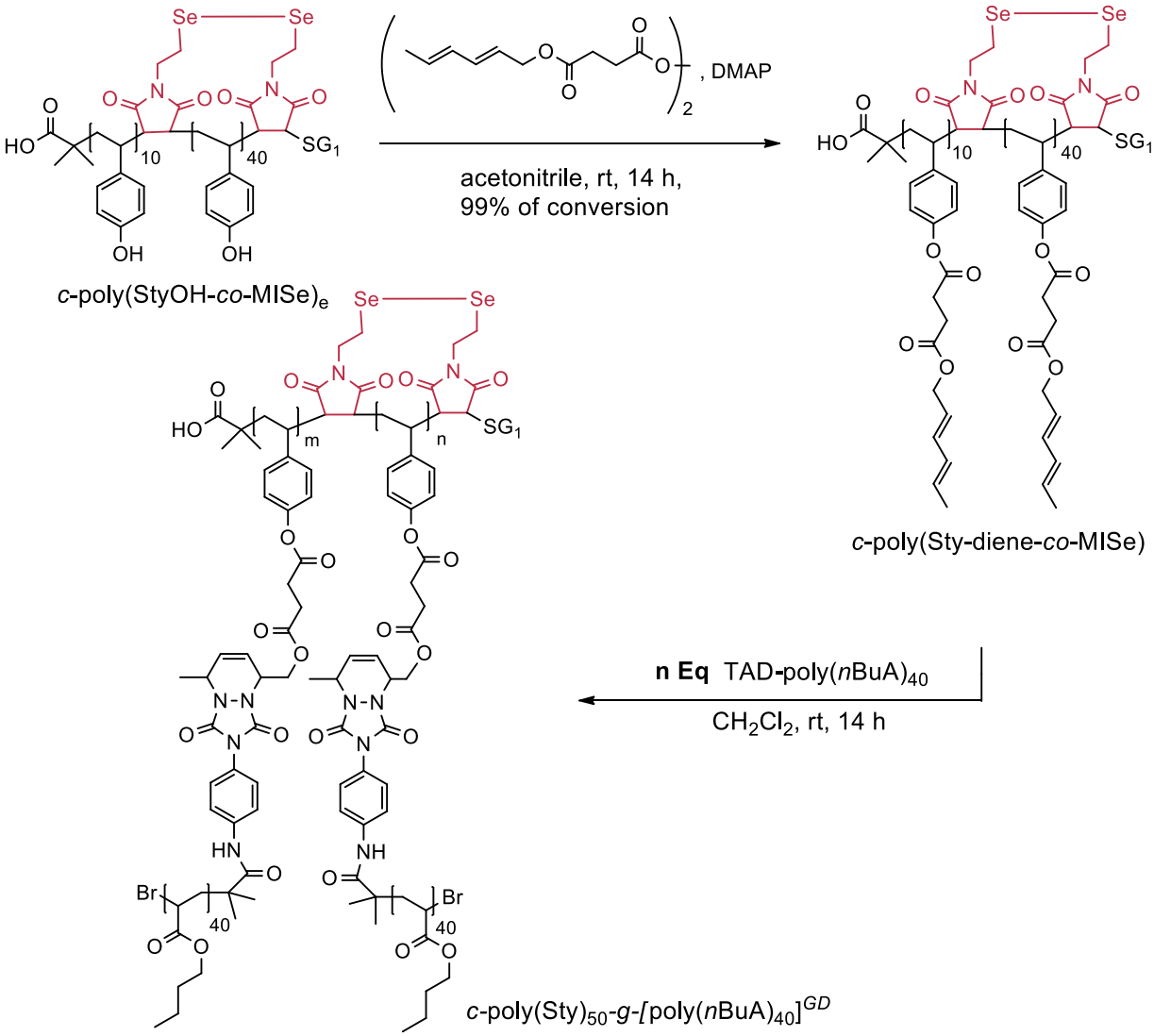

Scheme 19. Synthetic route toward grafted/brush polymers by using the « grafting onto » approach.

In the crude mixture of all grafting onto reactions, a significant amount of unreacted TAD-poly(*n*BuA)$_{40}$ could be found not attached to the backbone polymer. Especially in the case of the brush polymer with a GD of 100%, a larger excess of side chains was used, and a significant amount of unreacted side chains remained after purification by precipitation. The resulting brush polymer (GD= 100%) had to be further purified by standard analytical SEC set

up to isolate the cyclic brush polymers from free unreacted side chains (see section 6.3.9). The set of cyclic grafted/brush polymers was characterized by SEC in THF. **Figure 19** provides the SEC traces corresponding to the crude grafted polymers *c*-poly(Sty)$_{50}$-*g*-[poly(*n*BuA)$_{40}$]$^{0.27}$ (blue curve), the crude *c*-poly(Sty)$_{50}$-*g*-[poly(*n*BuA)$_{40}$]$^{0.65}$ (green curve) and the purified *c*-poly(Sty)$_{50}$-*g*-[poly(*n*BuA)$_{40}$]$^{1.0}$ (black curve). SEC elugrams showed a clear shift to higher apparent molecular weight region compared to the cyclic polymer precursor *c*-poly(Sty-diene-*co*-MISe). Moreover, all brush polymers (crude or purified) indicated dispersities between 1.03 and 1.10, suggesting that the synthesis proceeds in a controlled manner and confirming the tolerance of diselenide intramolecular crosslink with the coupling reaction.

Table 3. Reaction conditions of folded grafted/brush polymers synthesis and characterization.

Entry	Grafting: molar ratio TAD/diene[a]	GD_{NMR}[b] (%)	$M_{n,\,NMR}$[c] (g/mol)	$M_{n,SEC}$[d] (g/mol)	Đ[d]
***c*-poly(Sty)$_{50}$-*g*-[poly(*n*BuA)$_{40}$]$^{0.27}$**	0.7/1.0	27	86000	58000	1.08
***c*-poly(Sty)$_{50}$-*g*-[poly(*n*BuA)$_{40}$]$^{0.65}$**	1.0/1.0	65	182000	78000	1.06
***c*-poly(Sty)$_{50}$-*g*-[poly(*n*BuA)$_{40}$]$^{1.0}$**	2.0/1.0	100	280000	89000	1.03

[a] Coupling reaction of *c*-poly(Sty-diene-*co*-MISe) with TAD-poly(*n*BuA)$_{40}$ in DCM for 14 h at room temperature. [b] ^{1}H NMR spectroscopy in $CDCl_3$. GD_{NMR} calculated by using the equation $GD_{NMR} = (1 - [Diene]_t / [Diene]_{initial}) \times 100$. [c] Calculated from ^{1}H NMR spectroscopy by using the equation $M_{n,\,NMR} = M_n$ (*c*-poly(Sty-diene-*co*-MISe)) + $GD_{NMR} \times DP_{Backbone} \times M_n$ (poly(*n*BuA)$_{40}$). [d] Determined by SEC in THF, based on polystyrene calibration.

As a control sample for AFM studies, a linear brush analogue was synthesized by using the non-cyclized poly(4-hydroxystyrene) precursor *l*-poly(StyOH-*co*-MISeMob) and following the same synthetic strategy than the cyclic brush polymers. A linear backbone with pendant diene groups was prepared (*l*-poly(Sty-diene-*co*-MISeMob)$_{50}$, see section 6.4, **Figure 83**). Subsequent grafting reaction of TAD-poly(*n*BuA)$_{40}$ via TAD-diene cycloaddition by using a molar ratio of 1.0/1.0 (TAD to diene groups) resulted in the linear, not folded molecular brush analogue with a medium GD of 43% (*l*-poly(Sty)$_{50}$-*g*-[poly(*n*BuA)$_{40}$]$^{0.43}$, synthesis in section 6.3.8 and ^{1}NMR spectrum in **Figure 84**).

It must be noted that, the use of a molar ratio of 1.0/1.0 (TAD-diene groups) afforded a cyclic brush polymer with 65% GD, while the GD of the linear bottlebrush polymer analogue

resulted in only 43%. It is reasonable to assume that the « grafting onto » approach is not the most straightforward method toward bottlebrush polymer synthesis.

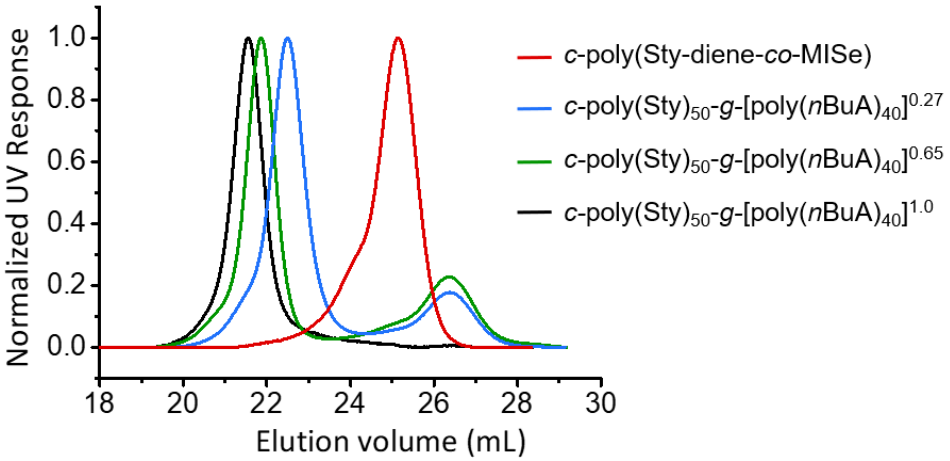

Figure 19. SEC traces of the macroinitiator *c*-poly(Sty-diene-*co*-MISe) (red curve) and the resulting brush polymers: crude *c*-poly(Sty)$_{50}$-*g*-[poly(*n*BuA)$_{40}$]$^{0.27}$ (blue curve), crude *c*-poly(Sty)$_{50}$-*g*-[poly(*n*BuA)$_{40}$]$^{0.65}$ (green curve) and purified *c*-poly(Sty)$_{50}$-*g*-[poly(*n*BuA)$_{40}$]$^{1.0}$ (black curve).

Indeed, the grafting process is sensitive to various experimental parameters such as local GD, accessibility of functionalities to be grafted onto, variable osmotic pressure, and steric congestion in the brushes. Nevertheless, the different GDs might potentially indicate some effects of backbone topology on the achievable conversion. The cyclic polymer backbone precursor enabled more effective grafting density than the linear polymer analogue. This could be explained by the reduced degree of freedom exhibited by the cyclic polymer precursor compared to the more flexible linear segments adopted by the linear analogue. Such conformation restriction could potentially influence the diffusion of free side chains.

3.1.5. Macromolecular imaging of cyclic brush polymers

AFM characterization of the obtained cyclic brush macromolecules was studied. Generally, brush polymers composed of poly(*n*BuA) side chains are often effectively visualized on mica substrate due to strong polar interactions of lateral chains with mica substrates. The side chains are spreading on the substrate surface which immobilize the macromolecule and promote the visualization by AFM.[224] Moreover, the lateral pressure arising from the high grafting density of side chains drives the brush backbone to adopt an extended chain structure instead of a statistical random coil structure.[225] By taking advantage of these aspects, it seemed very plausible to visualize the cyclic conformation of those brush polymers. To clearly evidence the resulting morphology, AFM characterization was investigated for both cyclic polymers and the linear bottlebrush polymer analogue to

distinguish the differences between the two topologies. For AFM studies, all samples were prepared by spin-coating a dilute solution of crude polymer in chloroform (ca. 0.01 mg/mL) on a freshly cleaved mica substrate to obtain a monomolecular film.

AFM characterization was primarily investigated for the cyclic brush polymer with GD = 65% (*c*-poly(Sty)$_{50}$-*g*-[poly(*n*BuA)$_{40}$]$^{0.65}$). Preliminary, the crude sample was characterized in the aim to visualize the integral sample and evaluate the possibility to observe the polymer conformation, even in the presence of free side chains. Already the crude cyclic brush polymer sample showed mainly round-shape structures with non-corrected diameters in the range of 20-30 nm **(Figure 20A**). Hard polymer backbone, surrounded by soft coronas of poly(*n*BuA) side chains spread-out on the mica surface, were visualized and would meet the expectations for a compacted brush topology. However, a significant amount of free side chains was also observed in the sample and decreased the achievable image resolution. Moreover, it must be noticed that the presence of free side chains in the sample most likely swell the core-shell brush structures and thus could yield in misleading nano-object dimensions and morphologies. In the aim to improve the visualization, removal of the unconnected side chains was required and purification of cyclic brush polymer from the free poly(*n*BuA)$_{40}$ remained not trivial even by means of standard SEC chromatography. One single run was conducted and the high molecular weight peak eluting between 20 and 24 mL in the SEC elugram was isolated. After purification, pure *c*-poly(Sty)$_{50}$-*g*-[poly(*n*BuA)$_{40}$]$^{0.65}$ was characterized by AFM and interestingly, the nano-objects still exhibited round-shape structures with an average, non-tip corrected diameter in the range of 26 nm (**Figure 20B**). Two cross-section profiles were operated on one nano-object structure from the AFM micrograph (B) and were obtained from two perpendicular scan directions (**Figure 20C**). Both profiles indicated similar dimensions with a height of approximatively 0.8 nm and an uncorrected average full width at half maximum (FWHM) in the range of 18 nm. These height profiles were practically identical, which confirmed that the nano-object exhibited an isometric structure. In general, bottlebrush macromolecules with significantly long side chains do not adapt a coil morphology but rather have a strong tendency to adapt an extended chain structure such as worm-like morphology.[16] Therefore, the observation of isometric objects could potentially suggest the presence of a collapsed backbone structure, where the full extension of the brush backbone is prevented due to intramolecular diselenide bridges that lock the backbone into a cyclic topology. Although the image resolution was not optimal and the statistics were extracted from a small ensemble of nano-objects, the estimated dimensions of the globular objects seemed to be close to the expected theoretical

structure. The theoretical size of the nano-object was determined by considering the most extended and idealized cyclic structure. In other words, the maximal length of monomer unit l_{max} = 0.24 nm for a fully extended all-trans repeated unit bond conformation, was considered to estimate the theoretical size of nano-objects. A cyclic polymer backbone *c*-poly(Sty-*co*-MISe) composed of 50 repeating units could span until a circumference (c) of 12 nm (c = 50 × 0.24 nm). Consequently, the most extended cyclic structure could exhibit a diameter (d) of 3.8 nm (c = π × d). To this backbone was added the corona of poly(*n*BuA)$_{40}$ side chains, stretching-out in all directions and measuring in the range of 9.6 nm (40 × 0.24 nm). Thus, the idealized cyclic-shape brush polymer had a theoretical diameter in the range of 23 nm (d = 3.8 nm + 2 × 9.6 nm). This expected diameter was calculated by considering a fully extended morphology. In fact, the poly(*n*-butyl acrylate) side chains of the brush polymer *c*-poly(Sty)$_{50}$-*g*-[poly(*n*BuA)$_{40}$]$^{0.65}$ were probably not fully all-trans extended due to a grafting density of only 65%. The resulting nano-objects could potentially adopt a less extended morphology and result in nano-object with smaller size. This could explain the experimental FWHM estimated in the range of 18 nm.

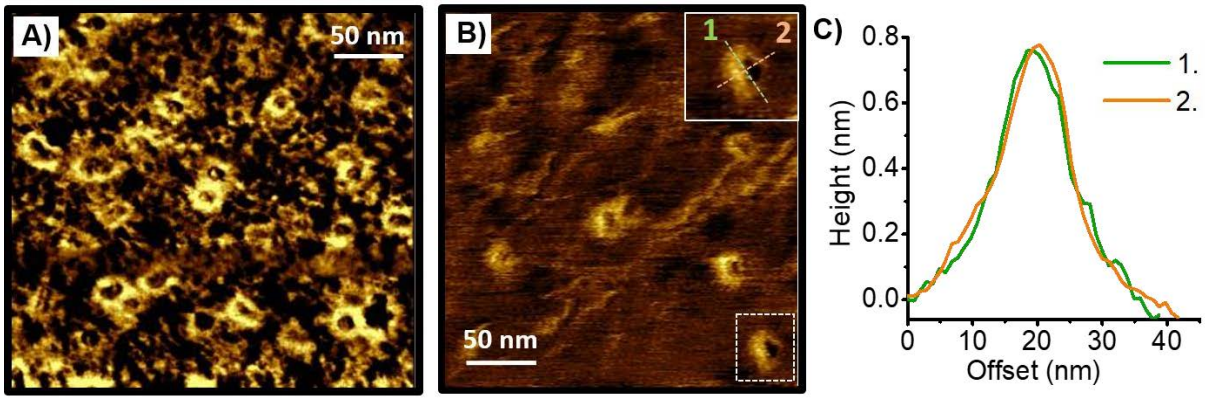

Figure 20. A) AFM micrograph of crude *c*-poly(Sty)$_{50}$-*g*-[poly(*n*BuA)$_{40}$]$^{0.65}$ brush polymer with a significant fraction of free TAD-poly(*n*BuA)$_{40}$ (phase image). B) AFM micrograph of purified *c*-poly(Sty)$_{50}$-*g*-[poly(*n*BuA)$_{40}$]$^{0.65}$ (phase image). C) Cross-section profiles of representative structures of cyclic brush in micrograph B.

To further confirm the isometric topology of the synthesized folded brush polymers, the cyclic brush polymer with GD = 27% (*c*-poly(Sty)$_{50}$-*g*-[poly(*n*BuA)$_{40}$]$^{0.27}$) was also purified by standard SEC chromatography and characterized by AFM (**Figure 21A**). Nano-object with similar round-shape structures were successfully visualized. Likewise, two cross-section profiles were operated on one nano-object structure from the AFM micrograph A) and were obtained from two perpendicular scan directions (**Figure 21B**). Both indicated similar dimensions with a height of approximatively 1.1 nm and an uncorrected average full width at half maximum (FWHM) in the range of 10 nm. The height profiles were nearly identical, which

confirmed the isometric structure of nano-objects and concurred with the previous results of the cyclic brush polymer with GD = 65%. It must be noticed that in this case, the FWHM is smaller (10 nm vs 18 nm for the cyclic brush with GD = 65%). This slight change in length could also be explained by the lower grafting density which is 27%. As suggested previously, the higher the grafting density of the brush polymer, the more the macromolecular conformation is extended and close to the theoretical diameter of 23 nm calculated for a fully extended cyclic structure. The current brush polymer had a lower grafting density and thus, could exhibit a less extended structure and smaller conformation in size.

AFM characterization was also investigated for the pure cyclic brush polymer with GD = 100% (*c*-poly(Sty)$_{50}$-*g*-[poly(*n*BuA)$_{40}$]$^{1.0}$). However, in this case, aggregation of brushes was experienced with the standardized sample preparation conditions. Moreover, although the brush macromolecules were purified by SEC analysis, a significant amount of free side chains could be observed in the phase image, which decreased significantly the resolution and the brush polymers could not be clearly visualised (See section 6.5). Regarding the synthesis of the brush macromolecule, a large amount of reactive side chains was used to force the grafting reaction and reach high grafting density. It is reasonnable to assume that a fraction of free side chains were associating with the brush macromolecules during the purification by SEC. Brush polymers were not perfectly isolated and the presence of unreacted poly(*n*-butyl acrylate) might potentially cause the agregation of the brush macromolecules. Besides, free side chains in the sample most likely swell the core-shell brush structures and thus could yield in misleading nano-object dimensions and morphologies.

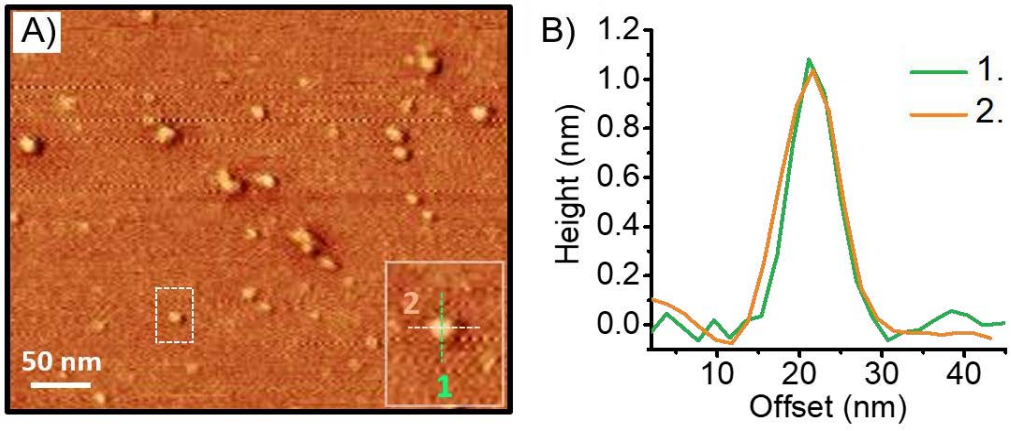

Figure 21. A) AFM micrograph of pure *c*-poly(Sty)$_{50}$-*g*-[poly(*n*BuA)$_{40}$]$^{0.27}$ (phase image). B) Cross-section profiles of representative structures of brush polymers from micrograph A.

For comparison with the cyclic brush polymers, the linear brush polymer analogue with GD = 43% (*l*-poly(Sty)$_{50}$-*g*-[poly(*n*BuA)$_{40}$]$^{0.43}$) was characterized by AFM microscopy, to

clearly distinguish the two different polymer topologies. As expected, the linear bottlebrush adopted a more extended morphology such as a worm-like structure (**Figure 22A**). Moreover, the phase image showed a significant polydispersity in length. On one hand, this observation could reflect the large distribution in molecular weight of the linear polymer precursor *l*-poly(StyOH-*co*-MISeMob). On the other hand, this large distribution in length could be potentially generated by different degree of backbone contraction, due to inhomogeneous and irregular grafting density along the polymer backbone.[32] Two cross-section profiles of one nano-object structure from the AFM micrograph were performed along two perpendicular scan directions (**Figure 22B**). The two profiles differed in length and confirmed the anisotropic structure of the obtained worm-like objects. The average structure width could be precisely evaluated by measuring height maximum distances of several molecular brushes in dense structure packages. An average width in the range of 22 nm was estimated, which was very close to the structure width determined before in the case of cyclic brush structures. The cross-section profile corresponding to the contour length (green curve) indicated an uncorrected average length at half maximum in the range of 27 nm.

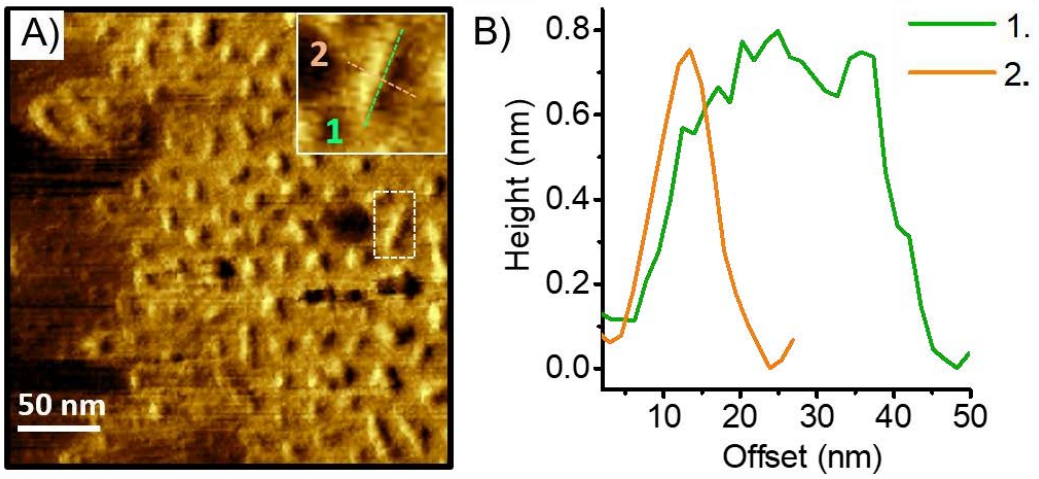

Figure 22. A) AFM micrograph of pure *l*-poly(Sty)$_{50}$-*g*-[poly(*n*BuA)$_{40}$]$^{0.43}$ (phase image). B) Cross-section profiles of representative linear brush structures of from micrograph A.

This value was compared with the theoretical length, determined by considering the most extended linear structure and a thus a maximal monomer repeating unit length of 0.24 nm. A linear polymer backbone (*l*-poly(Sty-diene-*co*-MISeMob) composed of 50 repeating units could span until a length of 12 nm (50 × 0.24 nm). To this backbone was added the corona of poly(*n*BuA)$_{40}$ side chains, stretching-out in all directions and measuring in the range of 9.6 nm (40 × 0.24 nm). The theoretical contour length (*l*) for the linear bottlebrush polymer was estimated in the range of 31 nm (l = 12 nm +2 × 9.6 nm), which is very close to experimental

contour length value (27 nm). The comparison of this micrograph corresponding to the linear bottlebrush polymer analogue with the micrographs of the potential cyclic brushes clearly evidenced different morphologies and confirmed the cyclic structure of the synthesized brush macromolecules.

The synthetic strategy developed here, consisting in the transformation of cyclic polymers into molecular cyclic brush polymers, enabled the direct visualization of single chain morphology by AFM. While the folded brushes exhibited round-shape structures with dimensions which met the range of the expected idealized structure, the linear analogue polymer showed the typical worm-like structure of molecular bottlebrushes. This strategy enabled to characterize single chain conformation and give access to a new analytic tool for complex single polymer chain folding. Although this preliminary study allowed to gain insights into the degree of structural control, both the synthesis and AFM characterization could be further improved. First, the synthetic approach for the preparation of brush polymers exploited the «grafting onto» method, which demanded an additional purification method for subsequent AFM analysis. Indeed, cyclic brush macromolecules required to be isolated by means of SEC chromatography to remove the unconnected polymer side chains in order to achieve a better visualization of nano-objects. Moreover, round-shape structures were clearly observed but the potential donut-shape polymer structure could not be visualized. Indeed, considering the small cyclic diameter exhibited by the polymer backbone, polymers side chains were stretching out in all directions and overlapping with each other, which is potentially an obstacle toward the visualization of the donut-shape structure. The small size of the macromolecules, which was about 20 nm, was in the range of the tip dimension (approximatively 8 nm). This aspect could also be a limitation toward macromolecular imaging with optimal resolution.

In the following study, the synthesis of higher molecular weight foldable macromolecules is targeted and investigated. On one hand, the use of larger polymer backbone could potentially lead to cyclic nano-objects with higher diameter and enable better macromolecular visualization by AFM. On the other hand, this current concept based on the use of sequence-controlled polymers toward subsequent oxidative single polymer chain folding, has proved to be highly efficient for macromolecules with intermediate molecular weight. Transferring this synthetic strategy to larger macromolecules is a step forward to the final goal to access more complex macromolecular folding that are closer to those of biopolymers.

3.2. Oxidative single-chain cyclization of large macromolecules

In the ultimate aim to fabricate functional synthetic materials that similarly exhibit the 3D structures and activities of biopolymers, the chain length, the microstructure uniformity and the precise positioning of crosslinks within a polymer chain are crucial parameters to access complex designs.[169] Although significant progress has been made toward the preparation of polymer chain displaying controlled and complex folding with intermediate molecular weight, the fabrication with larger macromolecule backbones is still out of reach.[5] Herein, the controlled oxidative cyclization of higher molecular weight polymer was targeted and explored. For this purpose, the sequence-controlled polymerization based on the styrene/*N*-substituted maleimide was studied for the synthesis of larger macromolecules ($DP_n = 400$) with locally inserted maleimides units. Oxidative single polymer chain folding was investigated by using positional disulfide bridge. While diselenide bond appeared to be incompatible with controlled radical polymerizations (see section 3.1.4.1), disulfide group remained inherent to radical polymerization process. Therefore, the use of the dynamic bond analogue allowed the subsequent transformation of folded polymers into folded brush polymers by exploiting the «grafting from» approach. This synthetic concept is an attracting approach for the transformation step of folded polymers into brush macromolecules due to the high achievable grafting density and the high purity of the resulting brushes. With such method, no additional purification by means of SEC chromatography is required to remove free side chains, which seemed to be a more suitable strategy for subsequent AFM characterization.

This project was also realized in collaboration with the group of Prof. Svetlana Santer and co-workers, who contributed to the study by performing the AFM characterizations.

3.2.1. Synthesis of polymers with positioned protected thiols

3.2.1.1. Design and synthesis of monomer

Sequence-controlled copolymerization of styrene and maleimide derivatives has proved to be highly efficient for functionalizing "on demand" local regions of polystyrene chains.[108] In this study, the introduction of reactive thiol groups at desired positions within a polymer chain was targeted, in the aim to subsequently induce controlled single-chain cyclization by forming intramolecular disulfide bridge. For this purpose, a *N*-functionalized maleimide bearing a protected thiol group was designed as acceptor monomer. To avoid interference of the functional groups in the polymerization process, the thiol was protected with a trityl moiety (Trt) which is an established protecting group for thiol side group in peptide chemistry.[241] Thus,

N-(2-tritylthio ethyl) maleimide (MISTrt) was designed and successfully synthesized over three steps (**Scheme 20**). First, 2-aminoethanethiol hydrochloride was treated with trityl chloride to afford 2-(tritylthio) ethylamine, bearing both a primary amine and the trityl-protected thiol. Then the resulting compound reacted with maleic anhydride by nucleophilic attack of the primary amine on the anhydride, leading to the formation of maleamic acid in extremely mild conditions. Dehydration of maleamic acid occurred at high temperature with an excess of sodium acetate in acetic anhydride to induce *N*-substituted maleimide cyclization.

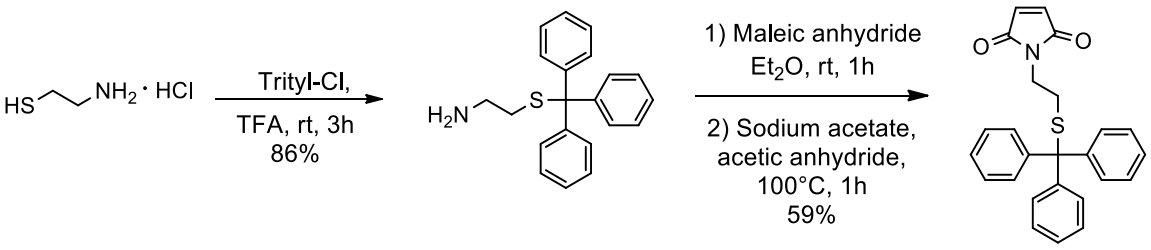

Scheme 20. Synthetic strategy for *N*-(2-tritylthio ethyl) maleimide in a two-step procedure.

3.2.1.2. Sequence-controlled polymerization by using a monofunctional initiator

As mentioned previously, transferring the synthetic concept, developed in this current study, to larger macromolecules is a step forward to the final goal to access more complex macromolecular designs. Thus, in this section, the sequence-controlled copolymerization concept was investigated for the preparation of larger macromolecules ($DP_n \approx 400$) with controlled microstructure. In a first attempt, NMP copolymerization of 4-*tert*-butoxystyrene and MISTrt was investigated by using similar reaction conditions than those described in the previous section for intermediate macromolecules (section 3.1.1).

The use of highly efficient acyclic nitroxides, such as SG1 fragment, enables a better NMP polymerization process for a large range of monomers compared to cyclic nitroxides such as TEMPO.[25,213] Therefore, the sequence-controlled copolymerization for high molecular weight polymer synthesis, was thus primarily investigated by using the established NMP initiator Blocbuilder MA, which is composed of a SG1 nitroxide. The copolymerization started with the homopolymerization of StyO*t*Bu with the molar ratio [BB: StyO*t*Bu] = [1: 900] in anisole at 115 °C. The polymerization kinetic was monitored by ^{1}H NMR spectroscopy. Injections of maleimide monomers were performed at different time during the homopolymerization of 4-*tert*-butoxystyrene. One equivalent of MISTrt was added to the polymerization at approximatively 7% of 4-*tert*-butoxystyrene conversion, and a second addition of one maleimide equivalent was performed at approximately 46%. The copolymerization was

stopped in the range of 50% of 4-*tert*-butoxystyrene monomer conversion to afford the linear poly(styrene) derivative with local pendant protected thiol groups (BB-poly(StyO*t*Bu-*co*-MISTrt)). The copolymerization kinetic calculated by ^{1}H NMR demonstrated the full consumption and insertion of the functional maleimide monomers on both sides of the formed polystyrene chains (**Figure 23A**). For the first maleimide addition, the conversion of maleimide reached 100%, while StyO*t*Bu conversion increased of 3.1%. Interestingly, regarding the monomer sequence, these monomer conversions indicated that the first maleimide unit was inserted somewhere in a polymer chain window constituted of 28 4-*tert*-butoxystyrene units in average. For the second maleimide insertion, the conversion of maleimide reached 100%, while StyO*t*Bu conversion gained 2.0%, indicating that the maleimide unit was inserted in a statistical window constituted of 18 units of 4-*tert*-butoxystyrene **(Figure 23B)**.

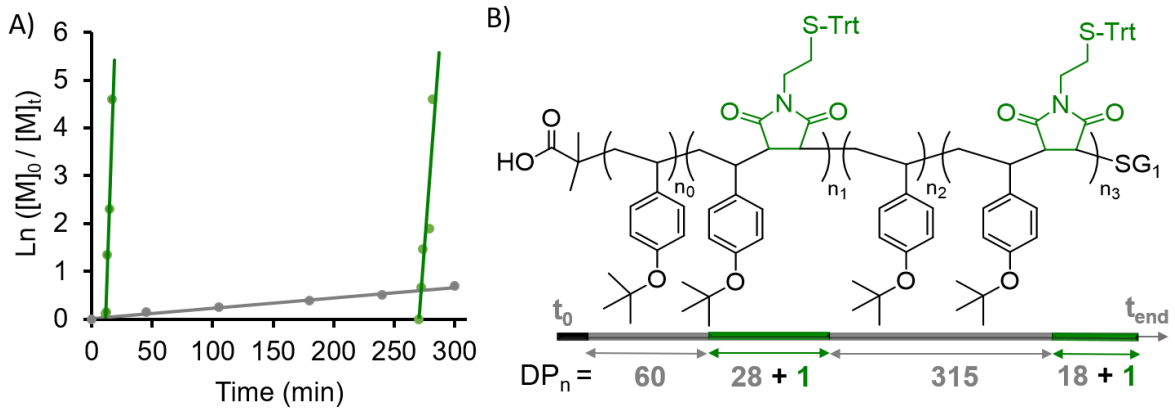

Figure 23. A) NMP sequence-controlled copolymerization of StyO*t*Bu with MISTrt initiated by Blocbuilder MA in anisole at 115 °C with the ratio [BB: StyO*t*Bu: MISTrt : anisole] = [1: 900: 2: 35% vol.]. B) Probable microstructure of the resulting copolymer BB-poly(StyO*t*Bu-*co*-MISTrt). Black, grey and green colours denote the initiator, StyO*t*Bu and MISTrt, respectively.

Compared to sequence-controlled polymerization for small polymer chains, the statistical maleimide incorporation windows increased significantly in the case of large polymer chains, which resulted in a less precise single monomer insertion within the chain. In fact, the higher is the donor/acceptor monomer ratio, the broader are sequence distribution and the incorporation window.[111] The insertion of maleimide units during the polymerization process is usually more precise with increasing conversion of donor monomer (*i.e.* when the ratio donor/acceptor monomer is lower).[111] Larger statistical windows were expectable since the amount of maleimide monomer was highly diluted in 4-*tert*-butoxystyrene comonomer in this study. The first maleimide incorporation was performed at early stage of the polymerization (approximatively 7%) when the donor/acceptor monomer ratio was very high. As expected, the

statistical window estimated for the first maleimide incorporation was larger than the one corresponding to the second maleimide incorporation.

For both maleimide insertions, a considerable amount of defaults in sequence-composition could result from these polymerisation conditions. Irregular *N*-substituted maleimide incorporations could lead to a significant fraction of polymer chain containing either only one maleimide or more than two maleimide units bearing the thiol group in a single polymer chain. These polymerization conditions could potentially reduce the control over the subsequent intramolecular disulfide bridge formation and decrease the yield of cyclic polymers. Besides, the SEC analysis indicated a broad molecular weight distribution with Đ = 1.43 (**Figure 24**). A peak tail was observed on the chromatogram, which suggested that some termination or transfer reactions were potentially occurring during the polymerization process. Termination reactions (such as disproportionation or radical coupling) more obviously appear during the synthesis of high molecular weight polymers.[242] Although the polymerization was stopped at relatively early stage of the polymerization to target a DP_n of 400 units (50% of StyO*t*Bu monomer conversion), it seemed that termination reactions occurred and such side reactions could potentially decrease the precision of the sequence-controlled polymerization process.

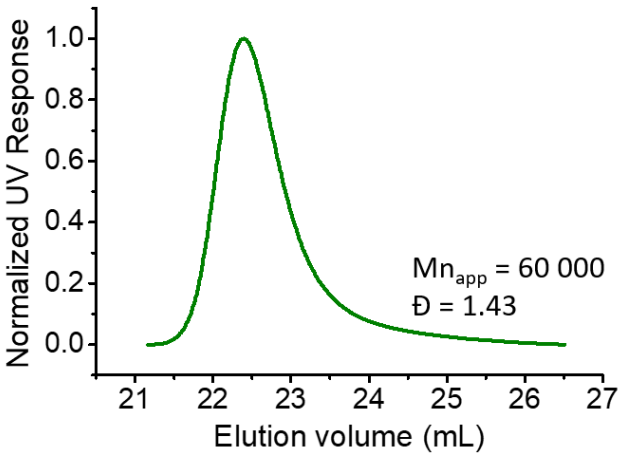

Figure 24. SEC trace of the isolated sequence-controlled copolymer BB-poly(StyO*t*Bu-*co*-MIStrt) after NMP polymerization in anisole at 115 °C with [BB: StyO*t*Bu: MISTrt : anisole] = [1: 900: 2: 35% vol.].

The NMP copolymerization conditions required some optimizations to ensure the synthesis of high molecular weight macromolecules exhibiting both a narrow molecular weight distribution and a regulated sequence to a certain degree. On one hand, it is known that high molecular weight macromolecules with narrow distribution are often more achievable by stopping the polymerization at low monomer conversion to minimize termination side

reactions.[242] On the other hand, performing maleimide injections at low monomer conversion would increase the statistical maleimide insertion windows and thus decrease the precision of the polymer microstructure. Moreover, it should be noticed that *N*-functional substituted maleimide incorporations require to be significantly spaced from each other in the latter aim to induce polymer cyclization and allow cyclic-shape visualization. Hence, it appeared that the standard NMP copolymerization initiated by the monofunctional Blocbuilder MA was not suitable to design high molecular weight macromolecules with narrow dispersity and precisely introduced maleimide units within the polymer chain.

The use of bi-directional initiators was a potential alternative to overcome this issue. Indeed, CRP polymerization initiated by a bifunctional initiator allows the polymer chain to grow on the initiator segment in two opposite directions simultaneously. Regarding the sequence-controlled polymerization initiated by such initiator, one single addition of maleimide would be required during the homopolymerization of 4-*tert*-butoxystyrene to introduce two maleimide units, statistically one on each side of the growing polymer chain. Moreover, this strategy would enable both maleimide insertions in the growing chain at medium donor monomer conversions (~50%) and avoid maleimide insertion at early stage of polymerization. Stopping the reaction at moderate monomer conversion would limit the appearance of radical-radical termination reaction. Therefore, it is plausible to assume that this copolymerization approach might lead to the synthesis of macromolecules with improved sequence-control. Nevertheless, it should be noticed that employing a bidirectional initiator is used for proof of principle of the global synthetic concept and such approach restricts the insertions of thiol functional groups at symmetric positions within the growing polymer chains.

3.2.1.3. Sequence-controlled polymerization by using bifunctional initiator

During the last decades, few NMP-bifunctional initiators have been described in literature, mainly for the preparation of ABA triblock copolymers.[243] Interestingly, a novel NMP bidirectional initiator has been synthesized in which two SG1 nitroxide fragments were spaced by a diester linker.[244] Although this bifunctional initiator could potentially provide satisfactory results for the targeted sequence-controlled polymerization, the diester linker could be accidently cleaved by hydrolysis in the following steps of the multistep synthesis and lead to a degradation of the macromolecules. Inspired by this bidirectional dialkoxyamine, a novel bifunctional initiator was designed, in which two SG1 nitroxide fragments were spaced by an diamide linker. Amide groups are known to be less prompt to hydrolysis than ester

groups.[245,246] A Blocbuilder MA-derived dialkoxyamine was synthesized in a two-step procedure (**Scheme 21**). The first step consisted in the esterification of the Blocbuilder MA compound with *N*-hydroxysuccinimide (NHS) in the presence of the coupling reagent *N,N'*-dicyclo-hexylcarbodiimide (DCC) to yield a Blocbuilder MA-derived with activated ester (BB-SG1-NHS).[247] Then, 1,4-diaminobutane (1 equiv) reacted by nucleophilic attack with BB-SG1-NHS (2 equiv) to afford the difunctional initiator bearing two SG1 nitroxide fragments spaced by an diamide linker (Bis-BB-SG1).

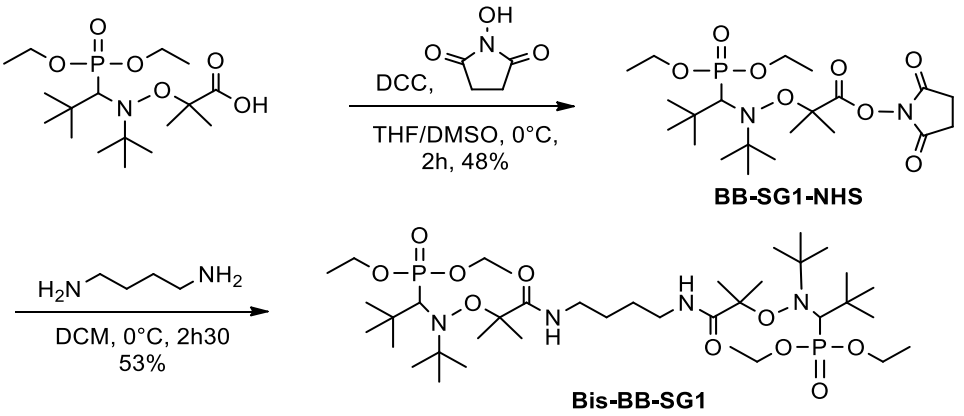

Scheme 21. Synthesis of bidirectional NMP initiator in a two-step procedure, bearing two SG1 nitroxide groups spaced by an amide linker (Bis-BB-SG1).

NMP polymerization initiated by the novel dialkoxyamine (Bis-BB-SG1) was investigated first with the homopolymerization of *tert*-butoxystyrene to test the efficiency of the novel initiator. The polymerization was conducted at 120 °C in anisole by using the ratio [Bis-BB-SG1: StyO*t*Bu] = [1: 1000] and stopped at 55% of monomer conversion to afford the homopolymer poly(*tert*-butoxystyrene) (poly(StyO*t*Bu)$_{550}$). Samples were taken during the polymerization to monitor the radical process by ^{1}H NMR spectroscopy and SEC in THF. The polymerization proceeded fast, with 55% of monomer conversion within 3 h. The semilogarithmic plot of monomer conversion exhibited a linear evolution with time, which suggested that the concentration of active species remained constant during the polymerization process and termination reaction barely occurred (**Figure 25A**).

SEC analysis recorded at various monomer conversions revealed monomodal molecular weight polymer distributions at low conversions (<49%). However, the appearance of a high molecular weight shoulder was noticed at monomer conversions above ~50% (**Figure 25B**). It seems plausible to attribute this shoulder to polymer dimers resulting of polymer-polymer radical coupling reactions commonly seen during radical polymerization *via* multi-functional

initiators, and particularly at higher conversions.[248] Thus, to synthesize well-defined poly(*tert*-butoxystyrene) chains with narrow molecular weight distributions, it was apparent that the reactions should be stopped at moderate conversions (up to 50%) in order to maintain a low dispersity and good control over the polymerisation.

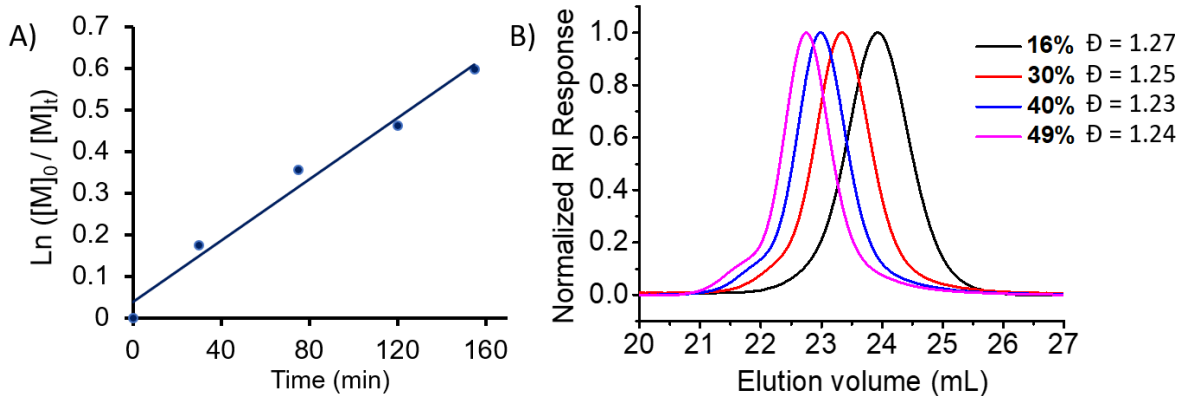

Figure 25. A) Semilogarithmic plot of monomer conversion *vs* time of the NMP homopolymerization of 4-*tert*-butoxystyrene initiated by the difunctional initiator in anisole at 120 °C with the ratio [Bis-BB-SG1: StyO*t*Bu] = [1: 1000]. B) SEC traces recorded at various conversions during the homopolymerization of 4-*tert*-butoxystyrene.

Subsequently, the sequence-controlled copolymerization of StyO*t*Bu with MISTrt was performed by using the novel difunctional initiator (Bis-BB-SG1) and the aforementioned experimental conditions. In this case, since the formed chains would be growing in two opposite directions due to the use of bidirectional initiator, one single addition of two equivalents of maleimide was required. The single injection of MISTrt (2 equiv) was performed during the homopolymerization of StyO*t*Bu at approximatively 44% of monomer conversion. The copolymerization was stopped in the range of 47% of 4-*tert*-butoxystyrene conversion to afford the sequence-controlled polymer (Bis-poly(StyO*t*Bu-*co*-MIStrt)). The copolymerization kinetic demonstrated the full and fast incorporation of the functional maleimide in the formed polystyrene chains (**Figure 26A**). The conversion of maleimide reached 100%, while StyO*t*Bu conversion increased of approximatively 3%. Regarding the monomer sequence, one unit of maleimide was introduced on both sides of the polymer chain in statistical regions composed of 15 units of 4-*tert*-butoxystyrene (**Figure 26B**).

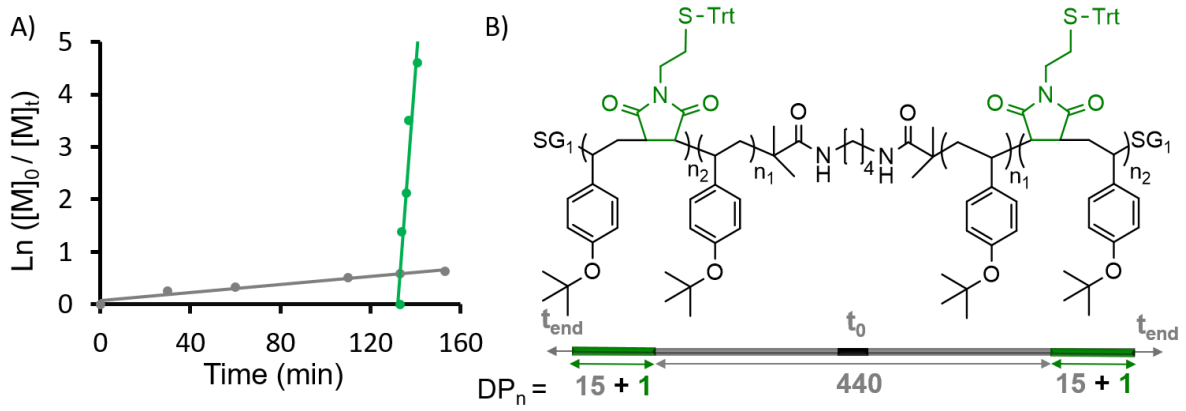

Figure 26. A) Semilogarithmic plot of monomer conversion *vs.* time of NMP sequence-controlled polymerization of 4-*tert*-butoxystyrene with maleimide MIStrt initiated by the difunctional initiator Bis-BB-SG1. B) Probable microstructure of the resulting copolymer Bis-poly(StyO*t*Bu-*co*-MIStrt). Black, grey and green colours denote the initiator, StyO*t*Bu and MISTrt, respectively.

A statistical region composed of 15 units remains rather broad. Due to radical-radical termination reactions evidenced at higher conversions, the maleimide injections required to be performed below 50% of donor monomer conversion which is not the ideal conversion to allow a narrow incorporation region (typically to conversion values > 60%). Thus, sequence defaults could be still significant generated with such polymerization conditions. Nevertheless, using a bifunctional initiator allowed to narrow down both incorporation windows compared to those in the sequence-controlled polymerization initiated by the monofunctional Blocbuilder MA. Besides, the SEC analysis evidenced the formation of macromolecules with controlled molecular weights and relatively narrow molecular weight distribution ($M_{n,\,app}$ = 90000 and Đ = 1.25, see section 6.3.14), which indicated that radical coupling termination reactions were limited. The obtained copolymer Bis-poly(StyO*t*Bu-*co*-MIStrt) was further characterized by proton NMR spectroscopy (**Figure 27**). Signals corresponding to the resonances of trityl protecting groups could be observed at 7.34, 7.27 and 7.24 ppm. An average of two maleimide units were inserted *per* polymer chain according to the integration of the trityl group signal peaks. Hence, it appeared that the use of bi-directional initiator for the sequence-controlled polymerization allowed an improvement in both the molecular weight distribution and in the precision of microstructure of the resulting macromolecules. This sequence-controlled copolymer was then exploited to study the oxidative cyclization of high molecular weight macromolecules.

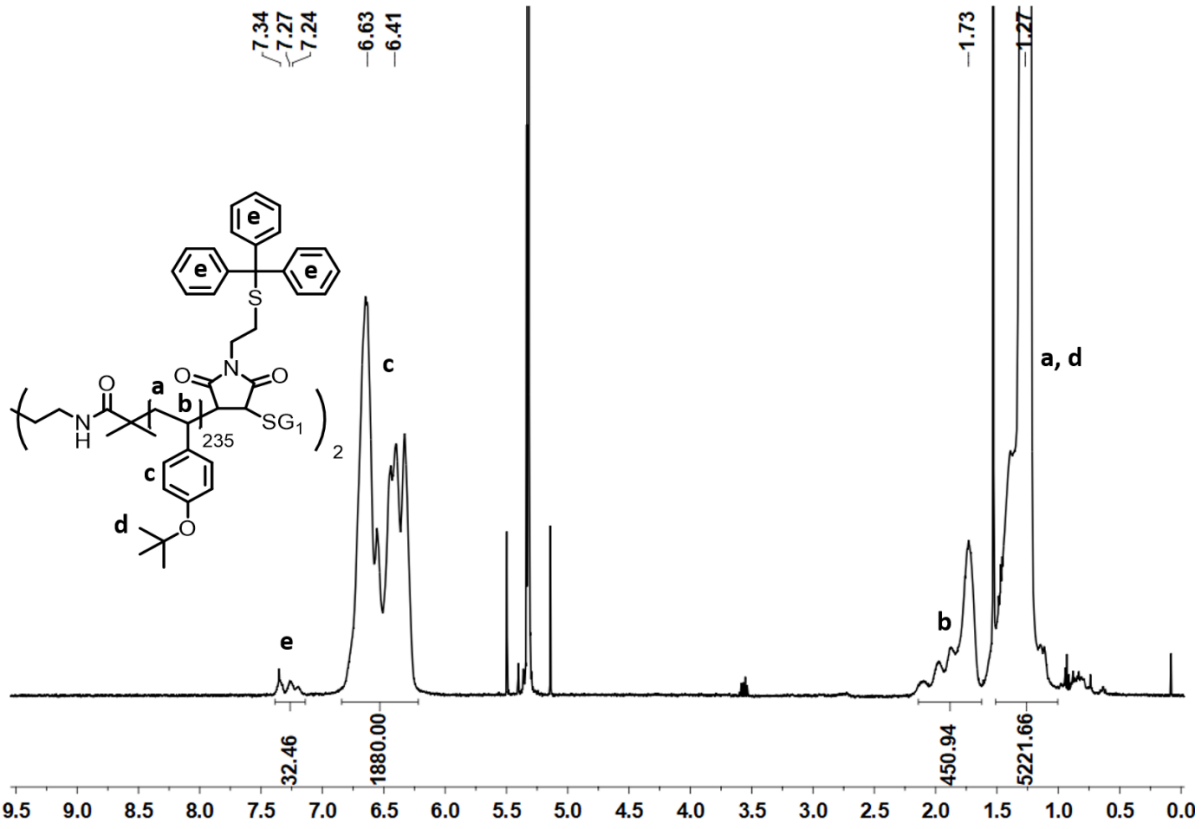

Figure 27. ^{1}H NMR spectrum in CD_2Cl_2 of the obtained sequence-controlled copolymer Bis-poly(StyO*t*Bu-*co*-MIStrt).

3.2.2. Deprotection reactions

3.2.2.1. Polymer backbone deprotection

The following step consisted in the deprotection of the phenolic backbone. As previously described, removal of *tert*-butyl groups was achieved by hydrolysis with aqueous hydrochloric acid (HCl) in dioxane at high temperature to afford the linear polymer with pendant 4-hydroxystyrene units (poly(StyOH-*co*-MISTrt)).[208] The deprotected polymer was characterized by proton NMR spectroscopy. The signals corresponding to the *tert*-butyl resonances at 1.0-1.5 ppm disappeared and confirmed a quantitative deprotection of the phenolic backbone units (see section 6.4, **Figure 93**). It must be noticed that approximatively 15% of trityl-thiol protecting groups were concomitantly removed during the hydrolysis. Furthermore, the polymer was also characterized by SEC chromatography in DMAc (**Figure 28**). The chromatogram revealed a minor shoulder at the high molecular weight flank of the polymer peak, which slightly increased the molecular weight distribution ($M_{n,\,app}$ = 93000 and Đ = 1.30).

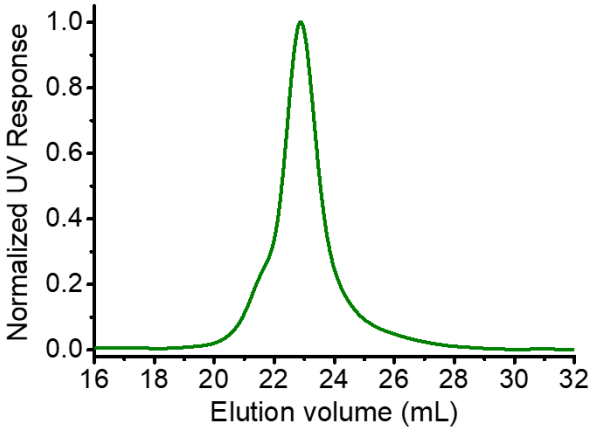

Figure 28. SEC trace of the resulting poly(StyOH-*co*-MISTrt) after deprotection reaction achieved by HCl catalysed hydrolysis at 105 °C.

The peak shoulder could be attributed to polymer chain dimers, probably arising from the small amount of deprotected thiols and their subsequent intermolecular oxidation into disulfide groups. This side reaction could potentially occur since the reaction was conducted in concentrated conditions (~10^{-3} M). However, this by-product could only be limited and not fully avoided even by conducting the hydrolysis in diluted conditions and under inert atmosphere to avoid oxidation. Some efforts were dedicated toward the concomitant removals of *tert*-butyl groups and trityl groups by using aqueous solution of HCl, since the trityl blocking group is also acid-labile cleavable.[241] Nevertheless, detritylation by using HCl solution in dioxane could not provide satisfactory results and often yielded in a mixture of protected and unprotected trityl thiol groups on the polymer chains. Hence, proceeding the detritylation in a subsequent step appeared to be the best option.

3.2.2.2. Trityl-thiol deprotection

As mentioned in the previous section, detritylation is effectively achieved under acidic conditions, by using either strong protic acids or Lewis acids.[241] The reaction conditions used in this study were slightly adapted according to a protocol previously described in literature.[176] Detritylation was achieved by using trifluoroacetic acid (TFA) in the presence of scavengers. A solvent mixture composed of TFA/dioxane (65/45) was used to carry out the deprotection since poly(4-hydroxystyrene) was not soluble in pure TFA. Triethyl silane (TES) was selected to scavenge trityl cations by reduction into unreactive triphenylmethane. The solution of polymer was intensively flushed with argon in order to remove oxygen and avoid undesirable intermolecular oxidation of the released thiol groups. The reaction was conducted for 4.5 h at room temperature (**Scheme 22**), to afford the fully deprotected linear precursor bearing two free thiol functional groups (*l*-poly(StyOH-*co*-MISH)) .

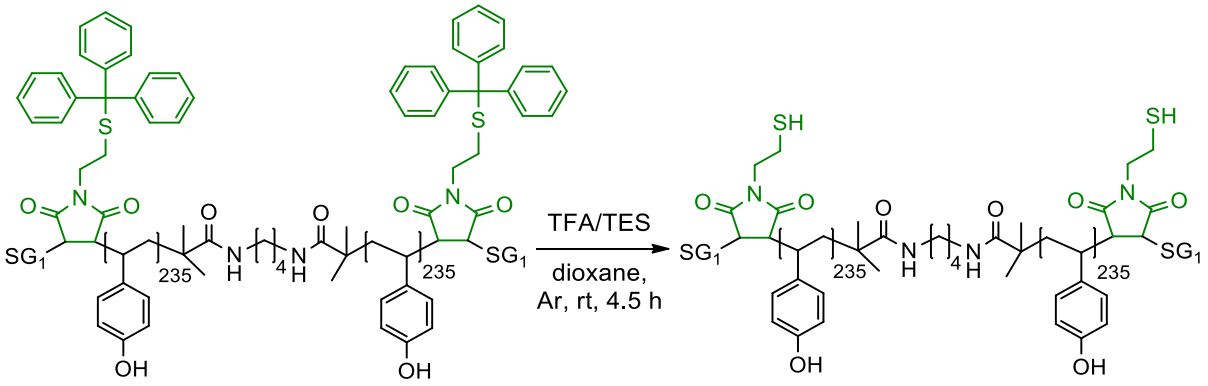

Scheme 22. Detritylation of thiol groups by using a TFA/dioxane solvent mixture solution in the presence of scavenger at room temperature to yield in the fully-deprotected linear polymer (*l*-poly(StyOH-*co*-MISH).

The deprotection fully occurred and was evidenced by ^{1}H NMR spectroscopy. The signals corresponding to the trityl resonances at 7.35 – 7.15 ppm disappeared and confirmed a quantitative deprotection of the thiol functional groups (see section 6.4, **Figure 94**). The resulting linear polymer (*l*-poly(StyOH-*co*-MISH)) was analysed by SEC in DMAc. The chromatogram could not evidence any shift to higher elution volume, i.e. lower molecular weight polymer. This was expectable, since only two trityl groups were removed from the linear polymer chain. Moreover, the chromatogram revealed that the minor shoulder at the high molecular weight flank of the polymer peak remained unchanged, indicating that the intermolecular side reactions were minimized in this second deprotection reaction ($M_{n,\,app}$ = 91500 and Đ = 1.32).

To further confirm the presence of free thiol among the linear polymer chains, an Ellman's test was performed. In both aqueous solutions and organic solvents, the presence of free thiols can be evidenced through the use of the reagent 5,5'-dithiobis-(2-nitrobenzoic) acid (DTNB) (**Figure 29A**).[249] This reagent is composed of a strong electrophilic disulfide bond, which can be easily reduced by free thiols and thus leading to the formation of a mixed disulfide and releasing one molecule of 5-thio-2-nitrobenzoic acid (TNB). Because the released fragment (TNB) is absorbing visible light (λ = 412 nm in water), free thiols concentration can be determined by measuring the absorption of TNB by UV-Vis spectroscopy. Herein, the Ellman's test was conducted in dimethylformamide (DMF). The polymer *l*-poly(StyOH-*co*-MISH) was dissolved in 1.0 mL of DMF (3×10^{-11} M of thiol groups). A stock solution of DTNB in DMF (10^{-8} M) with a small amount of base DIPEA (0.3% volume) was prepared separately. An excess of DTNB solution (0.1 mL) was added to the solution containing the polymer. The solution turned instantaneously orange, which suggested that the

free thiols located on the polymer reacted with DTNB and released the chromogenic TNB fragments. This observation was confirmed by measuring the absorbance by UV-Vis spectroscopy (**Figure 29B**). An absorbance band was evidenced at $\lambda = 500$ nm, which indicted that TNB adduct was released and confirmed indirectly the presence of free thiols on the sequence-controlled polymer.

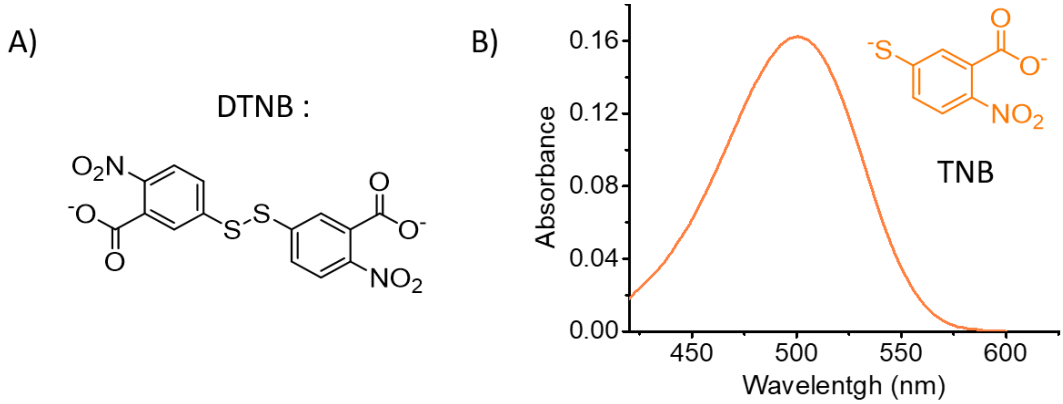

Figure 29. A) Chemical structure of the Ellman's test reagent. B) UV-Vis spectrum resulting from the Ellman's test performed on *l*-poly(StyOH-*co*-MISH) in dimethylformamide after thiol deprotection.

3.2.3. Formation of intramolecular disulfide bridge

Oxidative folding of individual polymer chain was investigated for high molecular weight macromolecules by forming one intramolecular crosslink. Oxidation of the two inserted thiol groups into disulfide bond was explored to generate an intramolecular dynamic bridge and lead to chain cyclization. So far, several synthetic strategies have been described in literature toward oxidative thiol coupling by exploiting oxidizing agents such as metals, dimethyl sulfoxide (DMSO), ionic liquids, halogens, electrochemical oxidation or even by simple air exposure.[250] DMSO and molecular oxygen (air-oxygen or oxygen pressure) has shown significant interests due to ease of handling and straightforward purification.[251] For both synthetic strategies, it has been reported that the oxidation of thiols into disulfide bonds are influenced by several external parameters, such as pH, temperature, solvent and thiols concentration.[252,253] Thiolate species are effectively able to form disulfide by simple air exposure while protonated thiols appear to be unreactive.[252] Therefore, thiol oxidations are strongly depending on the solution pH and can be promoted with the presence of base. Good yields have been described for reactions catalysed by amines.[254] Moreover, thiol oxidation conducted in polar-aprotic solvents, such as dimethylformamide, is known to increase the oxidation rate of thiols to disulfide.[251,255]

Oxidative single polymer chain folding was performed by using simultaneously air-oxygen and DMSO as oxidizing reagents according to a protocol adapted from the literature.[176] The linear polymer precursor *l*-poly(StyOH-*co*-MISH) was added dropwise via a syringe pump (48 h of addition) to a reaction mixture containing 5% vol. DMSO, 5% vol of the Hünig base *N,N*-diisopropylethylamine (DIPEA) and a large amount of DMF to avoid unwanted intermolecular cross-linking reactions (≈ 0.2 mg of polymer/mL after addition). The reaction was saturated with oxygen and was stirred for 6 days (**Scheme 23**) to afford the cyclic polymer locked *via* the formation of intramolecular disulfide bridge *(c*-poly(StyOH-*co*-MIS).

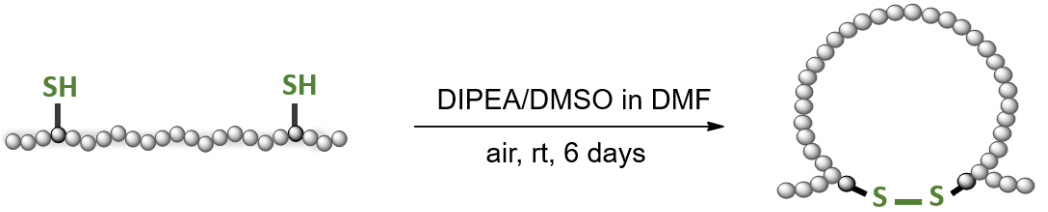

l-poly(StyOH-*co*-MISH) *c*-poly(StyOH-*co*-MIS)

Scheme 23. Schematic illustration of the cyclization reaction induced by thiol oxidations into disulfide bridge in DMF with the presence of DMSO and base.

The cyclization reaction was monitored by SEC analysis in DMAc. Interestingly, no change in the SEC curves between the starting material and the resulting product could be observed (**Figure 30A**). The SEC traces could not give conclusive evidence of a hydrodynamic volume reduction, which would be obviously indicative of intramolecular cyclization. The formation of intermolecular crosslinking bonds is generally the main side reaction during single-chain polymer cyclization. However, di- tri- or multimerization was neither visible in the SEC traces. It should be mentioned that the reduction of hydrodynamic volume, caused by the formation of an intramolecular crosslink, scales inverse with the degree of polymerization of the polymer chain (DP_n).[256] In other words, the more the macromolecular chain is long, the less is the difference in the hydrodynamic volume exhibited by a linear precursor and its cyclic polymer analogue. In literature, polymers with DP_n = 20-50 usually show a significant volume reduction in SEC measurements,[175,176] while large chains with DP_n = 470 as applied in this study, were not expected to indicate a visible volume reduction by ring formation. Therefore, additional characterizations are obviously required to get clear indication on the resulting polymer topology after the cyclization reaction.

To gain insights into the oxidation of free thiols into disulfides, Ellman's test was performed on the isolated cyclic polymer *c*-poly(StyOH-*co*-MIS). The experimental conditions

previously described for the Ellman's test of the linear precursor, were used here to investigate the final thiol concentration. After adding DTNB compounds in excess to a solution containing *c*-poly(StyOH-*co*-MIS) in DMF, the solution remained colourless. This observation was confirmed by measuring the absorbance by UV-Vis spectroscopy. The spectrum demonstrated an absorbance of approximatively 0.02 at λ = 500 nm, indicating a nearly quantitative consumption of free thiol moieties (**Figure 30B**).

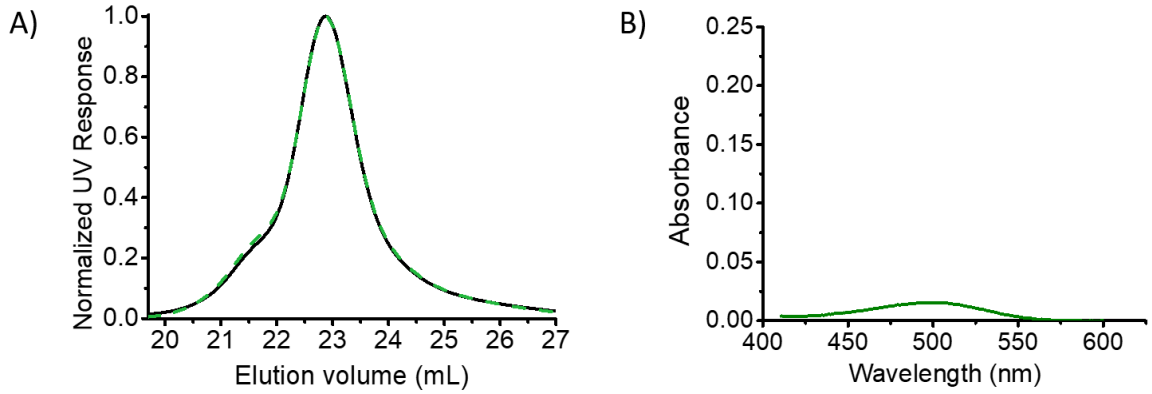

Figure 30. A) SEC traces of the polymers *l*-poly(StyOH-*co*-MISH) with free thiols (black solid line) and the resulting polymers *c*-poly(StyOH-*co*-MIS) after oxidation of the thiol group (dashed green line) B) UV-Vis spectrum resulting from the Ellman's test on *c*-poly(StyOH-*co*-MIS) (green curve).

This result was encouraging, since it could suggest that thiol oxidation potentially occurred. However, it also appeared that the consumption of thiol did not reached completion. This result was expectable considering the fact that a fraction of polymer chains could not be di-functionalized during the sequence-controlled copolymerization process. Statistically, it is plausible to assume that some macromolecules were mono-functionalized or tri-functionalized. Indeed, the fraction of mono-functionalized chains could not be able to generate intramolecular disulfide bridge formation and oxidation of thiols to intramolecular disulfide bridge could not be quantitative. On the other hand, the fraction of tri-functionalized polymer chains could potentially form local disulfide bridge on one side of the macromolecules with a remaining free thiol on the other side.

It must be pointed out that the Ellman's test on the linear precursor and cyclic polymer were performed to obtain a qualitative indication about the presence of thiols. The two obtained absorbance values were not quantitatively compared since both Ellman's test were performed separately on the isolated linear precursor and the isolated cyclic polymer by using similar experimental conditions. Thus, a minor difference in the sample concentration could lead to misleading comparison of thiol concentration. Moreover, the Ellman's test only indicated the potential disappearance of thiol functional groups and did not provide any information on the

resulting sulfur atom oxidation state. ^{1}H and 2D HSQC NMR spectroscopies were performed and could not give any evidence of -C*H*$_2$-S- proton resonance shift, since the maleimide concentration was not sufficient to provide any signals even for the characterization of concentrated samples. Due to limited amount of successful characterizations, no conclusion concerning the cyclization process could be determined at this stage. Hence, it appeared that the synthetic strategy developed in the current study, which consists in the transformation of the folded polymers into brush polymers to access AFM characterization, was highly required. Indeed, this situation clearly illustrated the high demand of additional characterization toward conformation analysis, for either complex macromolecular design or in this case, high molecular weight polymers. The transformation of the resulting polymer *c*-poly(StyOH-*co*-MIS) into brush polymers was performed for subsequent AFM microscopy characterization.

3.2.4. Synthesis of cyclic brush polymers

The transformation of the obtained polymers into brush polymers was targeted in the aim to gain insights into their morphology by AFM analysis. Previously, it was shown that disulfide bridges are chemically stable during controlled radical polymerization and do not interfere in the polymerization process. Hence, the «grafting from» approach which relies on the preparation of bottlebrush polymers by growing polymer side chains *via* CRP polymerization on a polymeric backbone,[225] was selected in this study. This method is more convenient for subsequent AFM characterization due to achievable high grafting densities and straightforward bottlebrush purification by filtration and precipitation. So far, grafting from reactions have been mostly conducted from polyethylene,[257] polyvinylchloride,[258] polyisobutylene[259] or even poly(meth)acrylic backbones.[38] To the best of our knowledge, the synthesis of densely brush macromolecules having a poly(styrene) backbone and poly(*n*-butyl acrylate) side chains by using the «grafting from» approach was not described in literature. Thus, a prior study was performed to investigate the controlled and successful preparation of linear brush polymers composed of such chemical structure.

3.2.4.1. Linear brush polymer synthesis via « grafting from approach »

The «grafting from» method allows the preparation of bottlebrushes with high grafting density and significant uniformity between macromolecules. The first requirement for a successful "grafting from" reaction is a preformed polymer backbone with distributed initiating groups for subsequent polymerization of side chains. So far, grafting side chains has been mainly achieved by performing ATRP process initiated by pendant α-bromoester groups on

poly(methacrylate) backbones.[226] In this section, the synthesis of brush polymers composed of styrenic backbone and *n*-butyl acrylate side chains was studied by using the «grafting from» approach. Synthesis of poly(*tert*-butoxystyrene) followed by a *tert*-butyl deprotection reaction afforded a functional polystyrene backbone. Then, polymer post-modification was implemented to introduce initiator groups on the styrenic backbone and ATRP polymerization was subsequently conducted.

A linear poly(*tert*-butoxystyrene) precursor , with a DP_n in the range of 380 monomer units (*l*-poly(StyO*t*Bu)$_{380}$), was prepared by NMP polymerization by using the novel bifunctional initiator (Bis-BB-SG1). The obtained homopolymer was successfully characterized by ^{1}H NMR spectroscopy and SEC analysis (SEC in DMAc, $M_{n,\,app}$ = 66000 and Đ = 1.16, see section 6.3.13). The following step consisted in the removal of *tert*-butyl groups present on the phenolic backbone. *Tert*-butyl deprotection was achieved by hydrolysis with hydrochloric acid (HCl) in dioxane at high temperature to afford the linear poly(4-hydroxystyrene) precursor (*l*-poly(StyOH)$_{380}$). ^{1}H NMR spectroscopy indicated a full deprotection of the 4-hydroxystyrene units, since the peak corresponding to the resonances of *tert*-butyl groups fully disappeared. The SEC analysis evidenced the formation of macromolecules with controlled molecular weight and narrow molecular weight distribution (SEC in DMAc, $M_{n,\,app}$ = 85000, and Đ = 1.23, see section 6.3.13).

The next step consisted in the introduction of α-bromoester groups on the poly(4-hydroxystyrene) backbone which are necessary for the subsequent ATRP polymerization. For this purpose, the hydroxyl functionalities of the linear homopolymer *l*-poly(StyOH)$_{380}$ were esterified by treatment with bromopropionyl bromide in the presence of pyridine to yield the poly(styrene) backbone bearing pendant α-bromoester segments (*l*-poly(StyBr)$_{380}$) (**Scheme 24**). The resulting ATRP macroinitiator was characterized by ^{1}H NMR and SEC analysis. The ^{1}H NMR spectrum showed the appearance of new signals at 4.58 and 1.94 ppm corresponding to the introduced C*H*-Br and C*H*$_3$-CH side groups, respectively (see section 6.4, **Figure 91**). Furthermore, by comparing the integration of the peak areas of the new formed signals with those of aromatic protons from the poly(styrene), a nearly quantitative conversion of hydroxyl group into bromoester was estimated (97% of conversion). SEC characterization demonstrated a shift to higher molecular weight region compared to the phenolic backbone precursor and indicated $M_{n,\,app}$ = 88000 with Đ = 1.24 (SEC trace shown in **Figure 31**).

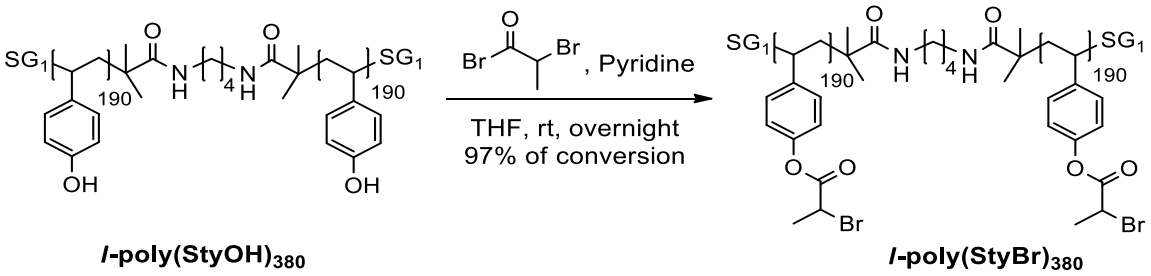

Scheme 24. Synthesis of the linear ATRP-macroinitiator (*l*-poly(StyBr)$_{380}$). Esterification of the hydroxyl groups of *l*-poly(StyOH)$_{380}$ with bromopropionyl bromide in the presence of pyridine at room temperature.

After the successful preparation of the poly(styrene) derivative macroinitiator, ATRP polymerization of *n*-butyl acrylate monomer could be implemented to grow polymer side chains on the macromolecules. It must be mentioned that polymerization on macroinitiators requires generally different experimental conditions than a traditional ATRP using low molecular weight monofunctional initiator. Due to a high local concentration of initiation sites of the polymer backbone, termination reactions such as radical-radical coupling can occur more likely during the controlled radical polymerization of side chains. To avoid these unwanted reactions, the polymerization of side chains are performed under dilute conditions. More precisely, the desired length of the side chains, is obtained by conducting the ATRP process in a large excess of monomer and subsequently stopping the reaction at low monomer conversions, usually around 10%.[38] Moreover, using a sub-stoichiometric amount of cuprous catalyst and adding a ~5% of copper (II) bromide ($Cu^{II}Br_2$) reversibly deactivate the growing polymer chains and thus suppress termination reactions.[38] In this study, ATRP of *n*-butyl acrylate was conducted at 80°C in ethyl methyl ketone, by using a small amount of $CuBr_2$, the catalytic complex CuBr/N,N,N′,N″,N″-pentamethyl diethylenetriamine (PMDETA) and *l*-poly(Sty-Br)$_{380}$ as macroinitiator, with a ratio of [Br: CuBr: PMDETA: $CuBr_2$: *n*BuA] = [1: 0.5: 0.525: 0.025: 500] (**Scheme 25**). The monomer conversion was monitored by ^{1}H NMR spectroscopy and the polymerization was stopped at approximatively 5% of conversion after 1.5 h. The average degree of polymerization for the poly(*n*BuA) side chains was approximatively of $DP_n = 25$ calculated from monomer conversion data and similar estimation was obtained from gravimetric method ($DP_n = 22$).

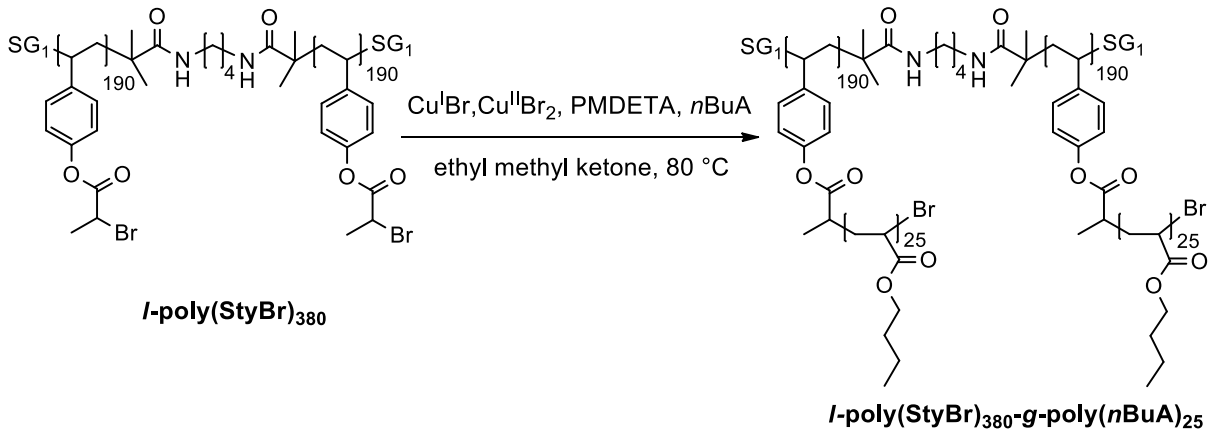

Scheme 25. Synthesis of linear brush polymer *l*-poly(Sty)$_{380}$-*g*-poly(*n*BuA)$_{25}$. ATRP polymerization of *n*-butyl acrylate initiated by the macroinitiator *l*-poly(StyBr)$_{380}$ in ethyl methyl ketone at 80°C with the ratio of reagents of [Br: CuBr: PMDETA: $CuBr_2$: *n*BuA] = [1: 0.5: 0.525: 0.025: 500].

The resulting linear brush polymer *l*-poly(Sty)$_{380}$-*g*-poly(*n*BuA)$_{25}$ was analysed by proton NMR and SEC chromatography. ^{1}H NMR spectrum indicated the appearance of new signals corresponding to the *n*-butyl acrylate units while the signals corresponding to the styrenic backbone remained unchanged (**Figure 92**). SEC traces of the brush copolymer clearly evidenced a shift toward lower elution volume, which is qualitatively indicative of an increase of molecular weight after ATRP polymerization (**Figure 31**, $M_{n,\,app}$ = 517000 and Đ = 1.28). It must be pointed out that the molecular weight indicated by SEC analysis was different than the molecular weight estimated by gravimetry or by monomer conversion from proton NMR. However, this observation was expectable since SEC data analysis using refractive index detection is calibrated *vs.* linear polystyrene standards and does not yield accurate molecular weight data.[38] In fact, due to the high compact structure of densely grafted bottlebrush polymers, the molecular weight to hydrodynamic volume relation strongly differs from linear polystyrene used for SEC calibration. Besides, the polydispersity of the brush is merely determined by the polydispersity of the backbone.[39,260] In this case, after the polymerization of side chains, the polydispersity nearly remained unchanged, indicating the good control of the *n*-butyl acrylate ATRP process. Using a high ratio of monomer to initiator and stopping the polymerization at low conversion avoided successfully the undesirable side reactions and enabled the preparation of the desired brushes with poly(*n*BuA)$_{25}$ side chains.

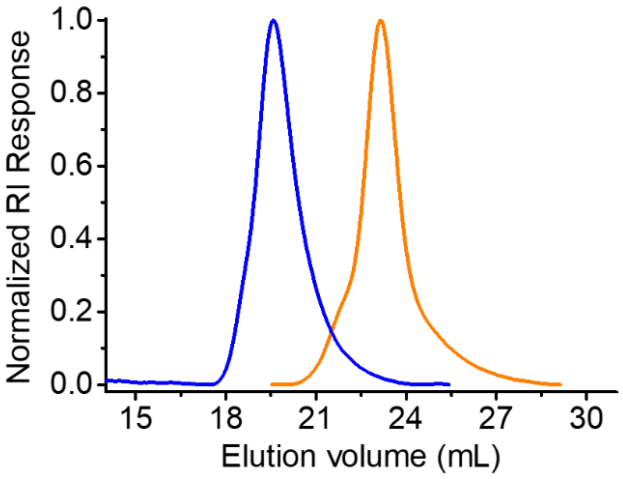

Figure 31. SEC traces of the macroinitiator precursor polymer *l*-poly(StyBr)$_{380}$ (orange curve) and the resulting linear bottlebrush polymer *l*-poly(Sty)$_{380}$-*g*-poly(*n*BuA)$_{25}$ (blue curve).

AFM microscopy was used to visualize the molecular morphology of the resulting linear bottlebrush polymer *l*-poly(Sty)$_{380}$-*g*-poly(*n*BuA)$_{25}$. For AFM studies, the sample was prepared by spin-coating a dilute solution of crude polymer in chloroform (ca. 0.01 mg/mL) on a freshly cleaved mica substrate to obtain a monomolecular film.

Figure 32 shows the obtained height and amplitude images. In both, bottlebrush polymers were clearly observed and as expected, exhibited worm-like molecular morphology. To further demonstrate the successful preparation of bottlebrush macromolecules with high grafting density, the backbone contraction was evaluated. Statistical molecular dimensions were determined by direct measurement of a significant ensemble of thirty bottlebrush macromolecules. The statistical average contour length, uncorrected full width at half maximum (FWHM) and height were estimated in the range of 98 ± 15 nm, 15 ± 3 nm, and 1.2 ± 0.2 nm, respectively. The statistical average contour length is very close to the theoretical maximal length estimated for polymer backbone of DP_n = 380 with fully extended all-trans repeated unit bond conformations ($l_{unit,\ max}$ = 0.24 nm) which is in the range of 91 nm (380 × 0.24 nm). Hence, in this case, it appeared that the bottlebrush morphology was fully extended, which indirectly suggested the high grafting density of poly(*n*-butyl acrylate) side chains on the styrenic backbone.

This investigation showed that the «grafting from» method led to well-controlled synthesis of bottlebrush polymers composed of poly(styrene) backbone and poly(*n*-butyl acrylate) side chains. Thus, this straightforward synthetic strategy seemed to be a promising pathway to transform cyclic polymers (previously cyclized by intramolecular disulfide bridge), into cyclic brush polymers in order to allow AFM microscopy characterization.

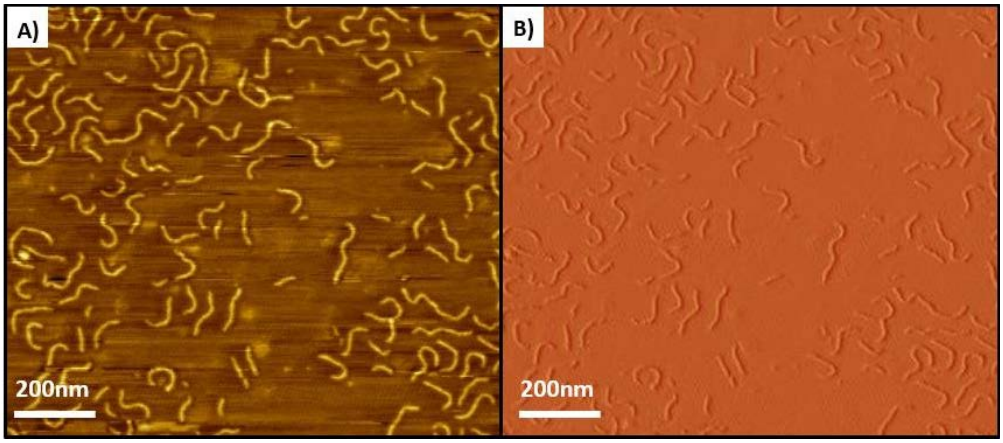

Figure 32. AFM micrograph of the linear bottlebrush polymer *l*-poly(Sty)$_{380}$-*g*-poly(*n*BuA)$_{25}$. A) Height image. B) Amplitude image.

3.2.4.2. Folded brush polymers synthesis

Previously, attempts toward single polymer chain compaction were conducted on high molecular weight macromolecules by forming one single intramolecular disulfide bridge (See section 3.2.3). However, standard characterization tools usually utilized to evidence cyclic polymer topology, such as SEC chromatography or NMR spectroscopy, could not prove in this case the cyclization process. In the aim to visualize directly the resulting polymer topology by AFM microscopy, the potential cyclic macromolecules were transformed into brush polymers. The grafting from approach was performed following the reaction conditions discussed in the previous section (see section 3.2.4.1). Pendant α-bromoester fragments were introduced on the polymer backbone *c*-poly(StyOH-*co*-MIS) by esterification of the hydroxyl units with bromopropionyl bromide in the presence of pyridine to yield the poly(styrene) macroinitiator with pendant α-bromoester segments (*c*-poly(StyBr-*co*-MIS)). The polymer was characterized by ^{1}H NMR (**Figure 33**). New signals appeared at 4.58 and 1.94 ppm, corresponding to the proton resonances located on the bromoester fragments. Nearly all the 4-hydroxystyrene backbone units were successfully transformed into initiating sites for subsequent ATRP polymerization (98% estimated by ^{1}H NMR). Furthermore, the macroinitiator was analysed by SEC chromatography in DMAc, which demonstrated a shift of the main peak toward higher molecular weight region and an unchanged molecular weight distribution ($M_{n,\,app}$ = 92000 and Đ = 1.30, SEC trace in **Figure 34**).

The obtained poly(styrene) derivative macroinitiator was then used to implement ATRP polymerization of *n*-butyl acrylate monomer and grow polymer side chains on the macromolecules. For this purpose, ATRP of *n*-butyl acrylate was conducted at 80 °C in ethyl

methyl ketone, by using a small amount of $CuBr_2$, the catalytic complex CuBr/N,N,N′,N″,N″-pentamethyl diethylenetriamine (PMDETA) and *c*-poly(StyBr-*co*-MIS) as macroinitiator, with a ratio of [Br: CuBr: PMDETA: $CuBr_2$: *n*BuA] = [1: 0.5: 0.525: 0.025: 500]. The monomer conversion was monitored by ^{1}H NMR spectroscopy and the polymerization was stopped at ~9% of conversion after 2 h, to afford the brush polymer (*c*-poly(Sty)$_{470}$-*g*-poly(*n*BuA)$_{40}$).

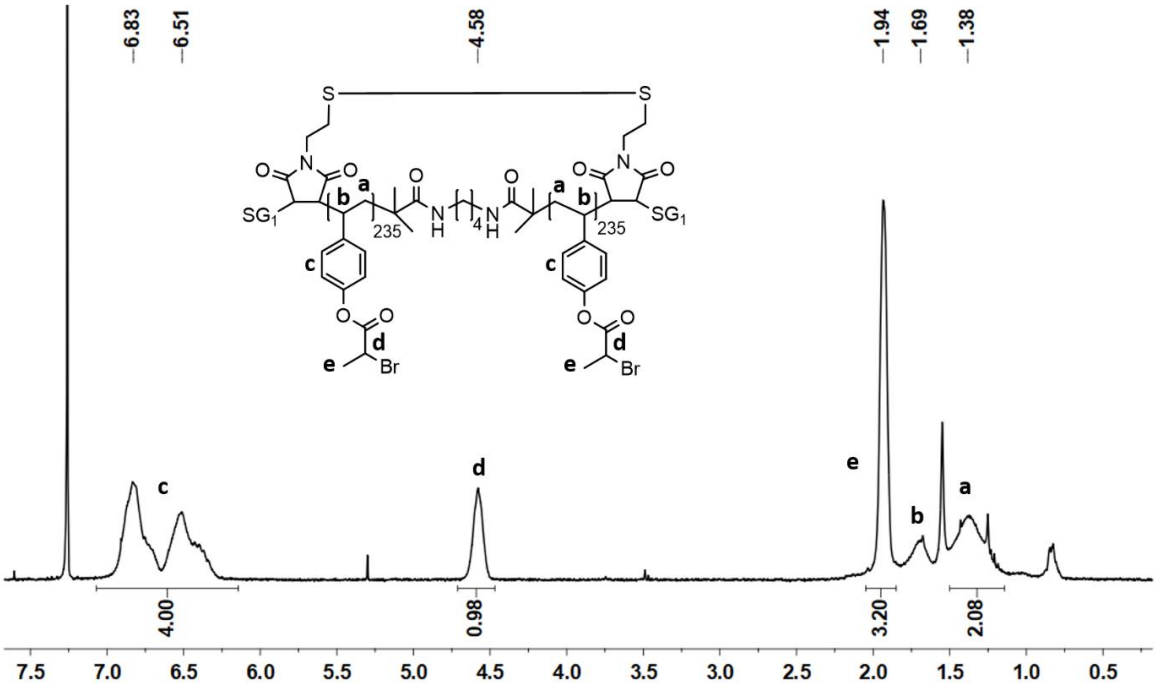

Figure 33. ^{1}H NMR spectrum of the obtained macroinitiator *c*-poly(StyBr-*co*-MIS) in $CDCl_3$ after esterification of the 4-hydroxystyrene backbone units by bromopropionyl bromide in presence of pyridine.

An average degree of polymerization for the poly(*n*BuA) side chains was estimated of DP_n = 40 units, calculated from monomer conversion data by NMR ($DP_{n,\ NMR}$ = 45) and gravimetry ($DP_{n,\ grav}$ = 35). The isolated cyclic brush macromolecule was characterized by proton spectroscopy and SEC chromatography. In the NMR spectrum, signals corresponding to *n*-butyl acrylate resonances appeared at 4.03, 1.90 - 1.38 and 0.92 ppm while signals corresponding to the proton resonances of backbone styrene units could still be observed at 7.03 – 5.81 ppm (see section 6.4, **Figure 96**). SEC chromatography indicated a peak shifted to lower elution time, demonstrating an obvious increase in molecular weight after the ATRP polymerization and a quantitative transformation of the macroinitiator into brush polymer (**Figure 34**). However, the elugram revealed a polymer peak with a significant shoulder at the high molecular weight flank and a broadening at the low molecular weight flank, which increased the molecular weight distribution ($M_{n,\ app}$ = 465000 and Đ = 1.43). The measured $M_{n,\ app}$ of the shoulder on the left-hand side is approximatively the double of the $M_{n,\ app}$

exhibited by the main peak ($M_{n,\,app\,(shoulder)}$ = 916000 *vs* $M_{n,\,app\,(main\,peak)}$ = 451000). These three different populations of polymer could potentially correspond to polymer chain dimers (high molecular weight shoulder), linear polymers (main peak) chain and the desired cyclic polymers (broadening at the low molecular weight flank). As mentioned previously, cyclic polymers exhibit smaller hydrodynamic volume compared to their linear analogue. This peak interpretation would indicate a poor cyclization yield while linear analogue polymers and linear polymer chain dimers could be the main macromolecular populations. Nevertheless, it remained difficult to get precise and clear information either on the topology of the obtained polymers or on the cyclization yield, with this conventional analytical technique. Deconvolution of SEC peak was tested in the aim to quantify each polymer populations. However, due to the excessive coelution of the main linear polymers with the two other populations (high and low molecular weight shoulder), the estimation could be obviously misled (data not shown).

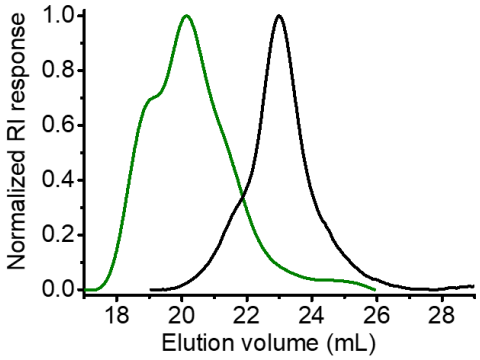

Figure 34. SEC traces of the macroinitiator *c*-poly(StyBr-*co*-MIS) (black curve) and the resulting cyclic bottlebrush polymers *c*-poly(Sty)$_{470}$-*g*-poly(*n*BuA)$_{40}$ (green curve) after ATRP polymerization of *n*-butyl acrylate monomers on the macroinitiator

Besides, it appeared that the high molecular weight peak shoulder observed in the elugram, which corresponded potentially to polymer chain dimers, increased considerably during the brush polymer synthesis step. Thus, this observation strongly indicated that side reactions probably occurred during the CRP process. Such chain dimerization of brush polymers could arise from termination reactions, such as radical-radical coupling. Indeed, in this case, the ATRP process was stopped at higher conversion of monomer (~10%), which could potentially cause radical coupling side reactions and could explain the significant increase of higher molecular weight brush polymers. Nevertheless, the obtained brush polymer was subsequently characterized by AFM microscopy to gain insight into the polymer topologies of the overall sample.

3.2.5. Macromolecular imaging of cyclic brush polymers

The folded polymers have been transformed into folded molecular brushes to allow conformation analysis by Atomic Force Microscopy. Indeed, while SEC analysis could only indicate the presence of three distinct polymer populations in the overall sample, AFM characterization would give more insight into polymer morphology and polymer population yields.

The cyclic brush polymer *c*-poly(Sty)$_{470}$-*g*-poly(*n*BuA)$_{40}$ was characterized by AFM and could be successfully visualised (**Figure 35A**). The absence of free side chains impurities in the sample allowed an AFM characterization with great resolution. Interestingly, only a small number of cyclic polymers were observed while most of the polymer chains exhibited linear worm-like structures. Due to the larger size of the nano-objects compared to the previous study (see section 3.1.5), the visualization and thus the differentiation of brush polymer topologies was significantly improved. Linear bottlebrush macromolecules with significantly long side chains do not adapt a coil morphology but rather have a strong tendency to adapt an extended chain structure such as worm-like morphology.[16] Thus, the observation of "donut-shape" nano-objects strongly suggested the presence of a collapsed backbone structure, where the full extension of the brush backbone is prevented due to intramolecular disulfide bridge that lock the backbone into a cyclic topology. Furthermore, the micrograph showed a rather obvious polydispersity in length. Regarding the dimension of the linear worm-like structures, two distinct sizes were estimated. Most of the linear structures exhibited an average contour length of approximatively ~121 nm (estimated from an ensemble of 20 macromolecules) while the longest linear polymer chains exhibited an average contour length of ~ 237 nm (estimated from 10 macromolecules). These estimations meet the range of the theoretical sizes expected for linear brush polymers with a $DP_{backbone}$ of 470 units (l_{max} = 470 × 0.24 = 112.8 nm) and linear chain dimers ($2l_{max}$ = 2 ×112.8 = 225 nm). Thus, it appeared that the AFM characterization was rather consistent with the SEC chromatogram interpretation, showing likely that single linear brush polymer and linear chain dimers were the main macromolecular populations compared to cyclic macromolecules.

A very low amount of cyclic nano-objects was observed in the AFM micrograph compared to linear analogue macromolecules, which suggested that the multistep synthesis required investigations and optimization. A statistic of 5 cyclic nano-objects for an ensemble of approximatively 300 macromolecules was estimated. However, this statistic is an

approximation and cannot be quantitatively interpreted. This estimation was determined from AFM characterization of the brush polymer sample, dropped and spin-coated on the mica substrate. Simple adsorption of bottlebrush macromolecules with long side chains on the substrate can induce not only conformational extension, but also spontaneous scission of covalent bonds in the polymer backbone.[261] This behaviour is attributed to the fact that the strong attractive interaction between the side chains and the substrate is maximized by the spreading of the side chains. In the current case, rupture of C-C bond in linear brush backbone could potentially occur and alter the statistic of the ratio cyclic/linear brush polymers after sample preparation. Moreover, cyclic brush polymer degradation could also occur, where ring opening at the chemically weakest S-S bond might be caused by the adsorption of the macromolecule on the substrate (E_{S-S} = 268 kJ/mol, E_{C-S} = 255 kJ/mol and E_{C-C} = 347 kJ/mol).[262] Moreover, the cyclic brush polymers nano-objects could be even more susceptible to cleavage considering the additional tension in the backbone from the forced curving.[195] In light to this degradation phenomenon, the initial ratio of cyclic and linear brush polymers could be slightly altered after sample preparation and thus the estimated statistic could not quantitatively reflect the overall sample of synthesized brush polymers. Nevertheless, the sample was prepared by spin coating the solution of brush polymers on the mica. This preparation method is probably the best suitable approach to minimize macromolecular backbone scission due to the short immobilization time of macromolecules on the substrate.

Although the multi-step synthesis lead to a poor statistic of cyclic polymers, this AFM characterization demonstrated also some positive aspects. As long polymer backbones were exploited to induce single polymer chain folding, size of the resulting nano-objects was significantly increased, and clear visualization of the cyclic structure could be successfully achieved. Cross-section profiles of each cyclic nano-objects were performed and are shown in **Figure 35B**. An uncorrected full width at half maximum (FWHM) in the range of about 18 nm could be estimated. This experimental width value was in the range of the expected theoretical width which was estimated of 19.2 nm for poly(nBuA)$_{40}$ side chains stretching maximum contour length of 9.6 nm in all directions (2 × 40 × 0.24 nm). Moreover, the graph confirmed the isometric structure of cyclic nano-objects and demonstrated highly uniform profile features with a diameter estimated at height maximum in the range of 44 nm. This dimension is slightly larger than the calculated diameter value estimated for a single brush contour length of 121 nm, which is approximatively of 38 nm. These values meet the theoretical dimensions of the length of a polymer backbone of DPn = 470 (470 × 0.24 = 112.8 nm) and the average width for

polymer side chains of DPn = 40 units (2 × 40 × 0.24 = 19.2 nm), which confirmed that the linear polymers are mainly single polymer chains and not dimers. The expected theoretical diameter value was determined in the range of 36 nm for a fully extended cyclic structure (d = l_{max} / π = (470 × 0.24) / π = 36 nm). It must be noticed that in this case, some cyclic brush polymers appeared to be cleaved on the mica substrate (blue, green and orange circle), probably caused by the previously discussed macromolecular backbone scission. Nevertheless, even if backbone scission seemed to take place, the cyclic polymers still exhibited a ring shape and the potential scission could explain the slightly higher experimental diameter compared to the expected value (44 nm *vs.* 38 nm respectively).

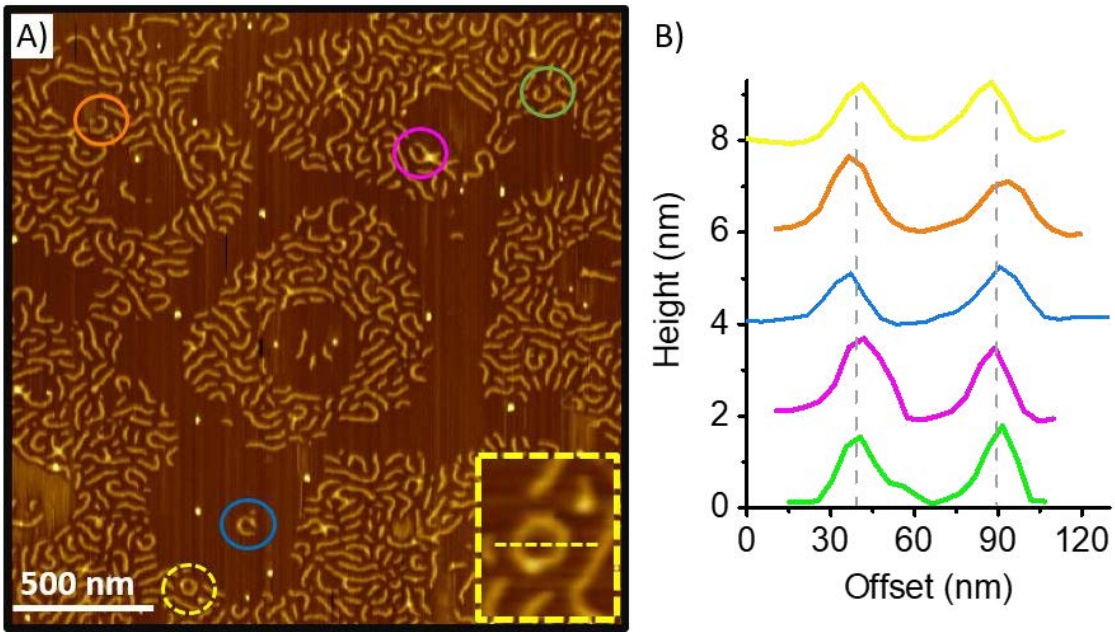

Figure 35. A) AFM micrograph of the brush polymer *c*-poly(Sty)$_{470}$-*g*-poly(*n*BuA)$_{40}$ with a zoom in of the brush macromolecule highlighted in yellow. B) Horizontal cross-section profiles of cyclic structures observed in image A).

Although the multi-step synthesis demanded optimizations, the first attempt toward single chain folding of larger macromolecules allowed to gain insights into the challenges. Two different hypothesis were considered to explain the poor statistic of cyclic polymers: 1) On one hand, the issue could originate from the first step of the total synthesis, which was the sequence-controlled copolymerization. In this study, long polymer chain backbones were targeted to ensure the visualization of folded polymer chains by AFM analysis. Therefore, the sequence-controlled polymerization conditions had to be modified and the amount of maleimide was diluted in a greater excess amount of styrene compared to the conditions described in literature. Going to larger molecular weight increases statistically the risk that the degree of sequence control decreases. All polymer chains might not contain two thiol moieties at requested

positions, which could potentially explain why the polymer cyclization did not properly occur. 2) On the other hand, ring-closing reaction for high molecular weight polymer chains remains more challenging, mainly for functional group proximity issue.[190] Indeed, it is highly likely that thiols on the same polymer chain could not be at a sufficient proximity to one another to react subsequently and form disulfide bridge. Consequently, the thiol-thiol coupling could be potentially slower than expected or could be inhibited. Based-Mediated β-Elimination of the thiol groups was considered to explain a potential inhibition of intramolecular disulfide bridges. However, activation of the thiol functional group into better electrophile, or the use of stronger base are generally required to induce an elimination of the thiol fragment.[263] Regarding the mechanism of thiol oxidation into disulfide bond by using DMSO and DIPEA, a possible stepwise mechanism is presented in **Scheme 26**. In excess of base (B), all thiol groups (RSH) are transformed into thiolates (Eq. 1), which can attack DMSO molecules, thereby forming thio-sulfoxide active adducts (Eq. 2). Subsequent attack by an additional thiolate molecule on such adducts then leads to the formation of the disulfide bond (Eq. 3).[253,264] Although recent mechanistical study confirmed the major conversion of the thio-sulfoxide adduct into disulfide bond, a possible production of a sulfenic acid intermediate was demonstrated (Eq. 4).[265] Sulfenic acid intermediates can subsequently react with thiol species to form disulfide bond, making their experimental detection difficult (Eq. 5). Nevertheless, in protein chemistry, it has been shown that sulfenic acid species could be stable and thus detected, either in large macromolecules which hinders their accessibility or in the absence of vicinal thiol groups.[265]

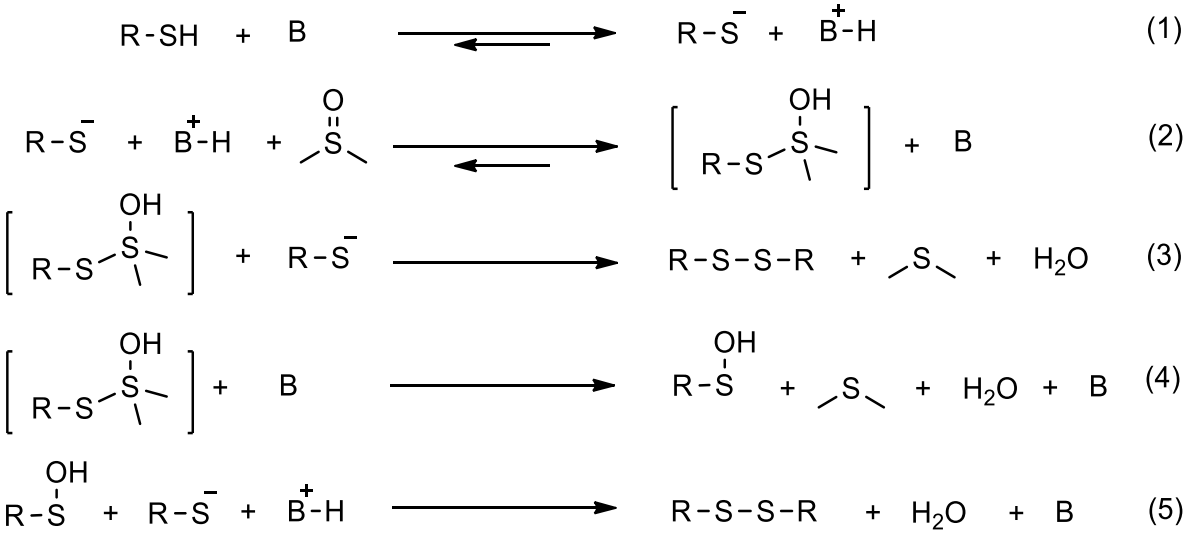

Scheme 26. Proposed mechanism for the oxidation of thiols into disulfide bond in the presence of DMSO and base (B).

According to the Ellman's test results, thiol groups were consumed, which could suggest that reactions (1) and (2) successfully occurred. However, no evidence of disulfide bridges were obtained, which led to believe that the two intramolecular thio-fragments could not react with each other (3 and 5). Indeed, this could result in the formation of copolymers containing sulfenic acid fragments, which are not detectable by Ellman's test.[266] Such sulfur group could potentially not further react with intramolecular thiol groups due to proximity issues and slow chain motion. Moreover, sulfenic acid could be inhibited by free amine impurities arising from dimethylformamide degradation by air and lead to stable sulfenamide groups.[266]

It is plausible to assume that the low statistic of cyclic polymers, obtained after this multi-step synthesis, arose from both of the sequence-controlled polymerization and the ring-closure reaction through the formation of disulfide bridge. Hence, these synthetic aspects were further investigated and slightly modified in the aim to improve the multi-step synthesis toward the folding of high molecular weight macromolecules and visualization of polymer conformation.

3.2.6. Investigations

Two hypotheses were considered to explain the resulting low statistic of cyclic polymers at the end of the multi-step synthesis: 1) the potentially sequence defects in the macromolecules originating from the sequence-controlled polymerization process. 2) the possible inefficiency of the intramolecular crosslinking reaction. In this section, these two aspects were separately investigated to understand the obstacles and attempts were made to overcome the issues.

3.2.6.1. Insertion of thiol moieties via local copolymer segments

The sequence-controlled polymerization for precise monomer insertion in high molecular weight polymer was hypothetically an obstacle. Indeed, in larger polymers, the degree of microstructure control decreases statistically and could result in the synthesis of polymer chains which might not contain two distant thiol groups. Therefore, insertion of several maleimides units instead of targeting a single maleimide insertion on each side of the polymer chain, could be a possible alternative to ensure the incorporation of thiol fragments at requested positions. Moreover, considering the second hypothesis which suggested that thiol-thiol coupling could not occur because of proximity issue, increasing the intramolecular concentration of thiols could also favour intramolecular reactions. It must be mentioned that with this approach, thiol functional groups could potentially react with another intramolecular neighbouring thiol to

form disulfide bridge on one side of the polymer chain. The insertion of thiols at requested positions was ensured to investigate the subsequent single chain folding and evaluate an improvement in the yield of cyclic polymers. For this purpose, two sequence-controlled polymers containing *n* MISTrt maleimide equivalents on each side of the polymer chains were synthesized (*n* = 3 or 6, respectively) (**Figure 36**). Then, the multi-step synthesis was performed, followed by AFM characterization.

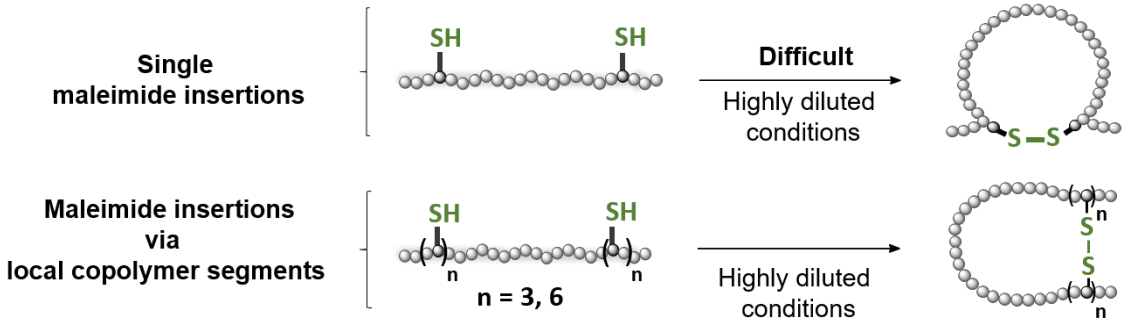

Figure 36. Schematic illustration of the synthetic approach *via* single maleimide insertions and *via* local copolymer segment insertions.

- **Sequence-controlled polymerizations**

Two sequence-controlled copolymers composed of 4-*tert*-butoxystyrene and MISTrt were prepared by NMP process and initiated by the bifunctional initiator (Bis-BB-SG1). Polymerization conditions were slightly modified to introduce *n* maleimide units on each side of the growing macromolecules and afford linear polymers with local copolymer segments (poly(StyO*t*Bu-*co*-MISTrt^{2n}) with *n* = 3 or 6). For both synthesis, a single addition of a solution of MISTrt in anisole, containing 6 or 12 maleimide equivalents, was performed during the homopolymerization of 4-*tert*-butoxystyrene to incorporate 3 or 6 thiol groups respectively on each side of the polymer chain. Kinetic data and characterizations are summarized in **Table 4**. The polymerizations were stopped after the full consumption of MISTrt to afford sequence-controlled polymers with *n* positioned protected thiol groups near each chain-end and narrow molecular weight distribution (**Table 4**, entry *a* for the synthesis of poly(StyO*t*Bu-*co*-MISTrt^{6}) and entry *b* for the synthesis of poly(StyO*t*Bu-*co*-MISTrt^{12})). In both cases, the copolymerization kinetics demonstrated the fast consumption of the functional maleimides (**Figure 37A** and **C**). Concerning poly(StyO*t*Bu-*co*-MISTrt^{6}), the conversion of maleimides reached 100%, while StyO*t*Bu conversion increased of approximatively 5%. Regarding the monomer sequence, 3 units of maleimide were introduced in average on both sides of the polymer chain in statistical regions composed of 25 units of *tert*-butoxystyrene. Concerning poly(StyO*t*Bu-*co*-MISTrt^{12}), 6 units of maleimide were inserted in average, on both sides of

the macromolecule, in a statistical monomer window composed of 30 *tert*-butoxystyrene monomer units (100% of MISTrt *vs*. 6% of StyO*t*Bu consumptions; **Figure 37B** and **D**).

Table 4. Kinetic data recorded and characterizations of the sequence-controlled polymerizations toward maleimide insertions via local copolymer segments. [a]

Entry	Equiv MI [b]	Conv. StyO*t*Bu at t_{add} [c]	Conv. StyO*t*Bu at $t_{f,\ add}$ [d]	Conv. StyO*t*Bu at t_{end} [e]	$M_{n,\ SEC}$ [f] (g/mol)	Đ [f]	DP_n [g]
a	6	0.39	0.44	0.44	66000	1.13	420
b	12	0.38	0.44	0.45	67500	1.15	430

[a] Experimental conditions: polymerization initiated by the bifunctional initiator Bis-BB-SG1, conducted in anisole at 120°C. [Bis-BB-SG1: StyO*t*Bu] = [1: 1000]. [b] Equivalents of maleimide injected during the polymerization. [c] StyO*t*Bu conversion at which the addition of MISTrt maleimides was performed. Calculated from ^{1}H NMR in $CDCl_3$. [d] 4-*tert*-butoxystyrene conversion at which Mal -STrt maleimides were fully consumed. [e] Final StyO*t*Bu conversion. [f] Measured by SEC in THF. [g] Estimated from SEC.

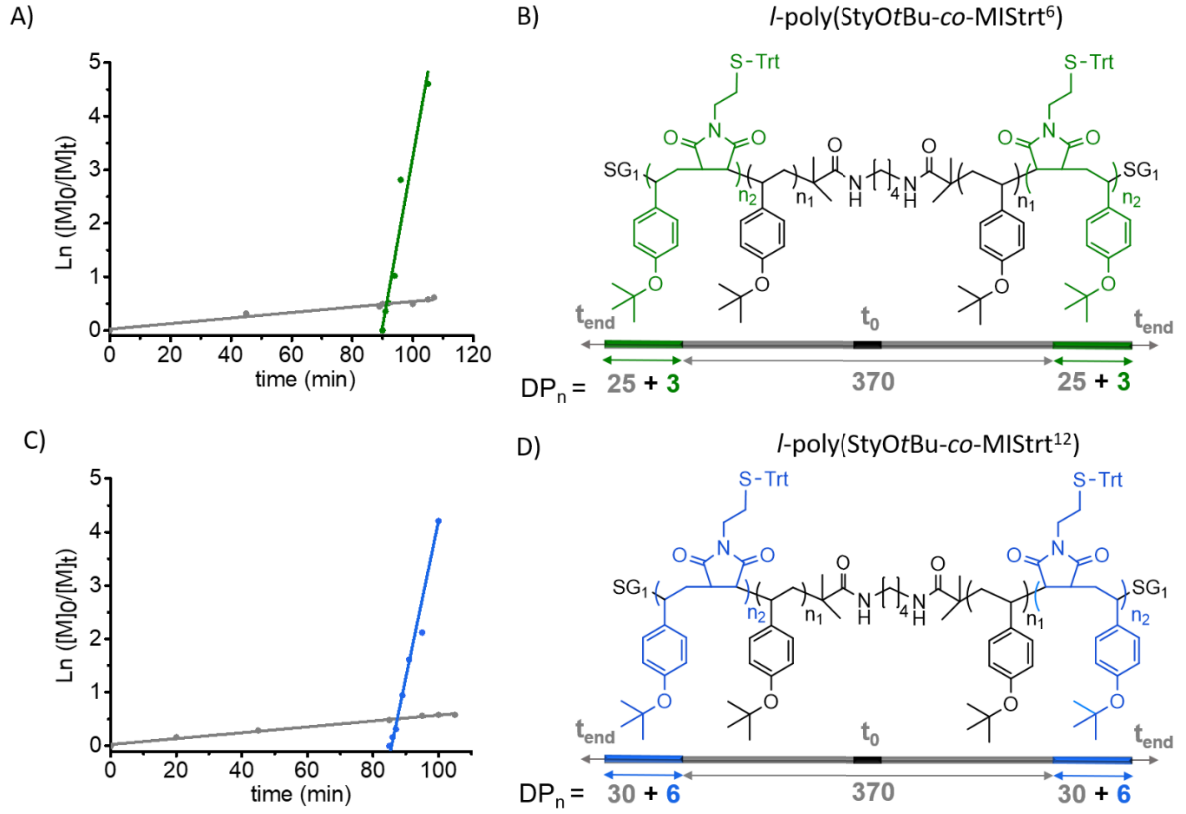

Figure 37. A) Semilogarithmic plot of monomer conversion *vs*. time recorded for the copolymerization of poly(StyO*t*Bu-*co*-MISTrt^6). B) Probable microstructure of the obtained linear copolymer poly(StyO*t*Bu-*co*-MISTrt^6). C) Semilogarithmic plot of monomer conversion *vs*. time recorded for the copolymerization of poly(StyO*t*Bu-*co*-MISTrt^{12}). D) Probable microstructure of the obtained copolymer poly(StyO*t*Bu-*co*-MISTrt^{12}).

Both statistical regions increased compared to the previous synthetic approach based on the insertion of two single maleimide units (section 3.2.1). This observation was expectable since

more maleimide equivalents were injected during the homopolymerization. Moreover, since sequence defects generally occur for one single maleimide insertion, incorporating several units of maleimide potentially decreased further the uniformity of chain microstructure. Nevertheless, the aim of this alternative approach was to ensure the introduction of protected thiol groups at desired positions. Targeting the insertion of several thiol-substituted maleimides within the polymer chain increased the probability to insert the functional groups on both side of the polymer chains. The rest of the multi-step synthesis was performed from these two linear polymer precursors toward the preparation and visualization of cyclic polymers.

- **Polymer deprotection reactions**

After the preparation of sequence-controlled copolymers, deprotections of 4-*tert*-butoxystyrene repeated units and trityl-thiol fragments were performed in a two-step procedure, as described in section 3.2.2. First, removal of *tert*-butyl groups was achieved by HCl catalysed hydrolysis at high temperature. Subsequently, detritylation of the thiol fragments was performed in the solvent mixture dioxane/TFA at room temperature in the presence of triethyl silane (TES) as a scavenger (**Scheme 27**). The deprotected linear sequence-controlled polymers (*l*-poly(StyOH-*co*-MISH^{6}) and (*l*-poly(StyOH-*co*-MISH^{12}) were successfully characterized by ^{1}H NMR spectroscopy and SEC analysis (NMR spectrums in section 6.4). Both SEC chromatograms indicated a small shoulder in the high molecular weight flank of the polymer peaks, indicating a minor formation of chain dimers linked by unwanted intermolecular disulfide bridge formation (SEC traces in **Figure 40A** and **B**, black curves).

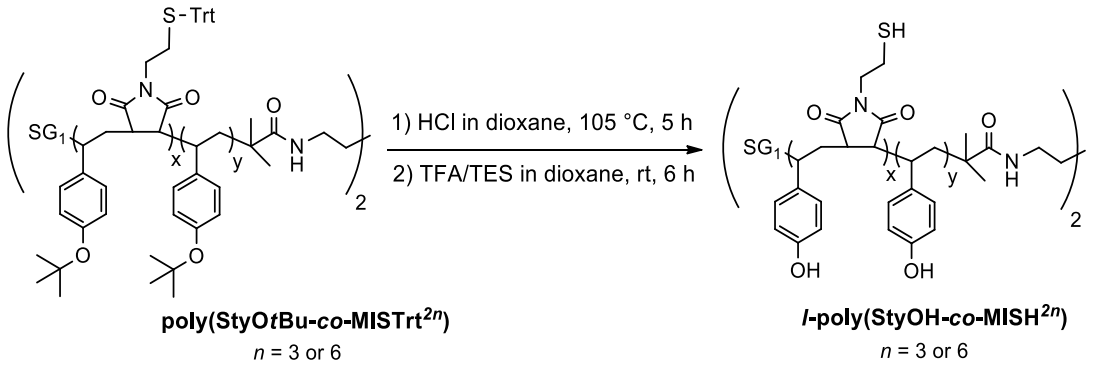

Scheme 27. Synthetic strategy toward the deprotection of 4-*tert*-butoxystyrene repeated units achieved by HCl catalysed hydrolysis at high temperature, followed by detritylation of thiol moieties in presence of TFA and scavenger, leading to the fully deprotected linear precursors *l*-poly(StyOH-*co*-MISH^{2n}).

- **Formation of intramolecular crosslinking by disulfide bridge**

The following step consisted in the formation of intramolecular crosslinking bonds based on thiol oxidation into disulfide bridges to generate single-chain cyclization. The same reaction

conditions were used as previously reported for intramolecular crosslinking (see section 3.2.3). For both synthesis, linear copolymer precursors (*l*-poly(StyOH-*co*-MISH^{6}) and *l*-poly(StyOH-*co*-MISH^{12})) were added via a syringe pump (48 h of addition) to the reaction mixture containing 5% vol. of DMSO and 5% vol. of DIPEA in a large amount of dimethylformamide (**Scheme 28**). The reaction was stirred for 8 days at room temperature to afford the cyclic copolymers locked by intramolecular disulfide bridges ((*c*-poly(StyOH-*co*-MIS^{6}) and *c*-poly(StyOH-*co*-MIS^{12}), respectively).

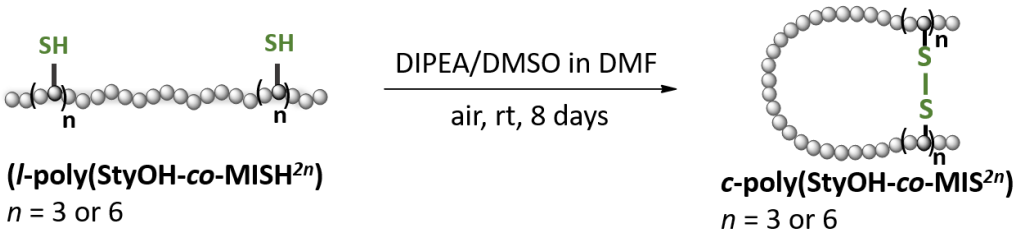

Scheme 28. Schematic illustration of the oxidation reaction conducted in DMF in the presence of DIPEA and DMSO at room temperature for 8 days, leading to the formation of cyclic macromolecules.

Herein, the polymer concentration was, in both cases, kept at 0.2 mg/mL as previously reported. Due to the incorporation of several maleimide units (6 and 12 thiols *per* chain respectively, instead of 2 thiols *per* chain), the thiol overall concentration was significantly increased. Thus, the experimental conditions used here allowed to monitor the thiol-thiol coupling reactions by Ellman's test. During the crosslinking reaction of the copolymer *l*-poly(StyOH-*co*-MISH^{6}), aliquots were taken after the end of polymer addition and Ellman's test were conducted to directly follow the decrease of the thiol concentration. **Figure 38** shows the resulting UV-VIS spectrum of Ellman's test performed on different aliquots. A substantial decrease of the absorbance was observed with time, which suggested that thiol groups were consumed. Interestingly, this monitoring demonstrated that the reaction proceeded slower than expected since traces of thiols were remaining after 5 days ($A < 0.03$). Nevertheless, quantitative consumption of thiol groups was not expected. Indeed, in this cases, several thiol groups (3 or 6 in average) were located on each side of the macromolecular chain. Such synthetic system could then undergo 3 different pathways when the oxidation reaction of thiol to disulfide bridge was performed (**Figure 39**): 1) Thiol group could react intermolecularly with a thiol located on another polymer chain and would lead to the formation of chain dimer. 2) Thiol group could react intramolecularly with a thiol located near the opposite chain-end of the same macromolecule, which would result in an "end-to-end" chain cyclization. 3) Thiol group could react intramolecularly with a neighbouring thiol present on the same side of the macromolecule and lead to a "one-side chain" cyclization of the macromolecule.

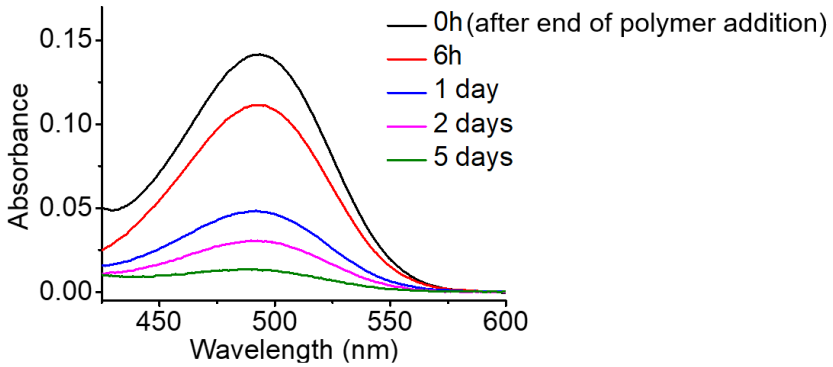

Figure 38. UV-Vis spectrum of Ellman's test performed on aliquots taken at different times after polymer addition during the crosslinking reaction.

Thus, it is reasonable to assume that the ideal pathway (2) consisting to form 3 or 6 intramolecular "end-to-end" disulfide bridges, respectively, cannot occur quantitatively. Moreover, the synthesized sequence-controlled macromolecules probably contained some defaults in the microstructure, resulting in a significant fraction of macromolecules which do not exhibit perfectly 3 or 6 thiol-functionalized maleimides on each side of the polymer chain. An error of ±1 inserted maleimide is expectable on each side of macromolecules Therefore, when thiol groups reacted intermolecularly (pathway 1) or possibly reacted with neighbouring thiol (pathway 3),it is highly possible that free thiols could remain unreacted on the polymer chain. Thus, a fraction of thiol could not be able to generate disulfide bond and quantitative oxidation was not expected.

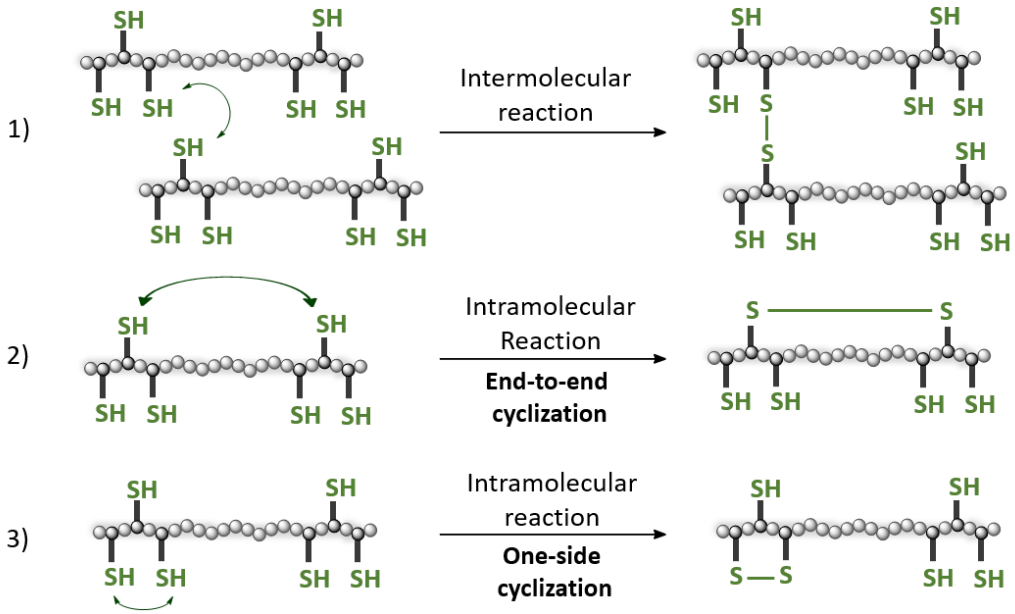

Figure 39. Schematic illustration of the possible pathways of thiol oxidation to disulfide bridge during the cyclization reaction of the sequence-controlled copolymers containing local copolymer segments (Example with the copolymer containing 3 thiols in average *per* chain-side of macromolecules).

The isolated cyclic macromolecules (*c*-poly(StyOH-*co*-MIS^{6}) and *c*-poly(StyOH-*co*-MIS^{12}), were characterized by SEC in DMAc. In both cases, similar SEC chromatograms were recorded before and after the crosslinking reaction (**Figure 40A** and **B**). A shift toward higher elution volume, which would indicate single chain compaction, could not be observed. However, intermolecular reactions did not seem to occur in either reactions, since the limited shoulders in higher molecular regions were nearly unchanged. The absence of chain dimers strongly suggested that either "end-to-end" or "on side" cyclic chains could have occurred, but evidence of any intramolecular disulfide bridge formations remained not obvious due to the high molecular weight of macromolecules. Thus, the copolymers were transformed into brush polymers for conformation analysis by AFM.

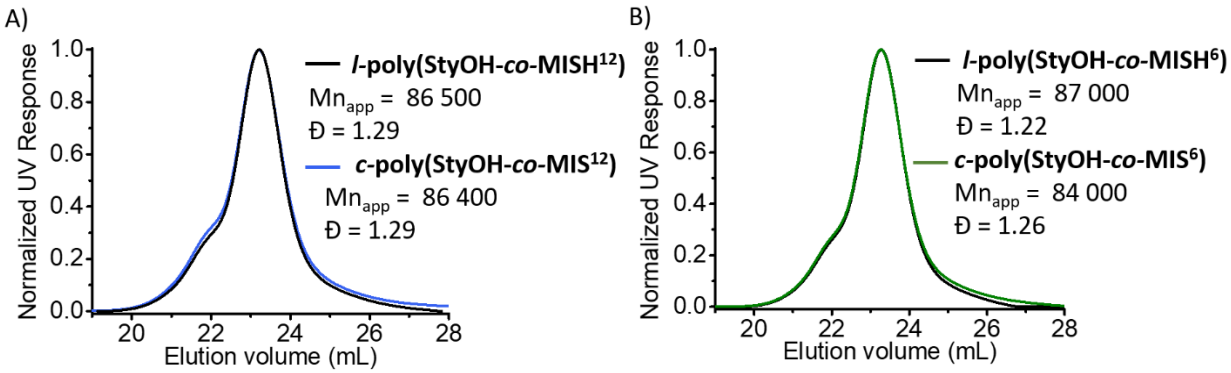

Figure 40. A) SEC traces of the linear precursor *l*-poly(StyOH-*co*-MISH^{12}) (black curve) and the resulting copolymer *c*-poly(StyOH-*co*-MIS^{12}) (blue curve) after thiol-thiol coupling reaction. B) SEC traces of the linear precursor *l*-poly(StyOH-*co*-MISH^{6}) (black curve) and the resulting copolymer *c*-poly(StyOH-*co*-MIS^{6}) (green curve) after oxidation(SEC in DMAc).

- **Transformation into brush polymers**

The obtained polymers were converted into brush polymers by using the «grafting from» approach. First, the polymer backbones were esterified with bromopropionyl bromide to introduce pendant α-bromoester groups on the 4-hydroxystyrene repeated units to afford the corresponding macroinitiators (*c*-poly(StyBr-*co*-MIS^{6}) and *c*-poly(StyBr-*co*-MIS^{12})). Then, ATRP polymerization of *n*-butyl acrylate was performed on each macroinitiator to grow side chains and lead to the corresponding cyclic bottlebrush polymers with poly(*n*BuA) side chains (*c*-poly[(Sty)$_{420}$-*g*-poly(*n*BuA)$_{20}$]^{6} and *c*-[poly(Sty)$_{430}$-*g*-poly(*n*BuA)$_{16}$]^{12} respectively). Synthesis and characterizations of the cyclic brush polymers are summarized in **Table 5**. Entry *1* corresponds to the polymerization conditions and analysis of the ATRP process conducted on the macroinitiator *c*-poly(StyBr-*co*-MIS^{6}), leading to the clean synthesis of the cyclic brush *c*-poly[(Sty)$_{420}$-*g*-poly(*n*BuA)$_{20}$]^{6}. Entry *2* corresponds to the synthesis and characterization of the ATRP polymerization of *n*-butyl acrylate performed on the cyclic macroinitiator

c-poly(StyBr-*co*-MIS^{12}), leading to the cyclic brush polymer *c*-[poly(Sty)$_{430}$-*g*-poly(*n*BuA)$_{16}$]^{12}. For both ATRP processes, the polymerizations were carefully stopped at low conversions (4-5%) to avoid undesired radical coupling side reactions. The obtained brush polymers were characterized by proton spectroscopy and SEC chromatography. ^{1}H NMR indicated the appearance of signals corresponding to the resonance of *n*-butyl acrylate repeated units, while the signals attributed to the polystyrene backbone remained unchanged (NMR spectrums in section 6.4, **Figure 99** and **Figure 102**).

Table 5. Synthesis and characterizations of the cyclic bottlebrush macromolecules (*c*-[poly(Sty)$_x$-*g*-poly(*n*BuA)$_y$]^{2n}).[a]

Entry	Macroinitiator	Conv. *n*BuA [b]	Conv. *n*BuA [c]	DP_n[d]	$M_{n,\,app}$[e]	Đ [e]
1	*c*-poly(StyBr-*co*-MIS^{6})	0.050	0.052	20	350000	1.43
2	*c*-poly(StyBr-*co*-MIS^{12})	0.050	0.032	16	263000	1.52

[a] Polymerization conducted at 80°C in methyl ethyl ketone (10% vol compared to monomer volume) with the ratio [Br: CuBr: PMDETA: $CuBr_2$: *n*BuA] = [1: 0.5: 0.525: 0.025: 400]. [b] Monomer conversion calculated by ^{1}H NMR in $CDCl_3$. [c] Monomer conversion calculated by gravimetry. [d] Average DP_n of poly(*n*-butyl acrylate). [e] Determined by SEC in DMAc.

Regarding the SEC analysis, similar elugrams of the one corresponding to the previous synthesized brush copolymer (n = 1) were obtained. Both chromatograms indicated a main polymer peak with a shoulder at the high molecular weight flank and a shoulder at the low molecular weight flank, which increased the molecular weight distribution of the resulting brush polymers (**Table 5** and **Figure 41**). Regarding the high molecular weight population in both elugrams, it must be pointed out that stopping the polymerization at lower monomer conversion allowed to decrease considerably radical-radical coupling side reactions and to limit additional formation of chain dimers.

Because SEC analysis could only indicate the presence of three distinct polymer populations in the overall sample, an additional study was performed to gain insights into the composition of the obtained brush polymer samples. The sample *c*-[poly(Sty)$_{430}$-*g*-poly(*n*BuA)$_{16}$]^{12} was subjected to reduction, to evidence the presence of any disulfide bridges. The reduction of intramolecular disulfide bridges could lead to a ring chain-opening.

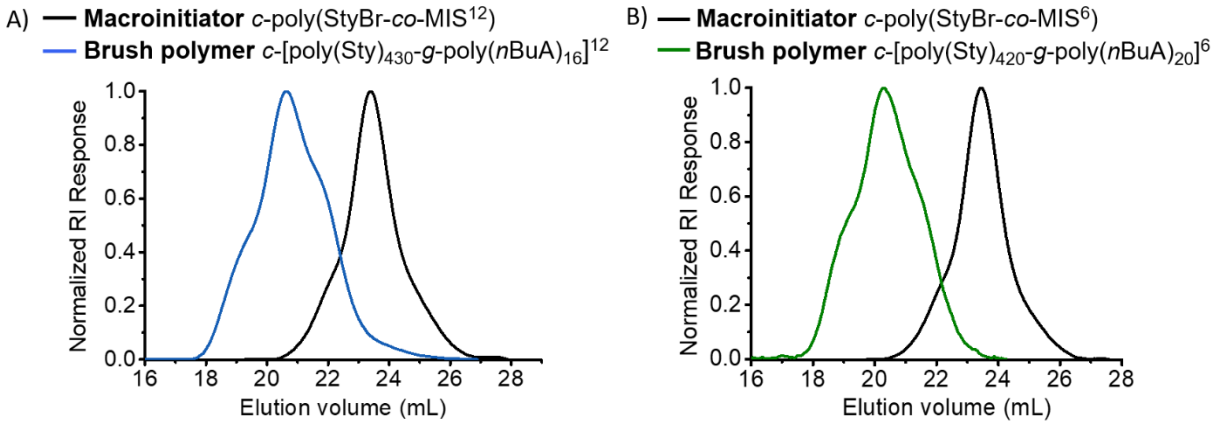

Figure 41. A) SEC traces of the macroinitiator *c*-poly(StyBr-*co*-MIS^{12}) (black curve) and the resulting cyclic brush polymer *c*-[poly(Sty)$_{430}$-*g*-poly(*n*BuA)$_{16}$]^{12} (blue curve). B) SEC traces of the macroinitiator *c*-poly(StyBr-*co*-MIS^{6}) (black curve) and the resulting cyclic brush polymer *c*-[poly(Sty)$_{420}$-*g*-poly(*n*BuA)$_{20}$]^{6} (green curve).

Such reverse topological transformation might induce an increase of the polymer hydrodynamic volume, which can be tracked by SEC chromatography and evidence indirectly a polymer cyclization. For this purpose, dithiothreitol (DTT) was used as reducing reagent in excess (400 equiv) and the reaction was conducted for 4 days under inter atmosphere. The reaction was performed in the solvent mixture DMAc/LiBr in quite diluted conditions in the aim to allow direct analysis by SEC chromatography and track the reaction. Very small changes in the SEC chromatogram could be observed over time. The shoulder at the low molecular weight flank of the main peak slightly shifted to lower elution volume, reflecting an increase of the hydrodynamic volume (**Figure 42**). This observation potentially suggested the presence of intramolecular disulfide bridges. A broadening and decrease of the high molecular weight shoulder could also be noticed, which indicated that polymer chain dimerization could occur via the formation of intermolecular disulfide bridges. It must be noticed that both shoulders did not fully disappear. The reduction of disulfide bridges by treatment with DTT seemed to proceed slowly even in the presence of a large excess of reducing reagents. The reaction was performed in quite diluted conditions (10^{-5} mM of thiol groups) to directly follow the reduction by SEC analysis. Such reaction conditions could be responsible of the low rate of reaction and potentially result in an incomplete reduction of disulfide bridges. Although this reduction study suggested the presence of intermolecular and intramolecular disulfide bridges in the obtained brush polymers, this short investigation certainly demands additional analysis to clearly evidence the polymer topologies and characterization by AFM microscopy was performed.

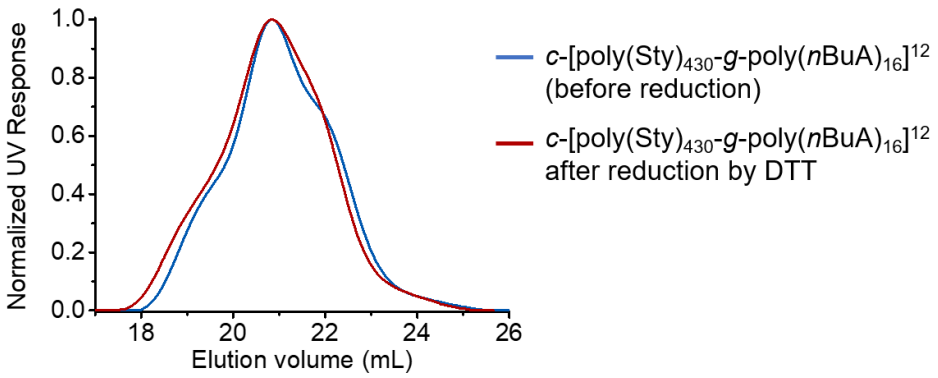

Figure 42. SEC traces corresponding to the cyclic brush polymers *c*-[poly(Sty)$_{430}$-*g*-poly(*n*BuA)$_{16}$]^{12} before reduction (blue curve) and after reduction by DTT(red curve) in dimethylacetamide.

- **Macromolecular imaging by Atomic Force Microscopy**

For AFM studies, the samples were prepared by spin-coating a dilute solution of brush polymers on a freshly cleaved mica substrate. **Figure 43A** and **Figure 44A** show the AFM images recorded for the brush polymers *c*-[poly(Sty)$_{420}$-*g*-poly(*n*BuA)$_{20}$]^{6} and *c*-[poly(Sty)$_{430}$-*g*-poly(*n*BuA)$_{16}$]^{12} respectively. Both micrographs revealed clear visualization of the nano-objects. Most of the individual brush macromolecules exhibited linear worm-like structures and only few cyclic topologies could be observed, which meet the interpretations of the SEC analysis. The non-homogeneity in size reflected also the broad size distribution. A statistical analysis of the AFM image of sample *c*-[poly(Sty)$_{420}$-*g*-poly(*n*BuA)$_{20}$]^{6} showed that the average contour length and the uncorrected full width at half maximum (FWHM) of linear brush polymers were determined to be approximatively 95 ± 15 nm and 15 ± 3 nm respectively. These values meet the theoretical dimensions of the length of a polymer backbone of DP_n = 420 (420 × 0.24 = 100.8 nm) and the average width for polymer side chains of DP_n = 20 (2 × 20 × 0.24 = 10.0 nm), which confirmed that the linear polymers are mainly single polymer chains and not dimers. Concerning the cyclic macromolecules, cross-section profiles of the cyclic objects were performed on each and are shown in **Figure 43B**. It appeared that in this case, the diameters of the observed rings were slightly differing, ranging from 21 nm to 29 nm approximatively. This dimension window fitted with the calculated diameter value estimated of 30 nm for a fully extended cyclic morphology with a contour length morphology of 95 nm. This comparison suggested that even if the polymer ring diameters were varying in size, all of them were single chain cyclic macromolecules. The difference of diameter could be explained by the different positions of thiols within the polymer chain since 3 thiols were inserted on both side in a relatively large statistical window composed of 25 styrene units.

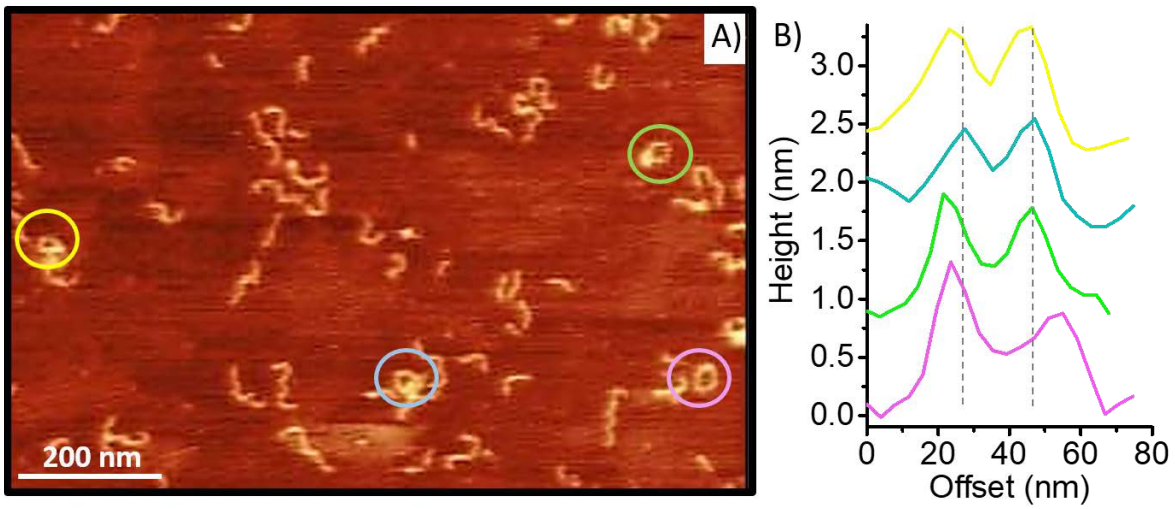

Figure 43. A) AFM height micrograph of the brush polymer *c*-[poly(Sty)$_{420}$-*g*-poly(*n*BuA)$_{20}$]^{6}. B) Cross-section profiles from horizontal scans of the representative cyclic structures observed in image A).

Regarding the AFM image of the sample *c*-[poly(Sty)$_{430}$-*g*-poly(*n*BuA)$_{16}$]^{12}, a statistical analysis of the linear nano-objects indicated that the average contour length and the uncorrected full width at half maximum (FWHM) of brush polymers were in the range of 97 ± 16 nm and 12 ± 5 nm respectively. This values meet the expectations for the fully extended linear brush polymers dimensions, theoretically estimated at approximatively 103 nm and 7 nm respectively. Concerning the observed cyclic polymers, cross-section profiles were performed for each found polymer rings and the experimental diameters were ranging from 16 nm to 37 nm, which were similar values than the calculated diameter estimated of 31 nm for a polymer chain with a contour length of 96 nm (**Figure 44B**). The different thiol positions, particularly in this case where the statistical window of maleimide insertion was rather broad, could explain the visualization of cyclic brush macromolecules exhibiting smaller diameters. However, the experimental diameter window was significantly large, suggesting that chain dimer cyclization could also have occurred. Moreover, it seemed that the found cyclic polymer chains significantly differed in shape, exhibiting either a cyclic topology or P-shape topologies. Because the experimental diameters meet the range of the theoretical diameter value for one single cyclic macromolecules, it appeared that P-shape polymers could also partially arise from the dimerization of one linear polymer chain with a cyclic chain (cyclic brush polymer highlighted with purple colour).

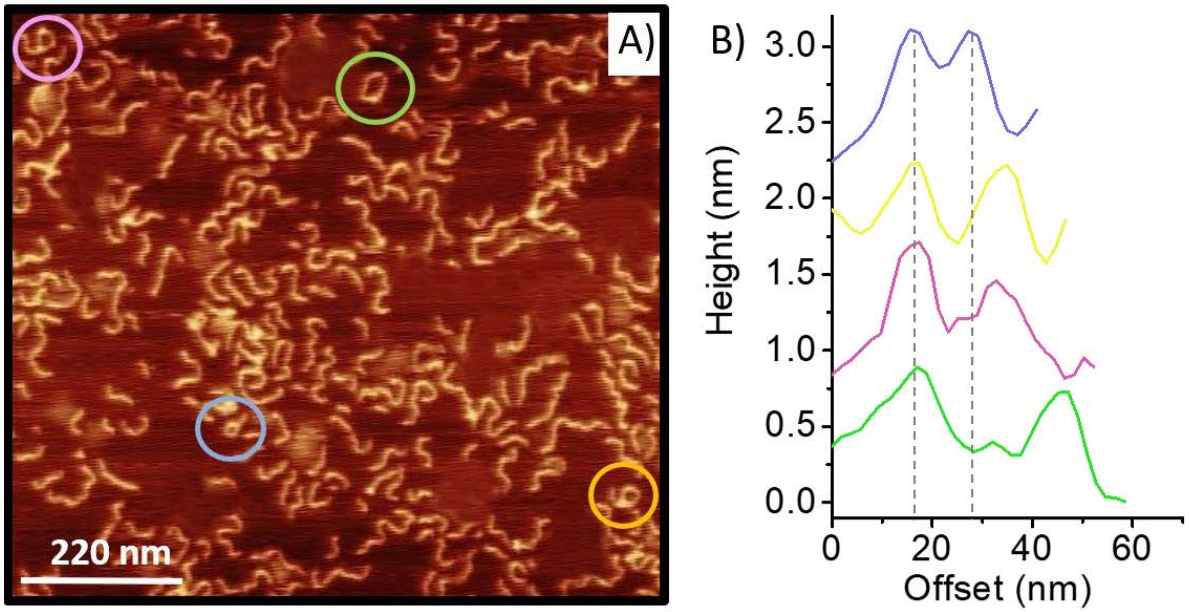

Figure 44. A) AFM height micrograph of the brush polymer *c*-[poly(Sty)$_{430}$-*g*-poly(*n*BuA)$_{16}$][12]. B) Cross-section profiles from horizontal scans of the representative cyclic structures in image A).

According to the AFM characterizations, it appeared that the copolymer with $n = 3$ allowed the preparation of uniform cyclic polymers while cyclization of the analogue copolymer with $n = 6$ resulted in different polymer ring sizes and shapes, reflecting a significant loss of structural control and uniformity. Moreover, it seemed that a better ratio of cyclic brush polymers (*vs.* linear analogue) was found when the sequence-controlled copolymer with $n = 3$ was exploited. Although, AFM characterizations of both synthesis suggested a slight improvement in the statistic of visualised cyclic nano-objects compared to the previous multi-step synthesis (with $n = 1$), the fraction of cyclic macromolecules remained low and most of the macromolecules exhibited linear topology. In this study, it is reasonable to believe that oxidation of thiols into disulfides were mainly occurring between two neighbouring thiols, leading to the formation of "one-side" cyclic polymers. Such resulting cyclic topology are expected to be visualized as worm-like structures by AFM, since the potential cycles within the polymer chain are too small to be observed. It is within reason that the oxidation of two neighbouring thiols is kinetically favoured for proximity reason compared to the oxidation of two thiols positioned at opposite chain-end. This hypothesis concurred with the fact that more cyclic nano-objects were statistically visualised after the multi-step synthesis conducted with the copolymer containing 3 + 3 thiol groups. Indeed, the copolymer exhibiting 6 + 6 thiols is statistically more prompt to "one-side" cyclization during the crosslinking reaction, since a higher amount of thiols, on one chain side, are located at proximity to another.

This investigation demonstrated that, while the insertion of thiol-functionalized maleimides was increased on both side of the macromolecules, linear brush polymers remained the main macromolecular topology of the overall samples. Nevertheless, this study based on the modification of the first step of the multi-step synthesis, allowed to progress in the understanding of the issues and the challenges: 1) It appeared that inserting 3 thiol units on both sides of the polymer chain ensured the incorporations of thiol moieties at the desired positions and seemed to slightly improve the "end-to-end" cyclic polymers statistic with narrow structural deviation. 2) The investigation conducted on the reduction by DTT suggested that the obtained cyclic polymers were produced via intramolecular disulfide bridge formations. 3) For kinetic reason, the formation of disulfide bond *via* neighbouring thiols appeared to be the main oxidation pathway and seemed, as expected, to be more pronounced in the crosslinking reaction performed with the copolymer containing 6+6 thiol groups. This last aspect concurred with the second general hypothesis, which suggested that thiol-thiol coupling in large macromolecules is rather challenging because of proximity issue. Indeed, regarding the previous multi-step synthesis conducted on copolymer $n = 1$, it was hypothesized that the thiols could be only converted into their intermediate species (sulfenic acid) and not into disulfide due to the absence of thiols at close distance. Herein, it is believable that "one-side" chain cyclization was favoured since the potential sulfenic acids intermediate species could be easily converted into disulfide with neighbouring thiols.

At this stage, it became evident that the major issue toward the obtention of cyclic brush polymers originates from the intramolecular crosslinking reaction step of the total synthesis. Regardless of the amount of inserted thiol groups within the linear macromolecule, the "end-to-end" polymer chain cyclization remained, in all cases, difficult to achieve due to the high molecular weight of the polymer chain. Therefore, the 4th step of the multi-step synthesis consisting in the formation of intramolecular disulfide bridge was investigated to evaluate the challenges and attempts to optimize the yield of cyclic polymers after the overall synthesis were performed.

3.2.6.2. Optimization of intramolecular crosslinking reaction

The hypothesis based on the low efficiency of the intramolecular "end-to end" crosslinking reaction step was studied. In this current work, the formation of disulfide bond within a high molecular weight polymer chain is targeted. Intramolecular thiols groups, located at opposite sides of the polymer chain required primarily to diffuse, therefore, to be at proximity to form

desired intramolecular disulfide bridges. However, the ease of macromolecule motion in solution increases inversely with the polymer molecular weight.[267] Due to the significant distance between intramolecular thiol groups and the probable limited motion in solution of these copolymers ($DP_n \approx 400$), it was reasonable to assume that the crosslinking reaction between two thiols far from each other is kinetically not favoured.

The first optimization attempt consisted to increase the reaction time. This investigation was performed with the sequence-controlled copolymers with $n = 3$, to ensure the presence of thiols on each side of the macromolecules. In such copolymers, it was reasonable to assume that intramolecular thiol-disulfide interchange could occur if the reaction time was increased, with the aim to convert "one-side" cyclic polymers into "end-to-end" cyclic polymers (**Scheme 29**). This reaction relies on the nucleophilic attack a thiolate (RS^-) on one of the sulfur atoms of the disulfide to produce a new disulfide bond while a free thiolate is released.[268,269] It seemed plausible that "one-side" chain cycle displayed higher tension in the backbone from the forced curving compared to an "end-to-end" chain cycle. Hence, the use of the thiol-disulfide interchange was believed to direct the formation of "end-to-end" cyclic chain which should be thermodynamically favoured. Thus, increasing the reaction time could promote thiol-disulfide interchange and lead to a higher statistic of visualizable cyclic brush polymers.

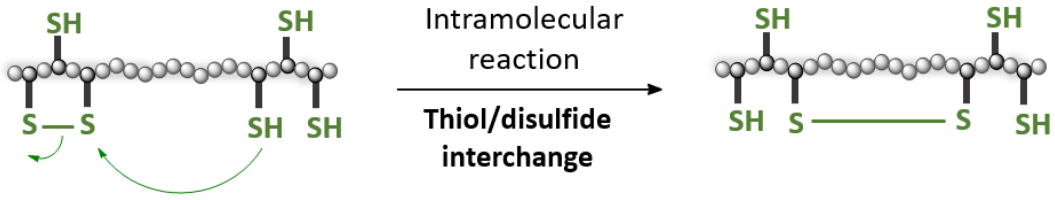

Scheme 29. Proposed thiol-disulfide intramolecular interchange toward the formation of "end-to-end" chain cyclization.

- **Effect of reaction time**

This investigation was conducted by using the fully deprotected copolymer *l*-poly(StyOH-*co*-MISH^6). In the previous multi-step synthesis, the intramolecular crosslinking reaction was stirred for 6 days in a large amount of DMF (0.2 mg copolymer/mL) in the presence of DMSO (5% vol.) and DIPEA (5% vol.). Similar experimental conditions were used to induce the cyclization of *l*-poly(StyOH-*co*-MISH^6), and the reaction was stirred for 3 weeks to afford potential cyclic polymers (*c*-poly(StyOH-*co*-MIS)$^{6\text{-a}}$) (**Scheme 30**).

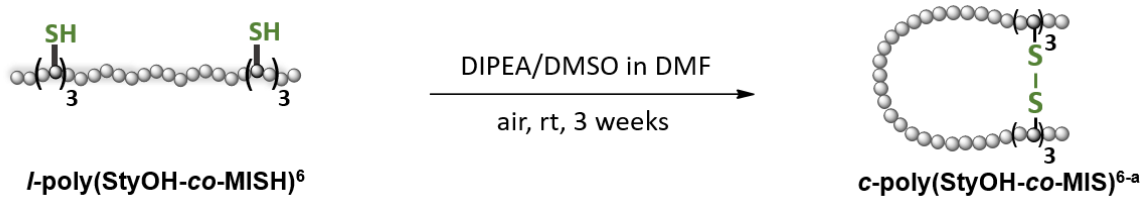

Scheme 30. Schematic illustration of the cyclization reaction of *l*-poly(StyOH-*co*-MISH)^{6} induced by thiol oxidations to disulfide bridge in DMF with the presence of DMSO and base for 3 weeks at room temperature to induce thiol oxidation to disulfide and potential thiol-disulfide interchanges.

The resulting copolymer was characterized by SEC chromatography. No change in the resulting SEC chromatogram could be observed before and after crosslinking reaction (see section 6.3.19). At this stage, it appeared that the time of reaction did not affect significantly the formation of either intermolecular or intramolecular disulfide bonds. The obtained copolymer was transformed into brush polymers by using the previously described «grafting from» approach (See section 6.3.19). Pendant α-bromoester groups were introduced on the copolymer *c*-poly(StyOH-*co*-MIS)$^{6\text{-a}}$ by esterification of the 4-hydroxystryrene repeated units with bromopropionyl bromide to yield in the ATRP macroinitiator. Polymerization of *n*-butyl acrylate monomer was conducted on the obtained macroinitiator to afford the corresponding cyclic brush polymer (*c*-[poly(Sty)$_{420}$-*g*-poly(*n*BuA)$_{20}$]$^{6\text{-a}}$) with an average DP_n side chain of 20 units. The SEC chromatogram indicated again a main polymer peak with minor shoulders in the high molecular and low molecular weight flanks of the peak, potentially corresponding to liner chain dimers, linear single polymer chains and cyclic single polymer chains.

AFM microscopy was used to characterize the obtained brush polymer *c*-[poly(Sty)$_{420}$-*g*-poly(*n*BuA)$_{20}$]$^{6\text{-a}}$ and evaluate the effect of crosslinking reaction time on the cyclic polymer statistic. The brush macromolecules could be successfully visualized (**Figure 45**). It appeared that single linear chains remained the dominant brush polymer population but interestingly, more individual cyclic brush could be observed. All obtained cyclic nano-objects exhibited similar cyclic architecture and dimensions, with an average diameter estimated to be approximatively 28 nm. This value meet the range of the theoretical diameter estimated of approximatyvely 32 nm for a fully extended cyclic structure of a polymer chain with a DP_n backbone of 420 units. It appeared that a larger amount of cyclic nano-objects could be visualized with an approximative statistic of 5% of cyclic structure. Thus, it seemed that increasing the reaction time moderately improved the yield of folded macromolecules.

This observation concurred with the previous explanation, in which thiol-disulfide interchange could potentially shuffle the installed disulfide bonds and direct the formation of

"end-to-end" chain cyclization for thermodynamic reasons. Nevertheless, linear brush macromolecules remained the main topological population in the resulting brush polymer sample. The crosslinking reaction was stirred for approximatyvely 3 weeks in highly diluted conditions, which strongly suggested that either the reaction rate of the oxidation of thiols into disulfide bonds was slow, or the thiol/disulfide shuffling was slow. In this study, the crosslinking reaction was investigated by using the sequence-controlled polymer exhibiting 3 + 3 thiols on each side of the macromolecules.

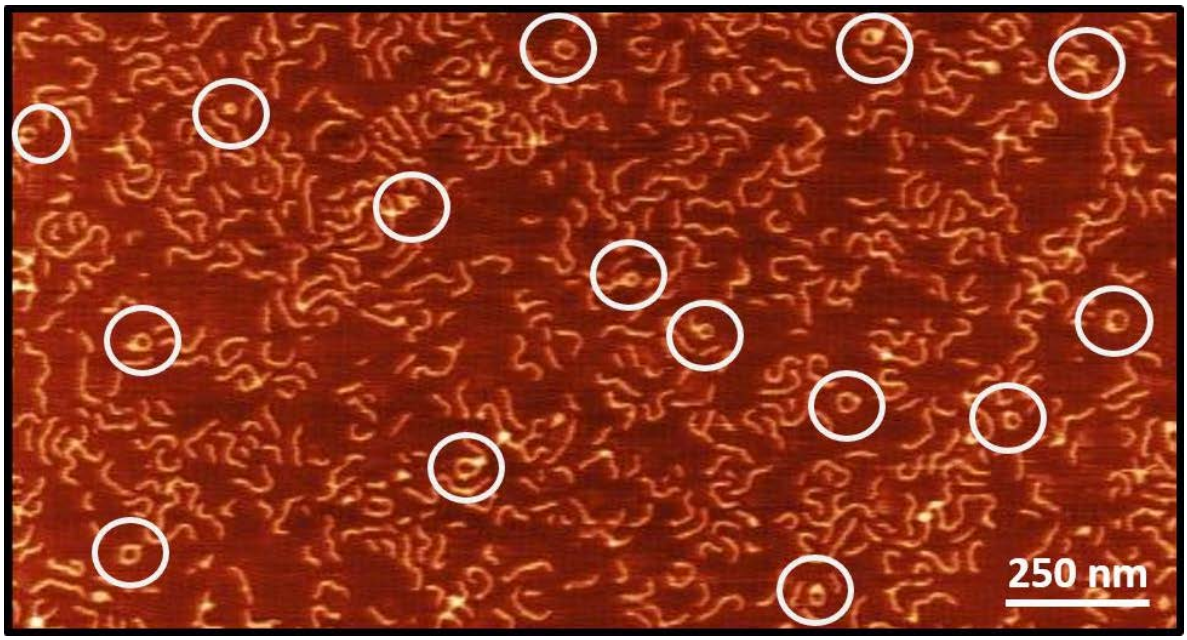

Figure 45. AFM micrograph of the brush polymers *c*-[poly(Sty)$_{420}$-*g*-poly(*n*BuA)$_{20}$]$^{6\text{-a}}$ (height image)at the end of the multi-step synthesis, in which the crosslinking reaction was conducted for 3 weeks in DMF to induce thiol-disulfide interchange and direct "end-to-end" chain cyclization.

It was reasonable to assume that the oxidation of two neighbouring thiols into disulfide bonds could occurred efficiently within 3 weeks, and lead to "one-side" chain cyclization. Thus, the reaction rate of thiol/ disulfides exchange with this reaction conditions was believed to take place slowly and therefore could not lead to a considerable improvement in the statistic of cyclic polymers. Indeed, such dynamic reaction highly relies on the proximity between, the frustrated thiols located on one chain-end, with the opposite "one-side" disulfide bridges, and on the polymer diffusion in solvent reaction.

A second investigation was performed, by switching the reaction solvent. The polymer conformation and motion, as well as the considerable distance between two reactive thiols located on each side of the polymer chain could potentially decrease the rates of the crosslinking reaction and also the eventual thiol disulfide interchange reaction. So far, the

intramolecular crosslinking reaction was conducted in DMF as solvent. It is reasonable to assume that changing the solvent could result in different polymer conformations in solution or different ease of motion, and therefore, could have an influence on the formation of intramolecular "end-to-end" disulfide bonds.

- **Solvent effect**

Dimethylformamide is a good solvent for poly(4-hydroxystyrene) polymer chain. The greater the affinity of solvent for polymer, the larger will be the sphere, that is, the hydrodynamic volume.[270] In this case, the poly(4-hydroxystyrene) macromolecule seemed to exhibit a large hydrodynamic volume in DMF. Indeed, after the second step of the multi-step synthesis (deprotection of 4-*tert*-butoxystyrene repeated units into 4-hydroxystyrene), the resulting polymers were analysed by SEC in DMAC, and a shift of the polymer peak to higher elution volume was expected after removal of the *tert*-butyl fragments. However, a shift to lower elution volume was noticed, indicating a higher hydrodynamic volume. This observation reflected a potential swelling of the polymer chain due to polymer-solvent interaction via hydrogen-bond interaction (H-bond) in dimethylacetamide, which is a very similar solvent to DMF. Thus, it seems reasonable to assume that during the crosslinking reaction conducted in DMF, the linear polymers were swollen with solvent molecules and the positions of two intramolecular thiols at requested proximity could be even more challenging. Moreover, polymer-solvent interactions could also limit the motion of the polymer chain and using a solvent without H-bond acceptor motif (in general carbonyl groups) could prevent the formation of H-bond with the 4-hydroxystyrene repeated units of the polymer backbone. Consequently, according to these observations, it seemed that the use of DMF as solvent could have an important impact on the intramolecular crosslinking reaction rate and yield.

A solvent switch could lead to significant change in the overall polymer hydrodynamic volume and chain conformation.[271] Conducting the cyclization process under theta solvent conditions could promote the formation of intramolecular crosslinks over intermolecular bonds. In such solvent, solvent–polymer interactions decrease and thus polymer-polymer interactions become more important, leading to a contraction of the hydrodynamic volume.[270] The more compacted macromolecular chain and smaller radius of gyration (R_G) could favour the intramolecular thiols to be at requested proximity.[190] Methanol was selected to conduct the crosslinking reaction since poly(4-hydroxystyrene) chains are soluble in this solvent. Moreover, it has been shown that due to hydrogen-bond interactions

formed between methanol and DMSO, a reduction of the electron density on the sulfur atom of DMSO, makes the attack by a thiol group more accessible.[253] Therefore, the use of methanol could also accelerate the first reaction step generating thiol-sulfoxide adducts. The crosslinking reaction in methanol was investigated with the fully deprotected copolymer (*n* = 3, *l*-poly(StyOH-*co*-MISH^6)) as linear precursor. Reactions conditions and characterizations are summarized in **Table 6**. The cyclization process was monitored by SEC in dimethylacetamide (DMAc). In a first attempt, similar reaction conditions were used as previously described and only the reaction solvent was changed, from DMF to methanol. The polymer was added in one portion to the flask containing methanol, DMSO and DIPEA. The reaction was stirred for 6 days at room temperature (**Table 6**, **entry *b***). After reaction, the SEC chromatogram showed a bimodal molecular weight distribution. The measured $M_{n,\,app}$ of the high molecular weight peak is approximatively the double of $M_{n,\,app}$ exhibited by the second peak ($M_{n,\,app\,(first\,peak)}$ = 188000 *vs* $M_{n,\,app\,(second\,peak)}$ = 89000). Mainly intermolecular crosslinks were formed, resulting in the formation of chain dimers (**Figure 46**, red curve). This result was very encouraging since the conversion of thiols into disulfide groups seemed to occur to a large polymer fraction. To favour the formation of intramolecular disulfide bond and reduce intermolecular side reaction, a second attempt was performed by adding dropwise a solution of polymer to the flask containing methanol, DMSO and DIPEA. After the complete addition of polymer into the mixture, the reaction was stirred for 6 days at room temperature (**Table 6**, **entry *c***). SEC traces indicated a reduction of the shoulder at the high molecular weight flank of the peak, suggesting a decrease of intermolecular disulfide bond formation (**Figure 46**, green curve). It seemed that slowing down the addition of polymer into the reaction mixture could not fully prevent intermolecular crosslinking reaction, probably because of a low reaction rate. Thus, either the reaction required higher diluted conditions or required some optimization to increase the rate. According to the literature, it was shown that increasing both the reaction temperature and the amount of DMSO clearly accelerated the thiol-thiol coupling into disulfide bond in methanol with an excess of DIPEA.[253] Thus, in the following attempt, the polymer was added dropwise to a mixture containing a larger ratio of DMSO (30% volume) in methanol. The reaction was conducted at 40 °C, for 5 days in the aim to minimize polymer-polymer coupling by increasing the reaction rate (**Table 6**, **entry *d***). A slight improvement could be noticed in the SEC chromatogram, since the shoulder peak corresponding to the chain dimer decreased (**Figure 46**, blue curve). However, no shift toward higher elution volume could be observed, and thus, no evidence of the formation of cyclic polymer could be obtained.

Table 6. Reaction conditions and characterizations of the crosslinking reaction in methanol to afford the cyclic copolymers *c*-poly(StyOH-*co*-MIS)$^{6\text{-}x}$.

Entry (x)	DMSO (% vol.)	Temperature (°C)	Polymer Concentration (M)	$M_{n,\,app}$ [a]	Đ [a]
b	5	rt	5 x 10^{-5}	82000	1.69
c	5	rt	5 x 10^{-5} [b]	88200	1.48
d	30	40 °C	5 x 10^{-5} [b]	86000	1.44

[a] Determined by SEC in DMAc. [b] Polymer was added dropwise to the solution via a syringe pump.

Performing the crosslinking reaction in methanol suggested that the formation of intermolecular disulfide bond was highly promoted in such solvent. To gain insights into the ratio of produced dimer polymer chains compared to cyclic polymers, the obtained copolymer *c*-poly(StyOH-*co*-MIS)$^{6\text{-}d}$ was then transformed into brush polymers to characterize the crosslinking bond formation by AFM microscopy.

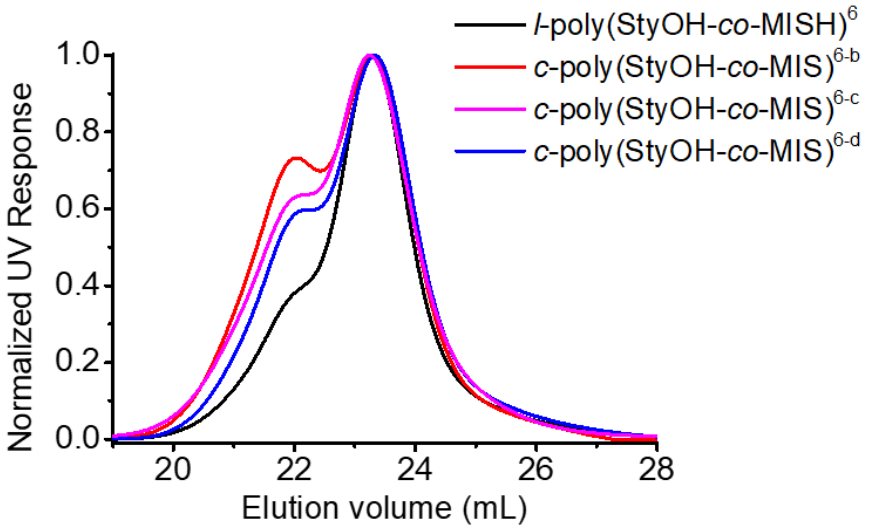

Figure 46. SEC traces of the linear deprotected precursor *l*-poly(StyOH-*co*-MISH)^{6} (black curve) with the obtained cyclic copolymers after oxidation of thiols into disulfide in methanol (Table 6): *c*-poly(StyOH-*co*-MIS)$^{6\text{-}b}$ (red curve), *c*-poly(StyOH-*co*-MIS)$^{6\text{-}c}$ (green curve) and *c*-poly(StyOH-*co*-MIS)$^{6\text{-}d}$ (blue curve).

The copolymer was transformed into brush polymers by using the previously described «grafting from» approach. Polymerization of *n*-butyl acrylate was performed to grow side chains on the macroinitiator and afford a brush polymer (*c*-[poly(Sty)$_{420}$-*g*-poly(*n*BuA)$_{17}$]$^{6\text{-}d}$) with an average DP_n side chain of 17 units. The brush polymer was successfully characterized by proton spectroscopy and SEC chromatography, evidencing the full conversion of the macroinitiator into brush macromolecules (See section 6.3.20).

AFM microscopy was used to characterize the morphology of the obtained cyclic brush polymer *c*-[poly(Sty)$_{420}$-*g*-poly(*n*BuA)$_{17}$]$^{6\text{-d}}$. The sample was prepared by spin-coating a dilute solution of crude polymer in chloroform (ca. 0.01 mg/mL) on a freshly cleaved mica substrate. As expected, linear polymers chains remained the major fraction of the polymer sample (**Figure 47**). However, an improvement of the statistic of cyclic polymers could be noticed (~10% yield). Regarding the linear macromolecules, an experimental average size of the observed nano-objects was estimated approximately of 180 ± 35 nm, which appeared to be significantly higher than the expected chain length estimated to be 100 nm for a fully extended linear structure with a DP_n of 420 units. Thus, these estimations strongly suggested the large obtention of linear chain dimers. Regarding the dimensions of the cyclic macromolecules, theoretical diameter was estimated in the range of 32 nm for a fully extended cyclic structure with a contour length of 100 nm. However, the AFM micrograph evidenced ring morphologies differing relatively in diameter size. Some cyclic polymers exhibited a diameter in the range of 44 nm (cyclic brush polymers highlighted in green), while a major fraction of rings had an estimated diameter of 25 nm (cyclic brush polymers highlighted in white). These experimental diameters potentially indicated that some cyclic nano-objects were formed by chain dimers. These observations concurred with the SEC chromatogram interpretation. Indeed, it seemed that limiting the swelling polymer chain effect allowed a better macromolecular motion and improved the accessibility of internal thiol groups.

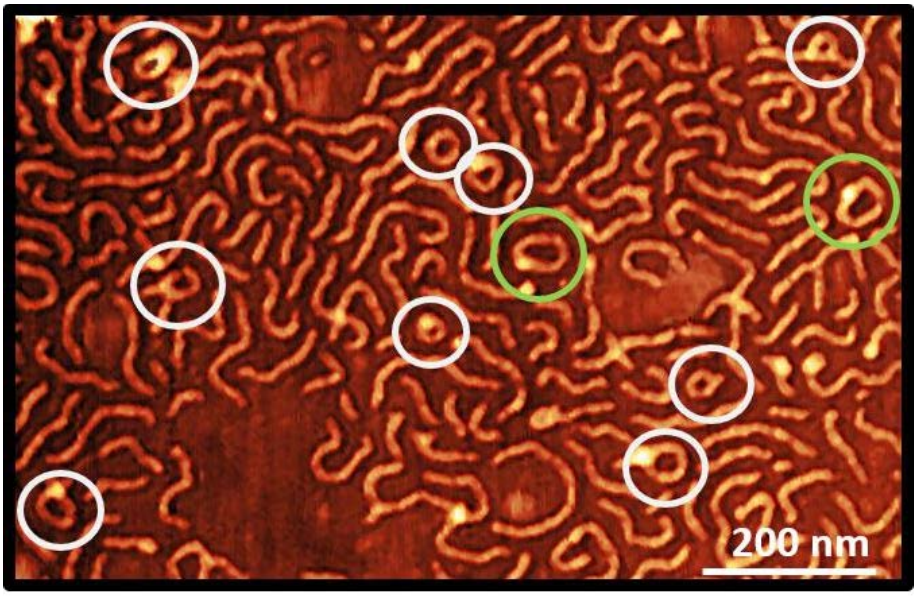

Figure 47. AFM micrograph of the obtained brush polymers *c*-[poly(Sty)$_{420}$-*g*-poly(*n*BuA)$_{17}$]$^{6\text{-d}}$ (height image), showing cyclic single polymer chain (white circle) and potentially cyclic chain dimer (green circle).

The formation of intramolecular end-to-end disulfide bridges was considerably enhanced but a major fraction of linear dimers was obtained, reflecting that mainly intermolecular disulfide bridges were generated. The obtention of dimers could be potentially explained by the kinetics of the competing intermolecular *vs.* intramolecular crosslinking reactions. First, with increasing molecular weight, intermolecular reactions dominate kinetics over cyclization process.[190] Indeed, in the ring-closure approach, the two reactive groups must preliminarily diffuse toward each other to enable subsequently intramolecular crosslinking bond formation. The higher the distance between the reactive groups, the more macromolecular diffusion is required. Secondly, when the functionalities are potentially at requested positions, the crosslink bond formation requires a fast coefficient rate. Otherwise, the functionalities could then diffuse away from each other due to the macromolecule motion and therefore intermolecular crosslinking reaction could be promoted.[190] Herein, the two-step oxidation reaction, as well as the significant distance between intramolecular thiols were potentially favouring the formation of intermolecular disulfide bonds.

At this stage, it could be confirmed that folding high molecular weight polymers remained challenging when the oxidation of thiols into disulfide bridge was performed with the aforementioned experimental conditions. Conducting thiol oxidation via the use of DMSO in methanol resulted in a large fraction of chain dimers formed by intermolecular disulfide bridges and poor cyclic polymers statistic were obtained (up to 10%). Unfortunately, reaction conditions could not be further optimized, indicating an unexpected bottleneck. Nevertheless, the project was successful, as significant progress in understanding of functionality positioning and reactivity of high molecular weight entities have been made. Moreover, this study illustrated the need of additional characterization techniques to differ polymer topology and quantify a statistic of each populations after single polymer chain folding. The characterization of potential cyclic polymers by AFM microscopy was successful and undoubtedly crucial to get a clear evidence of the cyclization process and a statistic of linear *vs*. cyclic macromolecular populations.

4. SUMMARY AND CONCLUSION

Controlled single polymer chain cyclization of fully synthetic macromolecules was investigated by using oxidative dynamic covalent bonds. In order to access new analytic tools and reveal the degree of structural control, cyclic polymers were transformed into cyclic brush macromolecules to enable direct molecular visualization by AFM analysis. The global synthetic concept was primarily established with intermediate molecular weight macromolecules and was subsequently transferred to high molecular weight polymer chains with related difficulties. First, single polymer chain folding was investigated by using positional diselenide bridge to trigger single chain compaction. Controlled radical copolymerization of styrene derivatives with precisely injected amounts of *N*-substituted maleimides bearing protected selenol pendent functions was used to prepare macromolecules, with moderate molecular weight (DP_n = 50) and positioned selenol moieties. The oxidation of selenol groups into the diselenide bridge was exploited to induce controlled intramolecular crosslinking and generate chain cyclization. The ring-closure reaction was successfully characterized by SEC analysis, ^{1}H and 2D NMR spectroscopies. To gain insight into the degree of structural control, a synthetic route consisting in the transformation of the cyclic polymers into cyclic molecular brushes was developed and allowed direct visualization and conformation analysis by AFM. The «grafting from» synthetic approach was initially targeted for the preparation of cyclic brush macromolecules. However, unexpected side reactions of the diselenide moieties got evident as those could not tolerate ATRP process. This was more closely analysed by carefully control reactions, using low molecular weight compounds. The outcome of such study required a modification of the brush synthesis strategy. A synthetic route toward cyclic brush polymers was established by using the «grafting onto» approach by exploiting triazolinedione (TAD) −diene cycloaddition to graft side chain polymers onto the styrenic polymer backbone. Cyclic molecular brushes with different side chains grafting densities were synthesized and AFM characterization was used to investigate the brush polymer morphologies. Round-shape nano-objects could be successfully observed and confirm the obtention of controlled cyclic topology. Nevertheless, the incompatibility of the diselenide formation which only tolerates grafting onto methods requiring intense purification, and the small size of cyclic nano-objects, remained an evident bottleneck toward AFM characterization with high resolution. Thus, a second study was investigated on larger synthetic polymers *via* positional disulfide bridge to induce single chain collapse. While diselenide bond appeared to be incompatible with ATRP process, disulfide group remained inherent to radical

polymerization. Therefore, this oxidative crosslink allowed the use of the «grafting from» approach toward the preparation of brush macromolecules, which is a more straightforward method for subsequent AFM characterizations. Similarly, sequence-controlled polymer exhibiting thiol pendent function at specific positions among the polymer chains was successfully prepared. Thiol oxidation into disulfide bond was then investigated to induce single chain folding. While Ellman's tests qualitatively indicated the substantial consumption of free thiol moieties, the SEC chromatograms could not give conclusive evidence of reduction in hydrodynamic volume that would be indicative of intramolecular cyclization. The potentially cyclic polymers were transformed into brush polymers via the «grafting from» approach to allow AFM microscopy characterization. The brushes could be visualized in molecular resolution confirming a clean multi-step synthesis. Interestingly, only a small number of cyclic polymers were evidenced. Two different hypothesis were investigated. On one hand, going to larger molecular weight could increase statistically the risk that under the given conditions for sequence-controlled polymerizations, the degree of sequence control decreases and not all polymer chains might contain two thiol moieties at requested positions. Thus, a first investigation based on the insertion of more equivalents of thiol fragments during the sequence-controlled polymerization was performed, to ensure the incorporation of thiol moieties at desired positions. The multi-step synthesis was then similarly reproduced but AFM characterization indicated only a slight improvement of cyclic polymer statistic. On the other hand, the thiol-thiol coupling reaction in high molecular weight polymer chains was evidently slower than expected and could be responsible of the obtained low yield of cyclic polymers. Hence, time reaction of the crosslinking step was increased and indicated a clear improvement in the obtention of cyclic macromolecules. Moreover, it appeared that the solvent had a considerable effect on the reaction kinetic. While the linear polymer precursor was swelling and potentially immobilized in dimethylformamide, methanol enabled better diffusion of the thiol groups and a larger fraction of disulfide bridge could be formed. However, intermolecular disulfide bridges were essentially formed, instead of intramolecular disulfide bridges, resulting in the formation of chain dimers. Such investigations evidenced an unexpected bottleneck that could arise from the slow reaction rate of thiol oxidation into disulfide bridge and leading to the formation of competing intermolecular disulfide bridges for kinetic reasons. Nevertheless, the project was rather successful, as significant progress in understanding of both sequence-controlled polymerization for large macromolecules synthesis and crucial parameters impacting on the reactivity of high molecular weight entities have been made.

5. OUTLOOK

With the final aim of fabricating macromolecules exhibiting as advanced functions as natural polymers, gaining insights into the formation and morphological characteristics of simplified folded synthetic systems are crucial steps to move forward. Cyclic polymers are the simplest class of folded macromolecules and should be considered as a first attempt to improve understanding for the production of advanced materials. In this study, a cyclic folded system, induced by the formation of one single positional intramolecular crosslink was targeted. This cyclic polymer was used to further gain in understanding in the developed synthetic approach, as well as into oxidative macromolecular folding and morphology characterization. While controlled single chain compaction with intermediate molecular weight macromolecules was successfully promoted, the attempts conducted with larger macromolecules illustrated that the folding process becomes more challenging as the molecular weight increases. The more distance between the reactive entities, the more intramolecular bond formation efficiency is compromised. It is reasonable to assume that such issue could be overcome in further investigations, by inducing a pre-organization of the linear macromolecules to force the reactive entities to be at required proximity, and form subsequently the desired intramolecular crosslinks. For example, the insertion of H-bond motifs within the polymer chain could be a potential alternative to pre-organize compaction prior to form intramolecular disulfide or diselenide bridges. Although this study primarily focused on the insertion of one single intramolecular crosslink for proof-of-concept, it is believed that such synthetic strategy could allow the controlled insertion of additional oxidative intramolecular bridges within the polymer chain, and lead to the elaboration and characterization of advanced and dynamic macromolecular structures.

Although the simplest folded macromolecular structure was targeted in this study, cyclic polymers are known to exhibit already considerable difference in macroscopic properties compared to their linear analogues. Furthermore, cyclic polymers are interesting candidates for the elaboration of advanced crosslinked network.[272] Indeed, gels based on cyclic polymers often display good tensile strength and a large swelling capacity compared to the gels obtained from cross-linking linear polymers.[272,273] The cyclic polymers obtained in this study could be potential candidates for the fabrication of novel cyclic gels, with possible subsequent photo-responsive degradation due to the presence of dynamic covalent bonds.[274]

6. EXPERIMENTAL PART

6.1. Materials

The following chemicals were used as received, unless otherwise mentioned, and purchased from Abcr, TCI, Acros Organic, Sigma Aldrich, Carl Roth, and Arkema. Hydrazine monohydrate, sodium hydroxide (NaOH), elemental selenium, *p*-methoxybenzyl chloride, sodium borohydride ($NaBH_4$), magnesium sulfate ($MgSO_4$), 2-bromoethylamine hydrobromide, sodium bicarbonate (Na_2CO_3), sodium hydrogen carbonate ($NaHCO_3$), sodium chloride (NaCl), maleic anhydride, anhydrous sodium acetate, acetic anhydride, Bloc builder MA, hydrochloric acid 37%, 2,2′-dithiobis(5-nitropyridine) (DTNP), 5,5′-dithiobis(2-nitrobenzoic acid) (DTNB), hydrogen peroxide (H_2O_2) 30%, bis(2-hydroxyethyl) disulfide, pyridine, 2-bromopionyl bromide, *N*,*N*,*N*′,*N*″,*N*″-pentamethyldiethylenetriamine (PMDETA), copper(i) bromide (CuBr), bromopropanol, silica gel, alumina oxide (Al_2O_3), succinic anhydride, *trans,trans*-2,4-hexadien-1-ol, *N,N*-diisopropylethylamine (DIPEA), citric acid, *N*-(3-dimethylaminopropyl)-*N*′-ethylcarbodiimide hydrochloride (EDC.HCl), *N*,*N*′-dicyclohexylcarbodiimide (DCC), 4-dimethylaminopyridine (DMAP), 4-phenyl-1,2,4-triazoline-3,5-dione, ethyl carbazate, 4-nitrophenyl isocyanate, celite, α-bromoisobutyryl bromide, acetic acid, tris[2-(dimethylamino)ethyl] amine (ME_6TREN), copper (ii) bromide ($CuBr_2$), copper(0) pellets, 1,4diazabicyclo-[2.2.2]octane (DABCO), bromine, 2-aminoethanethiol hydrochloride**,** trityl chloride, *N*-hydroxysuccinimide, 1,4-diaminobutane, bromopropionyl bromide, triethylsilane, dimethylformamide, dichloromethane, hexane, ethanol, diethyl ether, chloroform, cyclohexane, ethyl acetate, anisole, methanol, dioxane, trifluoroacetic acid (TFA), hexane, tetrahydrofuran, dimethylacetamide, acetonitrile, dimethyl sulfoxide, ethyl methyl ketone, benzene.

Tert-butoxystyrene, styrene, anisole and dimethylformamide were passed through an alumina oxide column prior to use. *n*-butyl acrylate was distilled under reduced pressure before use. Dichloromethane was dried over CaH_2 and distilled under argon. Tetrahydrofuran and acetonitrile were dried over 4°A molecular sieves and through anhydrous alumina columns using an Innovative Technology Inc. PS-400-7 solvent purification system.

6.2. Methods/Instrumentations

NMR spectra were measured in chloroform-d1 ($CDCl_3$), dichloromethane-d2 (CD_2Cl_2), dimethyl sulfoxide-d6 (DMSO-d6) and methanol-d4 (CD_3OD). Measurements were performed by using a Bruker Avance III-400 spectrometer (operating at 400 MHz for ^1H NMR and 75 MHz for ^{13}C) and a Bruker Avance III-500 spectrometer (operating at 500 MHz for ^1H NMR and 125 MHz for ^{13}C) from Bruker Biospin GmbH (Rheinstetten, Germany) at room temperature. All chemical shifts are reported in ppm relative to solvent residual signals of the deuterated solvent.

Size Exclusion Chromatography (SEC) with dimethylacetamide (DMAc) as eluent was performed on an Agilent HPLC system equipped with a thermostated column compartment at 50 °C, UV detector and a refractive index detector. The column set consisted of one pre-column PSS GRAM 10 µm and three PSS GRAM columns (30 Å - 10 µm, 1000 Å - 10 µm, 1000 Å - 10 µm) from PSS Polymer Standards Service GmbH). The used solvent was N, N dimethylacetamide containing 1 g/L of LiBr at a flow rate of 1 mL/min. Molar mass and dispersity values were calculated against polystyrene standards.

SEC in tetrahydrofuran (THF) was carried out on a TOSOH System equipped with a UV detector and a refractive index detector. Measurements were performed at a flow rate of 1.0 mL/min at 35 °C in THF. The column set consisted of one pre-column PSS SDV 5 µm and three PSS SDV columns (1000000Å - 5µm, 100000Å - 5µm, 1000Å - 5µm) from PSS Polymer Standards Service GmbH). Commercially available polystyrene (PS) standards were used for calibration. The analytical SEC setup was used to fractionate and purify the crude brush polymers from excess of TAD-terminated P(*n*BuA) chains. The high molecular weight peaks that correspond to the molecular brushes and appear in the SEC traces at elution volumes between 20 to 24 mL were collected manually. One single SEC run was conducted to purify *c*-poly(Sty)$_{50}$-*g*-[poly(*n*BuA)$_{40}$]$^{0.27}$, *c*-poly(Sty)$_{50}$-*g*-[poly(*n*BuA)$_{40}$]$^{0.65}$ and *l*-poly(Sty)$_{50}$-*g*-[poly(*n*BuA)$_{40}$]$^{0.43}$, while multiple runs were performed to isolate larger fractions of *c*-poly(Sty)$_{50}$-*g*-[poly(*n*BuA)$_{40}$]$^{0.65}$. The FT-IR spectrum were recorded with a Bruker Vertex 70v FT-IR spectrometer (Bruker Optics GmbH, Ettlingen, Germany) in the range 4000-400 cm-1. The samples were measured as a solid at room temperature in a fine vacuum.

The atomic force microscope (AFM) measurements were performed using a Nanoscope V (Bruker, USA). Tapping mode images were acquired using commercial tips (NanoSensors) with a resonance frequency of ~320 kHz, and a spring constant of ~42 N/m. The AFM

micrographs were recorded in air at a relative humidity of 40–50% and at room temperature (~21 ºC). Open Source software (Gwyddion 2.53) was used for the image analysis.

UPLC-ESI-MS was carried out on an Acquity-UPLC H-class CM Core system (Waters Corporation, Milford, USA) with an Acquity-UPLC PDA and QDa detector. An Acquity-UPLC HSS T3 column (Waters) was used at 40 °C and Solvent A/Solvent B-mixtures (Solvent A: 99.9 % MilliQ H_2O: 0.1 % formic acid; Solvent B: acetonitrile) as solvents.

UV-Vis absorption spectrum were recorded on a Shimadzu UV-2501 PC spectrometer (Shimadzu, 604-8511 Kyoto, Japan) using PS-cuvettes or quartz cuvettes.

Ellman's test is used to detect the presence of thiol groups. Ellman's reagent solution was prepared: 6.2 mg of 5,5'-dithiobis(2-nitrobenzoic acid) was dissolved in 1.6 mL of dimethylformamide. Then 10 µL of DIPEA was added. 100µL of this solution was added to desired polymer solutions. The change of colour to orange in some minutes indicated the presence of thiol groups and the absorbance was measured by UV-Vis spectroscopy and was detected at λ = 500 nm.

6.3. Synthesis

6.3.1. Synthesis of *N*-(2-*p*-methoxybenzylselenoethyl) maleimide

Preparation of bis (p-methoxybenzyl) diselenide [210]

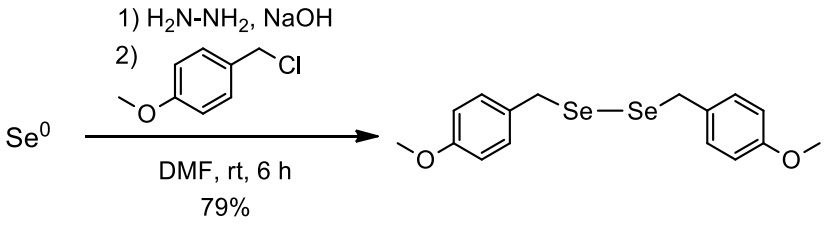

Hydrazine monohydrate (1.1 equiv, 55 mmol, 2.78 g) was added to a suspension of sodium NaOH (1.5 equiv, 76 mmol, 3.03 g) and elemental selenium (1.0 equiv, 50 mmol, 4.00 g) in 25 mL of dimethylformamide under inert atmosphere. The mixture was stirred at room temperature for 6 h. A dark red suspension was obtained. A solution of 4-methoxybenzyl chloride (0.5 equiv, 25 mmol, 3.96 g) in 15 mL of dimethylformamide was added dropwise to the mixture and the reaction was stirred for 45 min. The reaction was opened to air and water was added. The residue was extracted with dichloromethane (×3) and the collected organic phases were washed with 6N HCl (×1), water (×2), and brine (×1). The organic phase was dried over $MgSO_4$ and concentrated under reduced pressure. The resulting material was recrystallized from dichloromethane in hexane to afford a yellow solid (4.05 g, 79%).

Analysis : **^{1}H NMR** (500 MHz, $CDCl_3$) δ 7.15 (m, Ar, 4H), 6.85 (m, Ar, 4H), 3.83 (s, CH_2, 4H), 3.80 (s, CH_3, 6H) ppm. **^{13}C NMR** (126 MHz, $CDCl_3$) δ 158.77 (C4), 131.08 (C4), 130.10 (CH), 113.84 (CH), 55.28 (CH_3), 32.23 (CH_2) ppm. **IR** (KBr): ν = 2969 cm^{-1} (m), 2845 cm^{-1} (m), 1587 cm^{-1} (s, C=C), 1494 cm^{-1} (s, C=C), 1425 cm^{-1} (s, C=C), 1257 cm^{-1} (s, C-O-C), 1022 cm^{-1} (s), 801 cm^{-1} (s), 719 cm^{-1} (w, Se-Se), 701 cm^{-1} (s).

Preparation of 2-(p-methoxybenzylseleno) ethylamine [211]

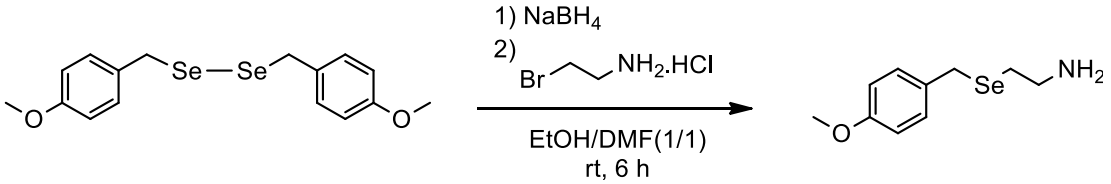

Bis(*p*-methoxybenzyl)diselenide (1.0 equiv, 12.5 mmol, 5.00 g) was dissolved in 100 mL of a solvent mixture (ethanol/dimethylformamide 1/1 v/v) the solution was bubbled with argon for 30 min. Sodium borohydride $NaBH_4$ (4.4 equiv, 55.0 mmol, 2.08 g) was added in small portions to the solution under inert atmosphere and the mixture was stirred for 1 h at room temperature. A solution of 2-bromoethylamine hydrobromide (2.5 equiv, 31.3 mmol, 6.41 g) in 10 mL of ethanol was then added dropwise to the mixture at 0 °C. The reaction was stirred for 6 h at room temperature. The resulting material was concentrated under reduced pressure and dissolved in a saturated aqueous solution of $NaHCO_3$. The compound was extracted with ethyl acetate (×3) and the collected organic phases were washed with brine (×1) and dried over $MgSO_4$. The desired product was used in the next step without any further purification.

Analysis : **^{1}H NMR** (400 MHz, $CDCl_3$) δ 7.20 (m, Ar, 2H), 6.81 (m, Ar, 2H), 3.78 (s, CH_3, 3H), 3.75 (s, CH_2, 2H), 2.85 (t, J = 6.6 Hz ,CH_2, 2H), 2.58 (t, J = 6.5 Hz, CH_2, 2H) ppm. **^{13}C NMR** (75 MHz, CDCl3) δ = 158.53 (C4), 131.28 (C4), 130.00 (CH), 114.06 (CH), 55.38 (CH_3), 41.71 (CH_2), 28.53 (CH_2), 26.37 (CH_2) ppm. **IR** (KBr): ν =3350 cm^{-1} (m, N-H), 2930 cm^{-1} (m), 1577 cm^{-1} (s), 1500 cm^{-1} (s, C=C), 1460 cm^{-1} (s), 1389 cm^{-1} (m), 1320 cm^{-1} (s), 1239 cm^{-1} (s), C-O-C), 1173 cm^{-1} (m), 1033 cm^{-1} (s), 844 cm^{-1} (m), 750 cm^{-1} (w), 615 cm^{-1} (w), 525 cm^{-1} (w).

Preparation of N-(2-p-methoxybenzylselenoethyl) maleimide [212]

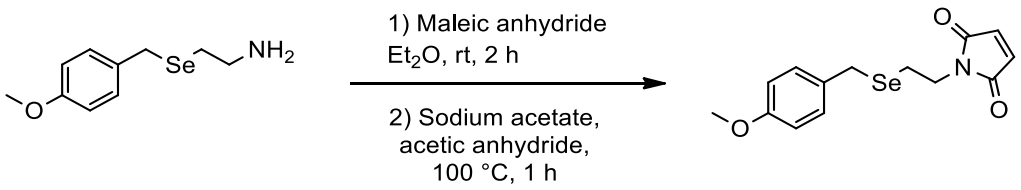

In a 25 mL flask, maleic anhydride (1.1 equiv, 15.9 mmol, 1.56 g) was dissolved in 70 mL of diethyl ether. After complete dissolution, a concentrated solution of 2-(*p*-methoxybenzylseleno) ethylamine (1.0 equiv, 14.5 mmol, 3.51 g) in a mixture of diethyl ether/chloroform (4/1 v/v), was added dropwise to the flask. A white suspension was obtained, and the reaction mixture was stirred for 2h at room temperature. The resulting N-(2tritylthioethyl) maleic acid was filtrated, washed with diethyl ether and dried under vacuum. The white solid was then added to a 3-neck-flask equipped with a condenser, containing a solution of anhydrous sodium acetate (2.30 g) in 15 mL of acetic anhydride. The reaction was stirred for 1h at 100 °C. The resulting mixture was cooled down in an ice bath and concentrated under reduced pressure. The residue was dissolved in chloroform and washed with water (x3) and brine (×1). The organic phase was dried over $MgSO_4$ and concentrated. The crude product was further purified via chromatography column over silica gel using cyclohexane/ethyl acetate (3/1) as eluent. The product was the recrystallized from chloroform in hexane to afford a yellow solid (32% over the last 3 steps). (^{1}H NMR spectrum in Section 6.4, **Figure 66**)

Analysis : **Rf** = 0.37 (eluent cyclohexane/ethyl acetate 3/1 vol.) **^{1}H NMR** (400 MHz, $CDCl_3$) δ 7.24 (m, Ar, 2H), 6.85 (m, Ar, 2H), 6.69 (s, CH, 2H), 3.85-3.79 (br, CH_2, CH_3, 5H), 3.73 (t, J = 1.9 Hz, CH_2, 2H), 2.63 (t, J = 7.1 Hz, CH_2, 2H) ppm. **^{13}C NMR** (75 MHz, $CDCl_3$) δ 170.68 (C=O), 134.20 (CH), 130.79 (C4), 130.07 (CH), 114.27 (CH), 55.35 (CH_3), 37.71 (CH_2), 26.38 (CH_2), 21.15 (CH_2) ppm. **IR** (KBr): ν = 3265-2900 cm^{-1} (w, HC=CH), 1784-1700 cm^{-1} (s, C=O), 1507 cm^{-1} (s), 1403 cm^{-1} (s), 1339 cm^{-1} (w), 1230 cm^{-1} (s, C-O-C), 1041 cm^{-1} (m), 802 cm^{-1} (m), 686 cm^{-1} (m).

6.3.2. Synthesis of cyclic macromolecules via diselenide bridge formation

Sequence-controlled polymerization of 4-tert-butoxystyrene and MISeMob

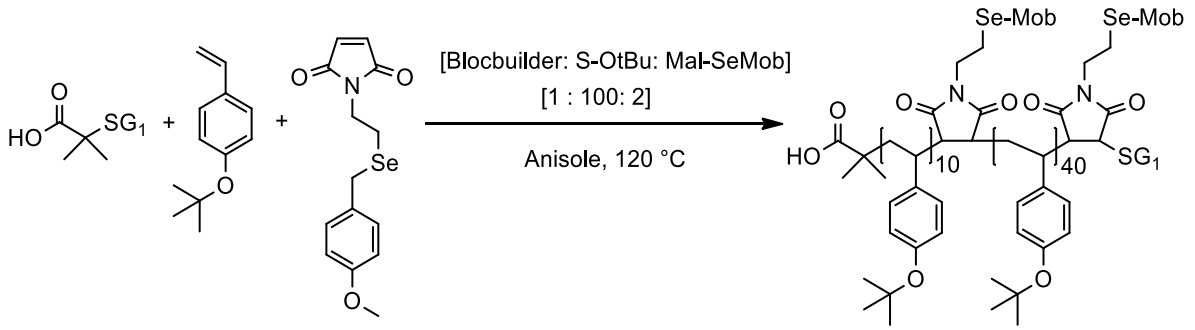

Synthesis of poly(StyO*t*Bu-*co*-MISeMob). Blocbuilder MA (1 equiv, 0.076 g) was dissolved in 2.0 mL of anisole and 3.8 mL of 4-*tert*-butoxystyrene (StyO*t*Bu) (100 equiv). The flask was deoxygenated by four freeze-pump thaw cycles and filled with argon. The mixture was then immersed in a pre-heated bath at 120 °C. At time intervals, aliquots were taken from the mixture with a degassed syringe to monitor the monomer conversion by ^{1}H NMR. When the conversion reached approximately 10%, a degassed solution of MISeMob (1.1 equiv, 0.071 g) in 0.2 mL of anisole was added to the polymerization. A second addition of degassed solution containing MISeMob (1.1 equiv, 0.071 g) in 0.2 mL of anisole was performed when the conversion of 4-*tert*-butoxystyrene reached 53%. The polymer was precipitated in cold methanol (×3) and dried.

Analysis : **^{1}H NMR** (500 MHz, CD_2Cl_2) δ 7.17 (br, Ar, 4H), 6.74 (br, Ar, 4H), 6.70-6.31 (m, Ar, 229H), 3.73 (br, CH_3, 6H), 3.65 (br, CH, 4H), 3.31 (br, CH_2, 4H), 2.08 (br, CH_2, 4H), 1.71 (br, CH, 50H), 1.23 (br, CH_2, CH_3, 580H) ppm. **HSQC 2D NMR** (500 MHz/126 MHz, CD_2Cl_2) δ 7.22/128.9 (ArMob, CH), 6.87/114.1 (Ar_{Mob}, CH), 6.72/123.4 (Ar, CH), 6.47/128.9 (Ar, CH), 3.80/54.3 (CH), 3.71/25.7 ($CH_{3,Mob}$), 3.39/37.9 ($CH_{2,Mob}$), 2.18/19.8 ($CH_{2,Mob}$), 1.85/38.7 (CH), 1.45/43.0 (CH_2), 1.29/28.6 (CH_3) ppm. **SEC in THF** $M_{n,\,app}$ = 10700 and Đ = 1.11.

Polymer backbone deprotection

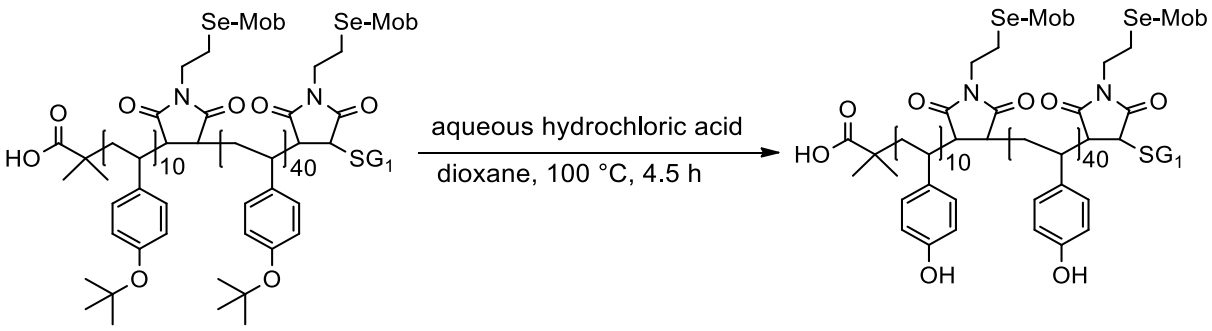

Synthesis of (*l*-poly(StyOH-*co*-MISeMob). The copolymer (M_n = 10000 g/mol, 0.300 g) was dissolved in 70.0 mL of dioxane and 1.5 mL of hydrochloric acid (37%) was added to the solution. The mixture was refluxed for 4.5 h at 105 °C. After completion of the hydrolysis, the polymer was precipitated in water and dried under reduced pressure. (^{1}H NMR spectrum in Section 6.4, **Figure 67**)

Analysis : **^{1}H NMR** (400 MHz, CD_3OD) δ 8.92 (br, OH, 1H), 7.17 (br, Ar, 4H), 6.80 (br, Ar, 4H), 6.75-6.24 (m, Ar, 220H), 3.70 (br, CH_3, CH, 10H), 3.43 (br, CH_2, 4H), 2.08 (br, CH_2, 4H), 1.78 (br, CH, 57H), 1.40 (br, CH_2, 96H) ppm. **HSQC 2D NMR** (500 MHz/126 MHz, CD_3OD) δ 7.17/131.0 (Ar_{Mob}, CH), 6.80/114.5 (Ar_{Mob}, CH), 6.58/115.4 (Ar, CH), 6.44/129.7 (Ar, CH), 3.80/55.6 (CH), 3.70/26.6 ($CH_{3,Mob}$), 3.42/38.6 ($CH_{2,Mob}$), 2.25/20.16 (CH_2-Se), 2.03/40.8 (CH), 1.46/45.2 (CH_2) ppm. **SEC in DMAc** $M_{n,\,app}$ = 13300 and Đ = 1.11.

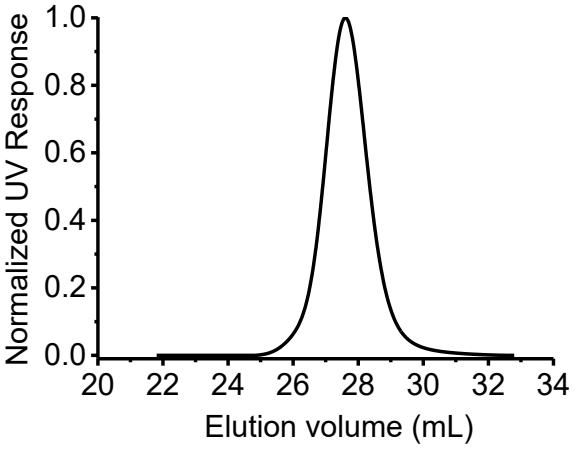

Figure 48. SEC chromatogram.

General procedure for polymer cyclization via the formation of diselenide bridge

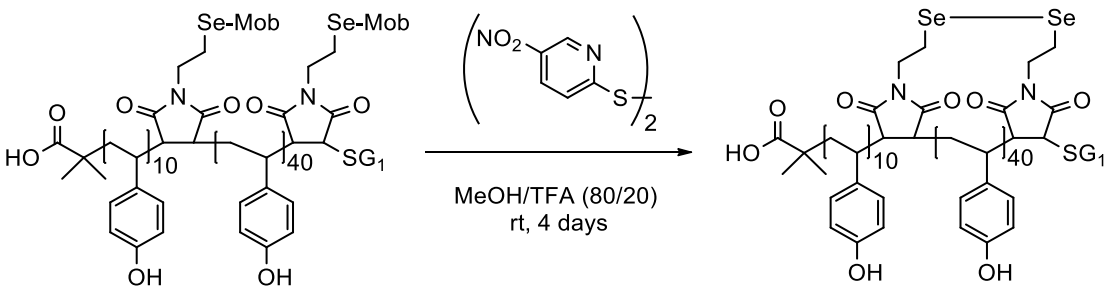

Synthesis of *c*-poly(StyOH-*co*-MISe)$_e$. 2,2′-Dithiobis(5-nitropyridine) (7 equiv, 0.043 g) was dissolved in 600 mL of the solvent mixture methanol/trifluoroacetic acid (80/20 v/v). The linear polymer precursor (1 equiv of selenol moieties, Mn = 7000 g/mol, 0.070 g) was dissolved in 8 mL of methanol and was added dropwise to the flask via a syringe pump. The reaction was stirred for 4 days at room temperature. The solvent was removed under reduced pressure. The polymer was precipitated in water (×2) and in hexane (×1). (^{1}H NMR spectrum in Section 6.4, **Figure 68**)

Analysis : **^{1}H NMR** (400 MHz, CD_3OD) δ 9.13 (br, N-Ar), 8.32 (br, N-Ar), 7.82 (br, N-Ar), 6.75-6.24 (m, Ar, 220H), 3.70 (br, CH_2, CH, 8H), 2.91 (br, CH_2, 4H), 1.78-1.40 (br, CH, CH_2, 160H) ppm. **HSQC 2D NMR** (500 MHz/126 MHz, CD_3OD) δ 6.57/115.00 (Ar, CH), 6.54/129.70 (Ar, CH), 3.68/53.90 (CH), 3.56/38.30 (CH_2), 2.82/29.30 ($CH_{2,Se}$), 1.82/39.60 (CH), 1.39/46.30 (CH_2) ppm. **SEC in DMAc** $M_{n,\,app}$ = 13200, $M_{p,\,app}$ = 13100 and Đ = 1.22.

6.3.3. Ring-chain opening

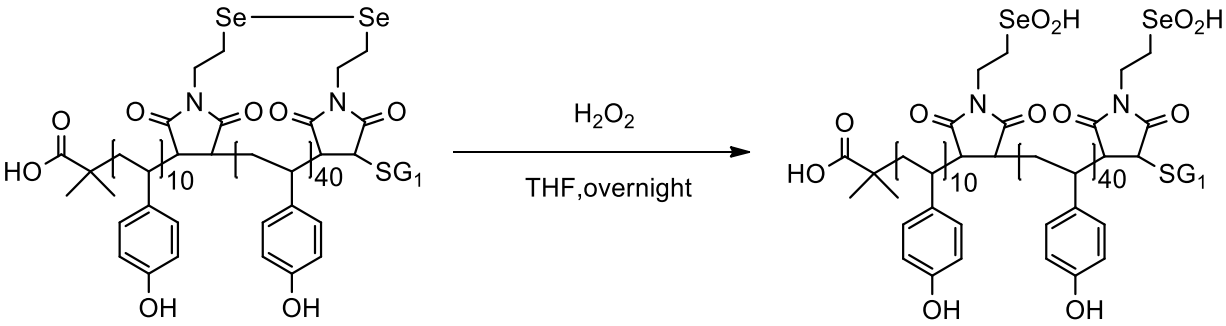

Synthesis of *l*-poly(StyOH-*co*-MISeO$_2$H). 3 mg of the cyclic polymer *c*-poly(StyOH-*co*-MISe)$_e$. were dissolved in 1 mL of tetrahydrofuran and 100 µL of hydrogen peroxide was added. The reaction was stirred overnight. The mixture was dried over $MgSO_4$ and concentrated under reduced pressure.

Analysis : **SEC in DMAc** $M_{p,\,app}$ = 14000 and Đ = 1.18.

6.3.4. ATRP polymerizations on disulfide and diselenide containing compounds

*Synthesis of Bis(2-ethyl-2-bromopropanoate) disulfide (**1**)*

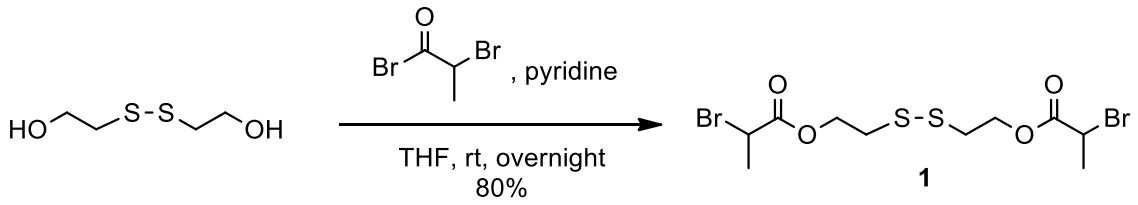

In a dry flask, bis(2-hydroxyethyl) disulfide (1 equiv, 16.8 mmol of hydroxyl group, 1.30 g) was dissolved in 140.00 mL of dry tetrahydrofuran. The solution was cooled down at 0 °C and pyridine (3 equiv, 50.5 mmol, 4.08 mL) was added. 2-bromopropionyl bromide (3 equiv, 50.5 mmol, 5.27 mL) was diluted in 3.00 mL of dry tetrahydrofuran and added dropwise to the reaction flask. The mixture was stirred overnight at room temperature under inert atmosphere. The reaction was then opened to air and the solvent was removed under reduced pressure. The resulting mixture was dissolved in dichloromethane and washed with water (×3) and brine (×1). The organic phase was dried over $MgSO_4$ and concentrated. The residue was further purified via column chromatography over silica gel by using ethyl acetate/cyclohexane (15/1) as eluent to afford a yellow oil (2.845 g, 80%).

Analysis : ^{1}**H NMR** (500 MHz, $CDCl_3$) δ 4.30 (m, CH_2, 4H), 4.21 (q, J = 6.9 Hz, CH, 2H), 2.96 (t, J = 6.6 Hz, CH_2, 4H), 1.84 (d, J = 6.9 Hz, CH_3, 6H) ppm.

ATRP of styrene on disulfide-containing initiator [227]

The difunctional initiator (1) (1 equiv, 2.6 x 10^{-4} mol of initiator groups, 54.4 mg), PMDETA (1 equiv, 2.6 x 10^{-4} mol, 44.0 mg), styrene (300 equiv, 0.077 mol, 8.91 mL) and anisole (1.00 mL) were introduced in a schlenk and the mixture was degassed by three freeze-pump-thaw cycles. In a separate flask, CuBr (1 equiv, 2.6 × 10^{-4} mol, 37.0 mg) was introduced and the flask was deoxygenated. The mixture was added to the flask containing CuBr under inert atmosphere and the reaction flask was then immersed in an oil bath at 90 °C. The polymerization was stopped at 98% of monomer conversion. The catalyst was removed by passing the reaction mixture over a column of Al_2O_3. The solvent was removed under vacuum. The polymer was precipitated in cold methanol (×3) and dried.

Analysis : **^{1}H NMR** (300 MHz, $CDCl_3$) δ 7.20 – 6.89 (br, Ar, 2H), 6.80 – 6.30 (br, Ar, 2H), 1.84 (br, CH, 1H), 1.42 (br, CH_2, 2H) ppm. **SEC in THF** $M_{n,app}$ = 48000 and Đ = 1.25.

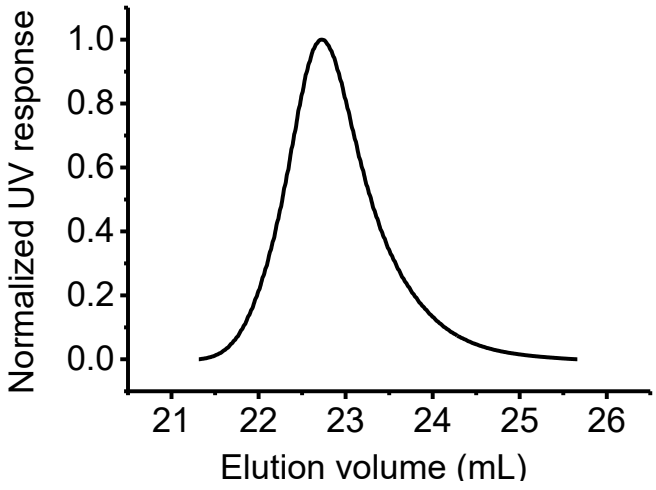

Figure 49. SEC chromatogram.

*Synthesis of diselenide-containing initiator (**2**) (2 steps)*

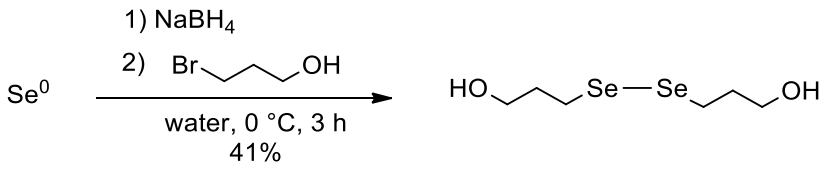

Synthesis of bis-(3-hydroxypropyl) diselenide.[275] $NaBH_4$ (1.1 equiv, 0.084 mol, 3.16 g) and Se^0 (0.5 equiv, 0.038 mol, 3.00 g) were introduced in a 3-necked flask equipped with an addition funnel and a condenser. The flask was flushed with an inert gas and cooled with an ice bath. 160 mL of water was added slowly. After 15 min, the ice bath was removed and a second portion of Se^0 (0.5 equiv, 0.038 mol, 3.00 g) was added. The mixture was then warmed up with a heat gun to complete the dissolution of the intermediate Se_2Na_2. A brownish solution was obtained. The mixture was cooled to room temperature and a solution of bromopropanol (1 equiv, 0.076 mol, 10.56 g) in 80 mL of water was added dropwise to the mixture. The resulting yellow solution was stirred for 3 h at room temperature. The aqueous layer was extracted with diethyl ether and ethyl acetate. Organic phases were combined, dried over $MgSO_4$, filtrated and concentrated under reduced pressure. The residue was further purified via column chromatography over silica gel by using ethyl acetate/cyclohexane (1/1) as eluent to afford a yellow oil (41%).

Analysis : **^{1}H NMR** (500 MHz, $CDCl_3$) δ 3.75 (t, J = 6.1 Hz, CH_2, 4H), 3.02 (t, J = 7.2 Hz, CH_2, 4H), 1.99 (m, CH_2, 4H) ppm. **^{13}C NMR** (126 MHz, $CDCl_3$) δ 61.92 (CH_2), 33.62 (CH_2), 26.22 (CH_2) ppm. **IR** (KBr): ν = 3300 cm^{-1} (s, O-H), 2900 cm^{-1} (s, C-H), 1429 cm^{-1} (w), 1235 cm^{-1} (w), 1 025 cm^{-1} (s, C-O), 893 cm^{-1} (w, Se-Se), 643 cm^{-1} (w).

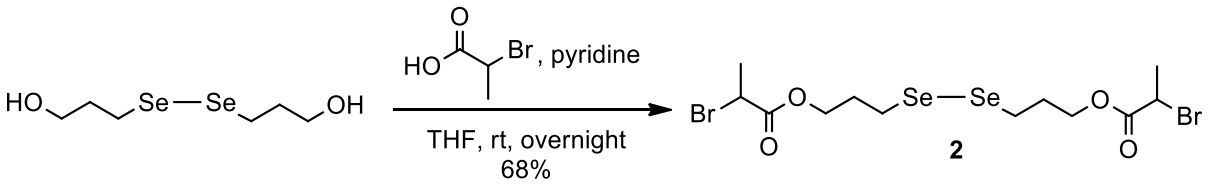

Synthesis of bis(3-propyl-2-bromopropanoate) diselenide (2). In a dry schlenk bis-(3-hydroxypropyl) diselenide (1 equiv, 0.005 mol of hydroxyl group, 0.70 g) was dissolved in 100 mL of dry tetrahydrofuran under inert atmosphere and the solution was cooled down with an ice bath. Pyridine (3 equiv, 0.015 mol, 1.99 g) was added, followed by the dropwise addition of bromopropionyl bromide (3 equiv, 0.015 mol, 3.26 g). The mixture was stirred overnight at room temperature. The residue was concentrated under reduced pressure and dissolved in dichloromethane. The organic phase was washed with water (×3) and brine (×1), dried over $MgSO_4$ and concentrated under reduced pressure. The crude product was further purified via chromatography column over silica gel using cyclohexane/ethyl acetate (10/1) as eluent to afford a yellow oil (0.925 g, 68%). (^{1}H NMR spectrum in Section 6.4, **Figure 70**)

Analysis : **^{1}H NMR** (500 MHz, $CDCl_3$) δ 4.37 (q, J = 6.9 Hz, CH, 2H), 4.27 (m, CH_2, 4H), 2.96 (t, J = 7.3 Hz, CH_2, 4H), 2.13 (m, CH_2, 4H), 1.83 (d, J = 6.9 Hz, CH_3, 6H) ppm. **^{13}C NMR** (126 MHz, $CDCl_3$) δ 170.30 (C=O), 65.00 (CH_2), 40.18 (CH), 29.97 (CH_2), 25.41 (CH_2), 21.73 (CH_3) ppm. **ESI-LCMS :** $[M + H]^+_{calc}$ = 545.81 g/mol; $[M+H]^+_{found}$ = 545.39 g/mol, 84%.

ATRP of styrene on diselenide-containing initiator

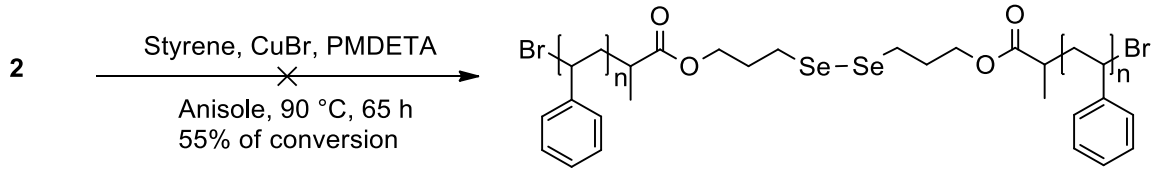

The difunctional initiator (**2**) (1 equiv, 2.0×10^{-4} mol of initiator groups, 54.4 mg), PMDETA (1 equiv, 2.0×10^{-4} mol, 34.0 mg), styrene (300 equiv, 0.077 mol, 6.87 mL) and anisole (0.70 mL) were introduced in a schlenk and the mixture was degassed by three freeze-pump-thaw cycles. In a separate flask, CuBr (1 equiv, 2.0×10^{-4} mol, 28.5 mg) was introduced and the flask was deoxygenated. The mixture was added to the flask containing CuBr under inert atmosphere and the reaction flask was then immersed in an oil bath at 90 °C. The polymerization was stopped at 55% of monomer conversion. The catalyst was removed by passing the reaction mixture over a column of Al_2O_3. The solvent was removed under vacuum. The polymer was precipitated in cold methanol (×3) and dried under vacuum.

Analysis : **^{1}H NMR** (300 MHz, $CDCl_3$) δ 7.23 – 6.85 (br, Ar, 2H), 6.88 – 6.25 (br, Ar, 2H), 1.86 (br, CH, 1H), 1.43 (br, CH_2, 2H) ppm. **SEC in THF** $M_{n,app}$ = 58000 and Đ = 1.90.

ATRP of n-butyl acrylate initiated by methyl bromopropionate

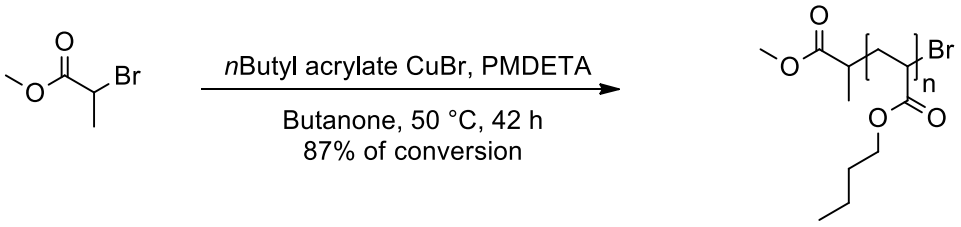

Methyl bromopropionate (MBrP) (1 equiv, 6.0×10^{-5} mol of initiator groups, 10.0 mg), PMDETA (1 equiv, 6.0×10^{-5} mol, 10.0 mg), *n*-butyl acrylate (200 equiv, 0.013 mol, 1.71 mL) and methyl ethyl ketone (0.20 mL) were introduced in a schlenk and the mixture was degassed by three freeze-pump-thaw cycles. In a separate flask, CuBr (1 equiv, 6.0×10^{-5} mol, 8.00 mg) was introduced and the flask was deoxygenated. The mixture was added to the flask containing CuBr under inert atmosphere and the reaction flask was then immersed in an oil bath at 50 °C. The polymerization was stopped at 87% of monomer conversion. The catalyst was removed by passing the reaction mixture over a column of Al_2O_3. The solvent and monomer were removed under vacuum.

Analysis : **^{1}H NMR** (300 MHz, $CDCl_3$) δ 4.03 (br, CH_2, 2H), 2.27 (br, CH, 1H), 1.59 (br, CH_2, 2H), 1.38 (br, CH_2, 2H), 0.93 (br, CH_3, 3H) ppm. **SEC in THF** $M_{n,\,app}$ = 20000 and Đ = 1.09.

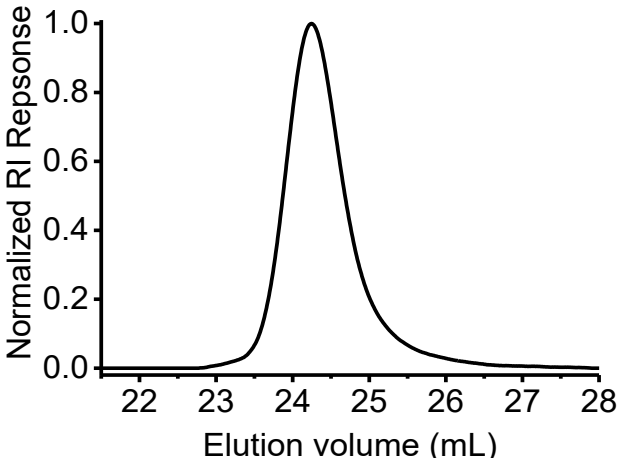

Figure 50. SEC chromatogram.

*ATRP of n-butyl acrylate on diselenide-containing initiator (**2**)*

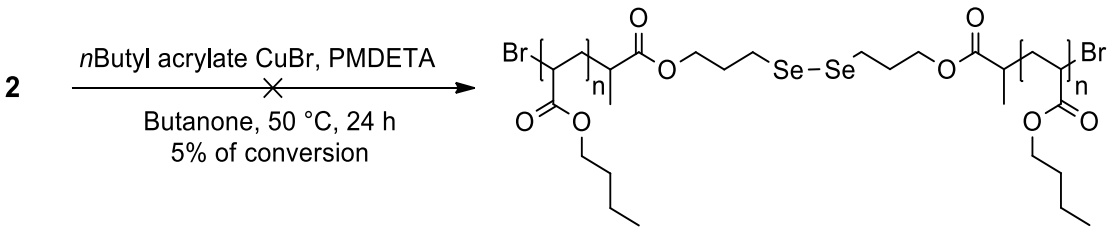

The monofunctional initiator (2) (1 equiv, 1.8×10^{-5} mol, 10.0 mg), PMDETA (2 equiv, 3.7×10^{-5} mol, 6.0 mg), *n*-butyl acrylate (400 equiv, 7.3×10^{-3} mol, 1.03 mL) and methyl ethyl ketone (0.10 mL) were introduced in a schlenk and the mixture was degassed by three freeze pump-thaw cycles. In a separate flask, CuBr (2 equiv, 3.7×10^{-5} mol, 5.00 mg) was introduced and the flask was deoxygenated. The mixture was added to the flask containing CuBr under inert atmosphere and the reaction flask was then immersed in an oil bath at 50 °C. The polymerization was stopped at 5% of monomer conversion after 24 h. The catalyst was removed by passing the reaction mixture over a column of Al_2O_3. The solvent and monomer were removed under vacuum. (^{1}H NMR spectrum in Section 6.4,**Figure 71**)

Analysis : **^{1}H NMR** (500 MHz, $CDCl_3$) δ 4.06 (m, CH_2-O, 116H), 3.28 (br, CH_2, 4H), 2.93 (m, CH_2, 4H), 1.37 (br, CH_2, 108H), 0.93 (br, CH_3, 150H) ppm. **^{13}C NMR** (126 MHz, $CDCl_3$) δ 174.65 (C=O), 64.55 ($CH_{2,\,acryl}$), 41.69 ($CH_{3,\,initiator}$), 30.68 ($CH_{2,\,acryl}$), 19.38 ($CH_{2,\,acryl}$), 13.86 ($CH_{3,\,acryl}$) ppm. **SEC in THF** $M_{n,app}$ = 3000 and Đ = 1.82.

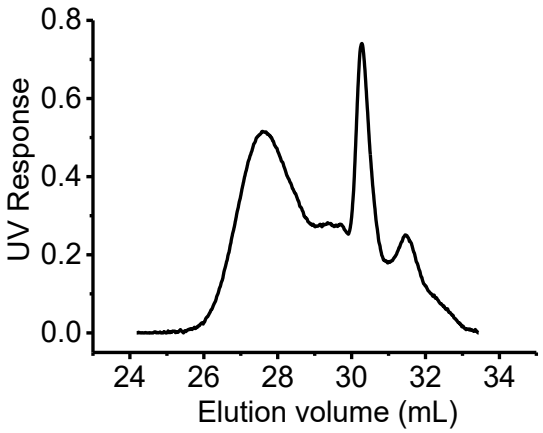

Figure 51. SEC chromatogram.

6.3.5. Symmetric anhydride of 2,4-hexadien-1-yl succinic acid monoester

*Synthesis of 2,4-hexadien-1-yl succinic acid (**3**)* [239]

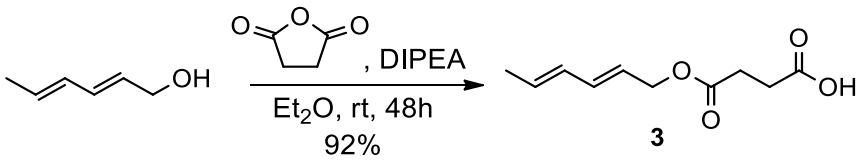

Succinic anhydride (1.15 equiv, 30 mmol, 2.99 g) and *trans, trans*-2,4-hexadien-1-ol (1.00 equiv, 26 mmol, 2.55 g) were dissolved in 10 mL of diethyl ether. *N, N*-diisopropylethylamine (1.00 equiv, 26 mmol, 3.35 g) was added to the flask and the mixture was stirred at room temperature for 2 days. Diethyl ether was removed under reduced pressure and the residue was dissolved in dichloromethane. The product was extracted with citric acid aqueous solution (5% w/w) three times, dried over $MgSO_4$, filtered, and concentrated under reduced pressure to afford a light brown solid (4.72 g, 92%). (^{1}H NMR spectrum in Section 6.4, **Figure 72**)

Analysis : **^{1}H NMR** (400 MHz, $CDCl_3$) δ 6.23 (m, 1H, CH), 6.03 (m, 1H, CH), 5.76 (m, 1H, CH), 5.62 (m, 1H, CH), 4.58 (d, J = 6.6 Hz, 2H, CH_2), 2.64 (m, 4H, CH_2), 1.74 (d, J = 6.7 Hz, 3H, CH_3) ppm. **^{13}C NMR** (126 MHz, DMSO-d6) δ 173.37 (C=O), 171.88 (C=O), 133.88(CH), 130.61 (CH), 130.57 (CH), 124.29 (CH), 64.22 (CH_2), 28.64 (CH_2), 17.86 (CH_3) ppm. **IR** (KBr): ν =2950 cm^{-1} (br, HC=CH), 1720-1697 cm^{-1} (s, C=O),.1428 cm^{-1} (m), 1299 cm^{-1} (m), 1162 cm^{-1} (m), 993 cm^{-1} (m), 948 cm^{-1} (m), 792 cm^{-1} (w), 643 cm^{-1} (w), 494 cm^{-1} (w).

Synthesis of the symmetric anhydride of 2,4-hexadien-1-yl succinic acid monoester [238]

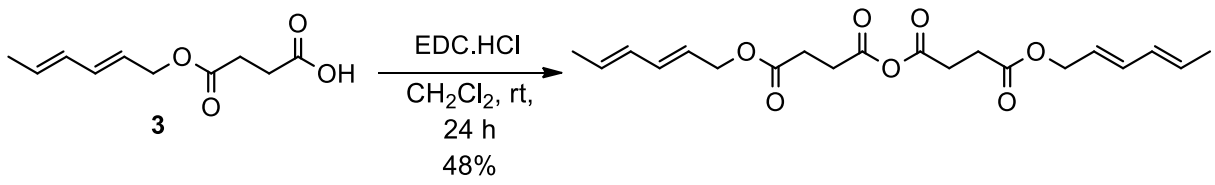

2,4-hexadien-1-yl succinic acid monoester (**3**) (1.0 equiv, 15.0 mmol, 3.00 g) was dissolved in 40 mL of dry dichloromethane under inert atmosphere and the resulting solution was cooled down at 0 °C. EDC.HCl (0.6 equiv, 9.1 mmol, 1.74 g) was dissolved in 10 mL of dry dichloromethane and was added dropwise to the flask. The mixture was stirred at room temperature for 24 h. The mixture was filtered and concentrated under reduced pressure. The residue was again dissolved in dichloromethane, cooled down at -20 °C and filtered to afford a brown solid (1.40 g, 48%). (^{1}H NMR spectrum in Section 6.4, **Figure 73**)

Analysis : **^{1}H NMR** (400 MHz, $CDCl_3$) δ 6.24 (m, 2H, CH), 6.03 (m, 2H, CH), 5.74 (m, 2H, CH), 5.60 (m, 2H, CH), 4.61 (d, 4H, CH_2), 2.79 (m, 4H, CH_2), 2.67 (m, 4H, CH_2), 1.77 (d, 6H, CH3) ppm. **^{13}C NMR** (126 MHz, DMSO-d6) δ 171.35 (C=O), 168.31 (C=O), 134.15 (CH), 130.82 (CH), 130.52 (CH), 124.04 (CH), 64.52 (CH_2), 29.85 (CH_2), 28.09 (CH_2), 17.90 (CH_3) ppm. **IR** (KBr): ν = 2962 cm^{-1} (br, HC=CH), 1730-1700 cm^{-1} (s, C= O, asym), 1679 cm^{-1} (m, C=O sym), 1446 cm^{-1} (m), 1325 cm^{-1} (m), 1196 cm^{-1} (m), 986 cm^{-1} (m), 906 cm^{-1} (m).

6.3.6. TAD-diene reaction on diselenide-containing compounds

*Synthesis of bis(2,4-hexadien-3-propyl succinic diester) diselenide (**4**)*

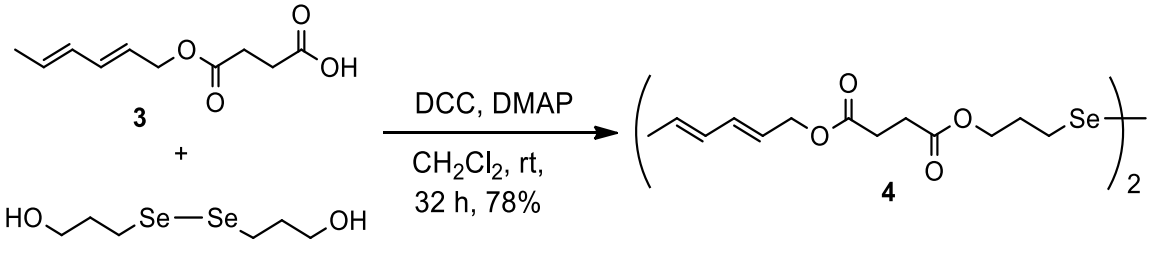

Bis-(3-hydroxypropyl) diselenide (1.0 equiv, 2.55×10^{-3} mol, 0.70 g) and 2,4-hexadien-1-yl succinic acid (2.1 equiv, 5.35×10^{-3} mol, 1.06 g) were dissolved in 10 mL of dry dichloromethane. DMAP (0.1 equiv, 2.55×10^{-4} mol, 0.03 g) was added and the mixture was cooled down at 0 °C. In a separated flask, dicyclohexylcarbodiimide (DCC) (2.2 equiv, 5.61×10^{-3} mol, 1.15 g) was dissolved in 2 mL of dry dichloromethane and was then added dropwise to the mixture. The reaction was stirred for 32 h at room temperature. The mixture was filtered, washed with aqueous hydrochloric acid (pH = 2) and water. The organic layer was dried over $MgSO_4$ and concentrated under reduced pressure. The residue was purified by liquid chromatography over silica gel with cyclohexane/ethyl acetate (10/1) as eluent to afford a yellow oil (1.27g, 78%). (^{1}H NMR spectrum in Section 6.4, **Figure 74**)

Analysis : **^{1}H NMR** (500 MHz, $CDCl_3$) δ 6.24 (m, CH, 2H), 6.04 (m, CH, 2H), 5.76 (m, CH, 2H), 5.61 (m, *J* = 15.2 Hz, CH, 2H), 4.58 (d, *J* = 6.7 Hz, CH_2, 4H), 4.18 (t, *J* = 6.2 Hz, CH_2, 4H), 2.93 (t, *J* = 7.3 Hz, CH_2, 4H), 2.08 (m, CH_2, 4H), 1.77 (d, *J* = 6.7 Hz, CH_3, 6H) ppm. **^{13}C NMR** (126 MHz, $CDCl_3$) δ 172.34 (C=O), 172.18 (C=O), 135.24 (CH), 131.59 (CH), 130.52 (CH), 123.57 (CH), 65.43 (CH_2-O), 63.91 (CH_2-O), 30.08 (CH_2), 29.27 (CH_2), 29.24 (CH_2), 25.64 (CH_2), 18.29 (CH_3) ppm. **IR** (KBr): ν = 2900 cm^{-1} (w, HC=CH), 1730-1700 cm^{-1} (s, C=O, asym), 1150 cm^{-1} (s, C=O sym).

*TAD-Diene click reaction with 4-Phenyl-1,2,4-triazoline-3,5-dione (**5**)*

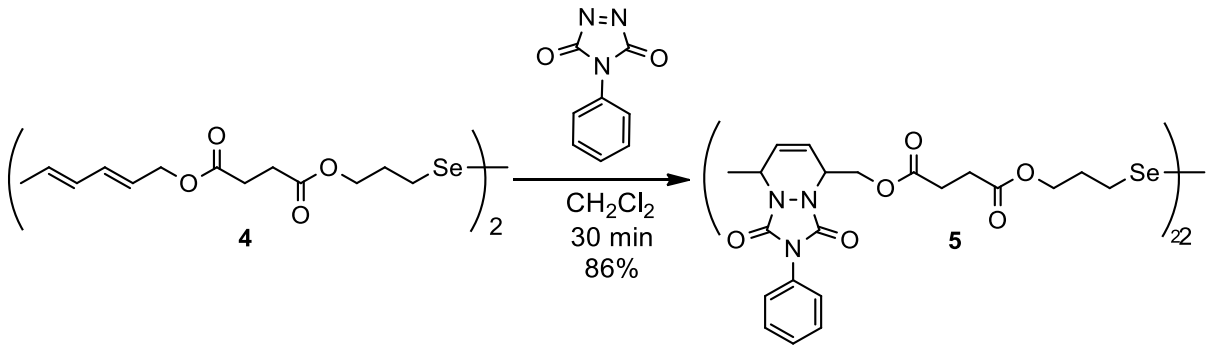

Diselenide (**4**) (1 equiv, 1.57×10^{-4} mol, 0.1 g) was dissolved in 2 mL of dry dichloromethane. 4-phenyl-1,2,4-triazoline-3,5-dione (2.1 equiv, 3.30×10^{-4} mol 0.058 g) was added to the solution under inert atmosphere. The pink solution turned instantaneously yellow. The reaction was stirred for 30 min at room temperature. The mixture was filtered and concentrated under reduced pressure to afford a yellow oil (0.109 g, 86%). (^{1}H NMR spectrum in Section 6.4, **Figure 75**)

Analysis : **^{1}H NMR** (500 MHz, $CDCl_3$) δ 7.48 (m, Ar, 8H), 7.37 (m, Ar, 2H), 5.90 (dddd, *J* = 10.4, 5.9, 3.6, 1.8 Hz, CH, 4H), 4.74 (br, CH, 2H), 4.56 (m, CH, 2H), 4.43 (br, CH2, 4H), 4.17 (m, CH_2, 4H), 2.93 (t, CH_2, 4H), 2.62 (m, CH_2, 8H), 2.08 (br, CH_2, 4H), 1.60 (t, CH_3, 6H) ppm. **^{13}C NMR** (126 MHz, CDCl3) δ 172.19 (C=O), 152.78 (C=O urazole group), 151.58 (C=O urazole group), 131.31 (C), 130.34 (CH, alkene), 129.22 (CH, Ar), 128.34(CH, alkene), 125.85 (CH, Ar), 120.84 (C), 63.94 (CH_2-O), 63.19 (CH_2-O), 52.97 (CH, cycle), 51.44 (CH, cycle), 30.05(CH_2Se), 28.99 (CH_2), 25.62 (CH_2), 19.68 (CH_3) ppm. **ESI-LCMS :** $[M + H]^+_{calc}$ = 989.87 g/mol; $[M+H]^+_{found}$ = 989.37g/mol, 78%.

6.3.7. Synthesis of TAD-terminated poly(*n*-butyl acrylate) side chains

Urazole-containing initiator was synthesized as previously described in literature.[239]

Synthesis of Urazole-containing initiator (4 steps)

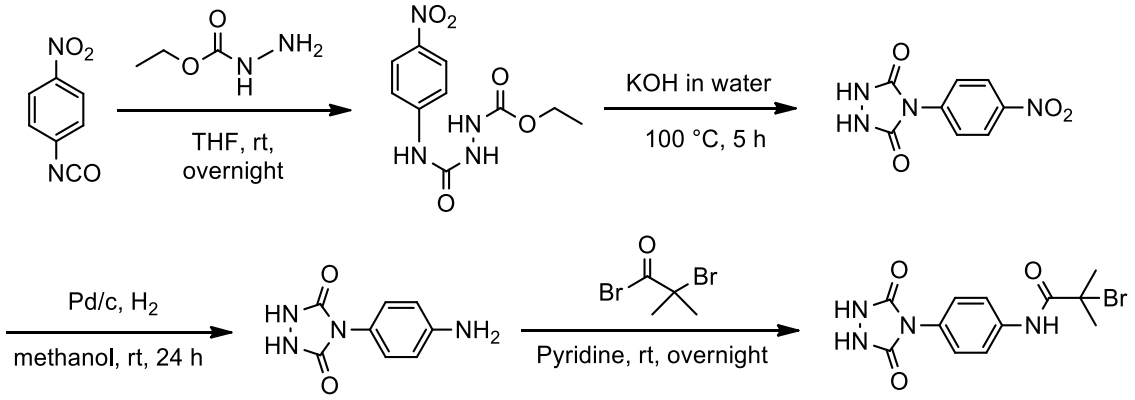

Scheme 31. Synthetic strategy of Urazole-containing initiator

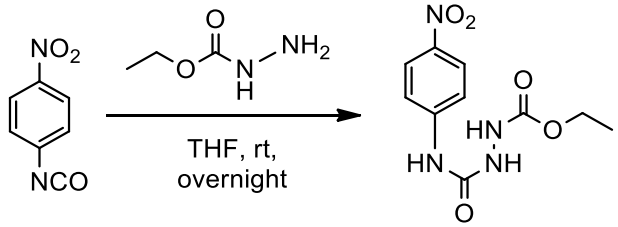

Synthesis of 4-nitrophenyl 1-(ethoxycarbonyl) semicarbazide.[276] Ethyl carbazate (1 equiv, 18.3 mmol, 1.90 g) was dissolved in 30 mL of dry tetrahydrofuran under inert atmosphere. 4-nitrophenyl isocyanate (1 equiv, 18.3 mmol, 3.00 g) was added to the solution. The mixture was stirred at room temperature overnight. The desired product was collected by filtration to afford a white solid (4.77 g, 97 %).

Analysis : **^{1}H NMR** (500 MHz, DMSO-d6) δ 9.54 (br, NH, 1H), 9.05 (br, NH, 1H), 8.39 (br, NH, 1H), 8.15 (d, J = 9.3 Hz, Ar, 2H), 7.73 (br, Ar, 2H), 4.08 (q, J = 7.1 Hz, CH_2, 2H), 1.20 (t, J = 7.1 Hz, CH_3, 3H) ppm. **^{13}C NMR** (126 MHz, DMSO) δ 156.84 (C), 146.48 (C=O), 141.08 (C), 124.97 (CH), 60.66 (CH2), 14.54 (CH_3) ppm. **ESI-LCMS :** $[M + H]^+_{calc}$ = 269. 08 g/mol; $[M+H]^+_{found}$ = 269.16 g/mol, 99%.

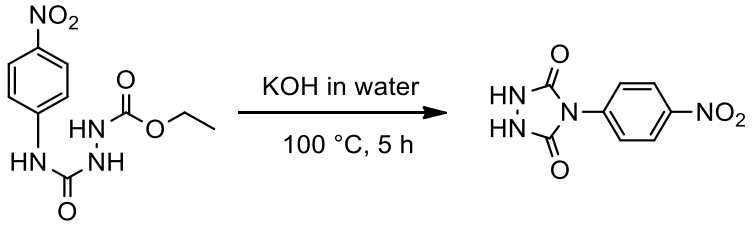

Synthesis of 4-nitrophenyl 1, 2, 4-triazolidine-3,5-dione. 4-nitrophenyl 1-(ethoxycarbonyl) semicarbazide (7.45 mmol, 2.77g) was dissolved in 7 mL of aqueous potassium hydroxide (4M). The mixture was refluxed at 100 °C for 5 h. The resulting product was warm filtered, cooled to room temperature and acidified with hydrochloric acid until pH 1. After cooling to room temperature, the precipitate was filtered to afford a yellow solid (1.38 g, 83%).

Analysis : **^{1}H NMR** (300 MHz, DMSO-d_6) δ 10.81 (br, NH, 2H), 8.33 (d, *J* = 9.3 Hz, Ar, 2H), 7.89 (d, *J* = 9.3 Hz, Ar, 2H) ppm. **^{13}C NMR** (126 MHz, DMSO-d_6) δ 152.00 (C=O), 125.64 (CH), 123.95 (CH) ppm.

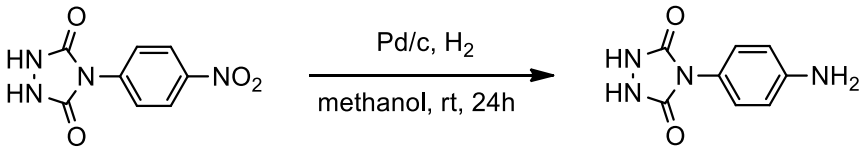

Synthesis of 4-aminophenyl 1,2,4-triazolidine-3,5-dione. 4-nitrophenyl 1,2,4-triazolidine-3,5-dione (5 mmol, 1.0 g) was dissolved in 200 mL of methanol. The whole compound was not completely soluble. A catalytic amount of palladium (5% on activated carbon, 0.1 g) was added to the suspension. Then a balloon containing hydrogen gas was placed on the reaction, this mixture was stirred for 24h at room temperature. The solution was filtered over a plug of celite to remove the catalyst and concentrated under reduced pressure to afford the desired product (0.92 g, 96%).

Analysis : **^{1}H NMR** (300 MHz, DMSO) δ 6.96 (d, *J* = 8.6 Hz, Ar, 2H), 6.58 (d, *J* = 8.6 Hz, Ar, 2H), 5.22 (br, NH2, 2H) ppm.

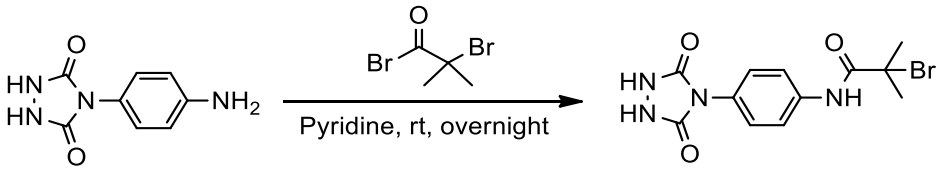

Synthesis of urazole initiator. In a dry flask, 4-aminophenyl 1,2,4-triazolidine-3,5-dione (1 equiv, 1.78 mmol, 0.34 g) was dissolved in dry pyridine (8 mL). The mixture was cooled down at 0 °C. α-bromoisobutyryl bromide (1.1 equiv, 1.80 mmol, 0.41 g) was added dropwise to the reaction flask under inert atmosphere. The reaction was stirred overnight at room temperature. Water was added to the mixture. The mixture was extracted with ethyl acetate (×3). The organic phases were collected, dried over $MgSO_4$ and concentrated. The crude product was further purified via chromatography column over silica gel using (ethyl acetate/methanol/acetic acid (95/5/1)) / cyclohexane (2/1) as eluent to afford a yellow solid (0.39 g, 65%). (^{1}H NMR spectrum in Section 6.4, **Figure 76**)

Analysis : **Rf** = 0.25. **^{1}H NMR** (500 MHz, DMSO-d6) δ 10.44 (s, NH, 2H), 9.96 (s, NH, 1H), 7.74 (d, *J* = 8.9 Hz, Ar, 2H), 7.39 (d, *J* = 8.9 Hz, Ar, 2H), 2.01 (s, CH_3, 6H) ppm. **^{13}C NMR** (126 MHz, DMSO-d6) δ 169.52 (C=O), 153.48 (C=O), 137.89 (C), 127.44 (C), 126.32 (CH), 120.71 (CH), 60.64 (C), 30.71 (CH_3) ppm. **ESI-LCMS :** $[M + H]^+_{calc}$ = 341.16 g/mol; $[M+H]^+_{found}$ = 341. 05 g/mol, 92%.

Synthesis of TAD-terminated poly(n-butyl acrylate)

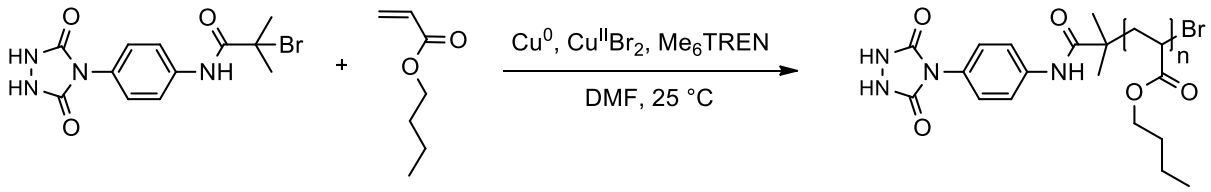

Synthesis of Ur-poly(*n*BuA)$_{40}$. Urazole-initiator (1.00 equiv, 0.060 g), *n*-butyl acrylate (45.00 equiv, 1.1 mL), Cu^0 (10 pellets) and 2.7 mL of dimethylformamide were degassed by four freeze-pump-thaw cycles and filled with inert gas. In a separate flask, ME_6TREN (0.15 equiv, 0.006 g), $CuBr_2$ (0.05 equiv, 0.001 g) and 3.0 mL of dimethylformamide were introduced and deoxygenated. The $CuBr_2$/ligand solution was added to the reaction mixture. The reaction flask was then immersed in an oil bath at 25 °C. The polymerization was stopped at 75% of monomer conversion. The catalyst was removed by passing the reaction mixture over a column of Al_2O_3. The solvent and the monomer were removed under reduced pressure. (^{1}H NMR spectrum in Section 6.4, **Figure 77**)

Analysis : **^{1}H NMR** (300 MHz, $CDCl_3$) δ 7.68 (br, Ar, 2H), 7.49 (br, Ar, 2H), 4.03 (br, CH_2, 80H), 2.28 (br, CH, 40H), 1.61 (br, CH_2, 80H), 1.38 (br, CH_2, 80H), 0.93 (br, CH_3, 120H) ppm. **HSQC 2D NMR** (500 MHz/126 MHz, $CDCl_3$) δ 7.64/120.2 (Ar, CH), 7.45/125.4 (Ar, CH), 4.00/64.5 (CH_2-O), 1.88/36.3 (CH), 1.57/30.3 (CH_2), 1.33/19.3 (CH_2), 0.89/13.2 (CH_3) ppm. **SEC in THF** $M_{n,\,app}$ = 5500 and Đ = 1.20.

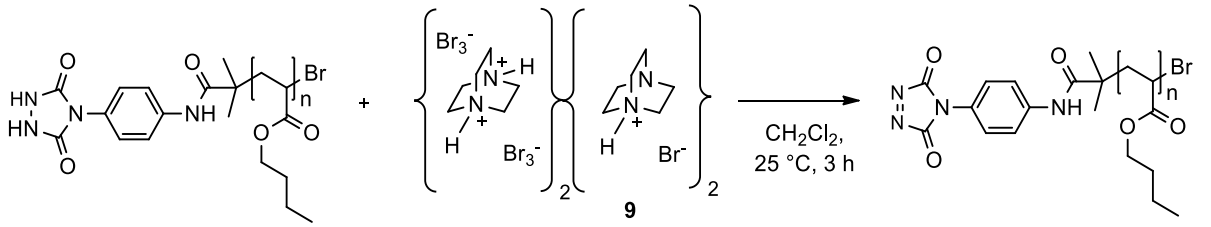

Synthesis of TAD-poly(*n*BuA)$_{40}$. Ur-poly(*n*BuA)$_{40}$ (1 equiv. of urazole group, 5 000 g/mol, 45 mg) was dissolved in 2 mL of dry dichloromethane. DABCO-Br (2 equiv, 29 mg) was added to the solution and the mixture was stirred at room temperature for 3 h. After filtration, a red solution was obtained, and TAD-poly(*n*BuA)$_{40}$ was directly used without any further purification.

Synthesis of Ur-poly(*n*BuA)$_{60}$. Urazole-initiator (1.00 equiv, 0.050 g), *n*-butyl acrylate (80.00 equiv, 1.7 mL), Cu^0 (10 pellets) and 3.5 mL of dimethylformamide were degassed by four freeze-pump-thaw cycles and filled with inert gas. In a separate flask, ME_6TREN (0.15 equiv, 0.005 g), $CuBr_2$ (0.05 equiv, 0.001 g) and 3.5 mL of dimethylformamide were introduced and deoxygenated. The $CuBr_2$/ligand solution was added to the reaction mixture. The reaction flask was then immersed in an oil bath at 25 °C. The polymerization was stopped at 75% of monomer conversion. The catalyst was removed by passing the reaction mixture over a column of Al_2O_3. The solvent and the monomer were removed under reduced pressure. (^{1}H NMR spectrum in Section 6.4, **Figure 78**)

Analysis : **^{1}H NMR** (300 MHz, $CDCl_3$) δ 7.70 (br, Ar, 2H), 7.48 (br, Ar, 2H), 4.03 (br, CH_2, 120H), 2.28 (br, CH, 60H), 1.61 (br, CH_2, 120H), 1.38 (br, CH_2, 120H), 0.96 (br, CH_3, 180H) ppm. **HSQC 2D NMR** (500 MHz/126 MHz, $CDCl_3$) δ 7.68/120.4 (Ar, CH), 7.49/125.2 (Ar, CH), 4.06/64.4 (CH_2-O), 1.88/36.8 (CH), 1.57/30.3 (CH_2), 1.34/19.2 (CH_2), 0.88/13.1 (CH_3) ppm. **SEC in DMAc** $M_{n,\,app}$ = 8300 and Đ = 1.20.

Synthesis of TAD-poly(*n*BuA)$_{60}$. Ur-poly(*n*BuA)$_{60}$ (1 equiv. of urazole group, 7500 g/mol, 80 mg) was dissolved in 2 mL of dry dichloromethane. DABCO-Br (2 equiv, 1573 g/mol, 30 mg) was added to the solution and the mixture was stirred at room temperature for 3h. After filtration, a red solution was obtained and TAD-poly(*n*BuA)$_{40}$ was directly used without any further purification.

6.3.8. Linear bottlebrush polymer synthesis via «grafting onto» approach

NMP homopolymerization of 4-tert-butoxystyrene

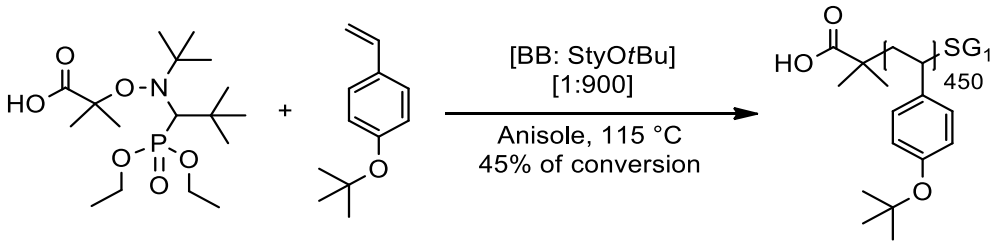

Synthesis of *l*-poly(StyO*t*Bu)$_{380}$. In a 25 mL-Schlenk, Blocbuilder MA (1 equiv, 0.015 mmol, 0.012 g) was dissolved in 2.60 mL of anisole and 5.34 mL of *4*-tert-butoxystyrene (900 equiv, 15.000 mmol) was added. The flask was sealed with a septum, deoxygenated by four freeze-pump-thaw cycles and filled with argon. The mixture was then immersed in a pre-heated bath at 115 °C. At timed intervals, aliquots were taken from the mixture with a degassed syringe to monitor the monomer conversion and polymer molecular weights by proton NMR and SEC in DMAC, respectively. The polymerization was opened to air when the monomer conversion reached approximatively 45%. The polymer was precipitated three times in cold methanol and dried under vacuum.

Analysis : **^{1}H NMR** (500 MHz, $CDCl_3$) δ 6.82 - 6.12 (br, Ar, 4H), 2.05 - 1.57 (br, CH, 1H), 1.51 - 1.01 (br, CH_2, CH_3, 11H) ppm. **HSQC 2D NMR** (500 MHz/126 MHz, $CDCl_3$) δ 6.64/123.0 (Ar, CH), 6.36/127.2 (Ar, CH), 1.80/39.1 (CH), 1.34/44.1 (CH_2), 1.29/29.5 (CH_3) ppm. **SEC in DMAc** $M_{n,\,app}$ = 77000 and Đ = 1.13.

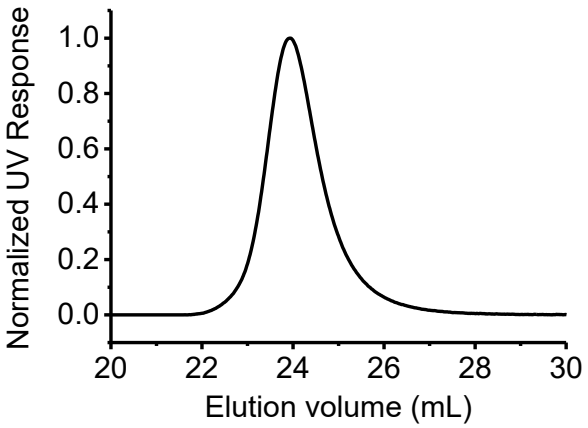

Figure 52. SEC chromatogram.

Backbone deprotection

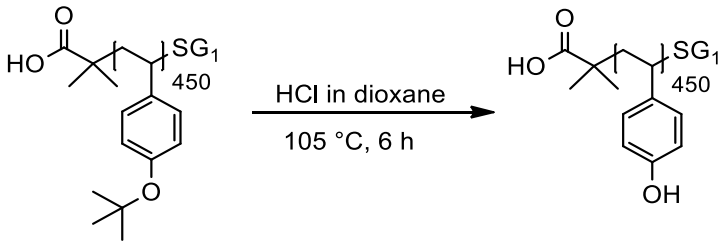

Synthesis of *l*-poly(StyOH)$_{450}$. The homopolymer *l*-poly(StyO*t*Bu)$_{380}$ (M_n = 77000 g/mol, 0.3 g) was dissolved in 70.0 mL of dioxane in a three-neck-flask. Then 1.5 mL of HCl (37%) was added to the solution and the mixture was refluxed for 6 h at 105 °C to afford the deprotected poly(4-hydroxystyrene). After completion of the hydrolysis, the mixture was cooled to room temperature. The polymer was then precipitated twice in cold water (×2), in cold hexane (×1) and dried under vacuum. (^{1}H NMR spectrum in Section 6.4, **Figure 79**)

Analysis : **^{1}H NMR** (400 MHz, CD_3OD) δ 6.80 - 6.14 (br, Ar, 4H), 2.30 - 1.65 (br, CH, 1H), 1.65 - 1.05 (br, CH_2, 2H) ppm. **HSQC 2D NMR** (500 MHz/126 MHz, CD_3OD) δ 6.55/114.5 (Ar, CH), 6.40/128.4 (Ar, CH), 1.84/40.0 (CH), 1.39/44.2 (CH_2) ppm. **SEC in DMAc** $M_{n,\,app}$ = 85000 and Đ = 1.23.

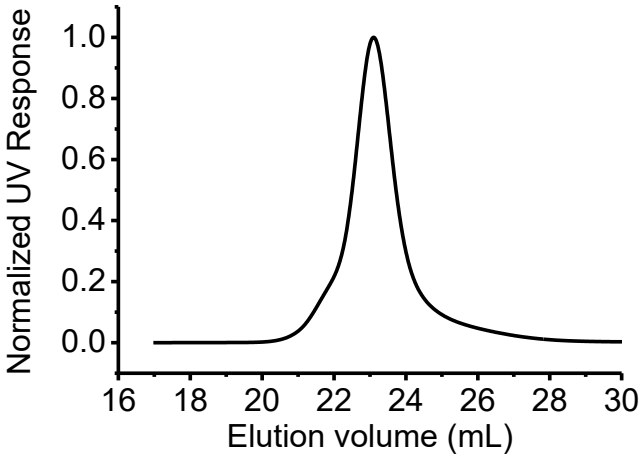

Figure 53. SEC chromatogram.

Macroinitiator synthesis [238]

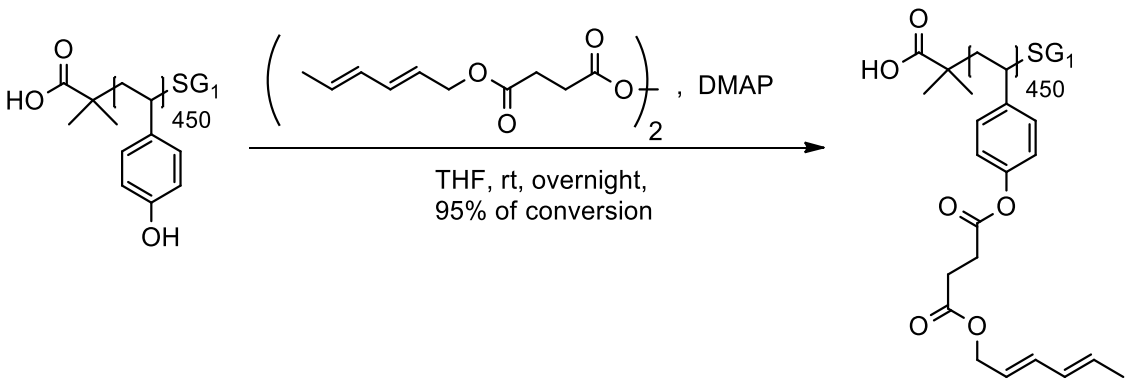

Synthesis of *l*-poly(Sty-diene)$_{450}$. In a dry flask, *l*-poly(StyOH)$_{450}$ (1 equiv of active centres, 55000 g/mol, 0.32 mmol, 0.040 g) was dissolved in 60 mL of dry tetrahydrofuran under inert atmosphere and the solution was cooled in an ice bath. The symmetric anhydride of 2,4-hexadien-1-yl succinic acid monoester (4 equiv, 1.28 mmol, 0.483 g) and DMAP (4 equiv, 1.28 mmol, 0.156 g) were added to the solution. The mixture was stirred at room temperature overnight. Then the solvent was removed under reduced pressure and the polymer was precipitated three times in cold methanol. The polymer was freeze-dried in benzene to afford a brownish polymer. (^{1}H NMR spectrum in Section 6.4, **Figure 80**)

Analysis : **^{1}H NMR** (300 MHz, $CDCl_3$) δ 7.01 – 6.15 (m, Ar, CH, 5H), 6.02 (m, CH, 1H), 5.67 (m, *J* = 38.9 Hz, CH, 2H), 4.61 (d, *J* = 6.5 Hz, CH_2, 2H), 2.90 - 2.70 (d, *J* = 31.6 Hz, CH_2, 4H), 1.72 (d, *J* = 6.5 Hz, CH_3, 3H), 1.28 (br, CH_2, 2H) ppm. **SEC in DMAC** $M_{n,\,app}$ = 92000 and Đ = 1.24.

Synthesis of linear bottlebrush polymer ($DP_{backbone}$ = 450) [238]

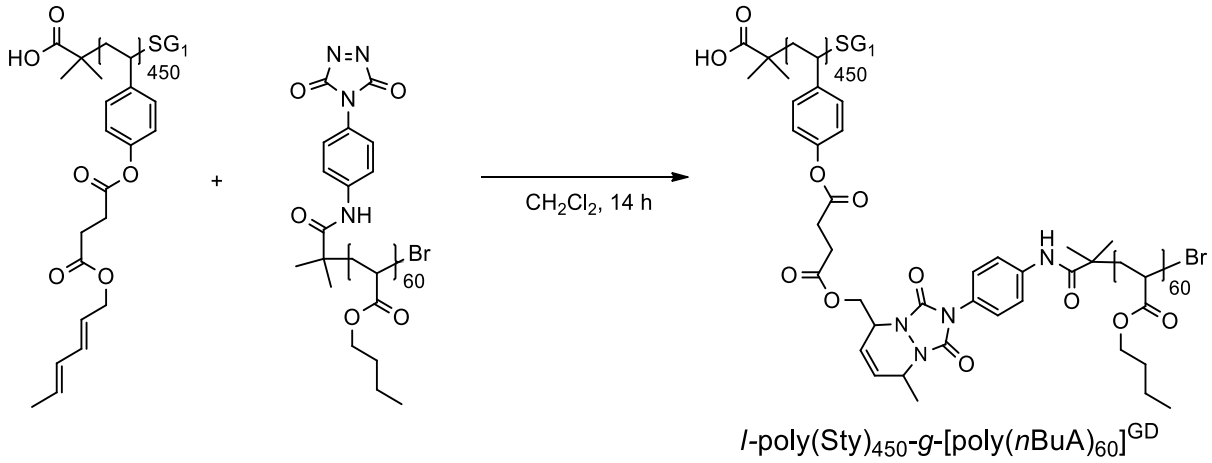

Synthesis of *l*-[poly(Sty)$_{450}$-*g*-poly(*n*BuA)$_{60}$]$^{0.7}$ (GD = 70%). In a dry flask, the polymer backbone *l*-poly(Sty-diene)$_{450}$ (1 equiv of diene groups, 135000 g/mol, 0.003 g) was dissolved in 0.6 mL of dry dichloromethane. In a separate dry flask, TAD-terminated polymer TAD-poly(*n*BuA)$_{60}$ was dissolved in 2.0 mL of dry dichloromethane (1.1 equiv of TAD end-groups, 7500 g/mol, 0.080 g) and was then added to the reaction flask under inert atmosphere. The grafting reaction was stirred at room temperature for 14 h. The reaction was then opened to air and the polymer was precipitated in cold methanol. The polymer was dried under vacuum. (^{1}H NMR spectrum in Section 6.4, **Figure 81**)

Analysis : **^{1}H NMR** (500 MHz, $CDCl_3$) δ 7.60, 7.39, 6.75, 6.60, 6.26, 6.00, 5.86, 5.73, 4.59, 4.48, 4.40, 4.03, 2.27, 1.59, 1.36, 0.93 ppm. **SEC in DMAc** $M_{n,\,app}$ = 44000 and Đ = 2.15 (crude).

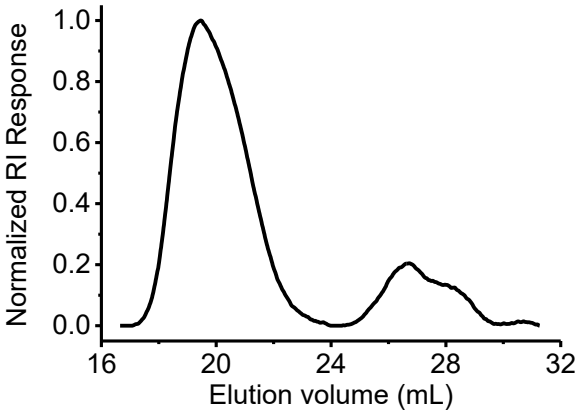

Figure 54. SEC chromatogram.

Synthesis of *l*-[poly(Sty)$_{450}$-*g*-poly(*n*BuA)$_{60}$]$^{1.0}$ (GD = 100%). In a dry flask, TAD-terminated polymer TAD-poly(*n*BuA)$_{60}$ was dissolved in 2.0 mL of dry dichloromethane (2 equiv of TAD end-groups, 7500 g/mol, 0.150 g). In a separate dry vial, the polymer backbone *l*-poly(Sty-diene)$_{450}$ (1 equiv of diene groups, 135000 g/mol, 0.003 g) was dissolved in 0.6 mL of dry dichloromethane and was then added to the reaction flask under inert atmosphere. The grafting reaction was stirred at room temperature for 14 h. The reaction was then opened to air and the polymer was precipitated in cold methanol. The polymer was dried under vacuum. (^{1}H NMR spectrum in Section 6.4, **Figure 82**)

Analysis : **^{1}H NMR** (500 MHz, $CDCl_3$) δ 7.62, 7.42, 6.72, 5.89, 5.79, 4.68, 4.53, 4.46, 4.04, 3.46, 2.72, 2.28, 1.90, 1.59, 1.38, 0.95 ppm (See spectrum in Section 6.4). **SEC in DMAc** $M_{n,\,app}$ = 415000 and Đ = 1.36.

Macroinitiator synthesis (DPn = 50)

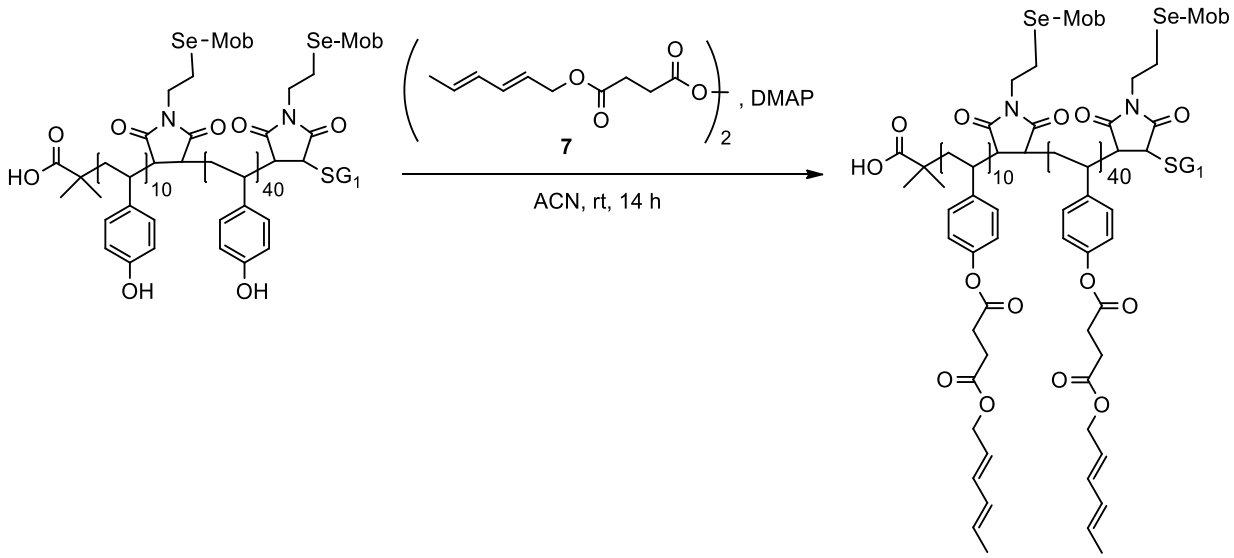

The linear macroinitiator *l*-poly(Sty-diene-*co*-MISeMob)$_{50}$ was synthesized from the linear copolymer precursor *l*-poly(StyOH-*co*-MISeMob).

Synthesis of *l*-poly(Sty-diene-*co*-MISeMob)$_{50}$. The linear copolymer *l*-poly(StyOH-*co*-MISeMob) (1 equiv of active centers, 7000 g/mol, 0.020 g) was dissolved in 50 mL of dry acetonitrile under inert atmosphere and the solution was cooled in an ice bath. The symmetric anhydride of 2,4-hexadien-1-yl succinic acid monoester (5 equiv, 0.320 g) and 4- dimethyl aminopyridine (5 equiv, 0.065 g) were added to the solution. The mixture was stirred at room temperature overnight. The solvent was removed under reduced pressure and the polymer was precipitated in methanol. The polymer was freeze-dried in benzene. (^{1}H NMR spectrum in Section 6.4, **Figure 83**)

Analysis : **^{1}H NMR** (300 MHz, $CDCl_3$) δ 7.08 – 6.15 (m, Ar, CH, 5H), 6.03 (m, CH, 1H), 5.66 (br, CH, 2H), 4.61 (br, CH_2, 2H), 2.90 - 2.70 (br, CH_2, 4H), 1.74 (d, J = 5.6 Hz, CH_3, 3H), 1.30 (br, CH_2, 2H) ppm. **SEC in THF** $M_{n,\,app}$ = 14300 and Đ = 1.11.

Synthesis of bottlebrush polymer (DPn $_{Backbone}$ = 50)

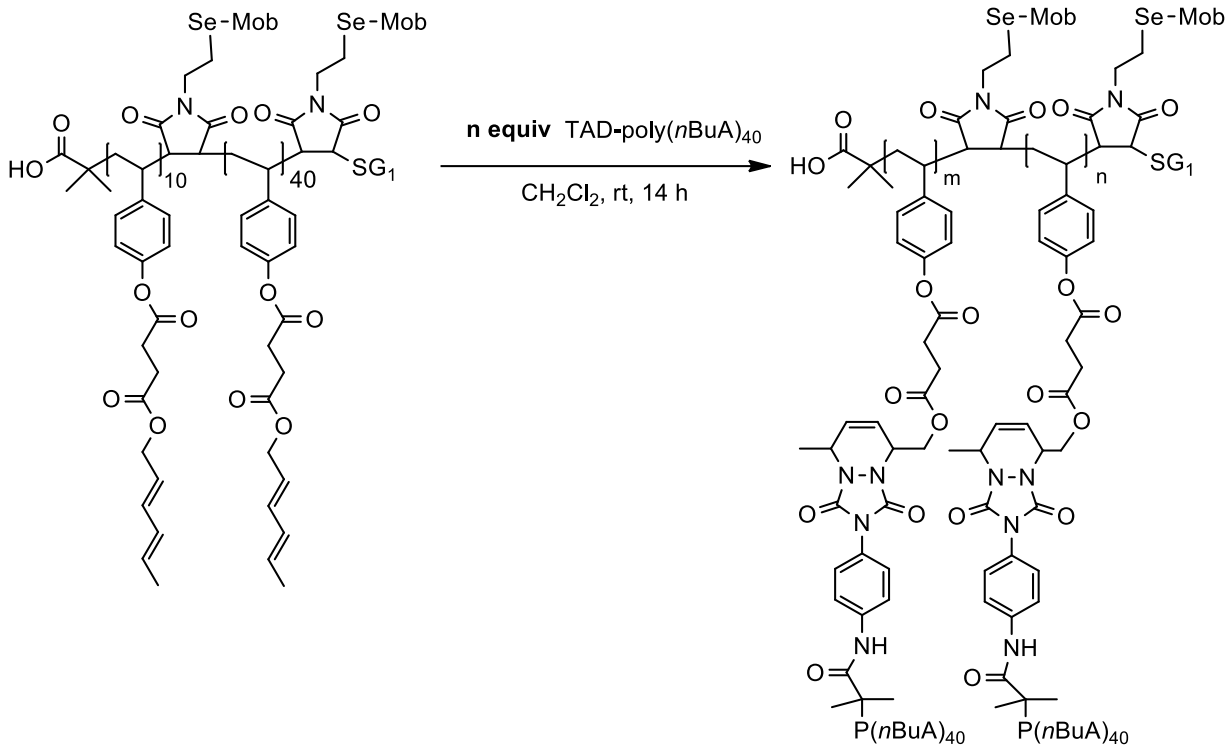

Synthesis of *l*-poly(Sty)$_{50}$-*g*-[poly(*n*BuA)$_{40}$]$^{0.43}$. The linear macroinitiator *l*-poly(Sty-diene-*co*-MISeMob)$_{50}$ polymer backbone (1.0 equiv, 9.0×10^{-6} mol of active centers, 16100 g/mol, 0.0029 g) was dissolved in 0.5 mL of dry dichloromethane and was added dropwise to a flask containing a solution of TAD-poly(*n*BuA)$_{40}$ polymer (1.0 equiv of TAD functionalities, 5000 g/mol, 9.0×10^{-5} mol, 0.0450 g) dissolved in 2.0 mL of dry dichloromethane. The grafting reaction was stirred at room temperature under inert atmosphere for 14h. The reaction was then opened to air and was dried under vacuum. The side chain grafting density (GD) was estimated approximatively at 43% by ^{1}H NMR. (^{1}H NMR spectrum in Section 6.4, **Figure 84**)

Analysis : **^{1}H NMR** (600 MHz, $CDCl_3$) δ 7.64, 7.44, 6.75, 6.47, 6.23, 6.02, 5.88, 5.79, 5.73, 5.60, 4.59, 4.03, 2.83, 2.72, 2.28, 1.91, 1.59, 1.37, 0.94 ppm. (See spectrum in Section 6.4)
SEC in THF $M_{n,\,app}$ = 75000 and Đ = 2.58.

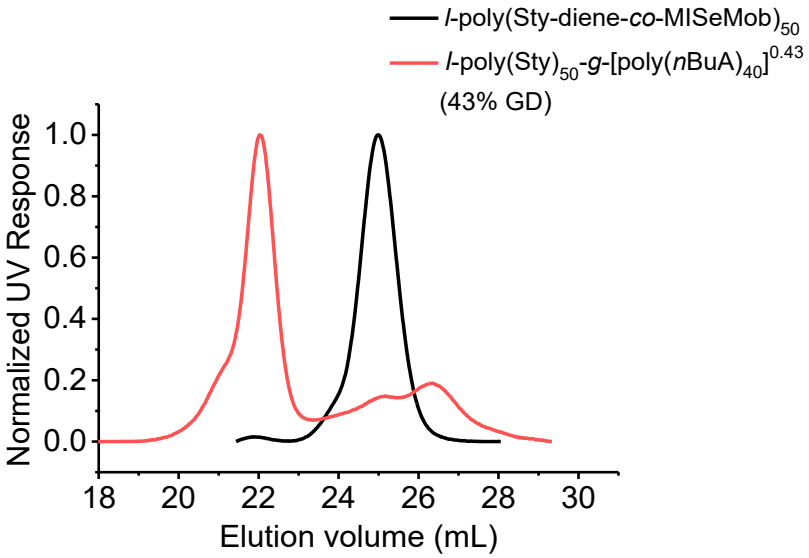

Figure 55. SEC traces of *l*-poly(Sty-diene-*co*-MISeMob)$_{50}$ and the crude linear grafted polymer *l*-poly(Sty)$_{50}$-*g*-[poly(*n*BuA)$_{40}$]$^{0.43}$.

6.3.9. Synthesis of cyclic brush polymers via «grafting onto» approach

Macroinitiator synthesis

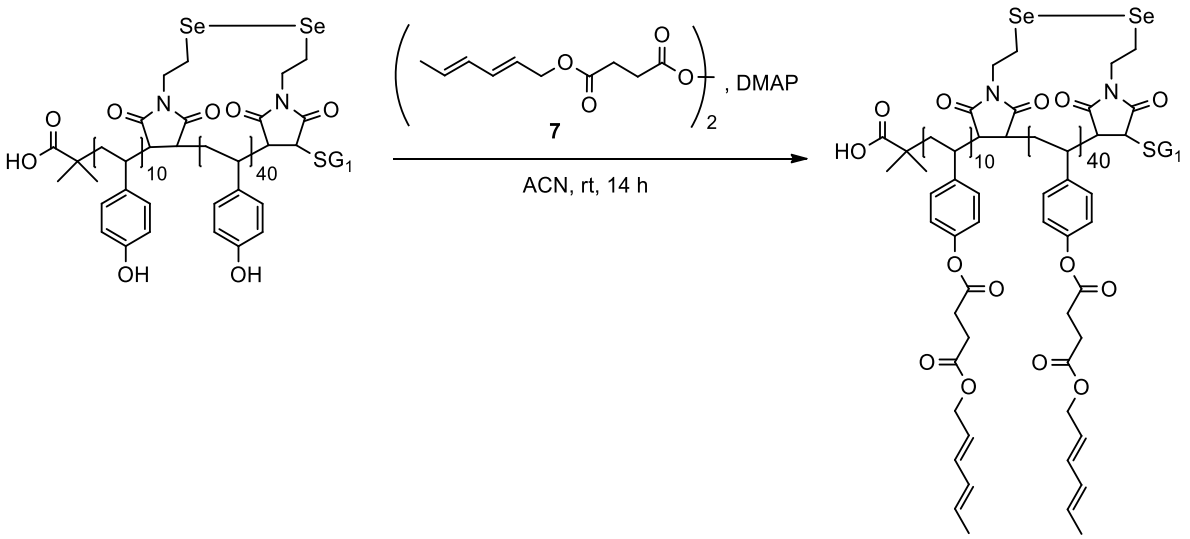

Synthesis of *c*-poly(Sty-diene-*co*-MISe). The cyclic polymer (1 equiv of active centers, 0.015 g) was dissolved in 60 mL of dry acetonitrile under inert atmosphere and the solution was cooled in an ice bath. The symmetric anhydride of 2,4- hexadien-1-yl succinic acid monoester (7) (5 equiv, 0.210 g) and 4dimethylaminopyridine (5 equiv, 0.065 g) were added to the solution. The mixture was stirred at room temperature overnight. The solvent was removed under reduced pressure and the polymer was precipitated in methanol. The polymer was freeze-dried in benzene. (^{1}H NMR spectrum in Section 6.4, **Figure 85**)

Analysis : **^{1}H NMR** (300 MHz, $CDCl_3$) δ 7.08 – 6.15 (m, Ar, CH, 5H), 6.03 (m, CH, 1H), 5.74 (m, CH, 1H), 5.61 (m, CH, 1H), 4.61 (d, CH_2, 2H), 3.74 – 3.68 (br, CH_2, CH, 8H), 2.90 - 2.50 (br, *J* = 31.1 Hz, CH_2, 4H), 1.74 (d, CH_3, 3H), 1.30 (br, CH_2, 2H) ppm. **SEC in THF** $M_{n,\,app}$ = 14400 and Đ = 1.22.

Synthesis of cyclic brush polymers c-poly(Sty)$_{50}$-g-[poly(nBuA)$_{40}$]^{GD}

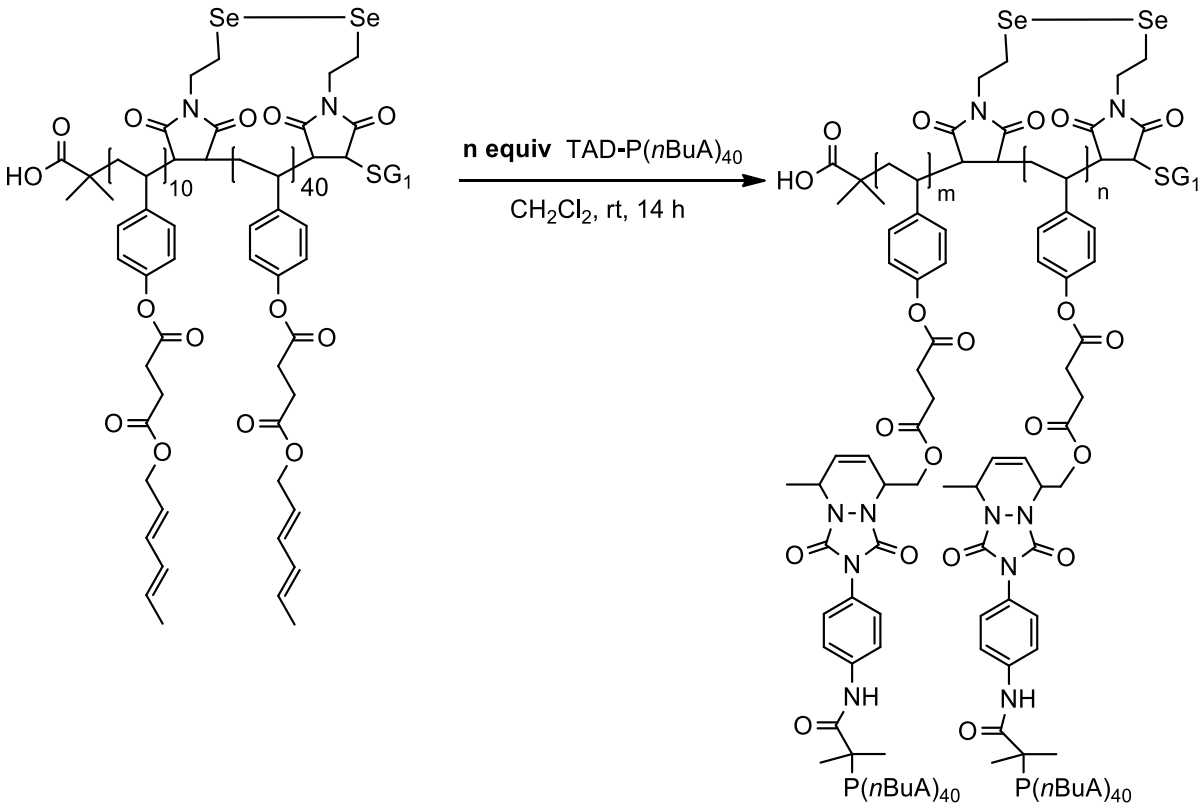

Synthesis of *c*-poly(Sty)$_{50}$-*g*-[poly(*n*BuA)$_{40}$]$^{0.27}$ (GD = 27%). *c*-poly(Sty-diene-*co*-MISe) (1.0 equiv of active centers, 15800 g/mol, 2.9 mg) was dissolved in 0.6 mL of dry dichloromethane. A solution of TAD-poly(*n*BuA)$_{40}$ polymer (0.7 equiv of TAD functionalities, 5000 g/mol, 0.0320 g) dissolved in 2.0 mL of dry dichloromethane was added dropwise to the reaction flask. The grafting reaction was stirred under inert atmosphere at room temperature for 14 h. The polymer was precipitated in methanol (×2) and dried under vacuum. (^{1}H NMR spectrum in Section 6.4, **Figure 86**)

Analysis : **^{1}H NMR** (600 MHz, $CDCl_3$) δ 7.64, 7.45, 6.76, 6.46, 6.24, 6.02, 5.88, 5.79, 5.73, 5.60, 4.59, 4.03, 2.84, 2.72, 2.27, 1.90, 1.59, 1.37, 0.93 ppm. (See spectrum in Section 6.4) **SEC in THF** $M_{n,\,app}$ = 58000 and Đ = 2.25 (crude).

Synthesis of *c*-poly(Sty)$_{50}$-*g*-[poly(*n*BuA)$_{40}$]$^{0.65}$ (GD = 65%). *c*-poly(Sty-diene-*co*-MISe) (1.0 equiv of active centers, 15800 g/mol, 2.9 mg) was dissolved in 0.6 mL of dry dichloromethane. A solution of TAD-poly(*n*BuA)$_{40}$ polymer (1.0 equiv of TAD functionalities, 0.0450 g) dissolved in 2.0 mL of dry dichloromethane was added dropwise to the reaction flask. The grafting reaction was stirred under inert atmosphere at room temperature for 14 h. The polymer was precipitated in methanol (×2) and dried under vacuum. (^{1}H NMR spectrum in Section 6.4, **Figure 87**)

Analysis: **^{1}H NMR** (600 MHz, $CDCl_3$) δ 7.63, 7.43, 6.74, 6.46, 6.23, 6.01, 5.87, 5.78, 5.72, 5.59, 4.58, 4.03, 2.70, 2.27, 1.90, 1.59, 1.36, 0.93 ppm. (See spectrum in Section 6.4) **SEC in THF** $M_{n,\,app}$ = 78000 and Đ = 3.18 (crude).

Synthesis of *c*-poly(Sty)$_{50}$-*g*-[poly(*n*BuA)$_{40}$]$^{1.0}$ (GD = 100%). *c*-poly(Sty-diene-*co*-MISe) polymer backbone (1 equiv of active centers, 15800 g/mol, 2.9 mg) was dissolved in 0.6 mL of dry dichloromethane and was added dropwise to a solution of TAD-poly(*n*BuA)$_{40}$ polymer (2 equiv of TAD functionalities, 0.0910 g) in 2.0 mL of dry dichloromethane. The grafting reaction was stirred under inert atmosphere at room temperature for 14 h. The polymer was precipitated in cold methanol (×2) and dried under vacuum. The polymer was further purified by standard SEC Chromatography in THF to removed unreacted side polymer chains. High molecular weight peak in the elugram, appearing between 20 and 24 mL was isolated. Multiple runs were conducted to purify *c*-poly(Sty)$_{50}$-*g*-[poly(*n*BuA)$_{40}$]$^{1.0}$. (^{1}H NMR spectrum in Section 6.4, **Figure 88**)

Analysis : **^{1}H NMR** (600 MHz, $CDCl_3$) δ 7.60, 7.39, 6.67, 6.42, 5.85, 5.76, 4.66, 4.51, 4.42, 4.03, 2.67, 2.27, 1.90, 1.59, 1.37, 0.93 ppm. **SEC in THF** $M_{n,\,app}$ = 89000 and Đ = 1.03.

6.3.10. *N*-(2-tritylthioethyl) maleimide synthesis

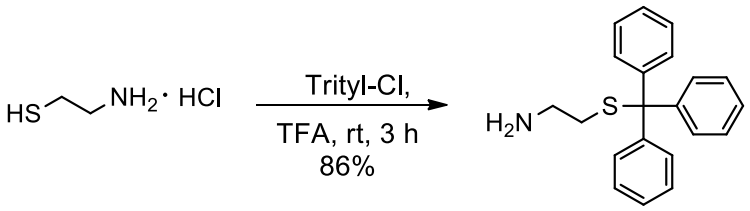

Synthesis of 2-(Tritylthio)ethylamine.[277] In a 100mL flask, 2-aminoethanethiol hydrochloride (1 equiv, 8.80 mmol, 1 g) was dissolved in 6.25 mL of trifluoroacetic acid and trityl chloride (1 equiv, 8.80 mmol, 2.45 g) was added to the solution. The mixture turned into a deep red solution and was stirred for 3 h at room temperature. The mixture was concentrated under reduced pressure. The residue was diluted in ethyl acetate and washed with 3N NaOH (×3), water (×1), and $NaHCO_3$ (×2). The organic phase was dried over $MgSO_4$ and concentrated. The resulting material was recrystallized from dichloromethane in hexane and dried under vacuum to afford a light yellow solid (2.39 g, 86%).

Analysis : **^{1}H NMR** (300 MHz, $CDCl_3$) δ 7.49 – 7.39 (m, Ar, 6H), 7.32 – 7.17 (m, Ar, 9H), 2.60 (t, J = 6.5 Hz, CH_2, 2H), 2.32 (t, J = 6.5 Hz, CH_2, 2H) ppm. **^{13}C NMR** (75 MHz, $CDCl_3$) δ 145.01(C), 129.71 (CH), 127.98 (CH), 126.77 (CH), 66.64 (C), 41.19 (CH_2), 36.46 (CH_2) ppm. **IR** (KBr): ν = 3365 cm^{-1} (w, N-H), 3200 cm^{-1} (br, C-H), 2899 cm^{-1} (w), 2800 cm^{-1} (w), 1600-1430 cm^{-1} (s, C=C), 1162 cm^{-1} (w), 1005 cm^{-1} (w), 735 cm^{-1} (s), 683 cm^{-1} (s), 616 cm^{-1} (m), 512 cm^{-1} (w).

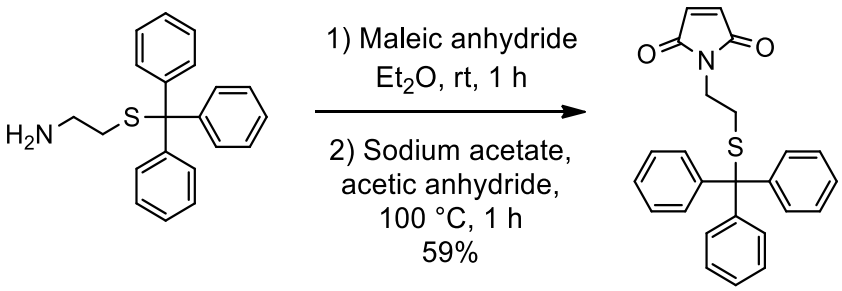

Synthesis of *N*-(2-tritylthioethyl) maleimide (MISTrt).[212] In a 25mL flask, maleic anhydride (1.2 equiv, 3.75 mmol, 0.37 g) was dissolved in 8.0 mL of diethyl ether. After complete dissolution, a concentrated solution of 2-(tritylthio)ethylamine in diethyl ether/chloroform (4/1) was added dropwise to the flask (1.0 equiv, 3.13 mmol, 1.00 g). A white suspension was obtained, and the reaction mixture was stirred for 1 h at room temperature. The mixture was cooled down in an ice bath. The *N*-(2-tritylthioethyl) maleanic acid was filtrated, washed with diethyl ether and dried under vacuum. The obtained maleamic acid (1.0 equiv, 3.13 mmol, 1.25 g) was then added to a 3-neck-flask containing a solution of anhydrous sodium acetate (0.8 equiv, 2.40 mmol, 0.24 g) in acetic anhydride (2.5 mL) and the reaction was stirred for 1 h at 100 °C. The resulting mixture was cooled down in an ice bath and concentrated under reduced pressure (oil bath at T = 40 °C). The residue was dissolved in chloroform and washed with water (×3) and brine (×1). The organic phase was dried over $MgSO_4$ and concentrated. The crude product was further purified via chromatography column over silica gel using cyclohexane/ethyl acetate (5/1) as eluent. The product was the recrystallized in ethyl acetate/cyclohexane (1/1) to afford a white solid (0.74 g, 59%). (^{1}H NMR spectrum in Section 6.4, **Figure 89**)

Analysis : **^{1}H NMR** (300 MHz, $CDCl_3$) δ 7.44 – 7.15 (m, Ar, 15H), 6.63 (s, CH, 2H), 3.40 (t, J = 7.2 Hz, 2H), 2.46 (t, J = 7.2 Hz, 2H) ppm. **^{13}C NMR** (75 MHz, $CDCl_3$) δ 170.19 (C=O), 144.54 (C), 134.02 (CH_{alkene}), 129.56 (CH_{Ar}), 127.97 (CH_{Ar}), 126.75 (CH_{Ar}), 36.69 (CH_2), 30.25 (CH_2) ppm. **IR** (KBr): ν = 3050 cm^{-1} (w, C-H), 1770 - 1699 cm^{-1} (s, C=O), 1600 - 1430 cm^{-1} (s, C=C), 1104 cm^{-1} (w), 851 cm^{-1} (m), 761 cm^{-1} (m), 688 cm^{-1} (s), 611 cm^{-1} (w).

6.3.11. Difuntional initiator synthesis

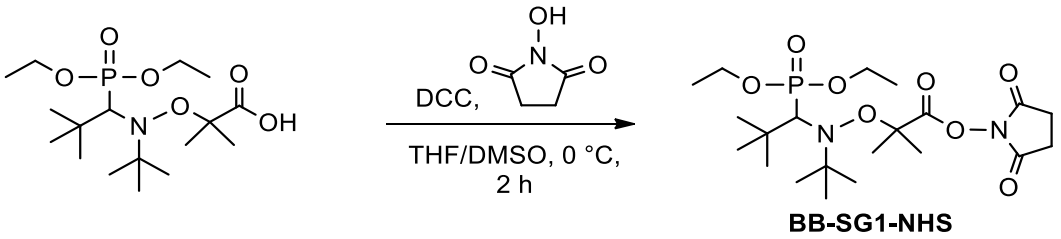

Synthesis of BB-SG1-NHS.[247] In a 100mL flask, N-hydroxysuccinimide (2.1 equiv, 21.7 mmol, 2.50 g) was dissolved in 4 mL of dimethyl sulfoxide. After complete dissolution, 16 mL of tetrahydrofuran were added followed by the addition of Blocbuilder MA (1.0 equiv, 14.3 mmol, 5.47 g) The mixture was bubbled with argon for 30 min. DCC was dissolved in 5 mL of tetrahydrofuran under argon and then was added to the mixture dropwise at 0 °C under inert atmosphere. The mixture was stirred for 2 h at 0 °C. The precipitate was removed by filtration and the residue was concentrated under reduced pressure. The resulting material was solubilized in the minimum amount of tetrahydrofuran and cooled down at -20 °C for 2h. The precipitate was removed by filtration. The product was precipitated in hexane, washed with water (×2) and dried. A white solid was obtained (3.21 g, 48%).

Analysis : **^{1}H NMR** (300 MHz, $CDCl_3$) δ 4.41 – 3.67 (m, CH_2, 4H), 3.30 (d, J = 26.0 Hz, CH, 1H), 2.83 (d, J = 25.9 Hz, CH_2, 4H), 1.89 (s, CH_3, 3H), 1.82 (s, CH_3, 3H), 1.33 – 1.16 (m, CH_3, 24H) ppm. **^{13}C NMR** (126 MHz, $CDCl_3$) δ 170.42 (C=O), 168.99 (C=O) 83.87 (C), 70.02 (d, J = 137.3 Hz, CHP), 62.79 (C), 62.07 (CH_2), 58.92 (CH_2), 36.22 (C), 30.22 (CH_3), 29.43 (CH_3), 28.33 (CH_3), 25.75 (CH_2), 22.09 (CH_3), 16.73 (CH_3), 16.33 (CH_3) ppm. **^{31}P NMR** (202 MHz, $CDCl_3$) δ 24.75 ppm.

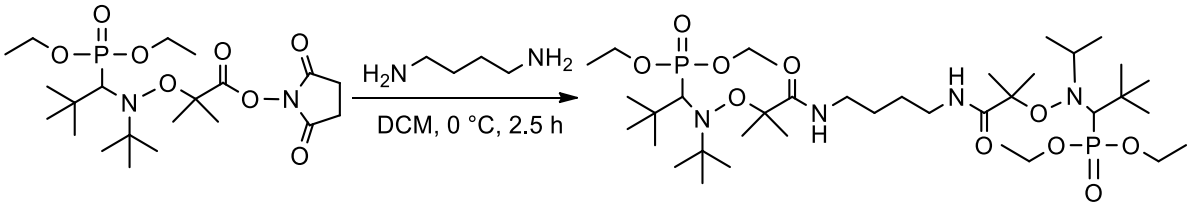

Synthesis of di-alkoxyamine NMP initiator (Bis-BB-SG1). BB-SG1-NHS (2.1 equiv, 1.78 mmol, 0.850 g) was dissolved in 30 mL of dry dichloromethane and bubbled with argon for 30 min. 1,4-diaminobutane (1.0 equiv, 0.84 mmol, 0.074 g) was diluted in 5 mL of dry dichloromethane and added to the solution under inert atmosphere at 0 °C. The mixture was stirred for 2.5 h at 0 °C and the released *N*-hydroxysuccinimide precipitated. The resulting material was filtrated and extracted with water (×3) and brine (×1), dried over $MgSO_4$, and concentrated under reduced pressure. The desired product was purified by chromatography over silica (eluent ethyl acetate /methanol, 2% to 10%). The product was freeze dried in benzene to afford a white solid (0.36 g, 53%). (^{1}H NMR spectrum in Section 6.4, **Figure 90**)

Analysis : **^{1}H NMR** (400 MHz, $CDCl_3$) δ 8.01 (br, NH, 2H), 4.25 – 4.20 (m, CH_2, 2H), 4.05 (ddd, *J* = 8.9, 5.1, 1.9 Hz, CH_2, 6H), 3.38 (br, CH_2, 2H), 3.34 (d, *J* = 22.3 Hz, CH, 2H), 3.04 (br, CH_2, 2H), 3.19 – 2.86 (m, 2H), 1.67 (s, CH_3, 6H), 1.55 (s, CH_3, 6H), 1.31 (dd, *J* = 12.0, 4.8 Hz, CH_3, 12H), 1.18 (s, CH_3, 18H), 1.09 (s, CH_3, 18H) ppm. **^{13}C NMR** (101 MHz, $CDCl_3$) δ 176.45 (*C*=O), 85.89 (NO*C*C=O), 71.20 (N*C*HP), 69.85 (N–*C*$(CH_3)_3$), 62.71 (*C*$H_2$$CH_2$NHC=O), 61.81 (d, *J* = 22.8 Hz, PO*C*$H_2$$CH_3$), 60.08 (d, *J* = 29.4 Hz PO*C*$H_2$$CH_3$), 39.25 ($CH_2$*C*$H_2$NHC=O), 36.37 (d, *J* = 7.1 Hz PCH*C*$(CH_3)_3$), 29.49 (d, *J* = 26.0 Hz, CHC(*C*H_3)$_3$), 27.26 (NC(*C*H_3)$_3$), 24.94 (*C*H_3CC=O), 21.24 (*C*H_3CC=O), 16.80 (d, *J* = 11.8 Hz, POCH$_2$*C*H_3), 16.34 (d, *J* = 7.5 Hz, POCH$_2$*C*H_3) ppm. **^{31}P NMR** (162 MHz, $CDCl_3$) δ 27.60 ppm. **ESI-LCMS :** $[M + H]^+_{calc}$ = 815. 63 g/mol; $[M+H]^+_{found}$ = 815.59 g/mol, 99%.

6.3.12. NMP homopolymerization of 4-*tert*-butoxystyrene by using dialkoxyamine

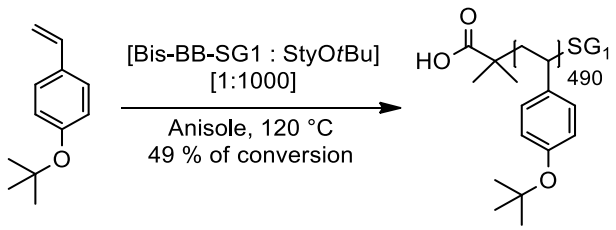

Synthesis of poly(StyO*t*Bu)$_{550}$. Difunctional initiator (Bis-BB-SG1) (1 equiv, 15×10^{-3} mmol, 0.012 g) was dissolved in 1.4 mL of anisole and 2.8 mL of 4-*tert*-butoxystyrene (StyO*t*Bu) (1000 equiv, 15 mmol). The flask was deoxygenated by four freeze-pump-thaw cycles and filled with argon. The mixture was then immersed in a pre-heated bath at 120 °C. At time intervals, aliquots were taken from the mixture with a degassed syringe to monitor the monomer conversion by ^{1}H NMR. The homopolymerization was stopped at 55%. The polymer was precipitated in cold methanol and dried under vacuum (0.7 g).

Analysis : **^{1}H NMR** (500 MHz, $CDCl_3$) δ 6.82 - 6.12 (br, Ar, 2200H), 2.05 - 1.57 (br, CH, 550H), 1.51 - 1.01 (br, CH_3, CH_2, 6050H) ppm. **SEC in THF** (49% of conversion) $M_{n,\,app}$ = 87000 and Đ = 1.23.

6.3.13. Linear bottlebrush polymer synthesis via «grafting from» approach

NMP homopolymerization of 4-tert-butoxystyrene

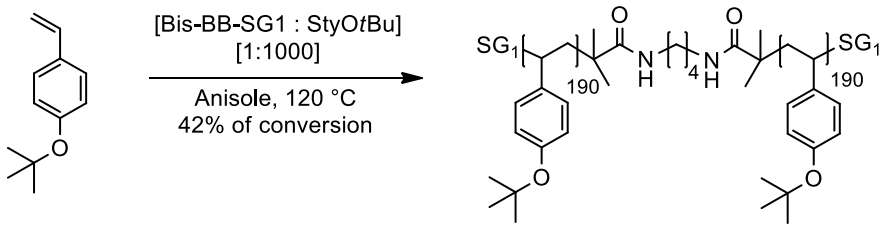

Synthesis of *l*-poly(StyO*t*Bu)$_{380}$. In a 25mL-Schlenk, difunctional NMP-initiator (Bis-BB-SG1) (1 equiv, 15×10^{-3} mmol, 0.012 g) was dissolved in 1.40 mL of anisole and 2.83 mL of 4-*tert*-butoxystyrene (1000 equiv, 15 mmol). The flask was sealed with a septum, deoxygenated by four freeze-pump-thaw cycles and filled with argon. The mixture was then immersed in a pre-heated bath at 120 °C. At timed intervals, aliquots were taken from the mixture with a degassed syringe to monitor monomer conversions and polymer molecular weights by NMR and SEC, respectively. The polymerization was opened to air when the monomer conversion reached 42%. The polymer was precipitated three times in cold methanol and dried under vacuum.

Analysis : **^{1}H NMR** (500 MHz, $CDCl_3$) δ 6.82-6.12 (br, Ar, 4H), 2.05-1.57 (br, CH, 1H), 1.51-1.01 (br, CH_2, CH_3, 11H) ppm. **2D HSQC NMR** (500 MHz/126 MHz, $CDCl_3$) δ 6.64/123.45 (Ar), 6.40/127.68 (Ar), 1.83/39.66 (CH), 1.34/44.81 (CH_2), 1.27/28.77 (CH_3) ppm. **SEC in DMAc** $M_{n,\,app}$ = 66000 and Đ = 1.16.

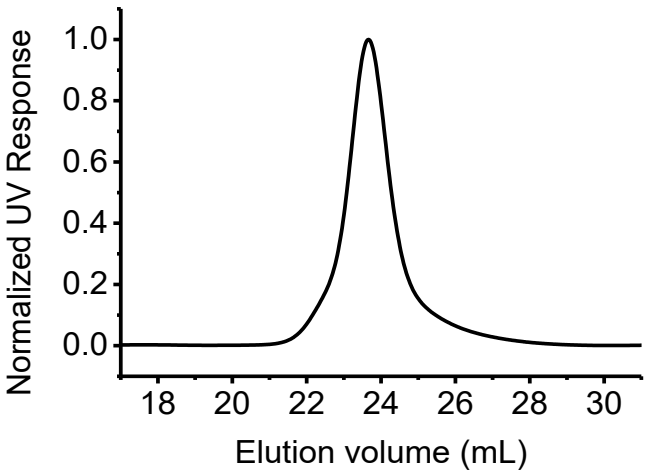

Figure 56. SEC chromatogram.

Removal of tert-butyl protecting group

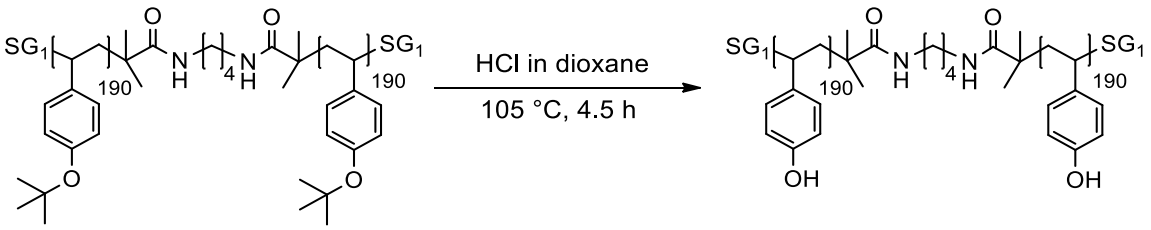

Synthesis of *l*-poly(StyOH)$_{380}$. *l*-poly(StyO*t*Bu)$_{380}$ (M_n = 66000 g/mol, 0.3g) was dissolved in 70.0 mL of dioxane in a three-neck-flask. Then 1.5 mL of HCl (37%) was added to the solution and the mixture was refluxed for 4.5 h at 105 °C. After completion of the hydrolysis, the mixture was cooled to room temperature. The polymer was then precipitated twice in cold water (×2), in cold hexane (×1) and dried under vacuum.

Analysis : **^{1}H NMR** (400 MHz, CD_3OD) δ 6.80-6.14 (br, Ar, 4H), 2.30-1.65 (br, CH, 1H), 1.65-1.05 (br, CH_2, 2H) ppm. **HSQC 2D NMR** (500 MHz/126 MHz, CD_3OD) δ 6.55/114.5 (Ar, CH), 6.40/128.4 (Ar, CH), 1.84/40.0 (CH), 1.39/44.2 (CH_2) ppm. **SEC in DMAC** $M_{n,\,app}$ = 85000 and Đ = 1.23.

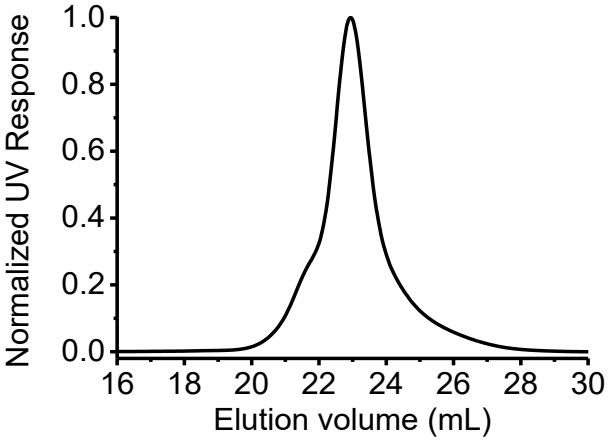

Figure 57. SEC Chromatogram.

Macroinitiator synthesis [39]

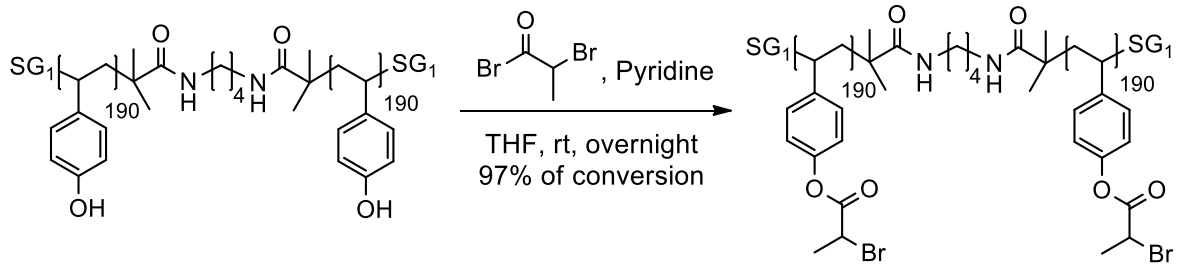

Synthesis of *l*-poly(StyBr)$_{380}$. A dry schlenk was charged with *l*-poly(StyOH)$_{380}$ (1 equiv of hydroxyl groups, 0.16 mmol, M_n = 45000 g/mol, 0.02 g) and purged with argon. 40.00 mL of dry tetrahydrofuran was added to the flask under argon, followed by the addition of pyridine (50 equiv, 8.40 mmol, 0.68 mL). Then 2-bromopropionyl bromide (50 equiv, 8.40 mmol, 0.87 mL) was added dropwise to the flask under argon at 0 °C. The mixture was stirred overnight at room temperature. The mixture was filtered and concentrated under reduced pressure. The polymer was precipitated three times in cold methanol, freeze-dried in benzene (98% of conversion determined by ^{1}H NMR). (^{1}H NMR spectrum in Section 6.4, **Figure 91**)

Analysis : **^{1}H NMR** (300 MHz, $CDCl_3$) δ 7.12-6.25 (br, Ar, 4H), 4.58 (br, CH, 1H), 1.94 (br, CH_3, 3H), 1.70 (br, CH, 1H), 1.36 (br, CH_2, 2H) ppm. **SEC in DMAc** $M_{n,\,app}$ = 88000 and Đ = 1.24.

Synthesis of linear molecular brush polymer [39]

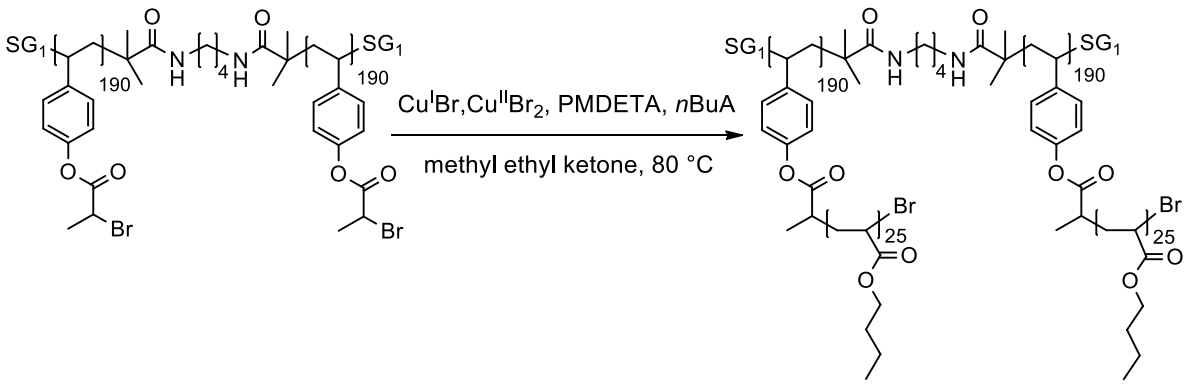

Synthesis of *l*-poly(Sty)$_{380}$-*g*-poly(*n*BuA)$_{25}$). In a 25mL-Schlenk, the ATRP-macroinitiator *l*-poly(StyBr)$_{380}$ (1 equiv of active centers, 1.94×10^{-5} mol, 0.0050 g) was dissolved in 0.20 mL of methyl ethyl ketone. *n*-butyl acrylate (500 equiv, 9.7×10^{-3} mol, 1.40 mL) was added to the reaction flask, followed by the addition of PMDETA (0.525 equiv, 1.02×10^{-5} mol, 0.0018 g). The flask was sealed with a septum, deoxygenated by four freeze-pump-thaw cycles and filled with inert gas. After stirring for 30 min, CuBr (0.5 equiv, 9.7×10^{-5} mol, 0.0014 g) and $CuBr_2$ (0.025 equiv, 4.9×10^{-7} mol, 0.0001 g) were added to the flask under inert atmosphere. An initial sample was taken, and the flask was then immersed in pre-heated oil bath at 80°C. The polymerization was monitored by ^{1}H NMR. At 5% of monomer conversion, the polymerization was stopped, and the flask was opened to air and cooled to room temperature. The catalyst was removed by passing the mixture through an alumina oxide column. The solvent and the monomer were removed under reduced pressure. Then the polymer was precipitated in cold methanol (×2) and freeze-dried in benzene. (^{1}H NMR spectrum in Section 6.4, **Figure 92**)

Analysis : **Gravimetry** 57 mg of brush polymer, 4.5 % of conversion. **^{1}H NMR** (500 MHz, $CDCl_3$) δ 7.00-6.30 (br, Ar, 4H), 4.03 (br, CH_2, 2H), 2.28 (br, CH, 1H), 1.58 (br, CH_2, 2H), 1.36 (br, CH_2, 2H), 0.93 (br, CH_3, 3H) ppm. **SEC in DMAc** $M_{n,\,app}$ = 517000 and Đ = 1.28.

6.3.14. Sequence-controlled polymerizations of 4-*tert*-butoxystyrene and MISTrt

Sequence-controlled polymerization by using monofunctional initiator (Blocbuilder)

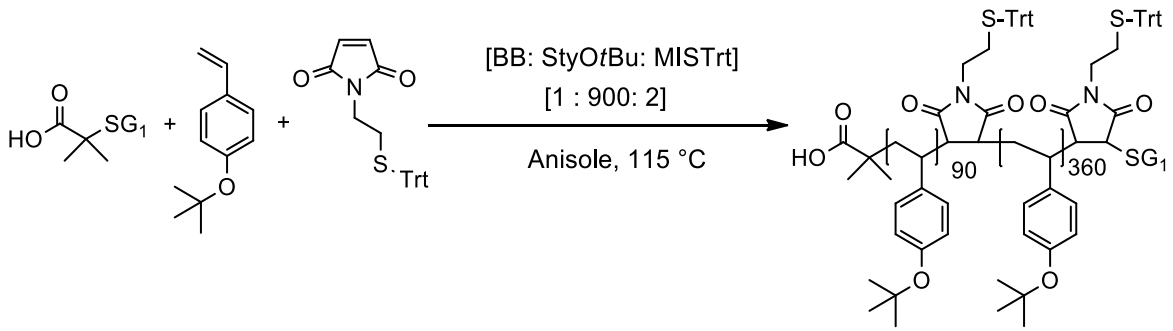

Synthesis of BB-poly(StyO*t*Bu-*co*-MISTrt). Blocbuilder MA (BB) (1 equiv, 0.0120 g) was dissolved in 2.0 mL of anisole and 5.3 mL of 4-*tert*-butoxystyrene (StyO*t*Bu) (900 equiv). The flask was deoxygenated by four freeze-pump thaw cycles and filled with argon. The mixture was then immersed in a pre-heated bath at 115 °C. At time intervals, aliquots were taken from the mixture with a degassed syringe to monitor the monomer conversion by ^{1}H NMR. When the conversion reached approximately 7%, a degassed solution of MISTrt (1 equiv, 0.0125 g) in 0.5 mL of anisole was added to the polymerization. A second addition of degassed solution containing MISTrt (1 equiv, 0.0125 g) in 0.5 mL of anisole was performed when the conversion of 4-*tert*-butoxystyrene reached 46%. The polymerization was stopped at approximatively 50%. The polymer was precipitated in cold methanol (×3) and dried.

Analysis : **^{1}H NMR** (300 MHz, $CDCl_3$) δ 7.29 (br, Ar_{Trt}, 15H), 6.88 – 6.16 (br, Ar, 1800H), 1.62 (br, CH, 450H), 1.25 (br, CH_2, CH_3, 4950H) ppm. **SEC in THF** $M_{n,app}$ = 57000 and Đ = 1.43.

Sequence-controlled polymerization of 4-tert-butoxystyrene and MISTrt by using Bis-BB-SG1

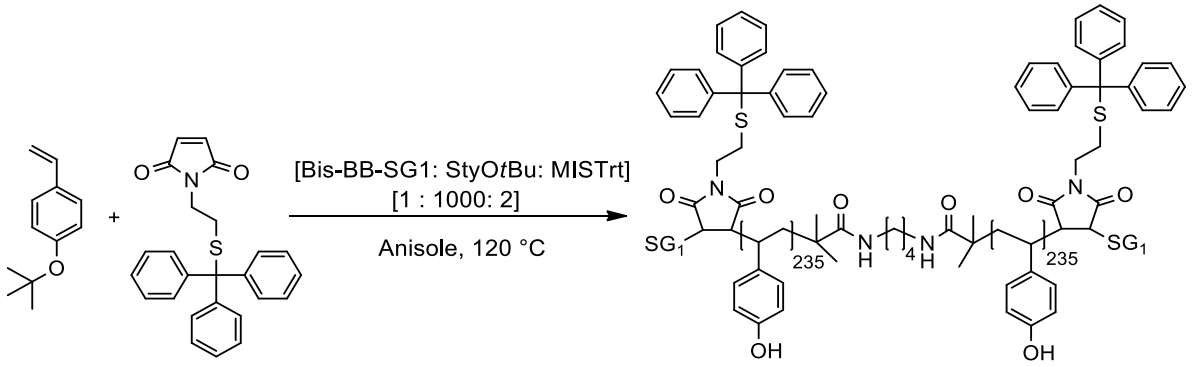

Synthesis of (Bis-poly(StyO*t*Bu-*co*-MIStrt)). The difunctional initiator Bis-BB-SG1 (1 equiv, 0.021 g) was dissolved in 2.5 mL of anisole and 5.0 mL of 4-*tert*-butoxystyrene (StyO*t*Bu) (1000 equiv). The flask was deoxygenated by four freeze-pump thaw cycles and filled with argon. The mixture was then immersed in a pre-heated bath at 120 °C. At time intervals, aliquots were taken from the mixture with a degassed syringe to monitor the monomer conversion by ^{1}H NMR. One single injection of MISTrt maleimide solution (2 equiv, 0.021 g) in 0.5 mL of anisole was performed during the homopolymerization of StyO*t*Bu at approximatively 44% of 4-*tert*-butoxystyrene conversion. The copolymerization was stopped in the range of 47% of 4-*tert*-butoxystyrene monomer conversion. The polymer was precipitated in cold methanol (×3) and dried.

Analysis : **^{1}H NMR** (500 MHz, CD_2Cl_2) δ 7.39 – 7.14 (m, Ar_{Trt}, 30H), 6.70 – 6.10 (m, Ar, 1880H), 1.73 (br, CH, 470H), 1.27 (br, CH_2, CH_3, 5170H) ppm. **HSQC 2D NMR** (500 MHz/126 MHz, CD_2Cl_2) δ 7.34/129.40 (Ar_{Trt}, CH), 7.25/127.55 (Ar_{Trt}, CH), 7.18/126.45 (Ar_{Trt}, CH), 6.57/123.37 (Ar, CH), 6.38/127.70 (Ar, CH), 3.67/67.66 (CH), 1.87/39.69 (CH), 1.42/30.84 (CH_3), 1.39/44.70 (CH_2) ppm. **SEC in THF** $M_{n,app}$ = 90000 and Đ = 1.25.

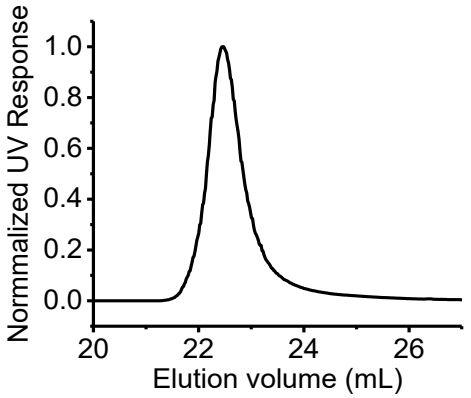

Figure 58. SEC chromatogram.

6.3.15. Synthesis of cyclic macromolecules via positional single disulfide bridge

Removal of tert-butyl protecting group

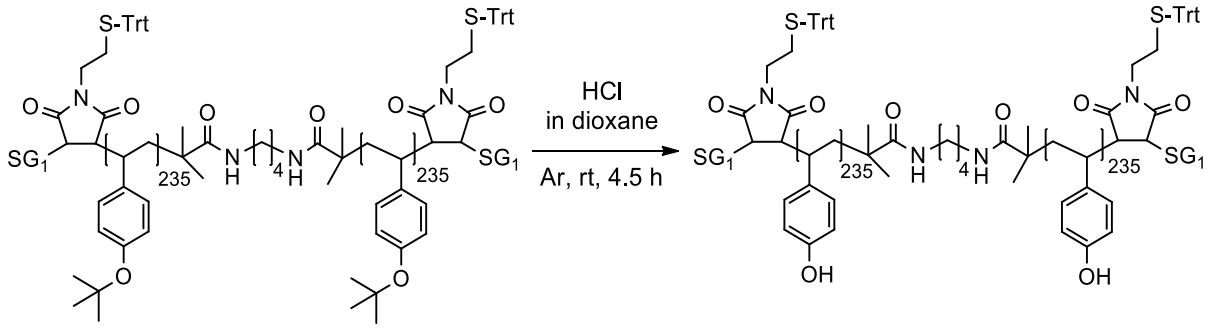

Synthesis of poly(StyOH-*co*-MISTrt). Bis-poly(Sty*O*t*Bu*-*co*-MIStrt) (M_n = 81800 g/mol, 0.30 g) was dissolved in 75.0 mL of dioxane in a three-neck-flask and bubbled with argon. Then 1.5 mL of HCl (37%) was added to the solution and the mixture was refluxed at 105 °C for 4.5 h. After completion of the hydrolysis, the mixture was cooled to room temperature. The polymer was then precipitated twice in cold water (×2) and dried under vacuum. (^{1}H NMR spectrum in Section 6.4, **Figure 93**)

Analysis : **^{1}H NMR** (500 MHz, CD_3OD) δ 7.31 – 7.16 (m, Ar_{Trt}, 27H), 6.80 – 6.20 (m, Ar, 1880H), 2.30-1.62 (br, CH, 470H), 1.60-0.90 (br, CH_2, 940H) ppm. **HSQC 2D NMR** (500 MHz/126 MHz, CD_3OD) δ 7.34/129.16 (Ar_{Trt}, CH), 7.23/127.11 (Ar_{Trt}, CH), 7.16/126.26 (Ar_{Trt}, CH), 6.55/114.30 (Ar, CH), 6.43/128.37 (Ar, CH), 1.78/39.41 (CH), 1.35/44.62 (CH_2) ppm. **SEC in DMAc** $M_{n,\,app}$ = 93000 and Đ = 1.30.

Removal of trityl protecting group

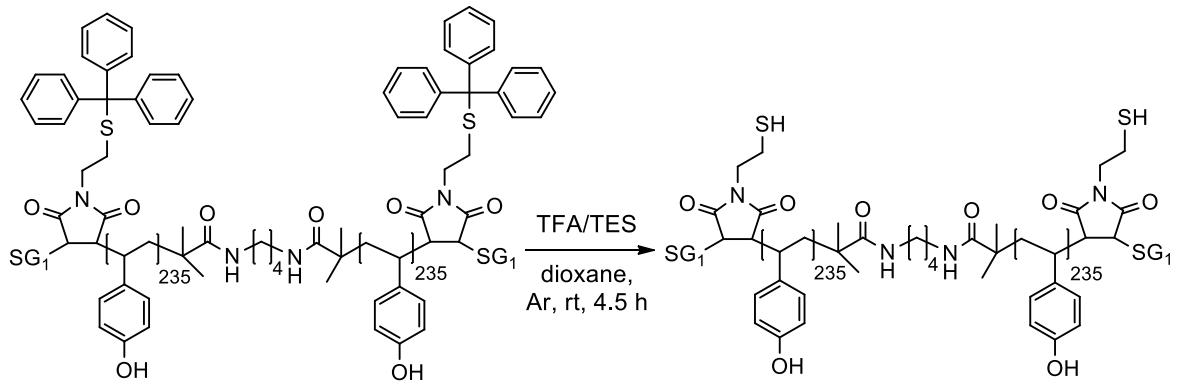

Synthesis of *l*-poly(StyOH-*co*-MISH). Poly(StyOH-*co*-MISTrt) (M_n = 55500 g/mol, 0.10 g) was dissolved in 3.2 mL of dioxane and 0.1 mL of triethyl silane was added to the solution. The mixture was deoxygenated by three freeze-pump-thaw cycles and filled with argon. A degassed solution of trifluoroacetic acid/dioxane (6.4 mL, 90/10 v/v,) was added to the mixture under argon and the reaction was stirred for 4.5 h at room temperature. The polymer was precipitated in water (×1) and then in hexane (×1). The polymer was dried under vacuum and stored under inert atmosphere. (^{1}H NMR spectrum in Section 6.4, **Figure 94**)

Analysis : **^{1}H NMR** (500 MHz, CD_3OD) δ 6.85 – 6.10 (m, Ar, 4H), 2.30 – 1.62 (br, CH, 1H), 1.60 – 0.90 (br, CH_2, 2H) ppm. **SEC in DMAc** $M_{n,\,app}$ = 91500 and Đ = 1.32. **UV-Vis spectroscopy of Ellman's test** (3×10^{-11} M of thiol groups) A = 0.16 at λ = 500 nm.

General procedure for polymer cyclization via the formation of disulfide bridge

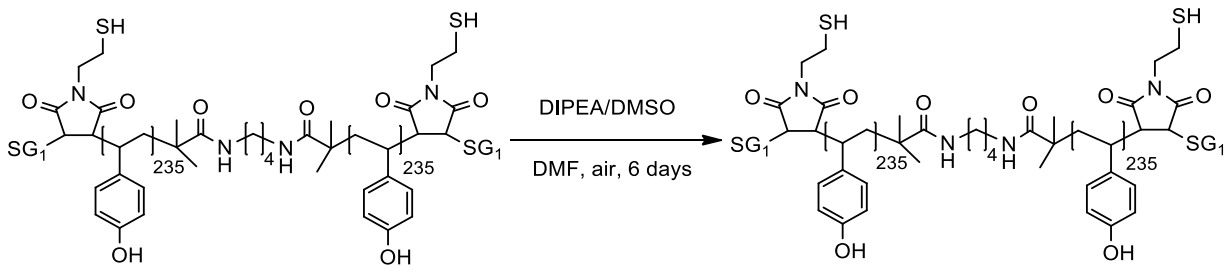

Synthesis of *c*-poly(StyOH-*co*-MIS). In a 500mL-flask, 280mL of dimethylformamide and 10 mL of dimethyl sulfoxide were introduced. DIPEA (5% vol.) was added to the solvent mixture. *l*-poly(StyOH-*co*-MISH) (M_n = 55000 g/mol, 0.060 g) was dissolved in 40 mL of degassed dimethylformamide and was added dropwise to the flask via a syringe pump. After addition, the reaction was stirred for 6 days at room temperature. The solvent was removed under reduced pressure. The resulting polymer was precipitated in water (×2) and in hexane (×1). The polymer was freeze dried in benzene/methanol (1/1 v/v). (^{1}H NMR spectrum in Section 6.4, **Figure 95**)

Analysis : **^{1}H NMR** (500 MHz, CD_3OD) δ 6.85 – 6.10 (m, Ar, 1880H), 2.30 – 1.62 (br, CH, 470H), 1.60 – 0.90 (br, CH_2, 940H) ppm. **SEC in DMAc** $M_{n,\,app}$ = 94500 and Đ = 1.30. **UV-Vis spectroscopy of Ellman's test** (2×10^{-11} M of sulfur groups) A = 0.02 at λ = 500nm.

6.3.16. Transformation into cyclic brush polymers via single disulfide bridge

Macroinitiator synthesis

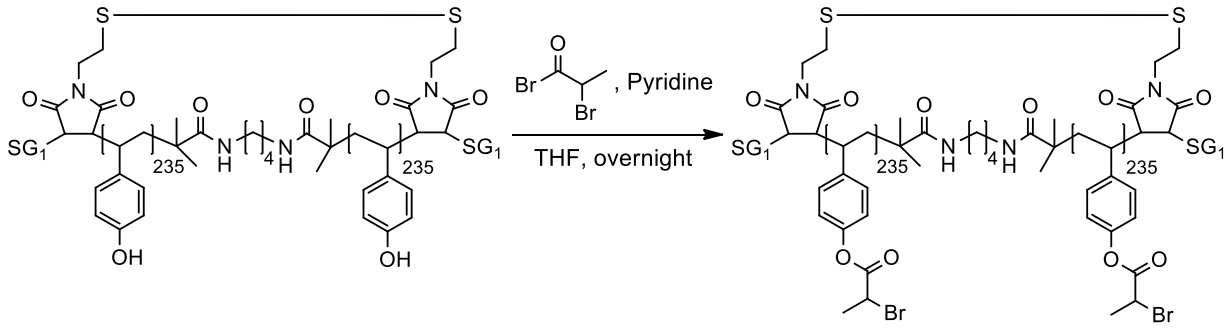

Synthesis of *c*-poly(StyBr-*co*-MIS). A dry schlenk was charged with *c*-poly(StyOH-*co*-MIS) (1 equiv, M_n = 57000 g/mol, assumed 0.25 mmol of hydroxyl group, 0.03 g) and purged with argon. 60.0 mL of dry tetrahydrofuran was added to the flask under argon, followed by the addition of pyridine (50 equiv, 12.00 mmol, 1.1 mL). Then 2-bromopropionyl bromide (50 equiv, 12.00 mmol, 0.31 mL) was added dropwise to the flask under argon at 0 °C. The mixture was stirred overnight at room temperature. The mixture was filtered and concentrated under reduced pressure. The polymer was precipitated three times in cold methanol, freeze-dried in benzene (98% of conversion determined by ^{1}H NMR).

Analysis : **^{1}H NMR** (300 MHz, $CDCl_3$) δ 6.90 – 6.20 (br, Ar, 4H), 4.58 (br, CH, 1H), 1.94 (br, CH_3, 3H), 1.69 (br, CH, 1H), 1.38 (br, CH_2, 2H) ppm. **SEC in DMAc** $M_{n,\,app}$ = 92000 and Đ = 1.30.

Transformation into brush polymers via «grafting from» approach

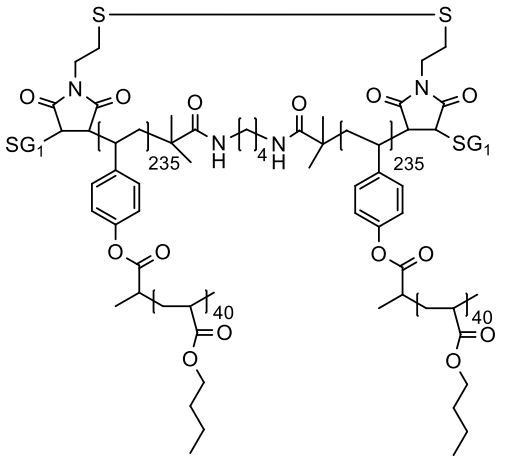

Synthesis of *c*-poly(Sty)$_{470}$-*g*-poly(*n*BuA)$_{40}$. In a 25mL-Schlenk, the ATRP-macroinitiator *c*-poly(StyBr-*co*-MIS) (1 equiv of active centers, 2.34×10^{-2} mmol, 6.0×10^{-3} g) was dissolved in 0.20 mL of methyl ethyl ketone and 1.68 mL of *n*-butyl acrylate (500 equiv, 11.72 mmol), followed by the addition of PMDETA (0.525 equiv, 1.23×10^{-2} mmol, 2.5×10^{-3} g). The flask was sealed with a septum, deoxygenated by four freeze-pump thaw cycles and filled with inert gas. After stirring for 30 min, CuBr (0.5 equiv, 1.17×10^{-2} mmol, 1.7×10^{-3} g) and $CuBr_2$ (0.025 equiv, 5.86×10^{-4} mmol, 1.3×10^{-4} g) were added to the flask under inert atmosphere. An initial sample was taken, and the flask was then immersed in pre-heated oil bath at 80 °C. The polymerization was monitored by ^{1}H NMR. At 9% of monomer conversion, the polymerization was stopped, and the flask was opened to air and cooled to room temperature. The catalyst was removed by passing the mixture through a neutral alumina oxide column. The solvent and the monomer were removed under reduced pressure. The polymer was precipitated in cold methanol (×2) and freeze-dried in benzene. (^{1}H NMR spectrum in Section 6.4, **Figure 96**)

Analysis : **Gravimetry** 107 mg of brush polymer, 7 % of conversion. **^{1}H NMR** (500 MHz, $CDCl_3$) δ 7.10 – 6.30 (br, Ar, 4H), 4.03 (br, O-CH_2, 2H), 2.27 (br, CH, 1H), 1.59 (br, CH_2, 2H), 1.37 (br, CH_2, 2H), 0.93 (br, CH_3, 3H) ppm. **SEC in DMAc** $M_{n,\,app}$ = 465000 and Đ = 1.43.

6.3.17. Multi-step synthesis of cyclic polymers via copolymer segments (*n* = 3)

Sequence-controlled polymerization of 4-tert-butoxystyrene and 6 equiv of MISTrt

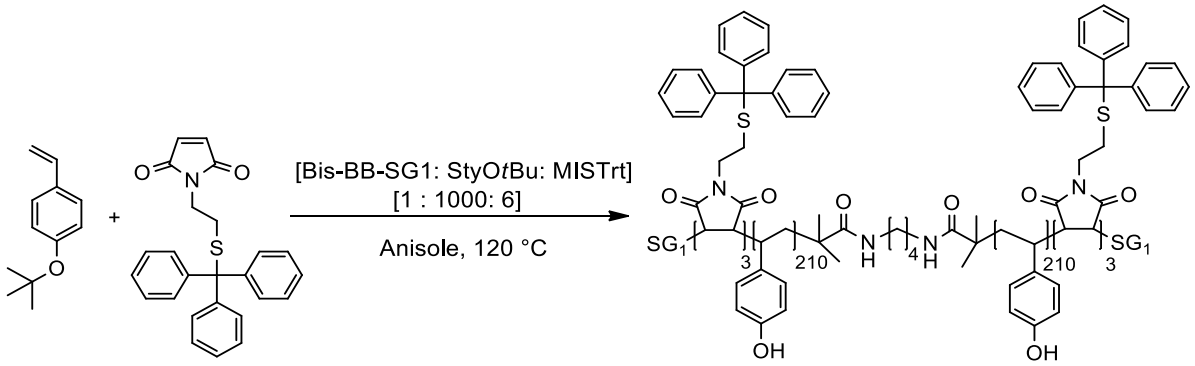

Synthesis of poly(StyO*t*Bu-*co*-MISTrt^6). Difunctional initiator (1 equiv, 2.210×10^{-5} mol, 0.018 g) was dissolved in 2.50 mL of anisole and 4.15 mL of 4-*tert*-butoxystyrene (1000 equiv, 0.022 mol). The flask was deoxygenated by four freeze-pump-thaw cycles and filled with argon. The mixture was then immersed in a pre-heated bath at 120 °C. At time intervals, aliquots were taken from the mixture to monitor the monomer conversion by ^{1}H NMR. One single injection of MISTrt maleimide (6 equiv, 1.300×10^{-4} mol, 0.021 g) in 0.50 mL of anisole was performed during the homopolymerization of StyO*t*Bu at approximatively 39% of conversion. The copolymerization was stopped at 44% and the polymer was precipitated in methanol (×3) and dried (1.050 g). (^{1}H NMR spectrum in Section 6.4, **Figure 97**)

Analysis : **^{1}H NMR** (500 MHz, CD_2Cl_2) δ 7.39 – 7.14 (m, Ar_{Trt}, 90H), 6.70 – 6.10 (br, Ar, 1680H), 1.77 (br, CH, 420H), 1.31 (br, CH_2, CH_3, 4620H) ppm. **HSQC 2D NMR** (500 MHz/126 MHz, CD_2Cl_2) δ 7.36/129.39 (Ar_{Trt}, CH), 7.28/127.82 (Ar_{Trt}, CH), 7.21/126.60 (Ar_{Trt}, CH), 6.66/123.44 (Ar, CH), 6.41/127.75 (Ar, CH), 3.67/67.50 (CH), 1.74/39.70 (CH), 1.35/44.13 (CH_2), 1.25/28.50 (CH_3) ppm. **SEC in THF** $M_{n,\,app}$ = 66000, $M_{p,\,app}$ = 73000 and Đ = 1.13

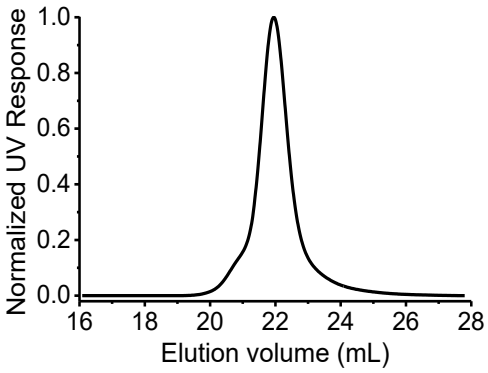

Figure 59. SEC chromatogram.

Removal of protecting groups

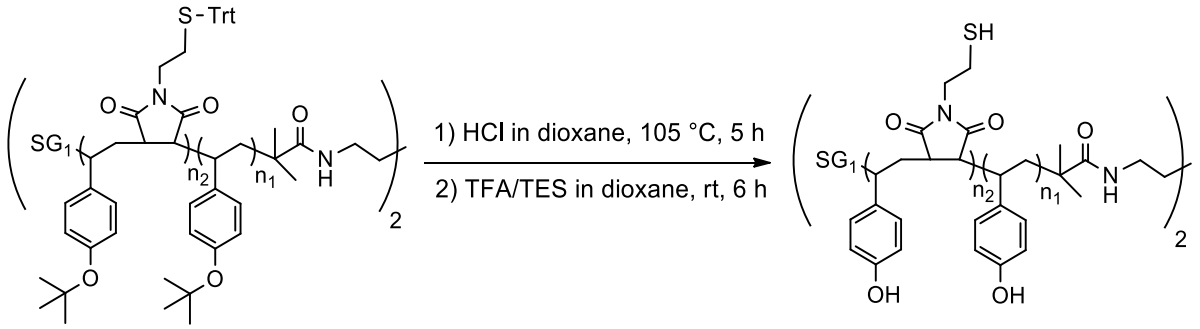

Synthesis of *l*-poly(StyOH-*co*-MISH[6]). The deprotection reactions were performed by using the experimental conditions as previously described in Section 6.3.15. *Tert*-butyl deprotection of poly(StyO*t*Bu-*co*-MISTrt[6]) was achieved by treatment with HCl in dioxane at 105 °C for 5 h.

Analysis : **^{1}H NMR** (400 MHz, CD_3OD) δ 7.39 – 6.97 (m, Ar_{Trt}, 32H), 6.47 (m, Ar, 1680H), 1.74 (br, CH, 418H), 1.37 (br, CH_2, 877H) ppm. **^{13}C NMR** (126 MHz, CD_3OD) δ 129.67 (Ar_{Trt}, Ar, CH), 40.80 (CH, CH_2) ppm. **SEC in DMAc** $M_{n,\,app}$ = 79700, $M_{p,\,app}$ = 91000 and Đ = 1.22.

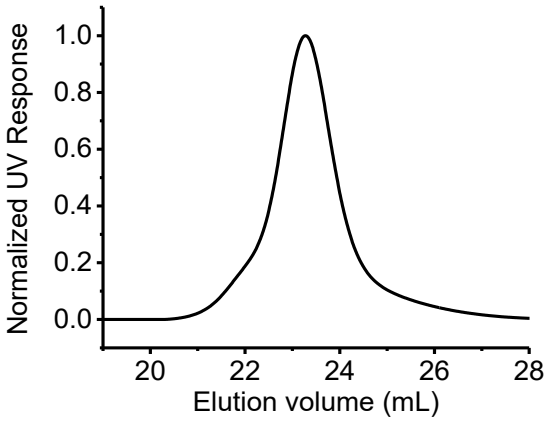

Figure 60. SEC chromatogram.

Detritylation was achieved by treatment with trifluoroacetic acid in presence of triethylsilane as scavenger in dioxane for 6 h at room temperature (98% of deprotected thiols determined by ^{1}H NMR). (^{1}H NMR spectrum in Section 6.4, **Figure 98**)

Analysis : **^{1}H NMR** (500 MHz, CD_3OD) δ 6.83 – 6.05 (m, Ar, 1680H), 2.12 – 1.52 (br, CH, 423H), 1.57 – 0.98 (br, CH_2, 831H) ppm. **SEC in DMAc** $M_{n,\,app}$ = 87500, $M_{p,\,app}$ = 91000 and Đ = 1.23.

Formation of intramolecular disulfide bridges

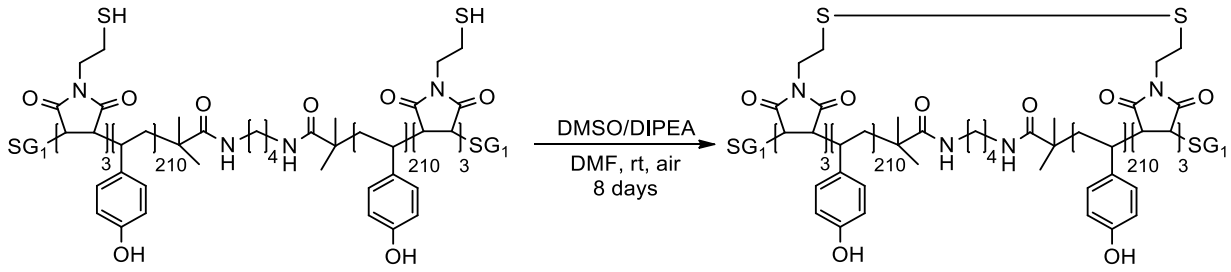

Synthesis of *c*-poly(StyOH-*co*-MIS[6]). The crosslinking reaction was performed by using the same experimental conditions as previously described in Section 6.3.15. The reaction was conducted at room temperature in dimethylformamide, in presence of dimethyl sulfoxide and DIPEA, for 8 days.

Analysis : **^{1}H NMR** (500 MHz, CD_3OD) δ 6.97 – 6.00 (m, Ar, 1680H), 1.84 (d, CH, 449H), 1.34 (br, CH_2, 940H) ppm. **SEC in DMAc** $M_{n,app}$ = 84000 and Đ = 1.26.

Macroinitiator synthesis

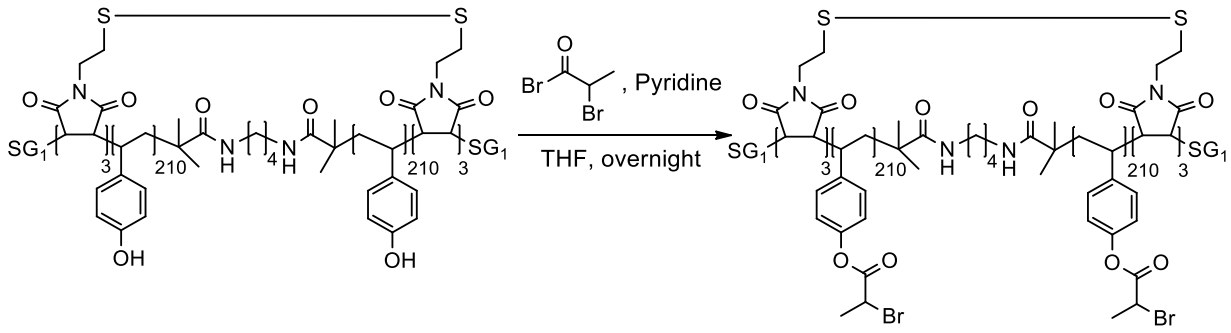

Synthesis of *c*-poly(StyBr-*co*-MIS[6]). The macroinitiator synthesis was performed by using the same experimental conditions as previously described in Section 6.3.15.

Analysis : **^{1}H NMR** (400 MHz, $CDCl_3$) δ 7.10 – 6.25 (m, Ar, 4H), 4.58 (br, CH, 1H), 2.05 – 1.93 (br, CH_3, 3H), 1.82 – 1.60 (br, CH, 1H), 1.48 – 1.00 (br, CH_2, 2H) ppm. **SEC in DMAc** $M_{n,\,app}$ = 74000 and Đ = 1.29.

Brush macromolecule synthesis

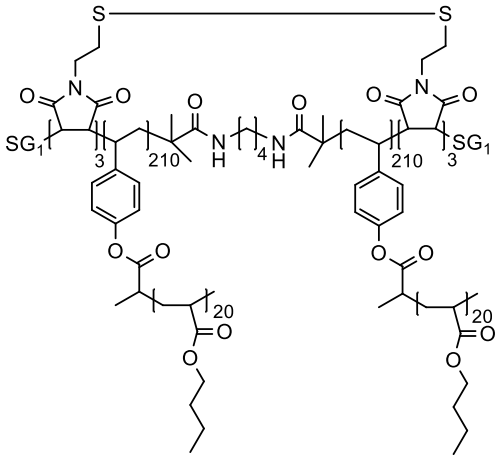

Synthesis of *c*-[poly(Sty)$_{420}$-*g*-poly(*n*BuA)$_{20}$][6]. In a 25mL-Schlenk, the ATRP-macroinitiator *c*-poly(StyBr-*co*-MIS[6]) (1 equiv of active centers, 1.94×10^{-5} mol, 5.0×10^{-3} g) was dissolved in 0.40 mL of methyl ethyl ketone and 1.11 mL of *n*-butyl acrylate (400 equiv, 7.7×10^{-3} mol), followed by the addition of PMDETA (0.525 equiv, 1.02×10^{-6} mol, 2.1×10^{-3} g). The flask was sealed with a septum, deoxygenated by four freeze-pump thaw cycles and filled with inert gas. After stirring for 30 min, CuBr (0.5 equiv, 9.72×10^{-6} mol, 1.4×10^{-3} g) and $CuBr_2$ (0.025 equiv, 4.86×10^{-7} mol, 1.0×10^{-4} g) were added to the flask under inert atmosphere. An initial sample was taken, and the flask was then immersed in preheated oil bath at 80 °C. The polymerization was monitored by ^{1}H NMR. At 5% of monomer conversion, the polymerization was stopped, and the flask was opened to air and cooled to room temperature. The catalyst was removed by passing the mixture through a neutral alumina oxide column. The solvent and the monomer were removed under reduced pressure. The polymer was precipitated in cold methanol (×2) and freeze-dried in benzene. (^{1}H NMR spectrum in Section 6.4, **Figure 99**)

Analysis : **Gravimetry** 56 mg of brush polymer, 5.2% of conversion. **^{1}H NMR** (500 MHz, $CDCl_3$) δ 7.10 – 6.30 (br, Ar), 4.03 (br, O-CH_2), 2.27 (br, CH,), 1.59 (br, CH_2), 1.37 (br, CH_2), 0.93 (br, CH_3) ppm. **SEC in DMAc** $M_{n,\,app}$ = 350000 and Đ = 1.43.

6.3.18. Multi-step synthesis of cyclic polymers via copolymer segments (*n* = 6)

Sequence-controlled polymerization

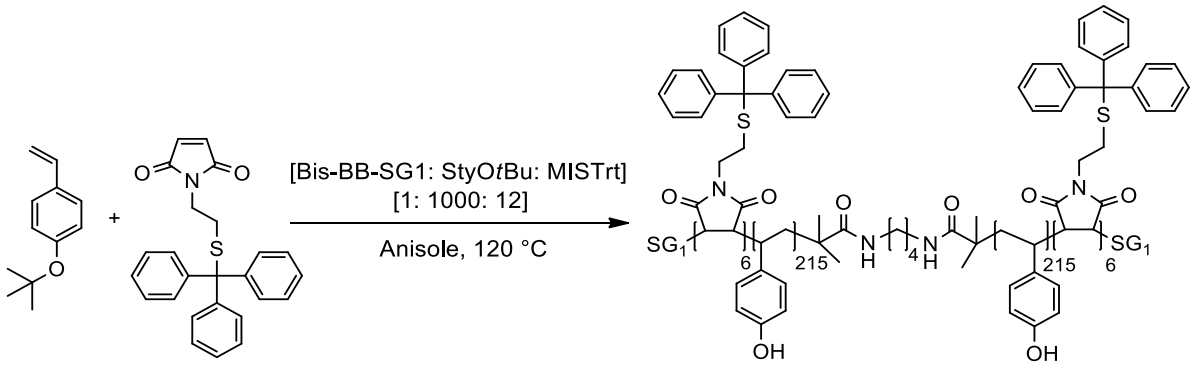

Synthesis of poly(StyO*t*Bu-*co*-MISTrt^{12}). Difunctional initiator (1 equiv, 2.210 × 10^{-5} mol, 0.018 g) was dissolved in 2.50 mL of anisole and 4.15 mL of *4-tert*-butoxystyrene (StyO*t*Bu) (1000 equiv, 0.022 mol). The flask was deoxygenated by four freeze-pump-thaw cycles and filled with argon. The mixture was then immersed in a pre-heated bath at 120 °C. At time intervals, aliquots were taken from the mixture with a degassed syringe to monitor the monomer conversion by ^{1}H NMR. One single injection of MISTrt maleimide (12 equiv, 2.600 × 10^{-4} mol, 0.100 g) in 0.50 mL of anisole was performed during the homopolymerization of StyO*t*Bu at approximatively 38%. The copolymerization was stopped at 45% and the polymer was precipitated in methanol (×3). (^{1}H NMR spectrum in Section 6.4, **Figure 100**)

Analysis : **^{1}H NMR** (500 MHz, CD_2Cl_2) δ 7.54 – 7.00 (m, Ar_{Trt}, 180H), 6.86 – 6.21 (br, Ar, 1720H), 1.73 (br, CH, 430H), 1.28 (br, CH_2, CH_3, 4730H) ppm. **HSQC 2D NMR** (500 MHz/126 MHz, CD_2Cl_2) δ 7.36/128.74(Ar_{Trt}, CH), 7.27/127.15 (Ar_{Trt}, CH), 7.21/125.97 (Ar_{Trt}, CH), 6.66/122.77 (Ar, CH), 6.41/127.28 (Ar, CH), 3.69/66.94 (CH), 1.75/39.03 (CH), 1.38/44.26 (CH_2), 1.25/27.87 (CH_3) ppm. **SEC in THF** $M_{n,app}$ = 67500, $M_{p,app}$ = 75500 and Đ = 1.15.

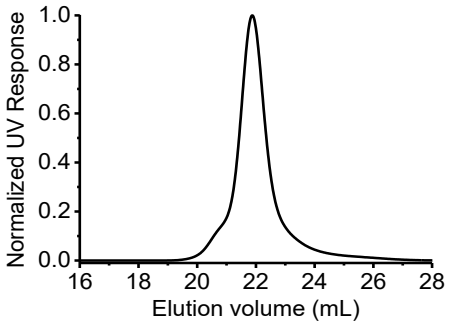

Figure 61. SEC chromatogram.

Removal of protecting groups

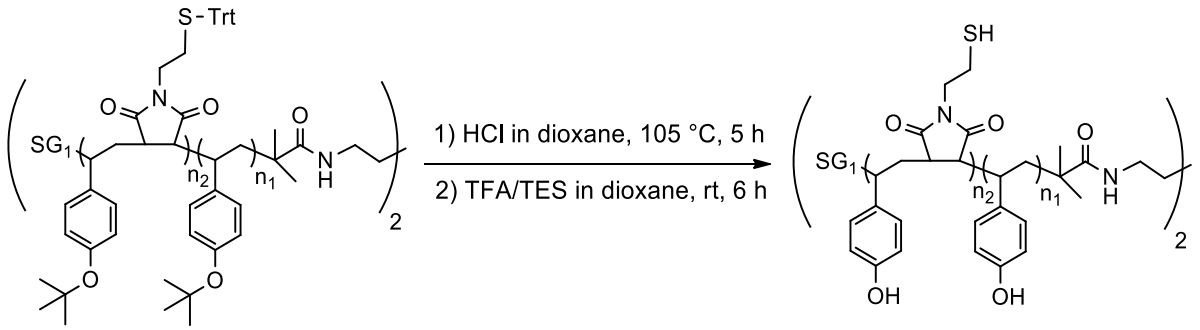

Synthesis of *l*-poly(StyOH-*co*-MISH^{12}). The deprotection reactions were performed by using the experimental conditions as previously described in Section 6.3.15. *Tert*-butyl removal of poly(StyO*t*Bu-*co*-MISTrt^{12}) was achieved by treatment with HCl in dioxane at 105 °C for 5 h.

Analysis : **^{1}H NMR** (400 MHz, CD_3OD) δ 7.39 – 6.97 (m, Ar_{Trt}, 52H), 6.47 (m, Ar, 1720H), 1.74 (br, CH, 467H), 1.37 (br, CH_2, 886H) ppm. **HSQC 2D NMR** (500 MHz/126 MHz, CD_3OD) δ 7.30/130.03 (Ar_{Trt}, CH), 7.23/128.10 (Ar_{Trt}, CH), 7.17/127.51 (Ar_{Trt}, CH), 6.56/114.98 (Ar, CH), 6.43/129.01 (Ar, CH), 3.31/41.36 (CH), 2.78/39.67 (N-CH_2), 2.28/21.37 (S-CH_2), 1.78/40.06 (CH), 1.40/43.50 (CH_2) ppm. **SEC in DMAc** $M_{n,\,app}$ = 83500, $M_{p,\,app}$ = 94000 and Đ = 1.20.

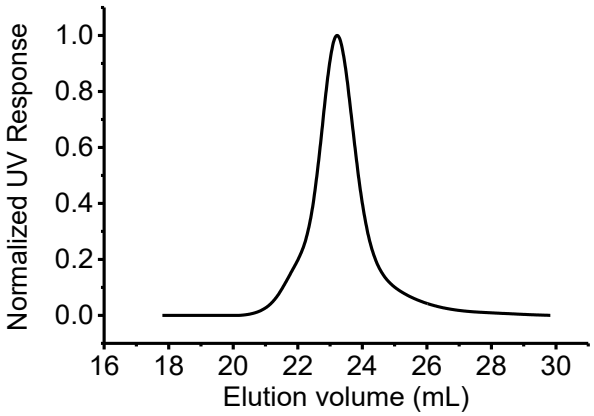

Figure 62. SEC chromatogram.

Detritylation was achieved by treatment with trifluoracetic acid in presence of triethylsilane as scavenger in dioxane for 6 h at room temperature (93% of deprotected thiols determined by ^{1}H NMR). (^{1}H NMR spectrum in Section 6.4, **Figure 101**)

Analysis : **^{1}H NMR** (400 MHz, CD_3OD) δ 6.83 – 6.05 (m, Ar, 1720H), 2.20 – 1.61 (br, CH, 422H), 1.58 – 1.00 (br, CH_2, 849H) ppm. **SEC in DMAc** $M_{n,\,app}$ = 86400, $M_{p,\,app}$ = 94000 and Đ = 1.29.

Formation of intramolecular disulfide bridges

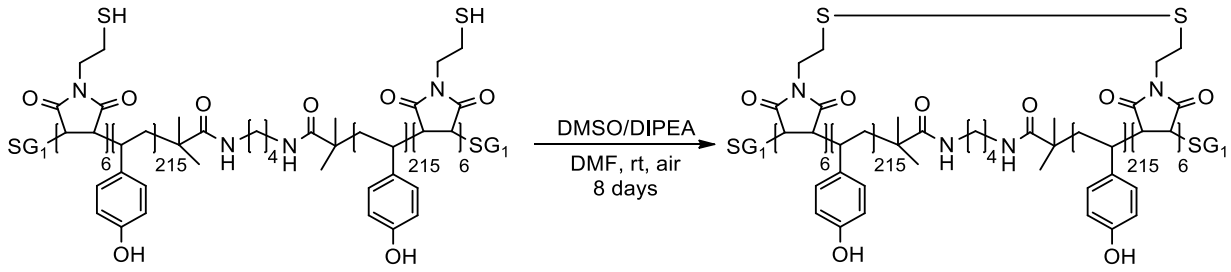

Synthesis of *c*-poly(StyOH-*co*-MIS[12]). The deprotection reactions were performed by using the same experimental conditions as previously described in Section 6.3.15. The crosslinking reaction was conducted at room temperature in dimethylformamide, in presence of dimethyl sulfoxide and DIPEA, for 8 days.

Analysis : **^{1}H NMR** (400 MHz, CD_3OD) δ 6.70-6.10 (m, Ar, 1720H), 1.76 (br, CH, 436H), 1.39 (br, CH_2, 879H) ppm. **SEC in DMAc** $M_{n,\,app}$ = 86500 and Đ = 1.29.

Macroinitiator synthesis

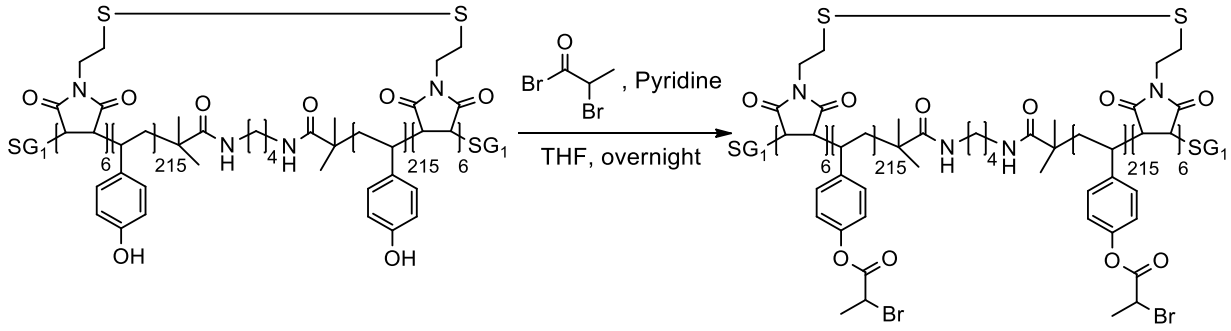

Synthesis of c-poly(StyBr-co-MIS[12]). The macroinitiator synthesis was performed by using the same experimental conditions as previously described in Section 6.3.16.

Analysis : **^{1}H NMR** (300 MHz, $CDCl_3$) δ 7.03 – 6.19 (m, Ar, 4H), 4.58 (s, CH, 1H), 1.94 (s, CH_3, 3H), 1.84 – 1.63 (br, CH, 1H), 1.51 – 1.11 (br, CH_2, 2H) ppm. **SEC in DMAc** $M_{n,\,app}$ = 73000 and Đ = 1.36.

Brush macromolecule synthesis

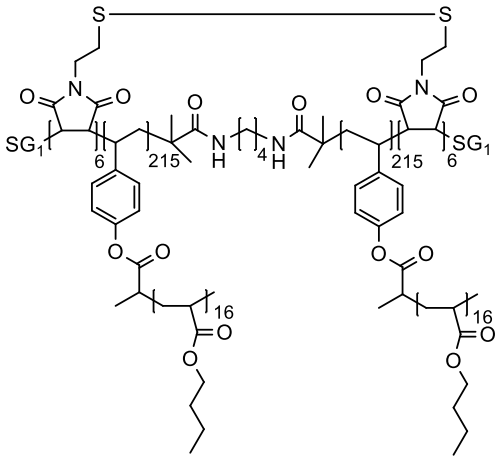

Synthesis of *c*-[poly(Sty)$_{430}$-*g*-poly(*n*BuA)$_{16}$]^{12}. The «grafting from» reaction was performed by using the same experimental conditions as previously described in Section 6.3.16. (^{1}H NMR spectrum in Section 6.4, **Figure 102**)

Analysis : **Gravimetry** 35 mg of brush polymer, 3.2% of conversion. **^{1}H NMR** (600 MHz, $CDCl_3$) δ 6.97 – 5.83 (m, Ar, 4H), 4.04 (s, CH_2, 74H), 2.27 (br, CH, 38H), 1.53 (br, CH_2, 76H), 1.37 (br, CH_2, 76H), 0.94 (br, CH_3, 112H) ppm. **SEC in DMAc** $M_{n,app}$ = 263000 and Đ = 1.52.

Reduction investigation

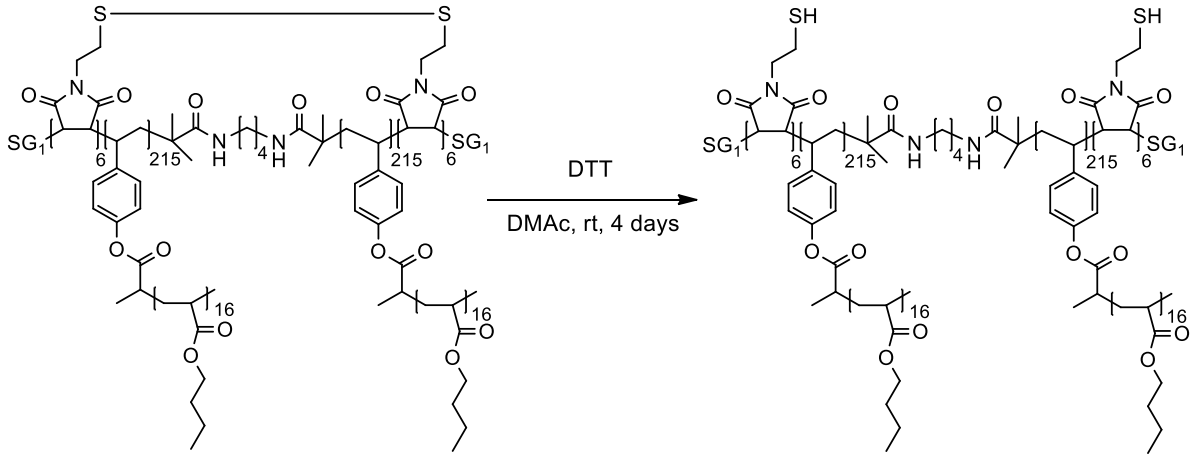

The brush copolymer *c*-[poly(Sty)$_{430}$-*g*-poly(*n*BuA)$_{16}$]^{12} (2.5 mg) was dissolved in 2 mL of dimethylacetamide containing LiBr salt (1 mg/mL, 1 equiv, 4.50 × 10^{-8} mol). The solution was bubbled with argon for 30 min and dithiothreitol (400 equiv, 1.8× 10^{-8} mol, 3 mg) was added. The reaction was stirred for 4 days under inert atmosphere and tracked by SEC.

Analysis: **SEC in DMAc** $M_{n,app}$ = 255000 and Đ = 1.47.

6.3.19. Study on thiol oxidation reaction time : multi-step synthesis

The fully deprotected sequence-controlled copolymer *l*-poly(StyOH-*co*-MISH)[6] was used as starting material to conduct the reaction time investigation.

Formation of intramolecular disulfide bridges

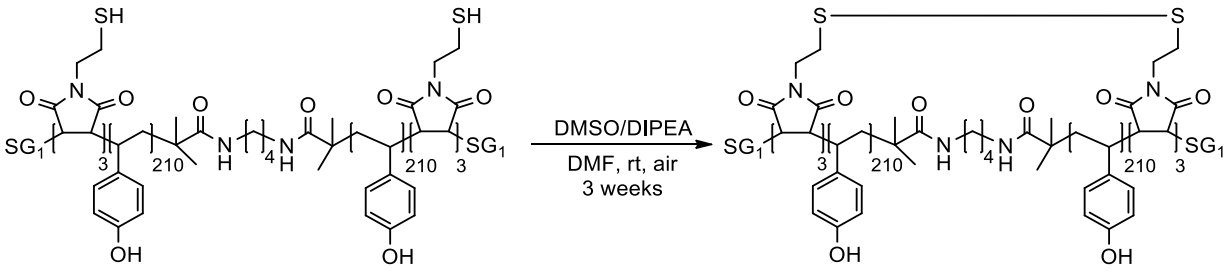

Synthesis of (*c*-poly(StyOH-*co*-MISH)$^{6\text{-a}}$). The crosslinking reaction was performed by using the same experimental conditions as previously described in Section 6.3.15. The copolymer was added in once to the reaction flask containing dimethylformamide, dimethyl sulfoxide (5%vol.) and DIPEA (5% vol.), and the mixture was stirred for 3 weeks.

Analysis : **^{1}H NMR** (500 MHz, CD_3OD) δ 6.97 – 6.00 (m, Ar, 1680H), 1.84 (br, CH, 449H), 1.34 (br, CH_2, 940H) ppm. **SEC in DMAc** $M_{n,\,app}$ = 79800 and Đ = 1.28.

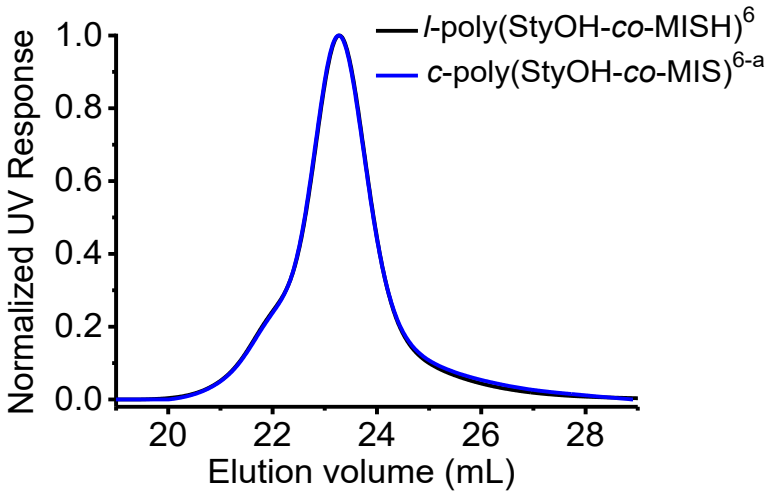

Figure 63. SEC chromatogram.

Macroinitiator synthesis

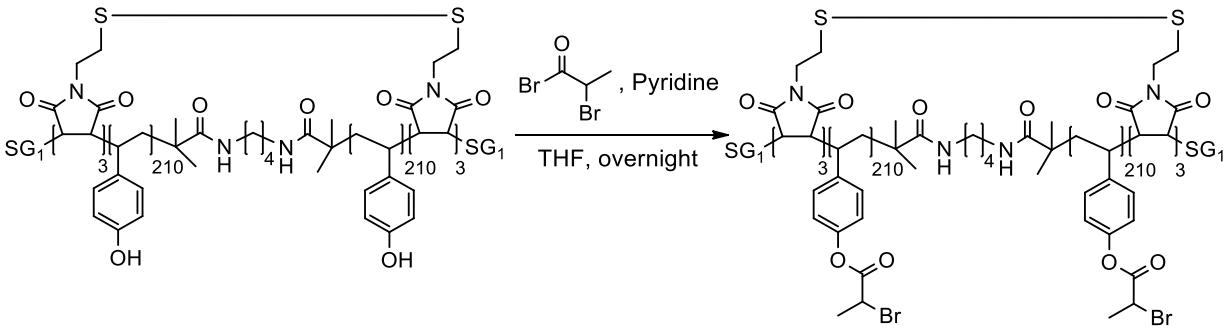

The macroinitiator synthesis was performed by using the same experimental conditions as previously described in Section 6.3.17.

Analysis : **^{1}H NMR** (400 MHz, $CDCl_3$) δ 7.10 – 6.25 (m, Ar, 4H), 4.58 (br, CH, 1H), 2.05 – 1.93 (br, CH_3, 3H), 1.82 – 1.60 (br, CH, 1H), 1.48 – 1.00 (br, CH_2, 2H) ppm. **SEC in DMAc** $M_{n,\,app}$ = 72600 and Đ = 1.29.

Brush macromolecule synthesis

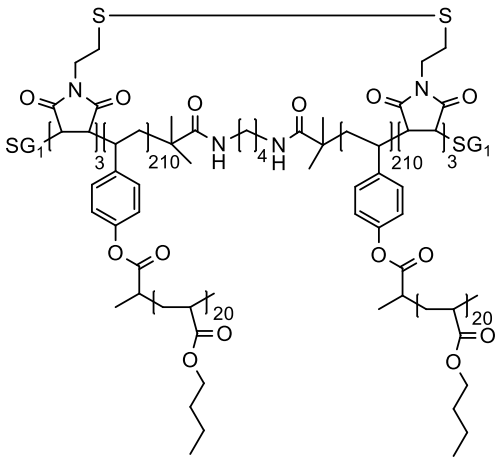

Synthesis of *c*-[poly(Sty)$_{420}$-*g*-poly(*n*BuA)$_{20}$][6-a]. The «grafting from» reaction was performed by using the same experimental conditions as previously described in Section 6.3.17. (^{1}H NMR spectrum in Section 6.4, **Figure 103**)

Analysis : **Gravimetry** 48 mg of brush polymer, 4.5 % of conversion. **^{1}H NMR** (500 MHz, $CDCl_3$) δ 7.10-6.30 (br, Ar), 4.03 (br, O-CH_2), 2.27 (br, CH,), 1.59 (br, CH_2), 1.37 (br, CH_2), 0.93 (br, CH_3) ppm. **SEC in DMAc** $M_{n,\,app}$ = 374000 and Đ = 1.35.

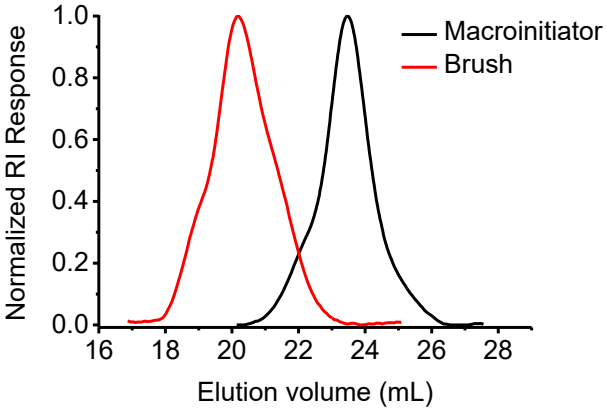

Figure 64. SEC chromatogram.

6.3.20. Study on thiol oxidation reaction solvent : multi-step synthesis

A fully deprotected sequence-controlled copolymer *l*-poly(StyOH-*co*-MISH)[6] was prepared from the sequence-controlled copolymer poly(StyO*t*Bu-*co*-MISTrt[6]) and was used as starting material to study the effect of solvent on the crosslinking reaction (SEC in DMAC, $M_{n,\,app}$ = 88700 and Đ = 1.25).

General procedure for polymer cyclization via intramolecular disulfide bridges in methanol

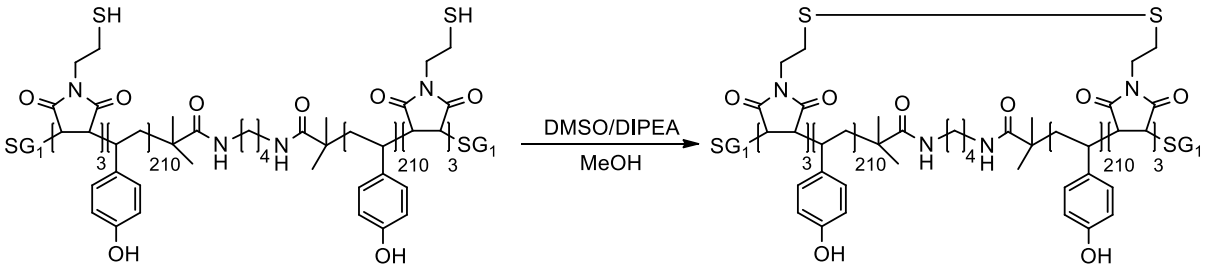

Synthesis of *c*-poly(StyOH-*co*-MIS)[6-d]. In a 250mL-flask, 30 mL of methanol and 25 mL of dimethyl sulfoxide were introduced. 5 mL of DIPEA was added to the solvent mixture. The fully deprotected copolymer *l*-poly(StyOH-*co*-MISH)[6] (M_n = 50000 g/mol, 0.025 g) was dissolved in 20 mL of degassed methanol and was added dropwise to the flask via a syringe pump. After addition, the reaction was stirred for 5 days at 40°C. The solvent was removed under reduced pressure. The resulting polymer was precipitated in water (×2) and in hexane (×1). The polymer was freeze dried in benzene/methanol (1/1 v/v). (^{1}H NMR spectrum in Section 6.4, **Figure 104**)

Analysis : ^{1}H **NMR** (500 MHz, CD_3OD) δ 6.97 – 6.00 (m, Ar, 1680H), 1.84 (br, CH, 449H), 1.34 (br, CH_2, 940H) ppm. **SEC in DMAc** $M_{n,\,app}$ = 86000 and Đ = 1.44.

Macroinitiator synthesis

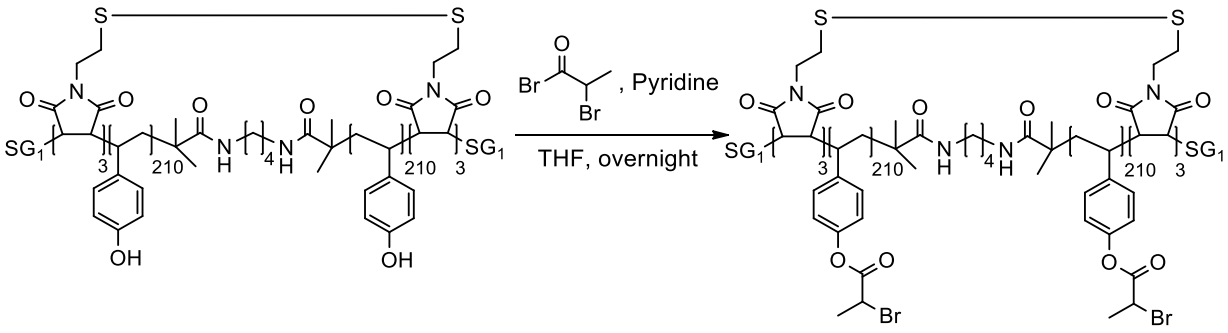

The macroinitiator synthesis was performed by using the same experimental conditions as previously described in Section 6.3.17.

Analysis : ^{1}H **NMR** (400 MHz, $CDCl_3$) δ 7.10 – 6.25 (m, Ar, 4H), 4.58 (br, CH, 1H), 2.05 – 1.93 (br, CH_3, 3H), 1.82 – 1.60 (br, CH, 1H), 1.48 – 1.00 (br, CH_2, 2H) ppm. **SEC in DMAc** $M_{n,\,app}$ = 80400 and Đ = 1.27

Brush macromolecule synthesis

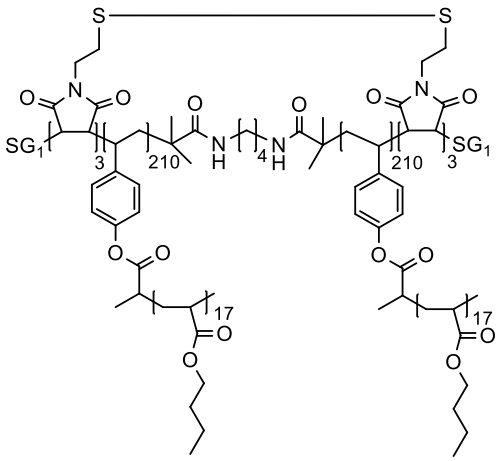

Synthesis of *c*-[poly(Sty)$_{420}$-*g*-poly(*n*BuA)$_{17}$]$^{6\text{-d}}$. The «grafting from» reaction was performed by using the same experimental conditions as previously described in Section 6.3.17. (^{1}H NMR spectrum in Section 6.4, **Figure 105**)

Analysis : **Gravimetry** 38 mg of brush polymer, 3.5 % of conversion. **^{1}H NMR** (500 MHz, $CDCl_3$) δ 7.10-6.30 (br, Ar), 4.03 (br, O-CH_2), 2.27 (br, CH,), 1.59 (br, CH_2), 1.37 (br, CH_2), 0.93 (br, CH_3) ppm. **SEC in DMAc** $M_{n,\,app}$ = 332000 and Đ = 1.27.

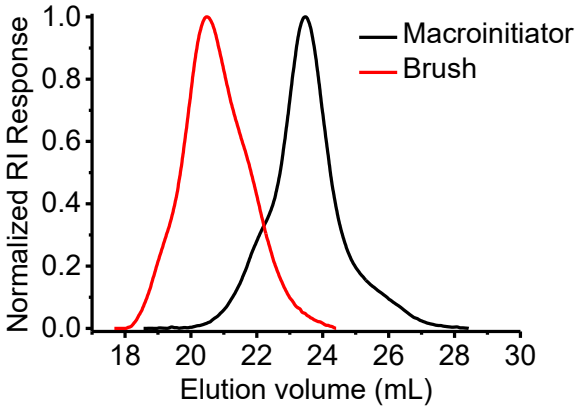

Figure 65. SEC chromatogram.

6.4. NMR analytic

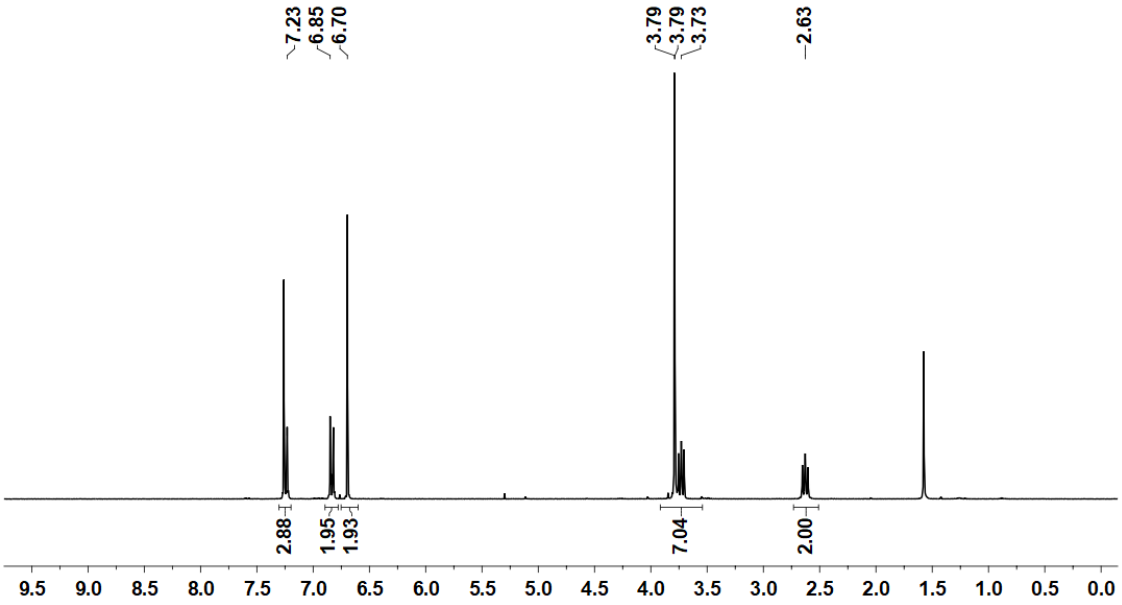

Figure 66. ^{1}H NMR spectrum of *N*-(2-p-methoxybenzylselenoethyl) maleimide in $CDCl_3$.

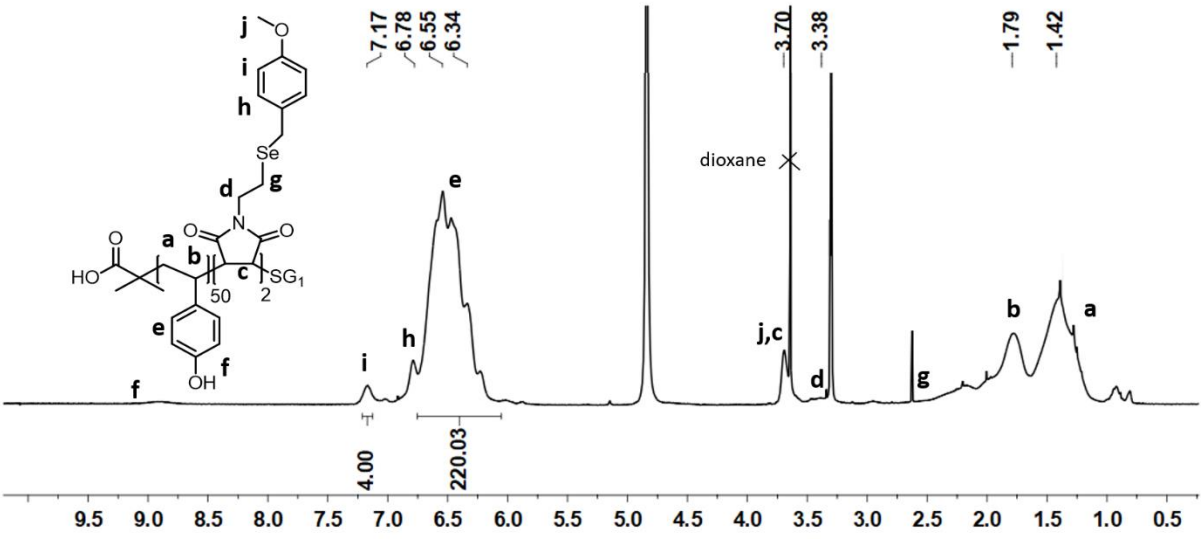

Figure 67. ^{1}H NMR spectrum in CD_3OD of the isolated copolymer *l*-poly(StyOH-*co*-MISeMob) after *tert*-butyl deprotection.

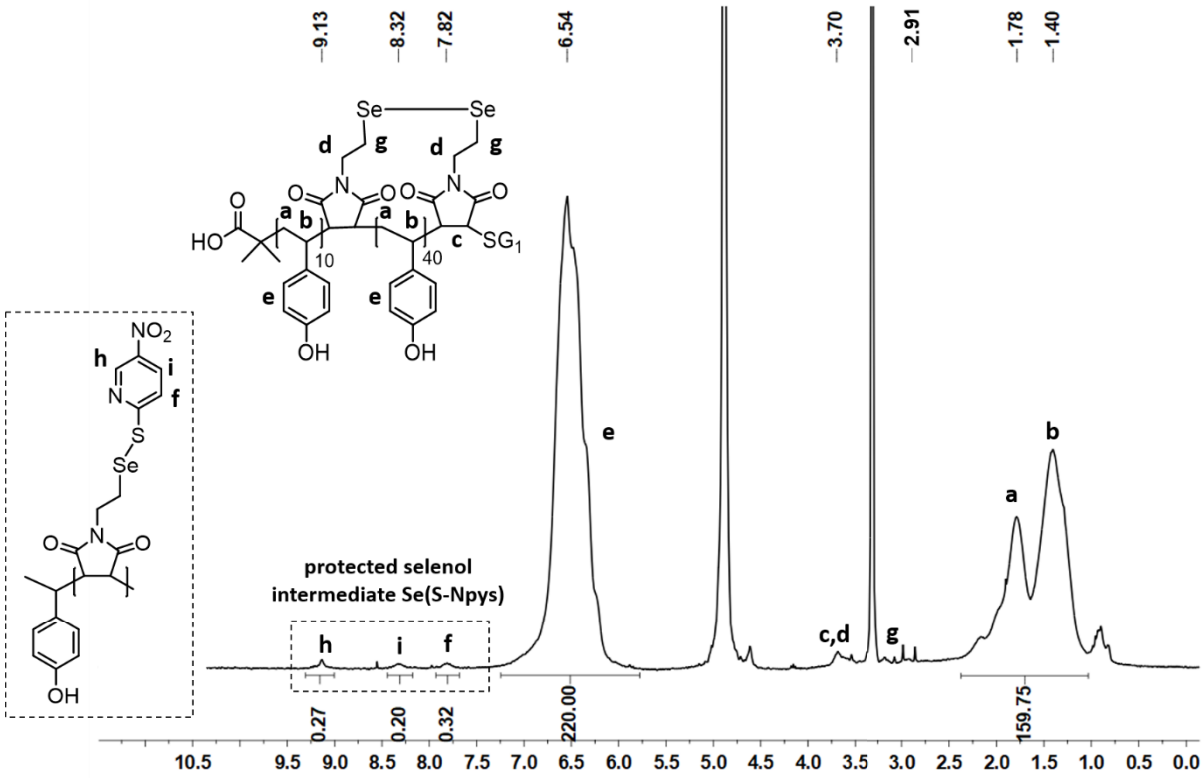

Figure 68. ^{1}H NMR spectrum of the isolated cyclic polymer *c*-poly(StyOH-*co*-MISe)^{e} in CD_3OD (Table 1, entry e).

Estimation of % of protected selenol intermediate by using the equation, where H_f and H_i are the integration areas corresponding to the protons f and I respectively:

$$\text{Se(S-Npys)}\ (\%) = \frac{2 \times \text{Hf}}{\text{Hi}} \times 100 = 14$$

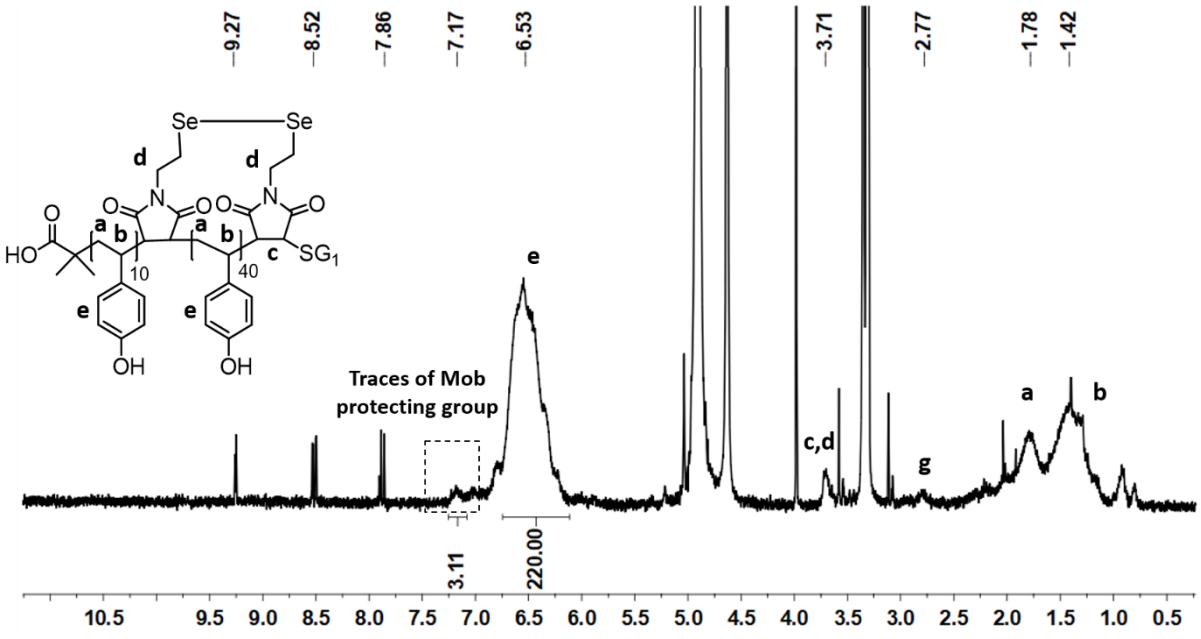

Figure 69. ^{1}H NMR spectrum in CD_3OD of the cyclic copolymer *c*-poly(StyOH-*co*-MISe)[a] in CD_3OD (Table 1, entry a). with 77% of Mob group remaining after cyclization reaction.

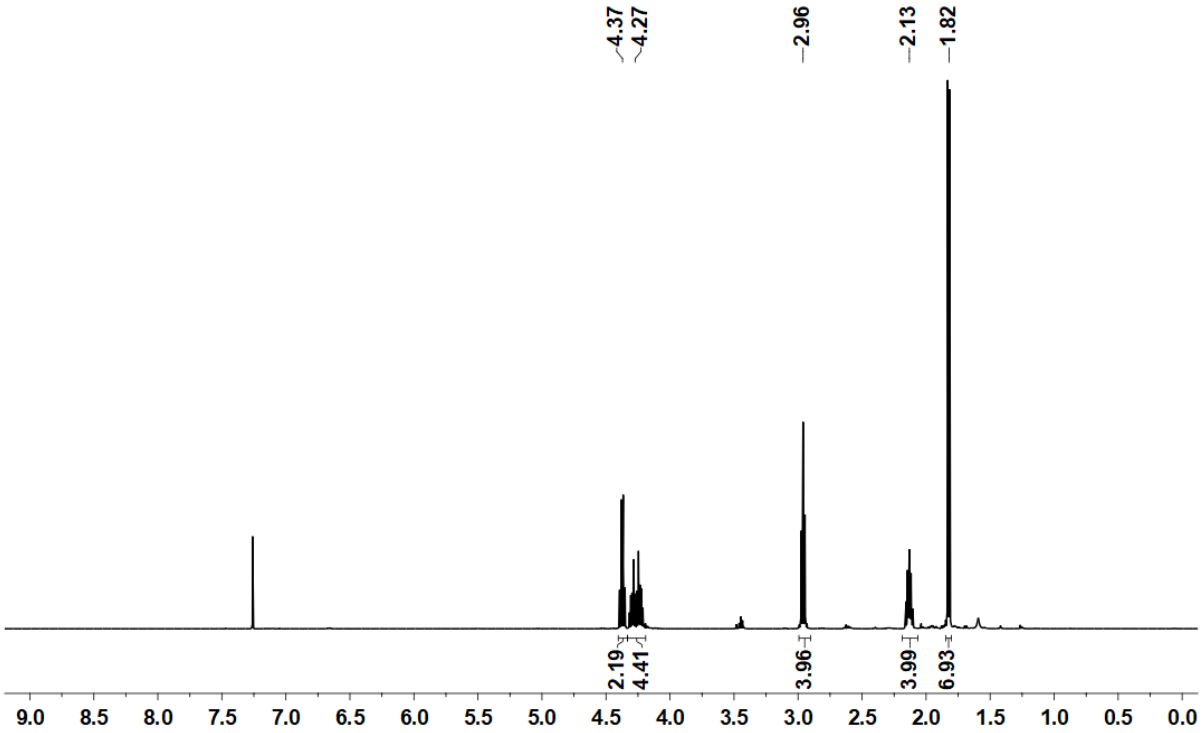

Figure 70. ^{1}H NMR spectrum of the diselenide-containing initiator (**2**) in $CDCl_3$.

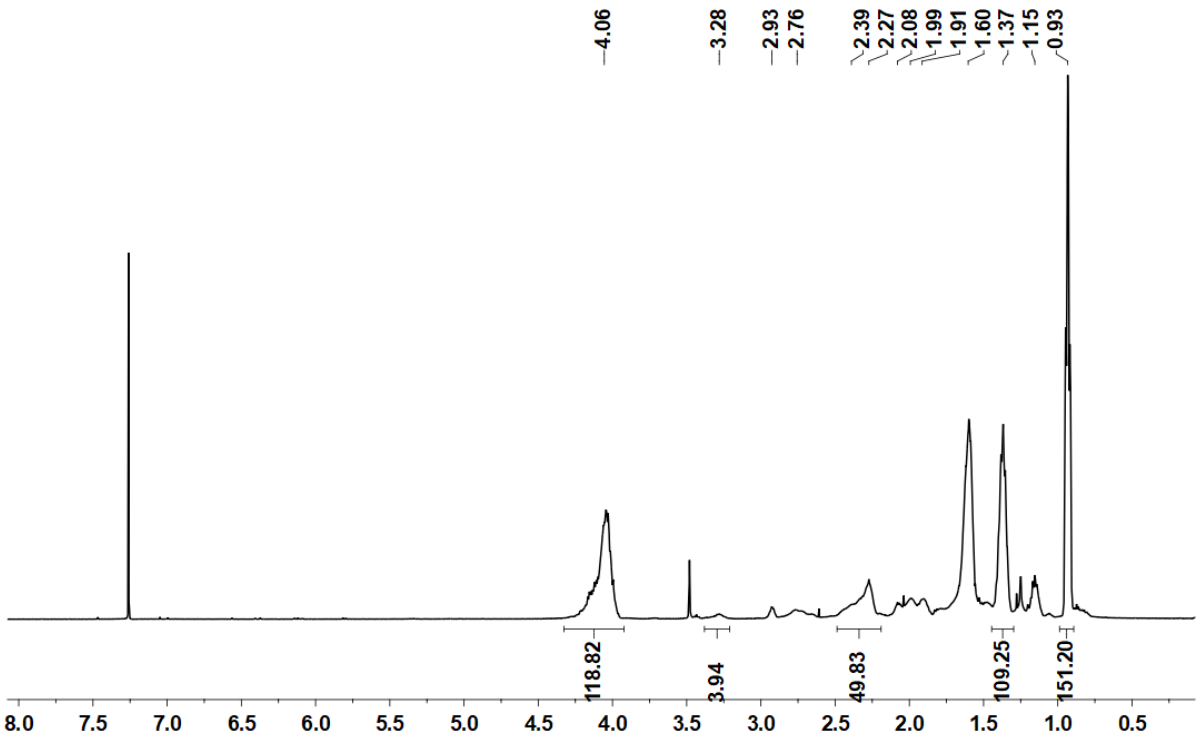

Figure 71. ^{1}H NMR spectrum of short poly(*n*-butyl acrylate) initiated by (**2**) in $CDCl_3$.

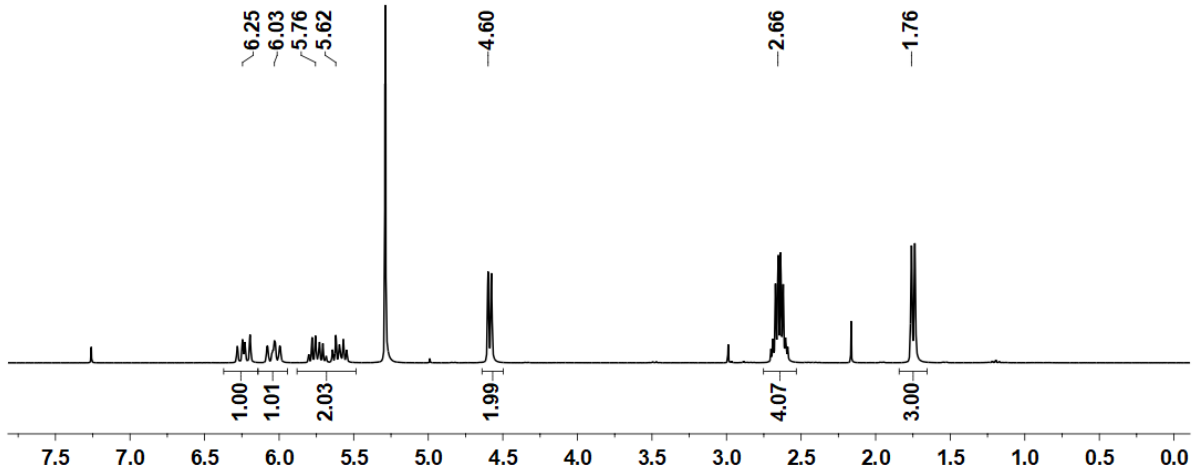

Figure 72. ^{1}H NMR spectrum of 2,4-hexadien-1-yl succinic acid monoester in $CDCl_3$.

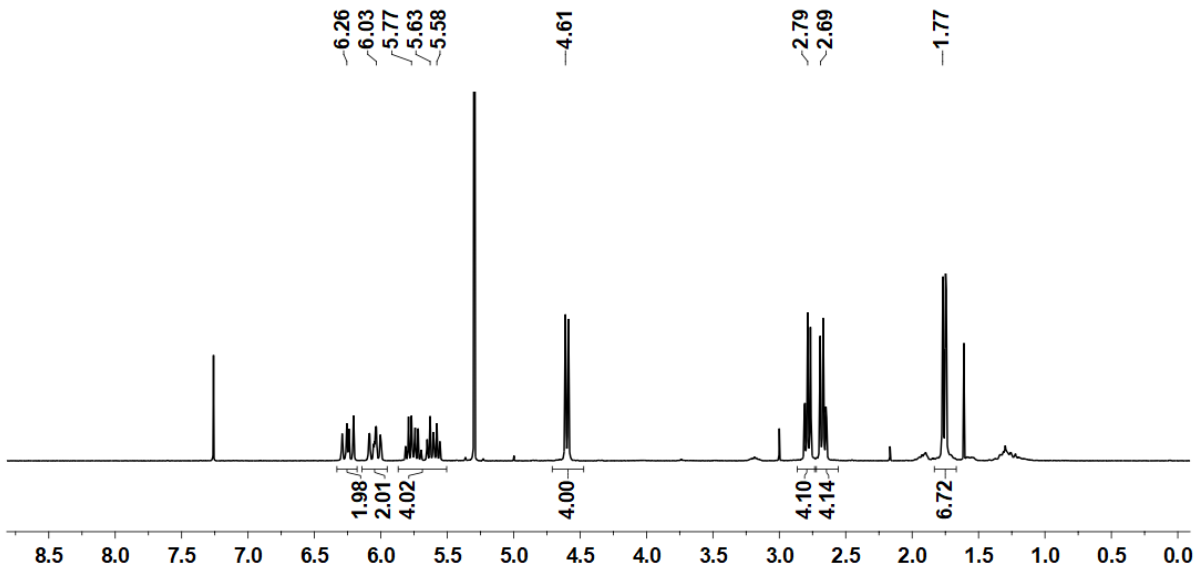

Figure 73. ^{1}H NMR spectrum of the symmetric anhydride of 2,4-hexadien-1-yl succinic acid monoester in $CDCl_3$.

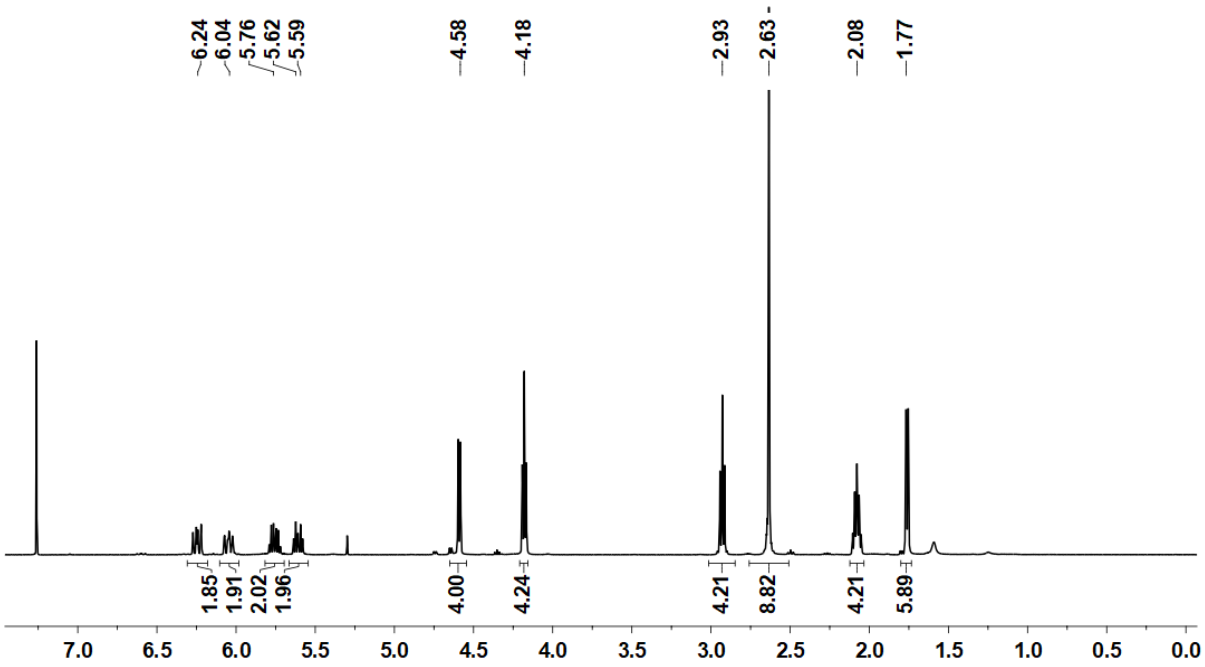

Figure 74. ^{1}H NMR spectrum of bis(2,4-hexadien-3-propyl succinic diester) diselenide (**4**) in $CDCl_3$.

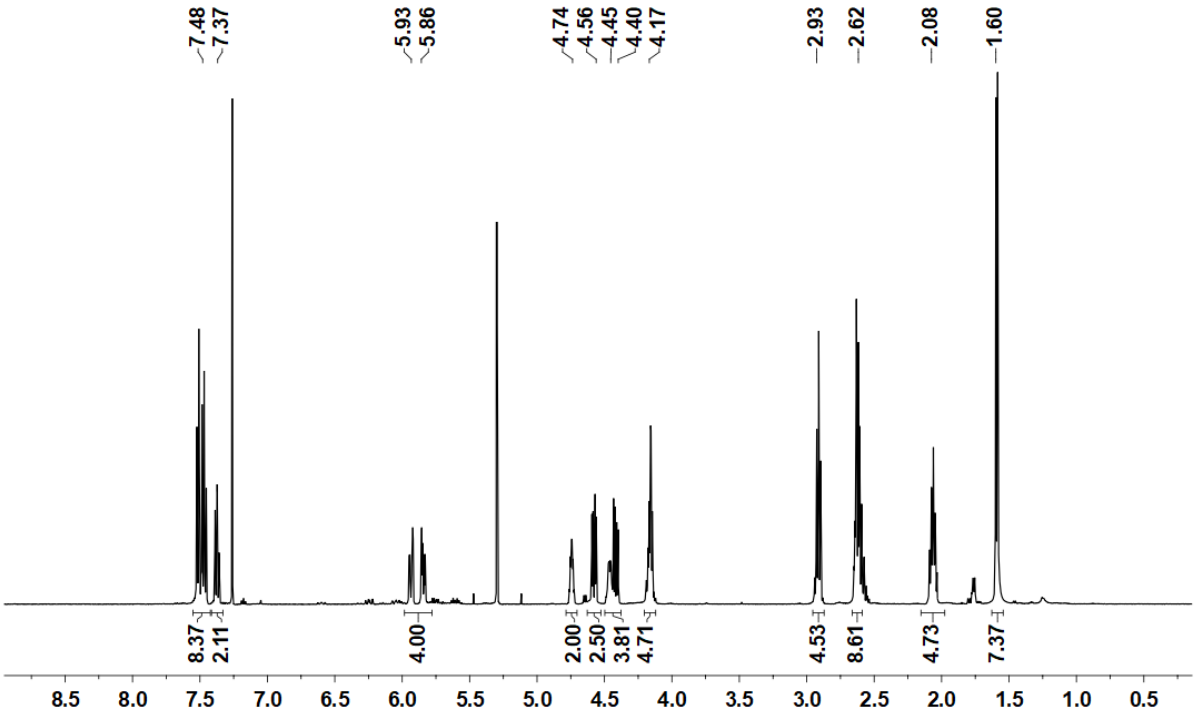

Figure 75. ^{1}H NMR spectrum of the TAD-diene DA adduct (**5**) on a diselenide containing compound in $CDCl_3$.

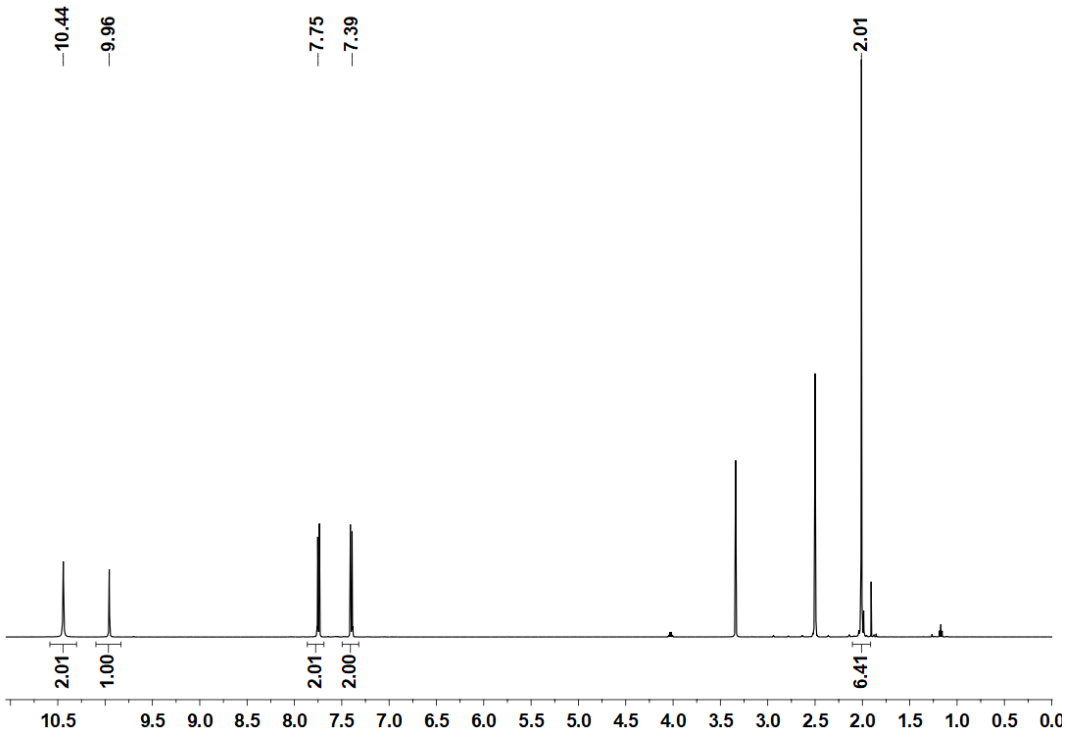

Figure 76. ^{1}H NMR spectrum of urazole-initiator in DMSO-d6.

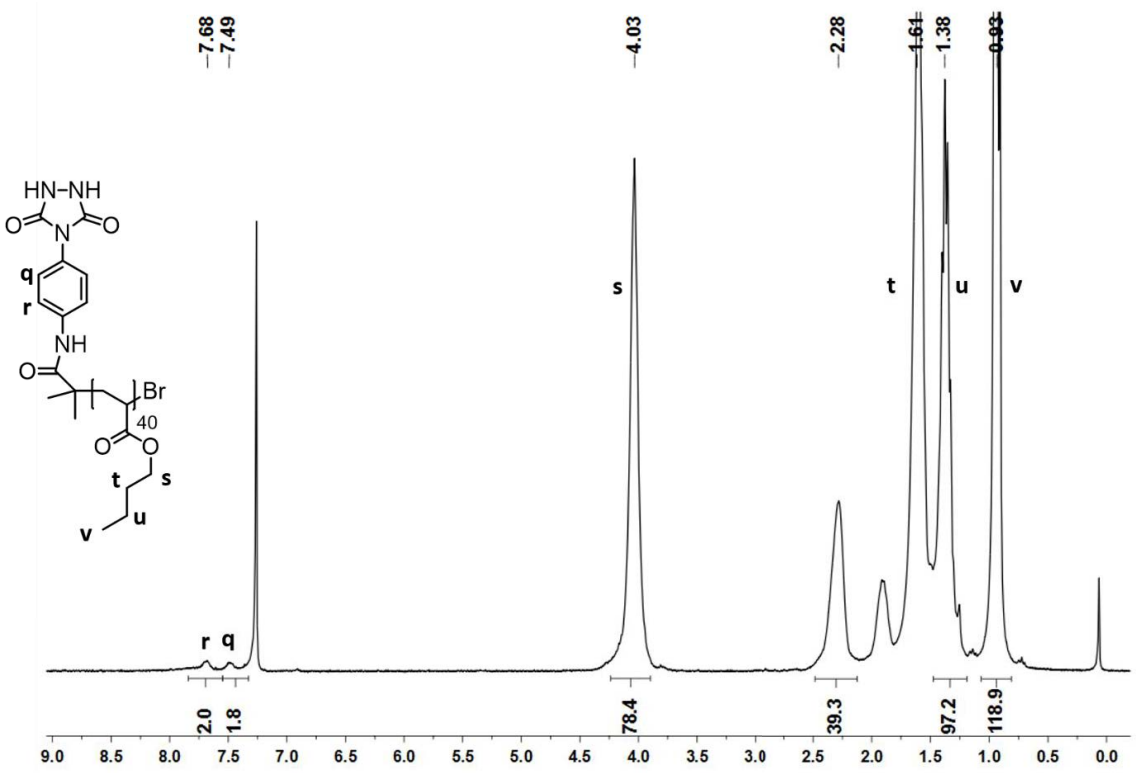

Figure 77. ^{1}H NMR spectrum of Ur-poly(*n*BuA)$_{40}$ in $CDCl_3$.

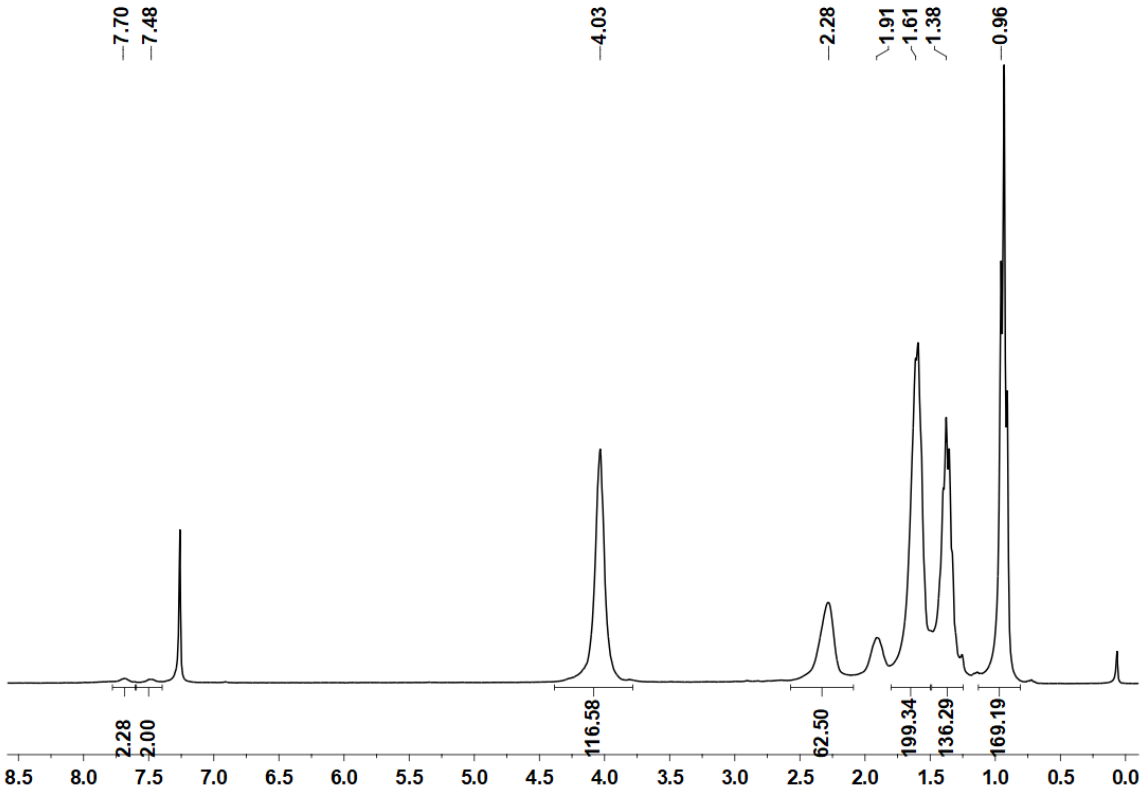

Figure 78. ^{1}H NMR spectrum of Ur-poly(*n*BuA)$_{60}$ in $CDCl_3$.

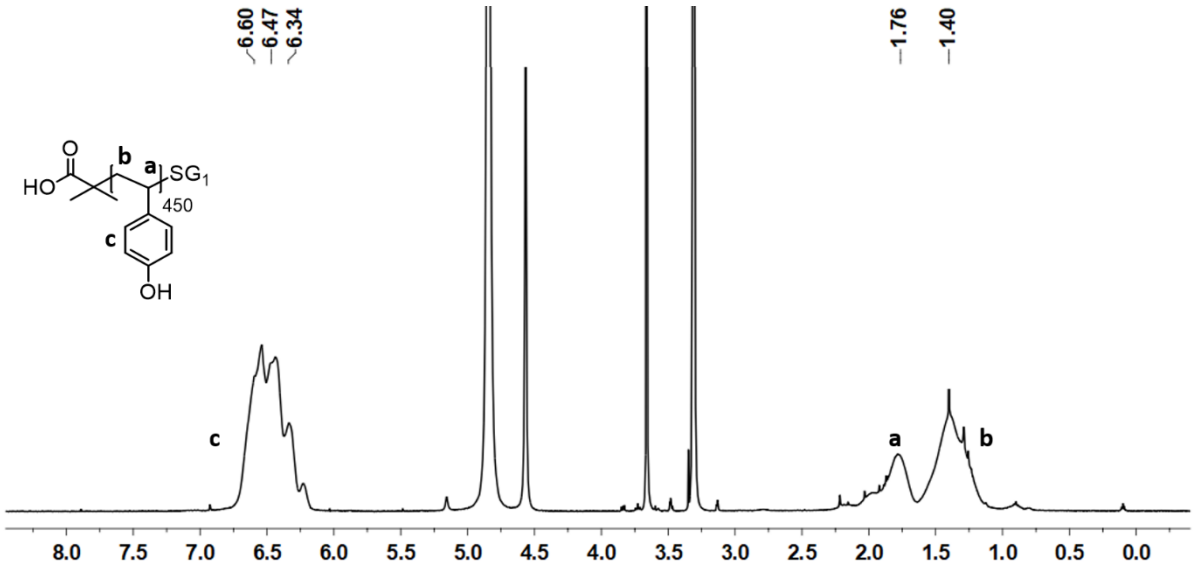

Figure 79. ^{1}H NMR spectrum of the linear homopolymer *l*-poly(StyOH)$_{450}$ in CD_3OD.

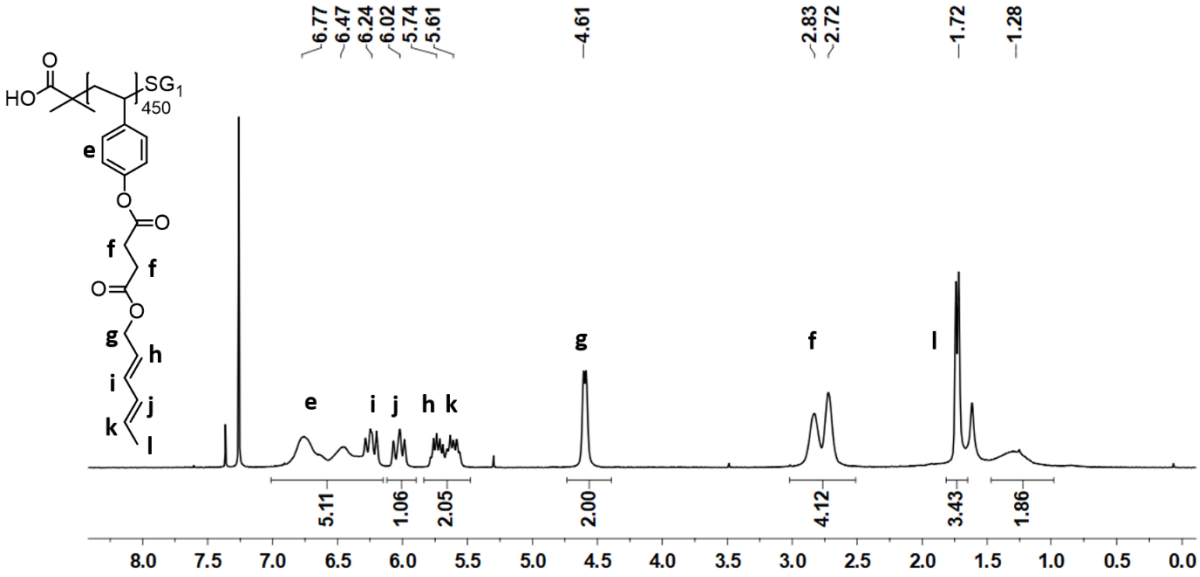

Figure 80. ^{1}H NMR spectrum of the linear macroinitiator *l*-poly(Sty-diene)$_{450}$ in $CDCl_3$.

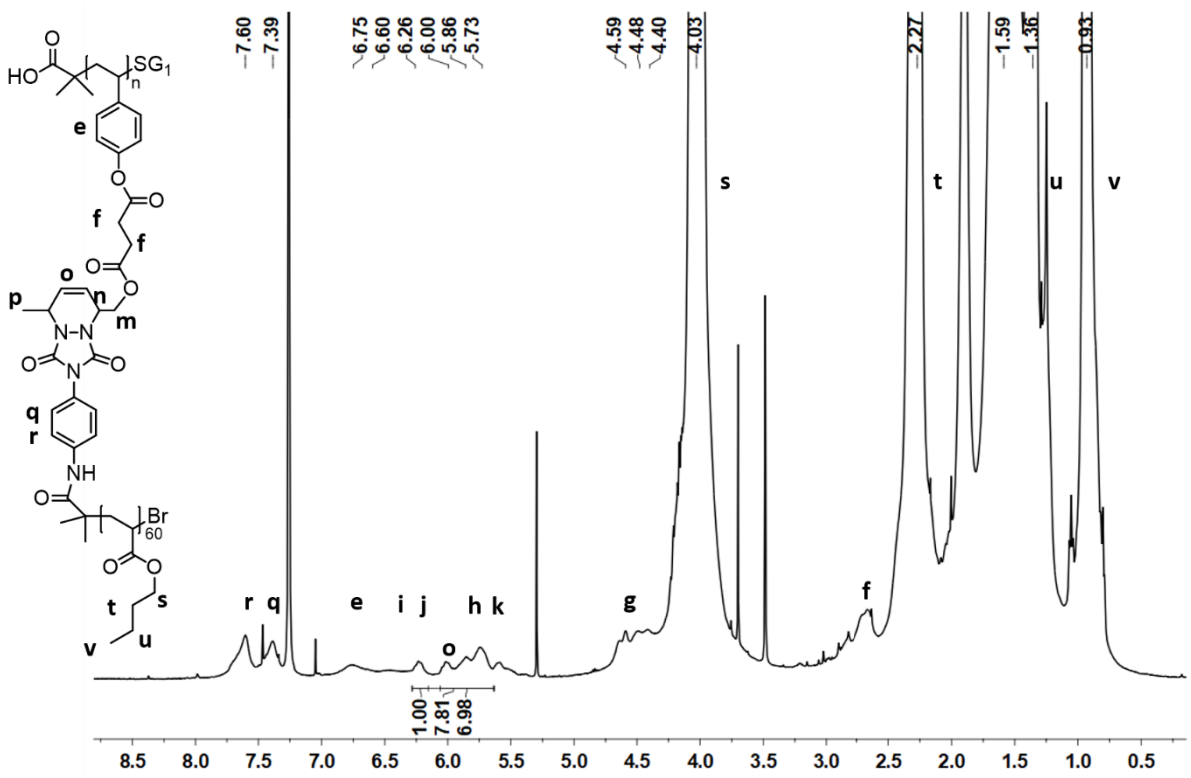

Figure 81. ^{1}H NMR of the linear bottlebrush polymer *l*-[poly(Sty)$_{450}$-*g*-poly(*n*BuA)$_{60}$]$^{0.7}$ in $CDCl_3$. (GD = 70%).

Estimation of the grafting density (GD) by using the following equation where H_h, H_i, H_j, H_k, and H_o are the integration areas corresponding to the protons H, I, J, K, and O respectively:

GD (%) = $\frac{H_{j,o,h} - 2H_k}{H_{j,o,k}}$ x 100 = 70

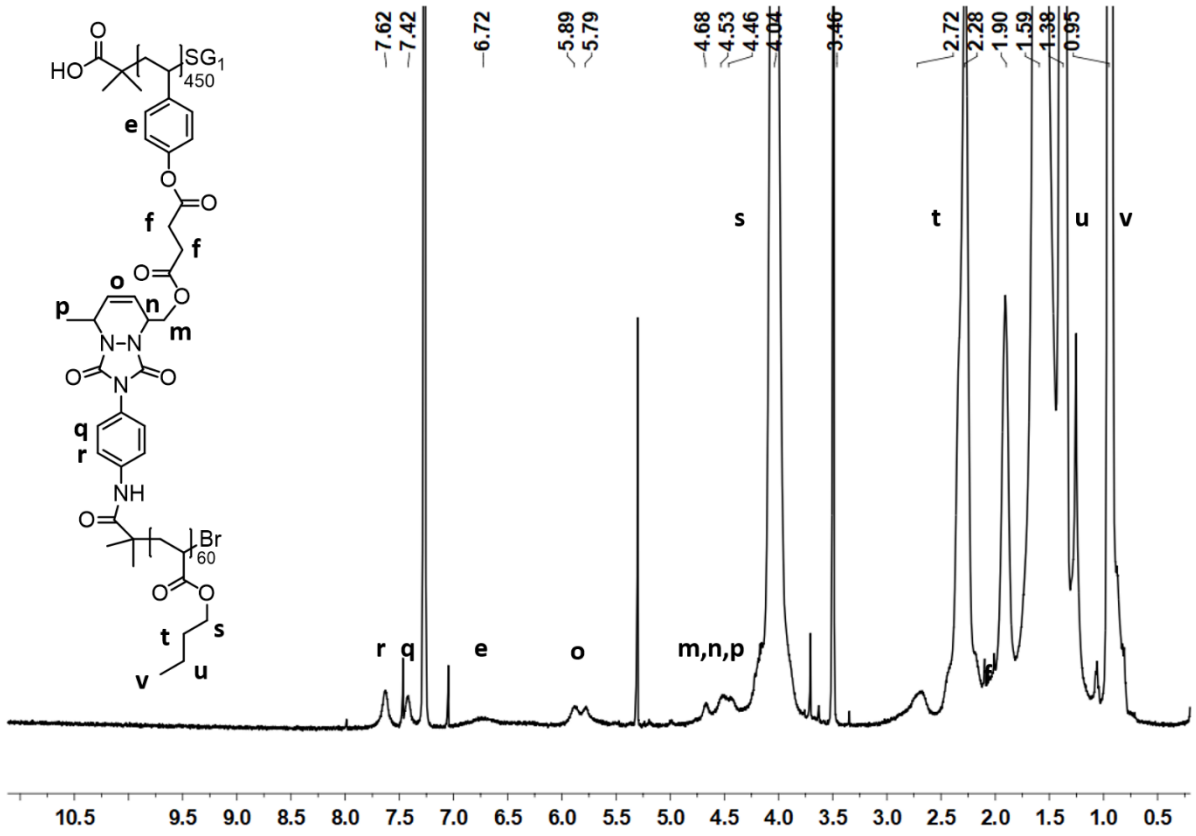

Figure 82. ^{1}H NMR of the linear bottlebrush polymer *l*-[poly(Sty)$_{450}$-*g*-poly(*n*BuA)$_{60}$]$^{1.0}$ in $CDCl_3$.

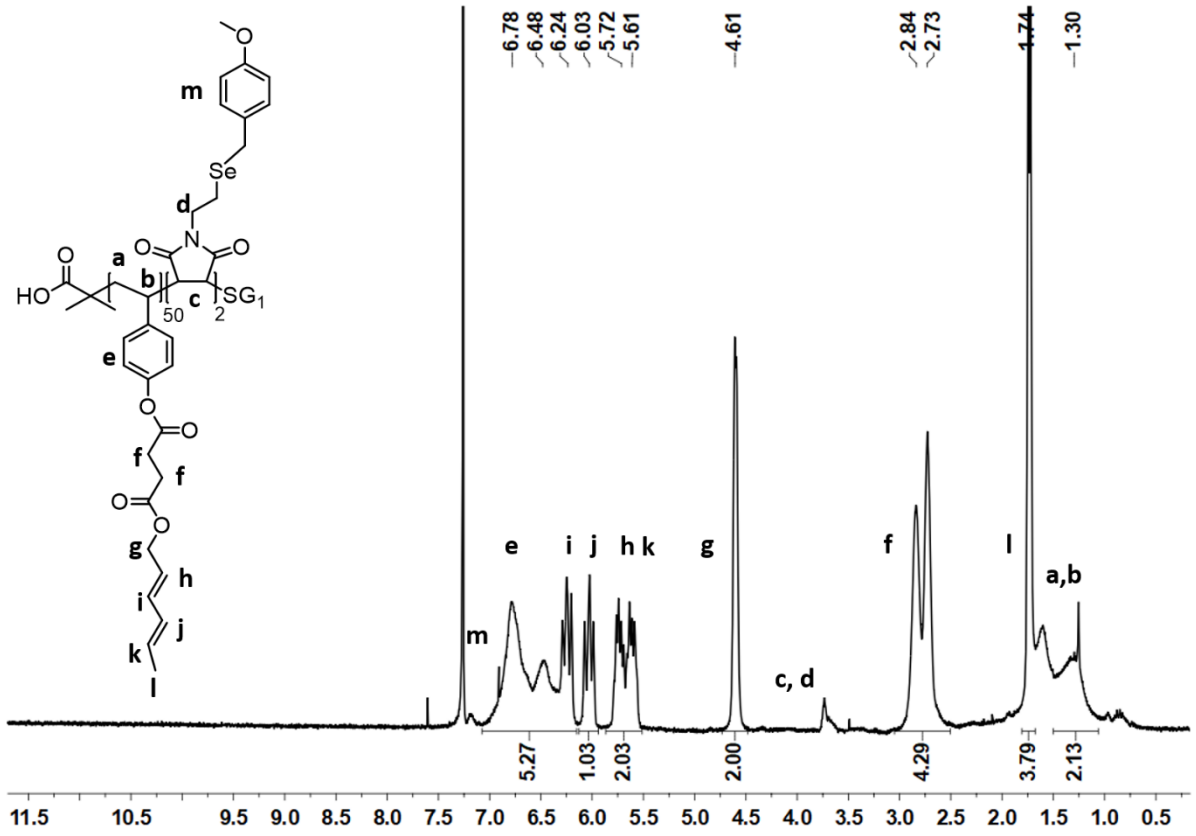

Figure 83. ^{1}H NMR spectrum of the linear macroinitiator analogue *l*-poly(Sty-diene)$_{50}$ in $CDCl_3$.

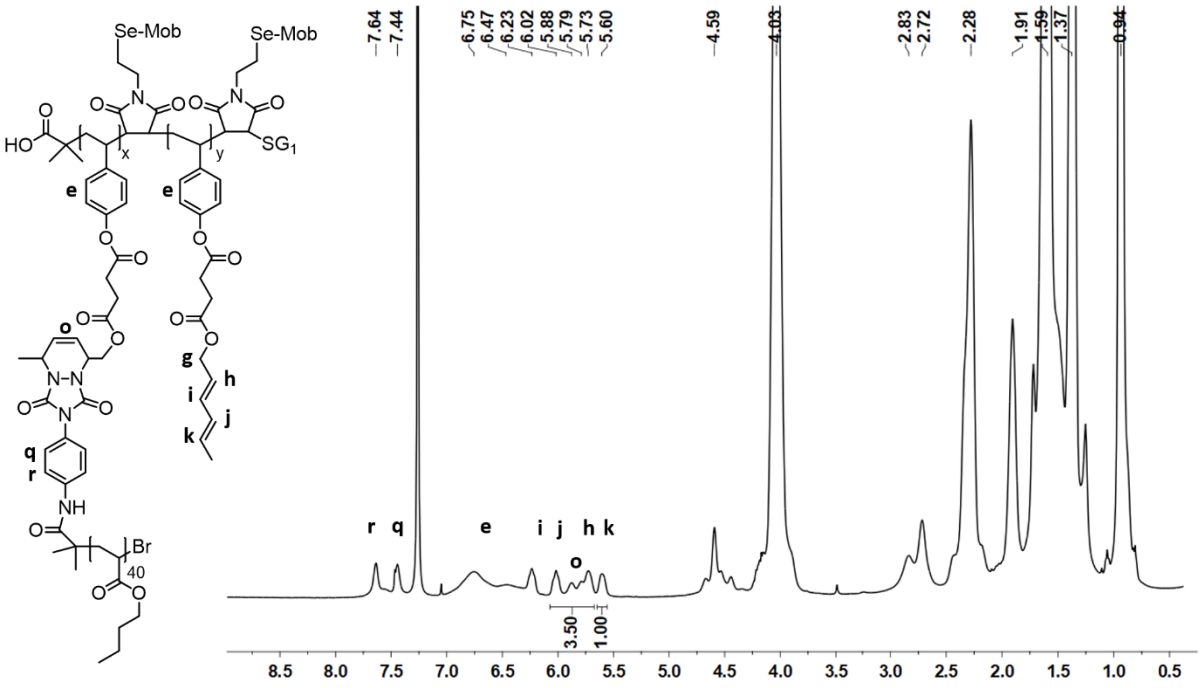

Figure 84. ^{1}H NMR of the linear grafted polymer *l*-poly(Sty)$_{50}$-*g*-[poly(*n*BuA)$_{40}$]$^{0.43}$ in $CDCl_3$.

GD = 43%.

Estimation of the grafting density (GD) by using the following equation where H_h, H_i, H_j, H_k, and H_o are the integration areas corresponding to the protons H, I, J, K, and O respectively:

GD (%) = $\frac{Hj,o,h-2Hk}{Hj,o,k}$ x 100 = 43

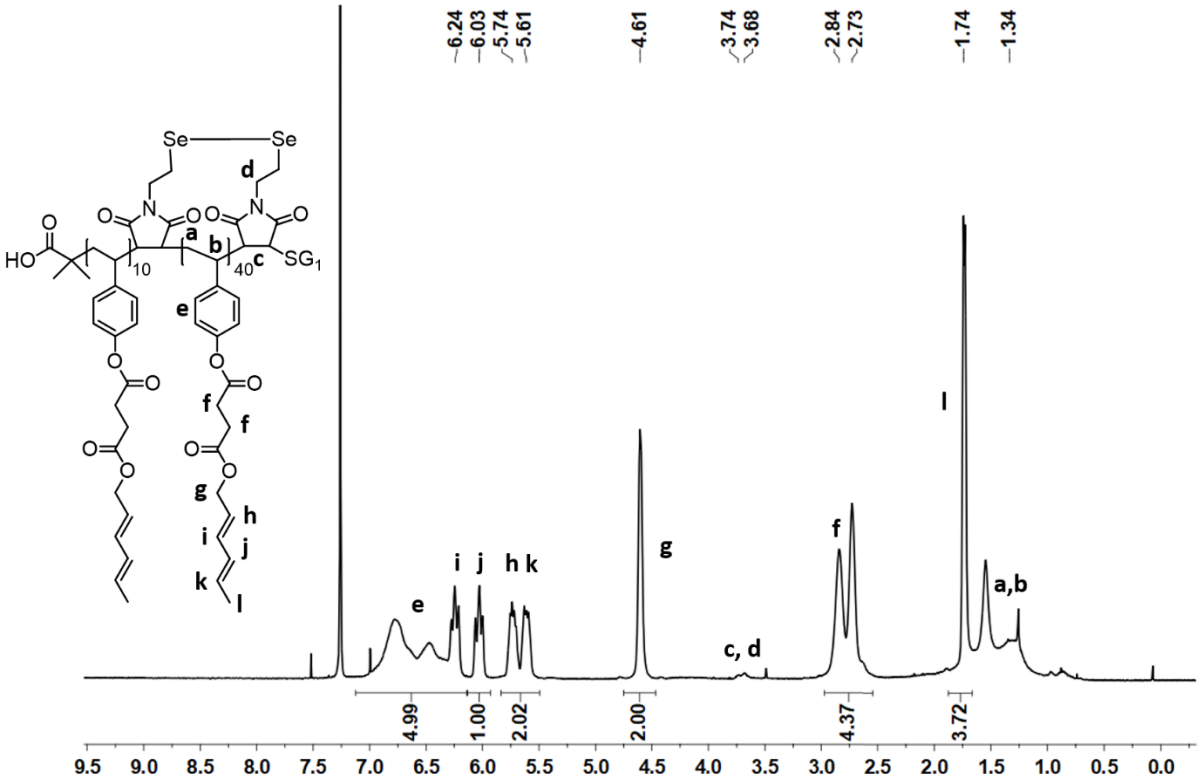

Figure 85. ^{1}H NMR spectrum of the cyclic macroinitiator *c*-poly(Sty-diene-*co*-MISe) in $CDCl_3$.

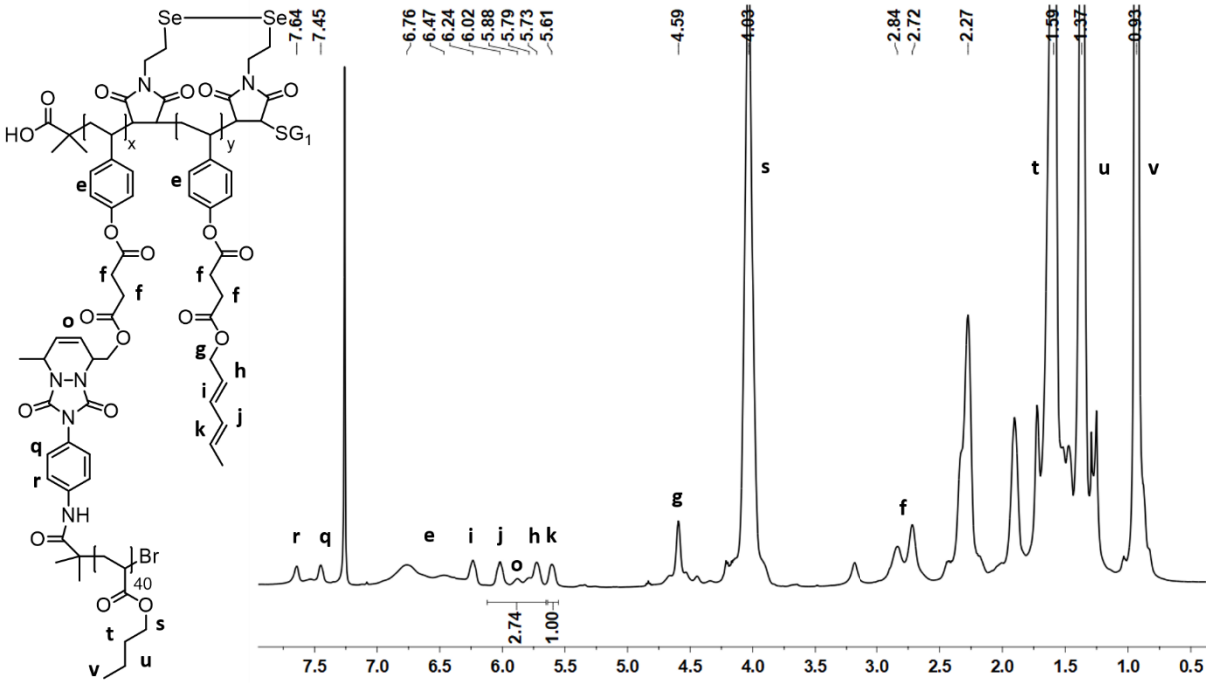

Figure 86. ^{1}H NMR spectrum of the cyclic grafted polymers *c*-poly(Sty)$_{50}$-*g*-[poly(*n*BuA)$_{40}$]$^{0.27}$ in $CDCl_3$.

Estimation of the grafting density (GD) by using the equation:

$$GD\ (\%) = \frac{Hj,o,h-2Hk}{Hj,o,k} \times 100 = 27$$

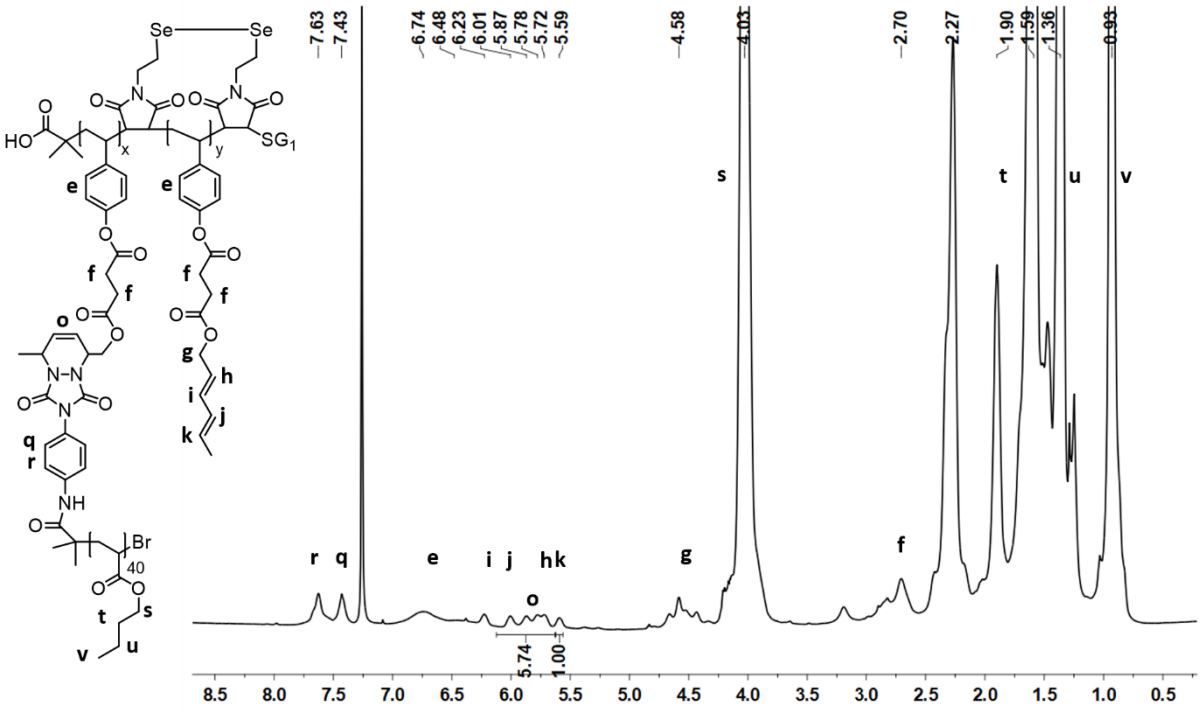

Figure 87. ^{1}H NMR spectrum of the cyclic grafted polymers *c*-poly(Sty)$_{50}$-*g*-[poly(*n*BuA)$_{40}$]$^{0.65}$ in $CDCl_3$. GD = 65%

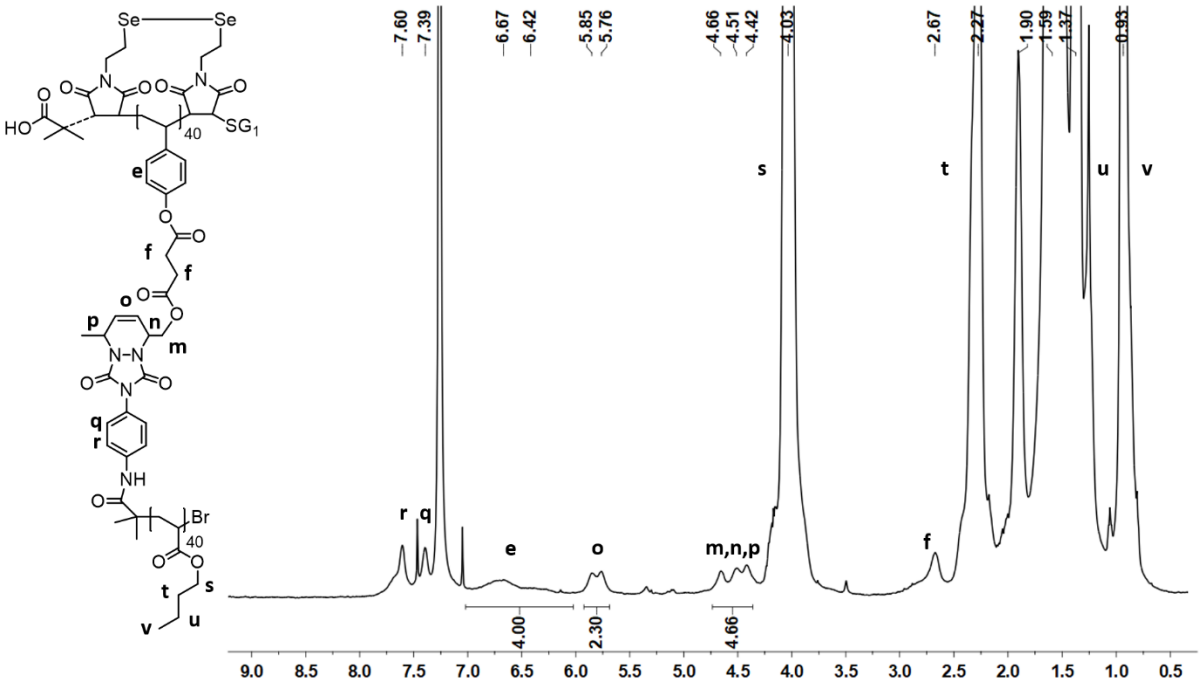

Figure 88. ^{1}H NMR spectrum of the brush polymers *c*-poly(Sty)$_{50}$-*g*-[poly(*n*BuA)$_{40}$]$^{1.0}$ in $CDCl_3$. GD = 100%

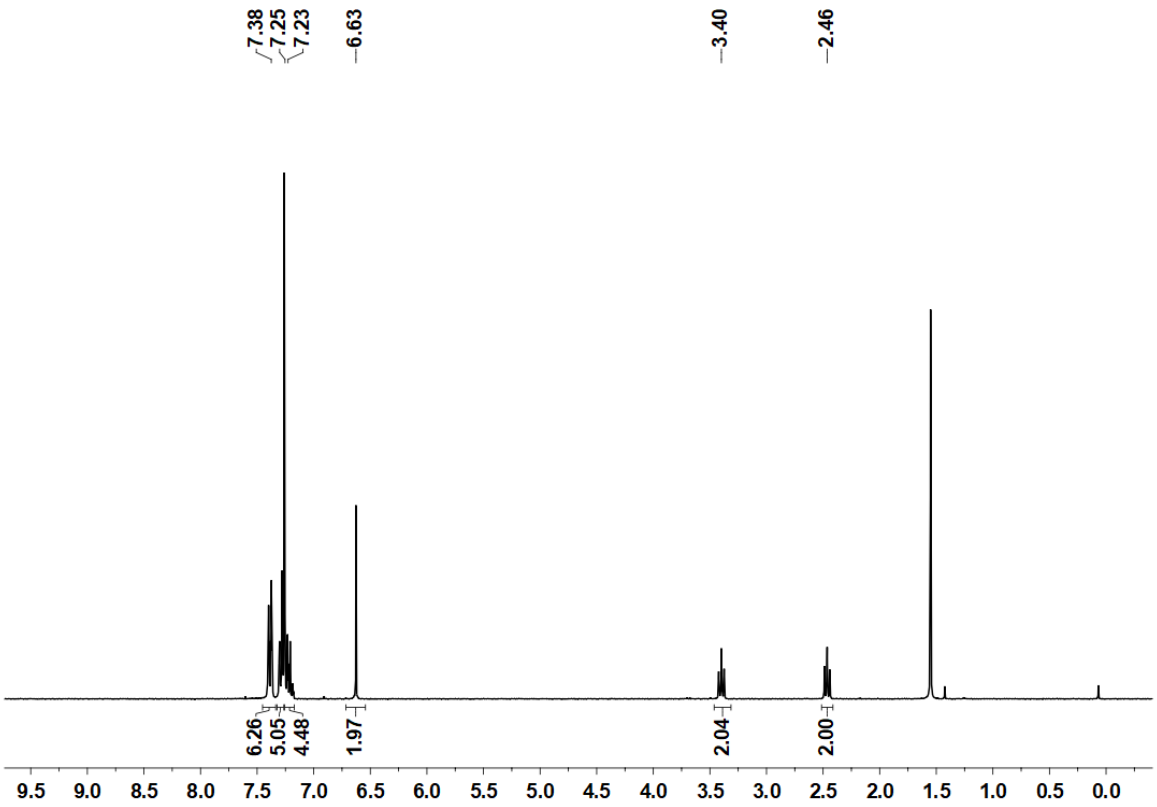

Figure 89. ^{1}H NMR spectrum of *N*-(2-tritylthioethyl) maleimide in $CDCl_3$.

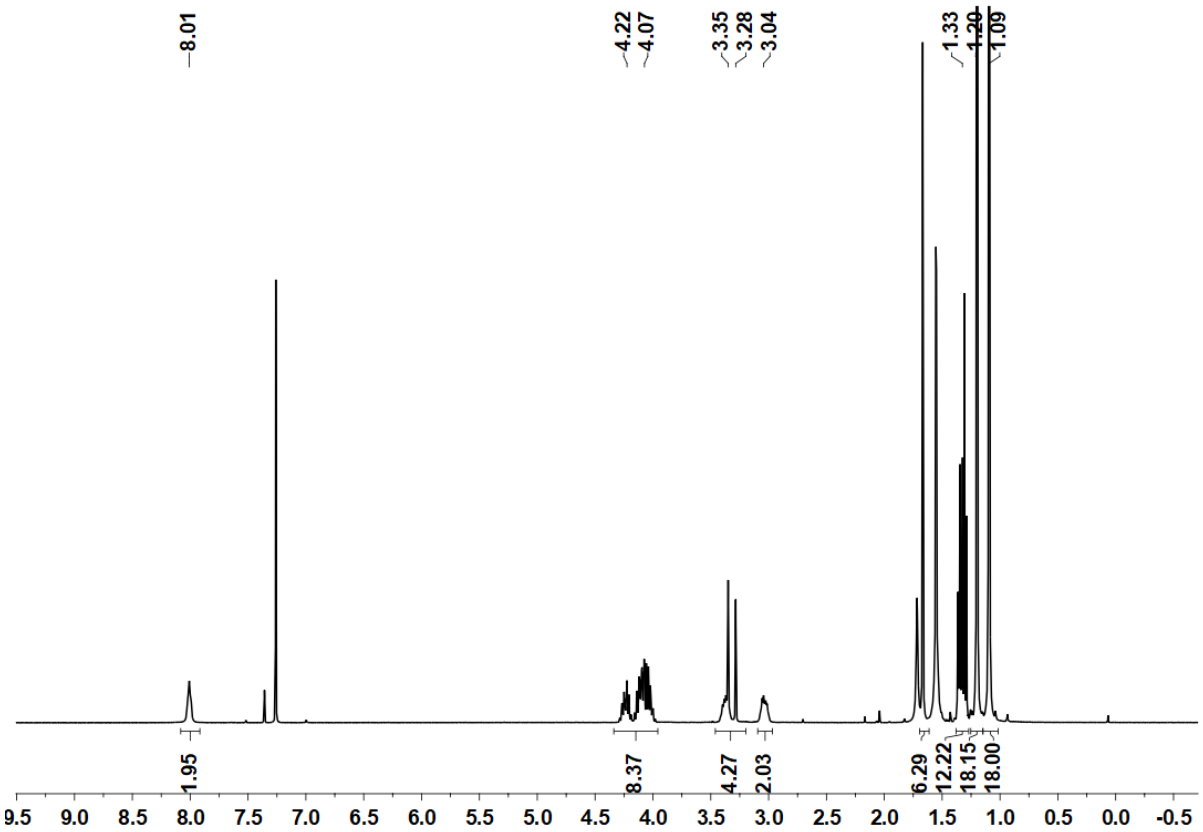

Figure 90. ^{1}H NMR spectrum of the novel NMP-difunctional initiator (Bis-BB-SG1) in $CDCl_3$.

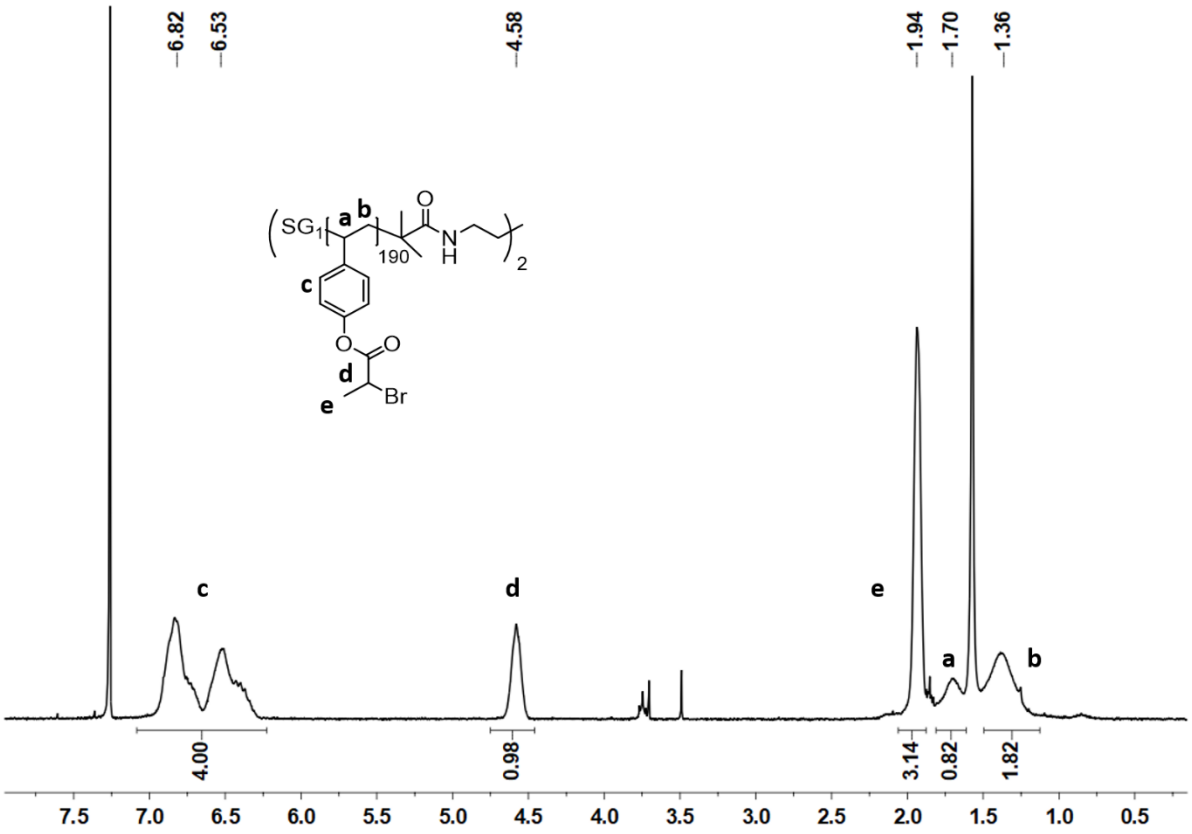

Figure 91. ^{1}H NMR spectrum of the linear brush polymer *l*-poly(StyBr)$_{380}$ in $CDCl_3$.

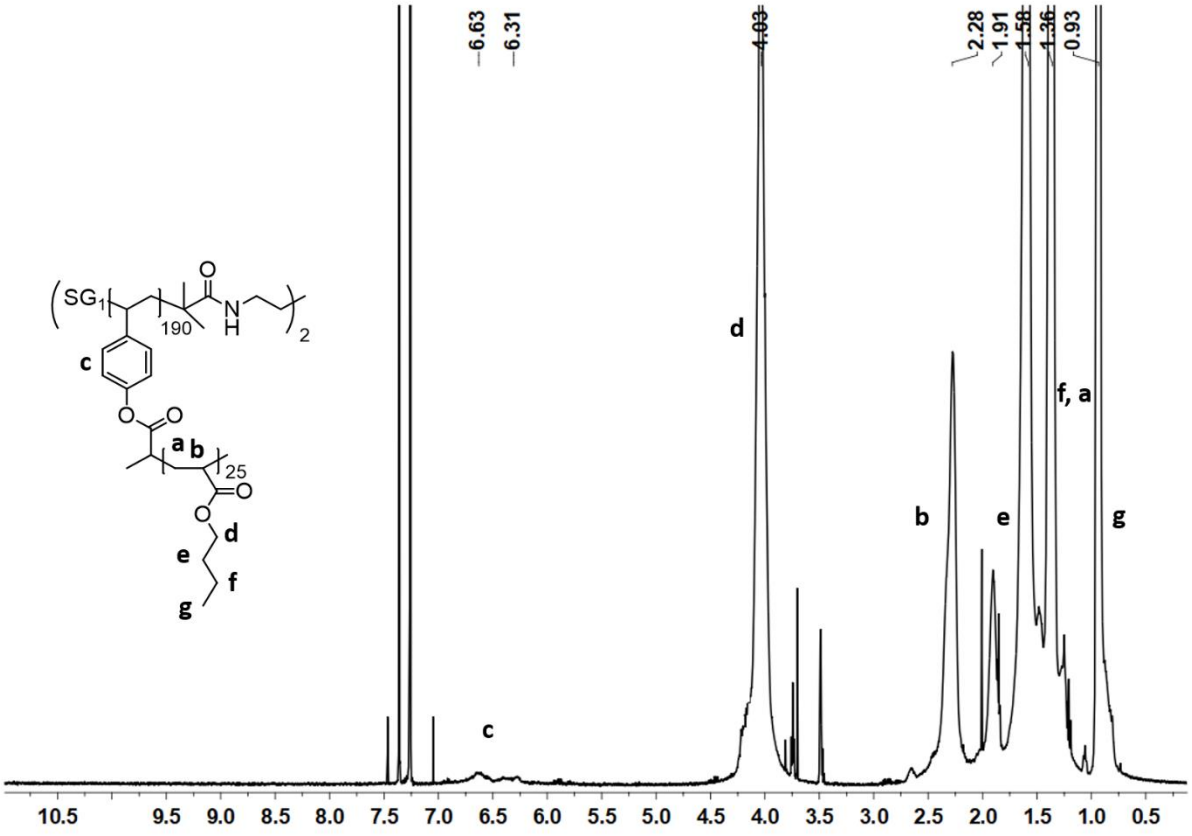

Figure 92. ^{1}H NMR spectrum of the linear brush polymer *l*-poly(Sty)$_{380}$-*g*-poly(*n*BuA)$_{25}$ in $CDCl_3$.

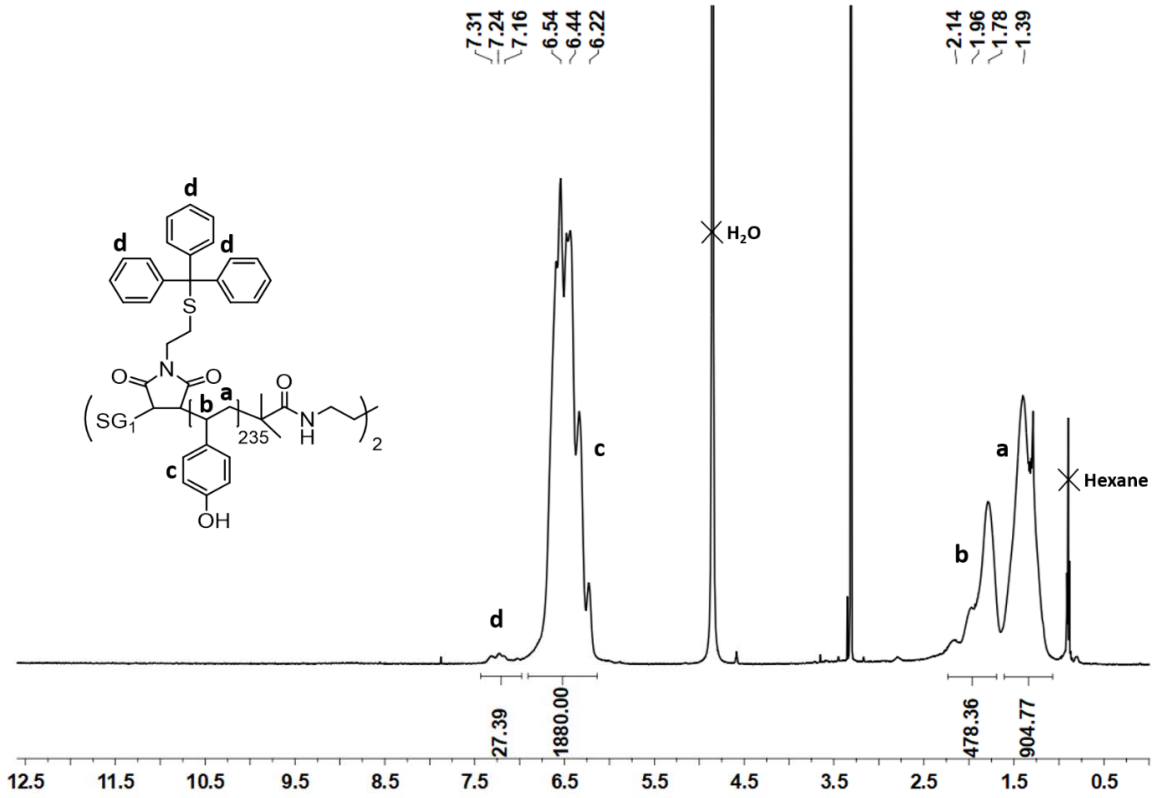

Figure 93. [1]H NMR spectrum of the copolymer poly(StyOH-*co*-MISTrt) after removal of *tert*-butyl groups in CD_3OD.

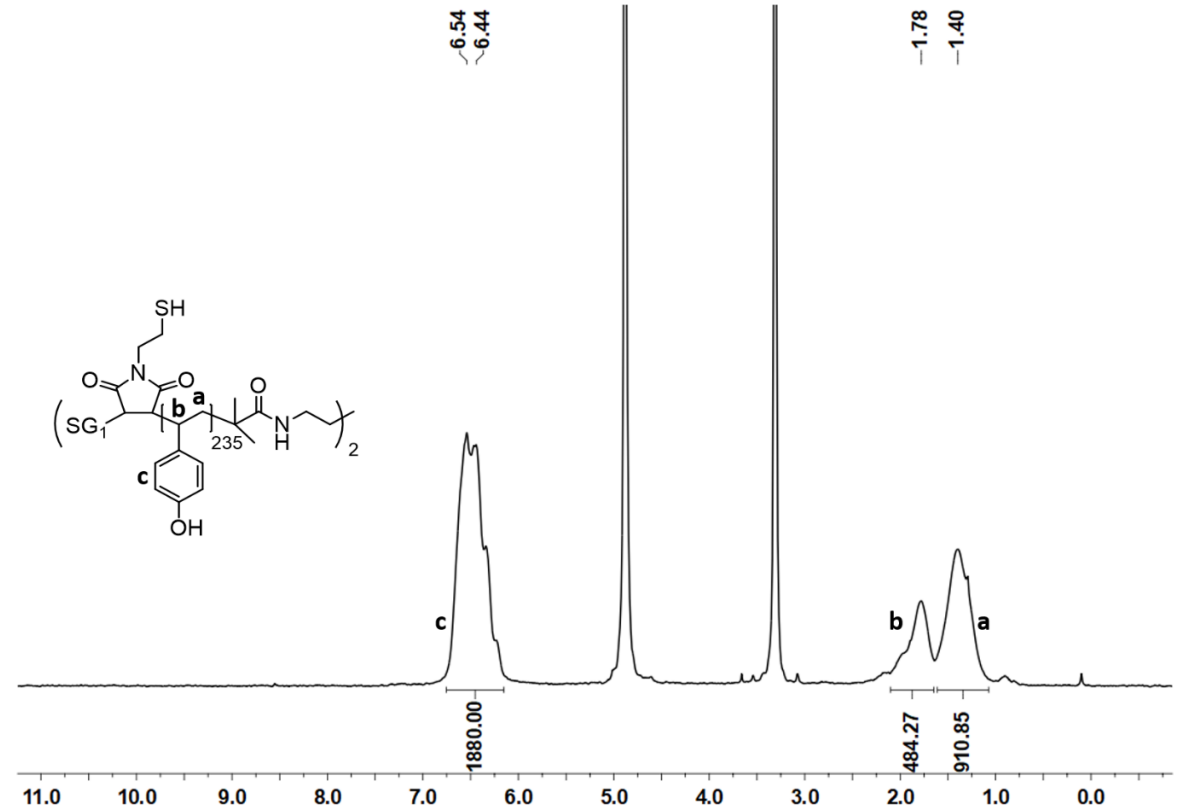

Figure 94. [1]H NMR spectrum of the fully deprotected copolymer *l*-poly(StyOH-*co*-MISH) in CD_3OD.

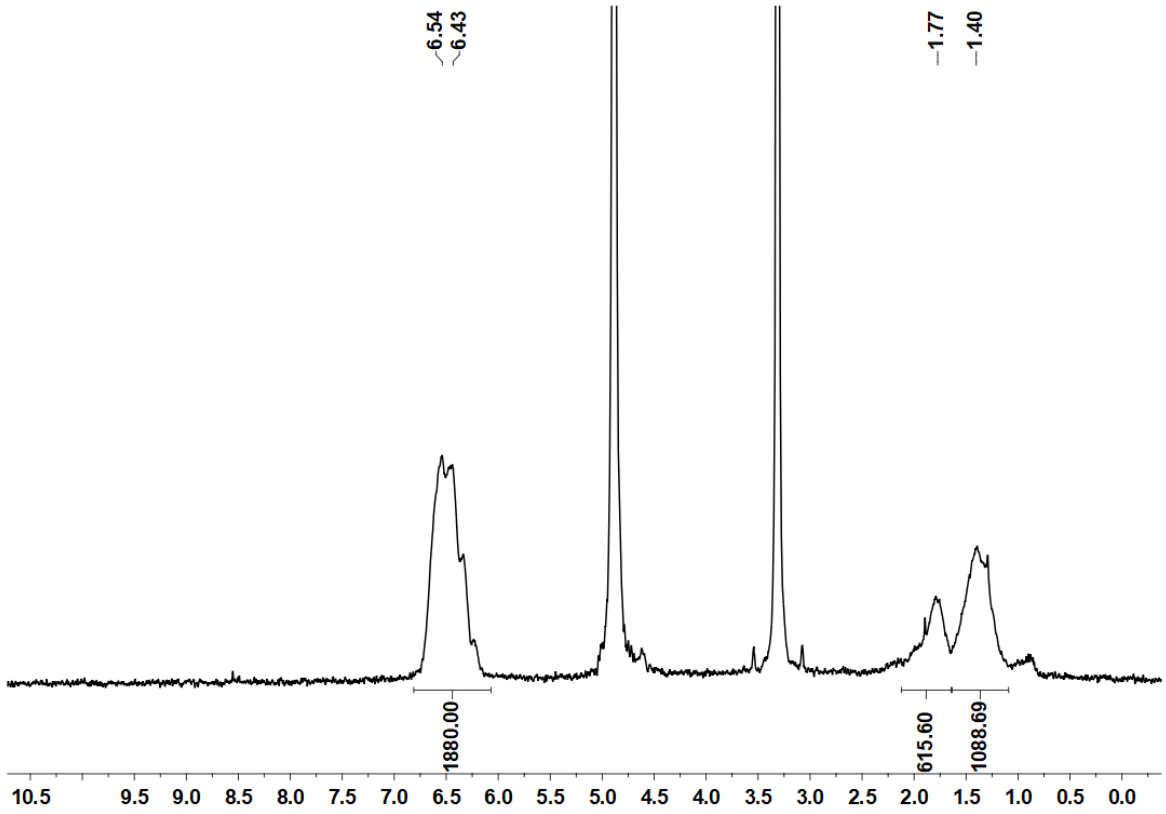

Figure 95. ^{1}H NMR spectrum in CD_3OD of the copolymer *c*-poly(StyOH-*co*-MIS) after crosslinking reaction.

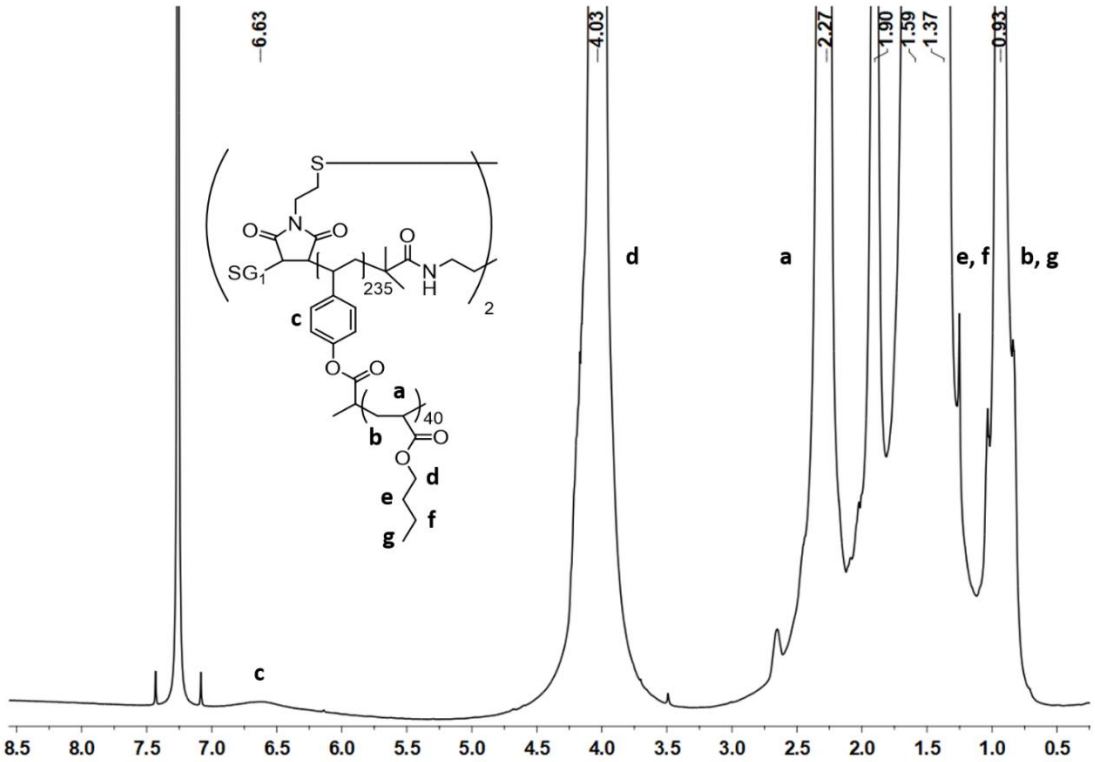

Figure 96. ^{1}H NMR spectrum in $CDCl_3$ of the brush copolymer (*c*-poly(Sty)$_{470}$-*g*-poly(*n*BuA)$_{40}$).

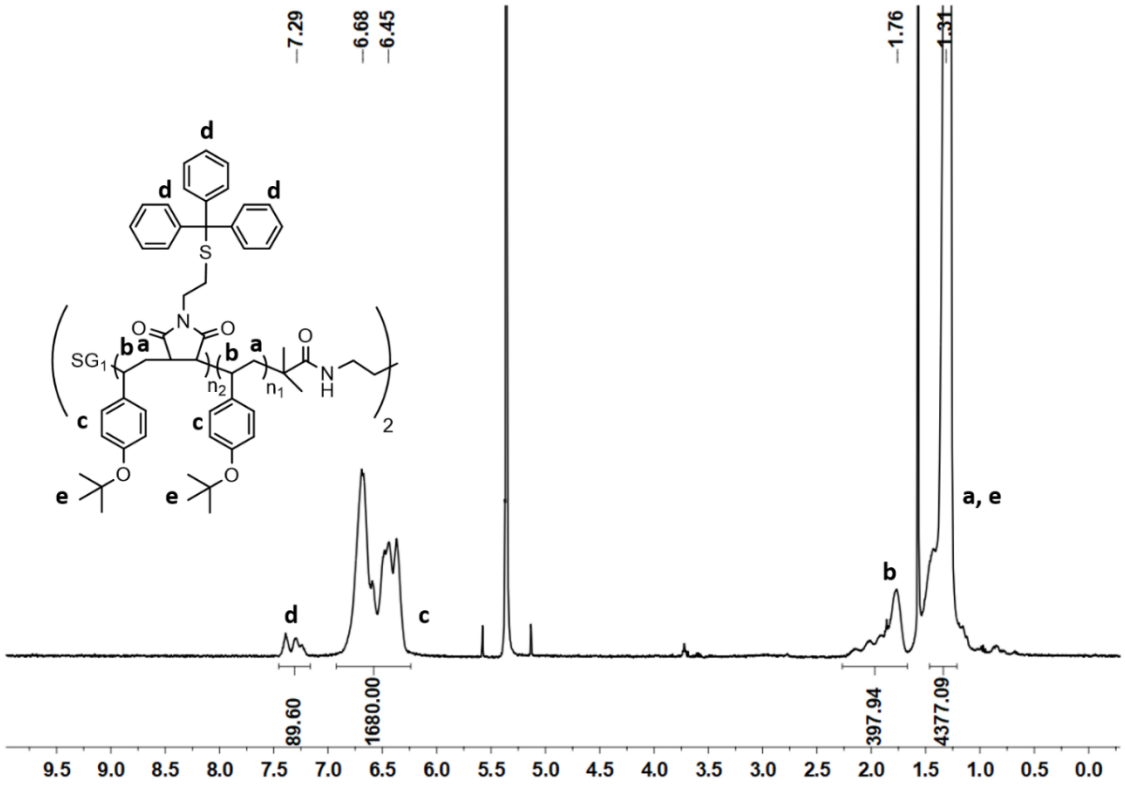

Figure 97. ^{1}H NMR spectrum of the sequence-controlled copolymer poly(StyO*t*Bu-*co*-MISTrt^{6}) in $CDCl_3$.

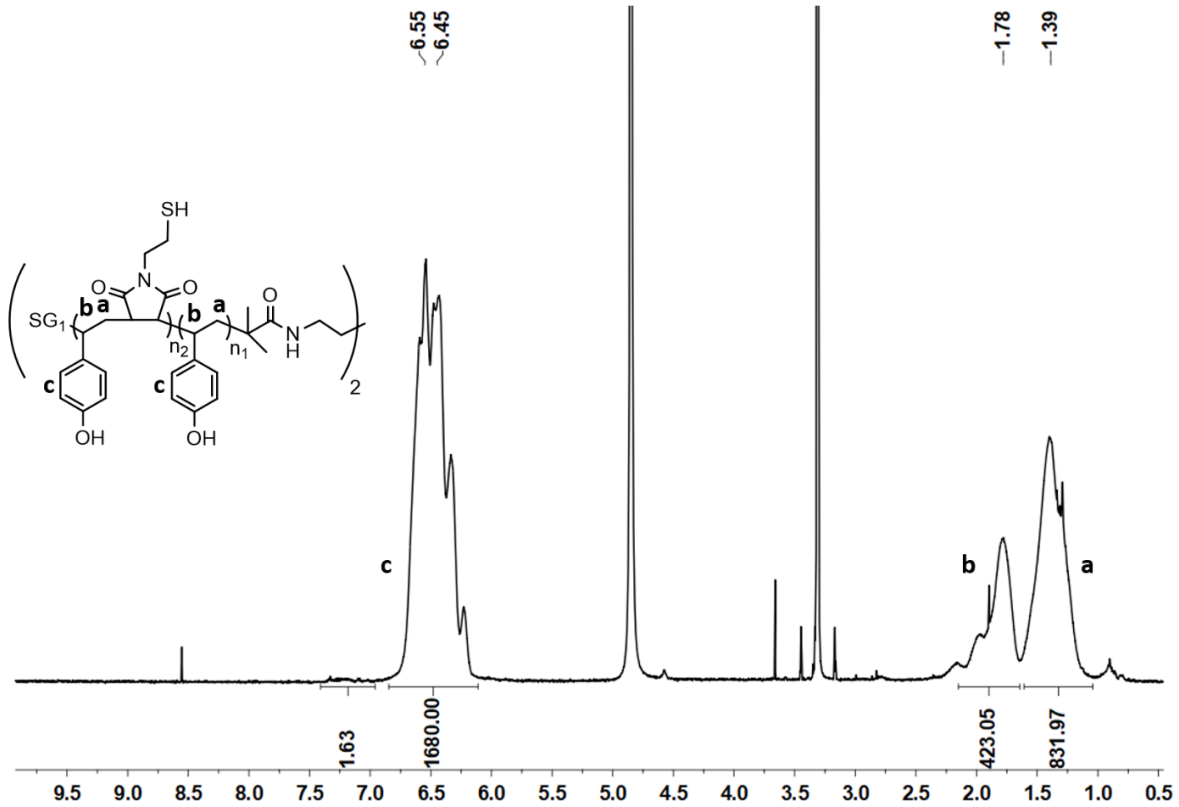

Figure 98. ^{1}H NMR spectrum of the fully deprotected copolymer *l*-poly(StyOH-*co*-MISH^{6}) in CD_3OD.

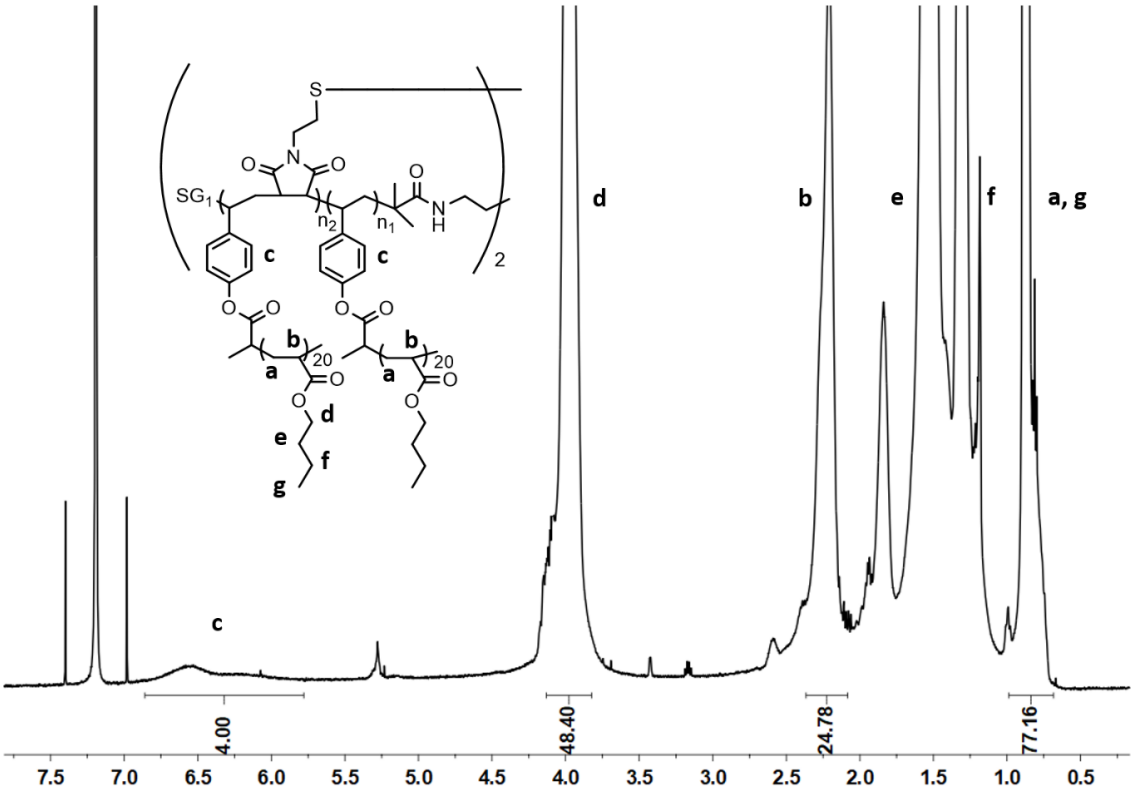

Figure 99. ^{1}H NMR spectrum of the fully deprotected copolymer *c*-[poly(Sty)$_{420}$-*g*-poly(*n*BuA)$_{20}$]^{6} in $CDCl_3$.

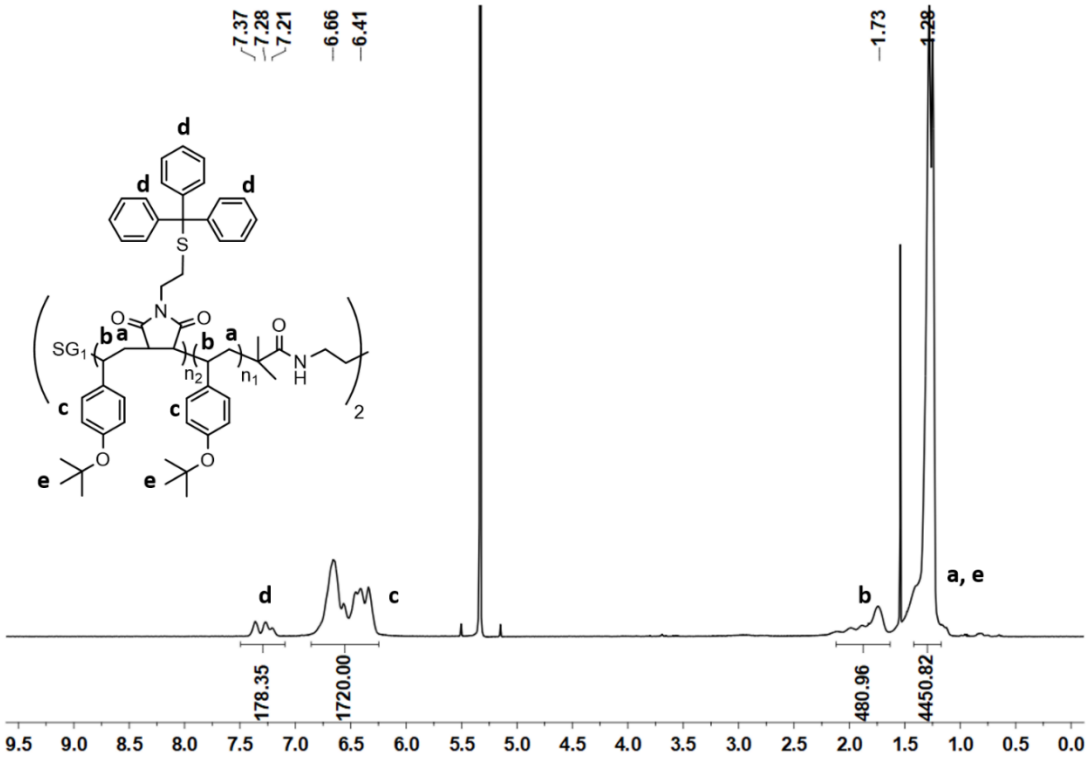

Figure 100. ^{1}H NMR spectrum of the sequence-controlled copolymer poly(StyO*t*Bu-*co*-MISTrt^{12}) in $CDCl_3$.

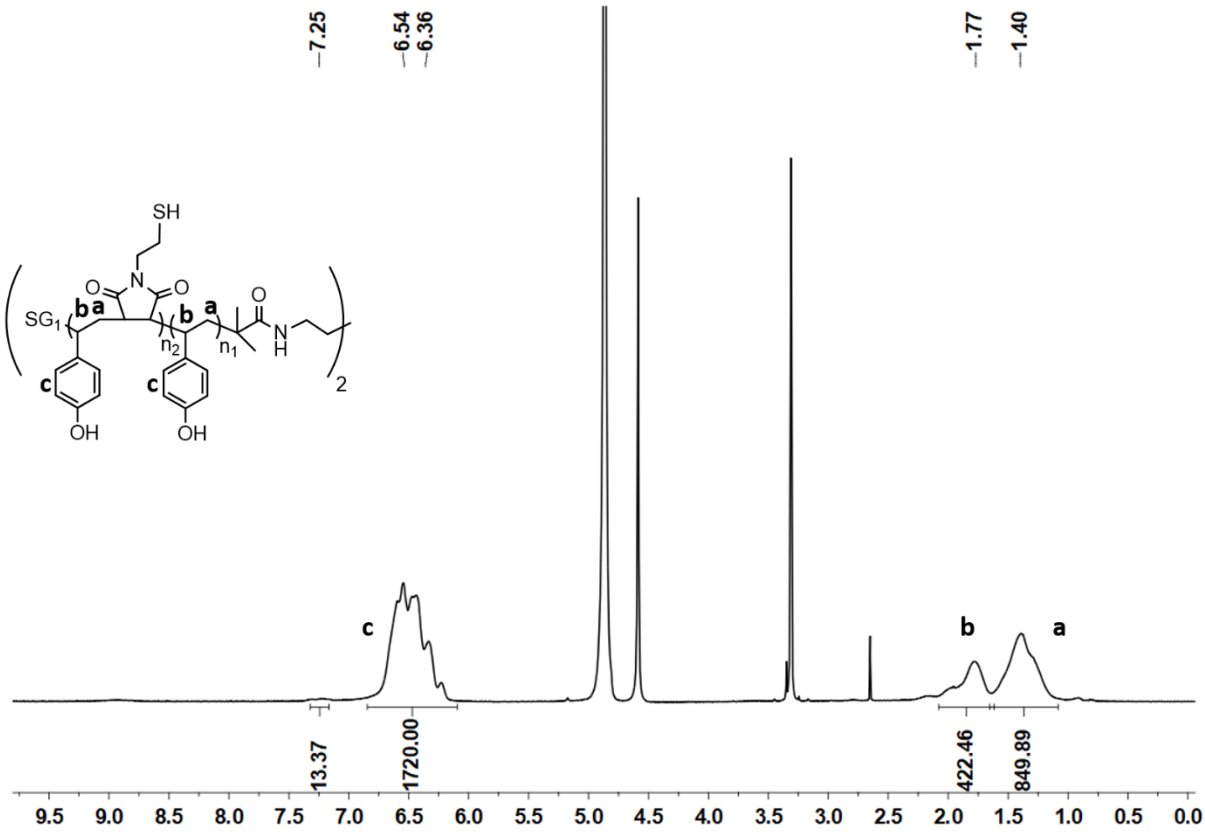

Figure 101. ^{1}H NMR spectrum of the fully deprotected copolymer *l*-poly(StyO*H*-*co*-MISH^{12}) in CD_3OD.

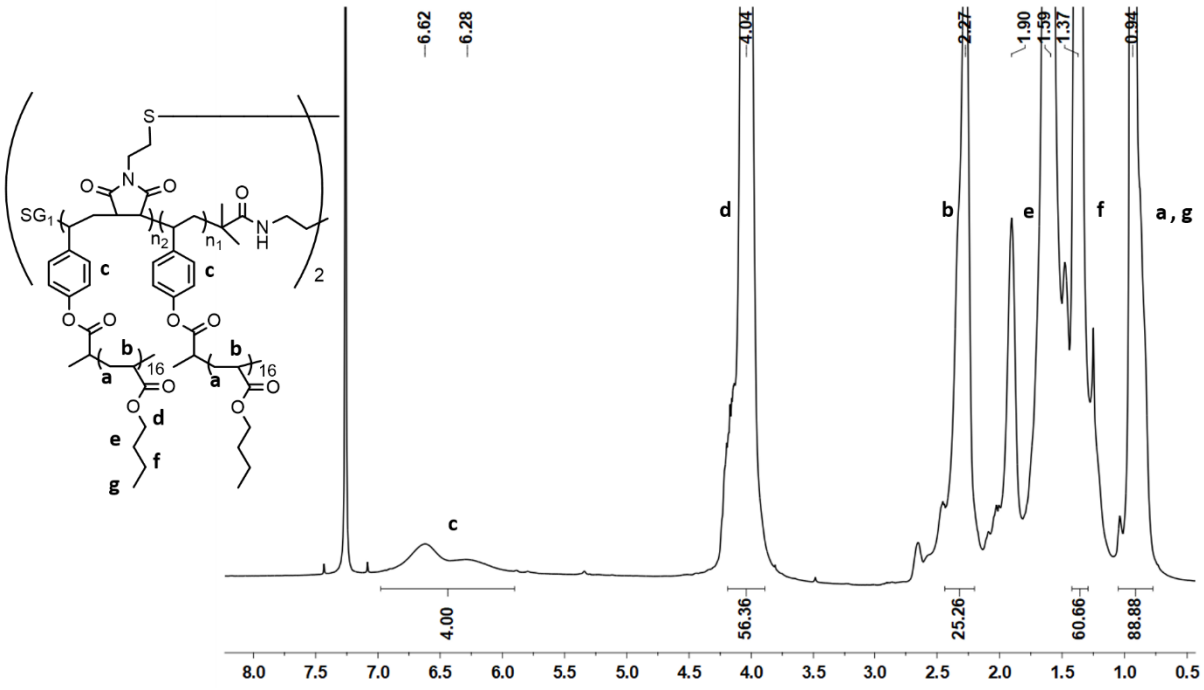

Figure 102. ^{1}H NMR spectrum of the brush copolymer *c*-[poly(Sty)$_{430}$-*g*-poly(*n*BuA)$_{16}$]^{12} in $CDCl_3$.

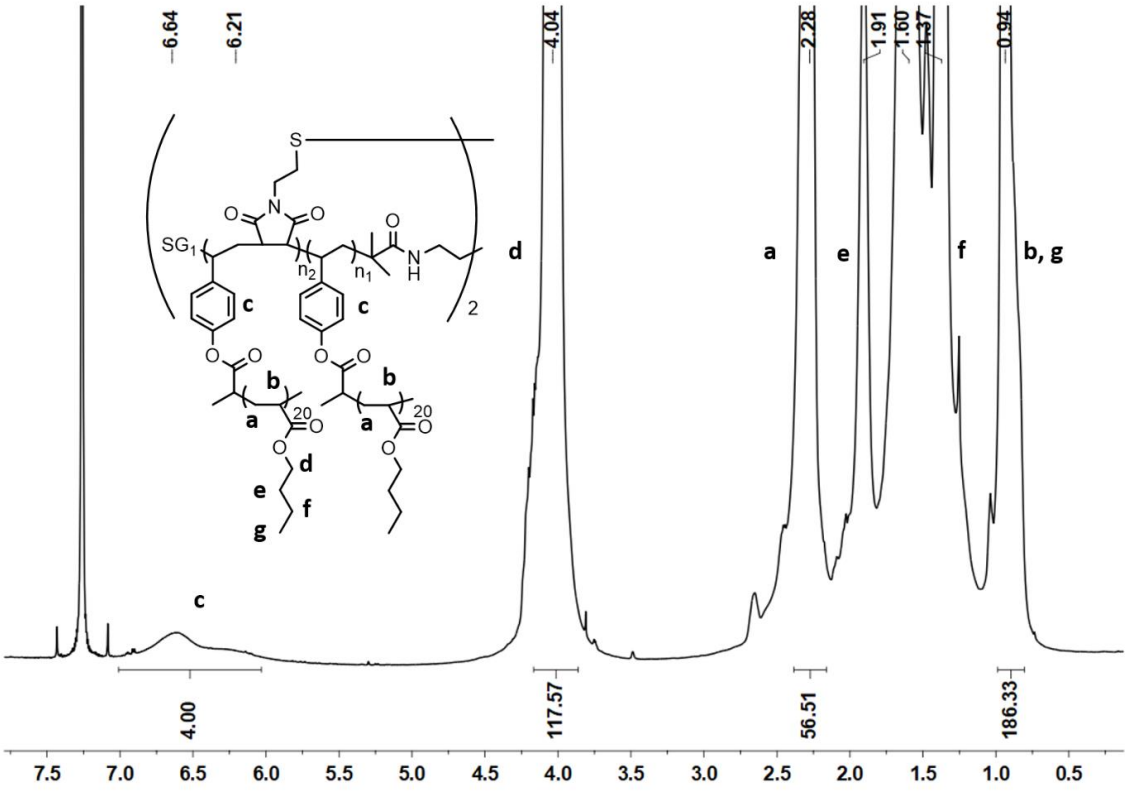

Figure 103. ^{1}H NMR spectrum in $CDCl_3$ of the cyclic brush copolymer *c*-[poly(Sty)$_{420}$-*g*-poly(*n*BuA)$_{20}$]$^{6\text{-a}}$.

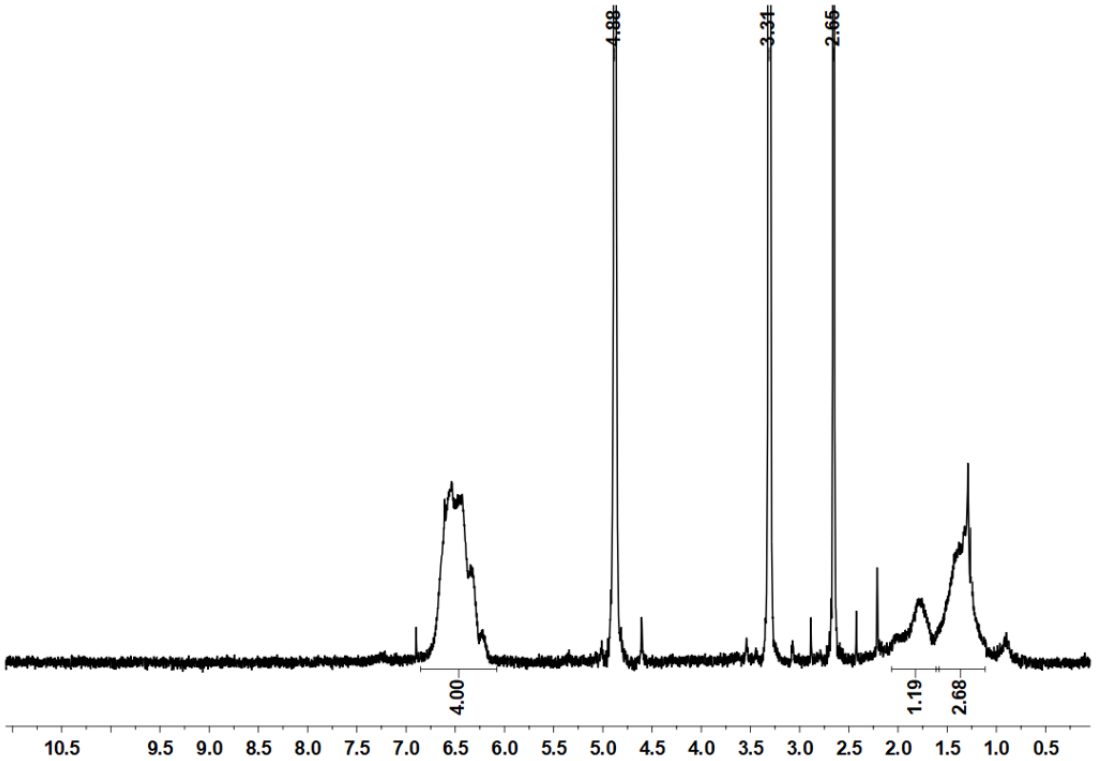

Figure 104. ^{1}H NMR spectrum in CD_3OD of the copolymer *c*-poly(StyOH-*co*-MIS)$^{6\text{-d}}$ after oxidative crosslinking reaction.

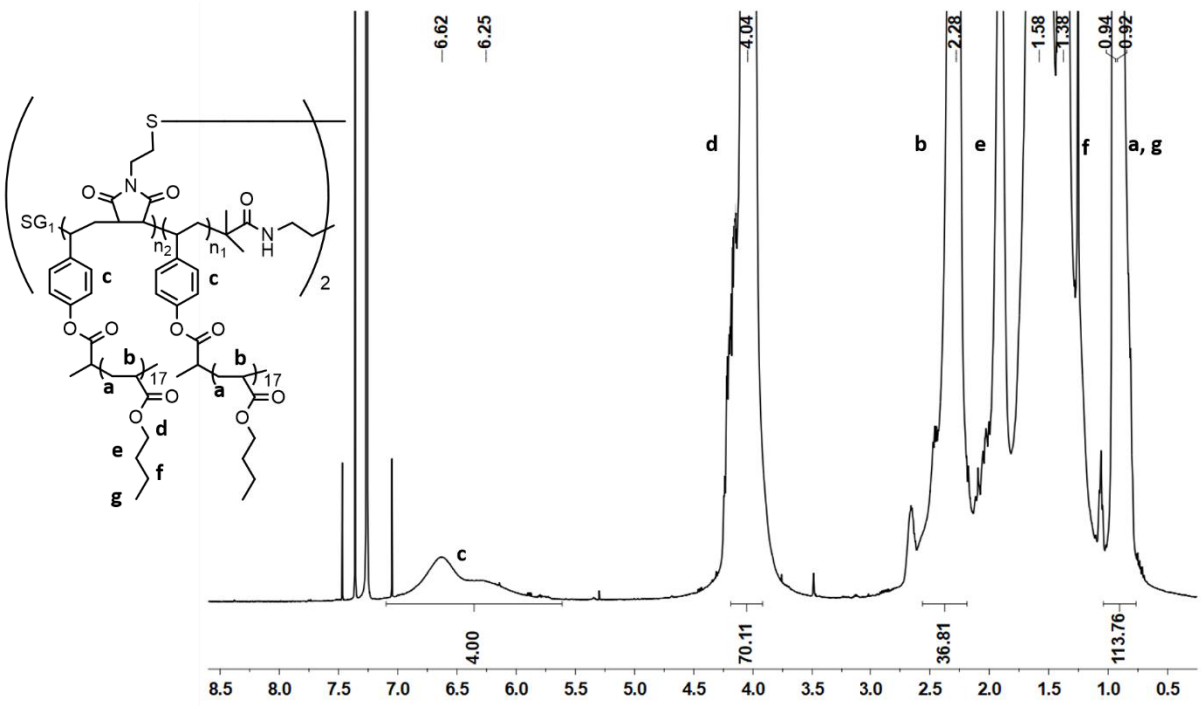

Figure 105. ^{1}H NMR spectrum of the brush copolymer *c*-[poly(Sty)$_{420}$-*g*-poly(*n*BuA)$_{17}$]$^{6\text{-d}}$ in $CDCl_3$.

6.5. Atomic Force Microscopy

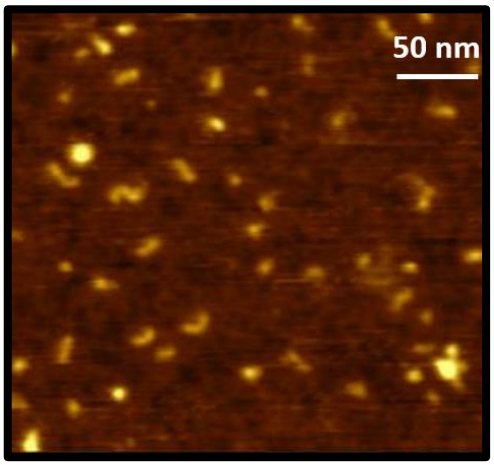

Figure 106. AFM microscopy, height image of crude *c*-poly(Sty)$_{50}$-*g*-[poly(*n*BuA)$_{40}$]$^{0.65}$.

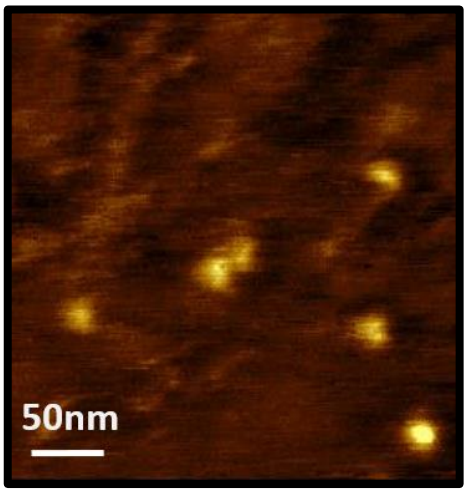

Figure 107. AFM microscopy, height image of pure *c*-poly(Sty)$_{50}$-*g*-[poly(*n*BuA)$_{40}$]$^{0.65}$.

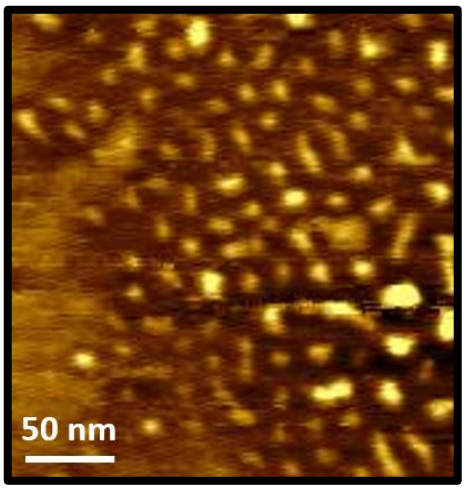

Figure 108. AFM microscopy, height image of pure *l*-poly(Sty)$_{50}$-*g*-[poly(*n*BuA)$_{40}$]$^{0.43}$.

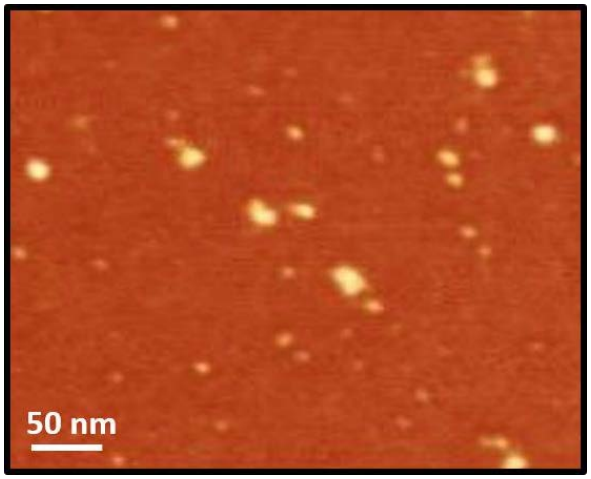

Figure 109. AFM microscopy, height image of pure *c*-poly(Sty)$_{50}$-*g*-[poly(*n*BuA)$_{40}$]$^{0.27}$.

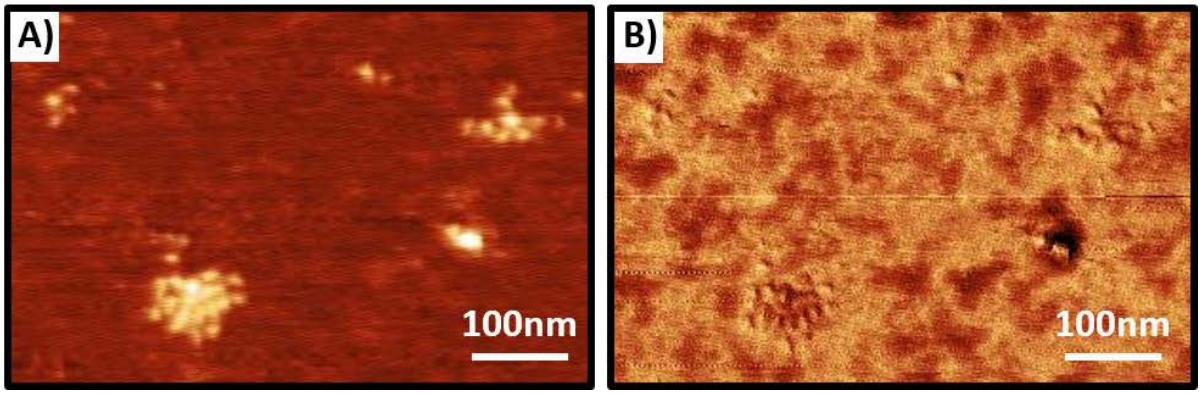

Figure 110. AFM height (A) and phase (B) micrographs of *c*-poly(Sty)$_{50}$-*g*-[poly(*n*BuA)$_{40}$]$^{1.0}$.

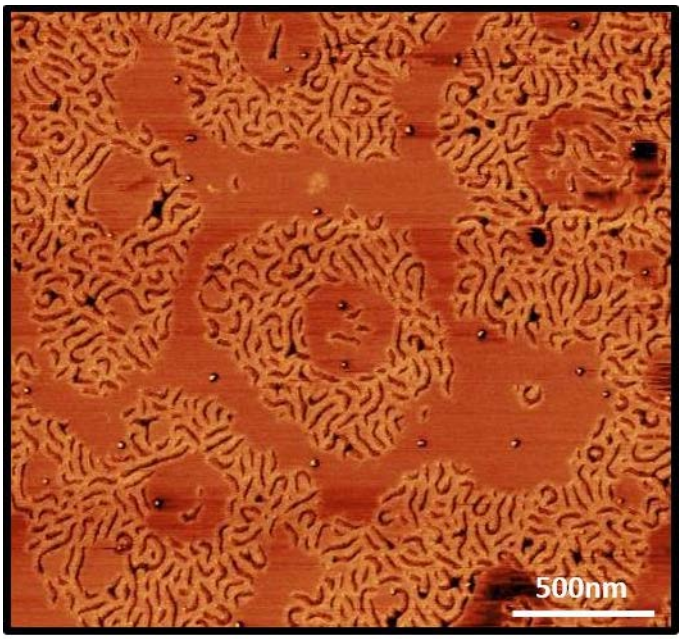

Figure 111. AFM phase micrograph of the cyclic brush copolymer *c*-poly(Sty)$_{470}$-*g*-poly(*n*BuA)$_{40}$.

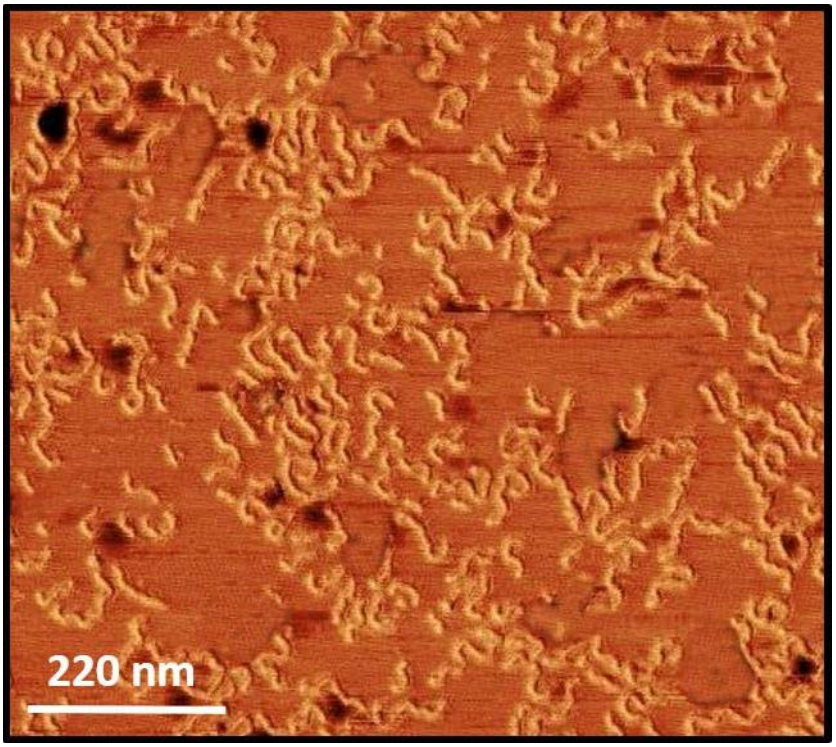

Figure 112. AFM phase micrograph of *c*-[poly(Sty)$_{430}$-*g*-poly(*n*BuA)$_{16}$][12].

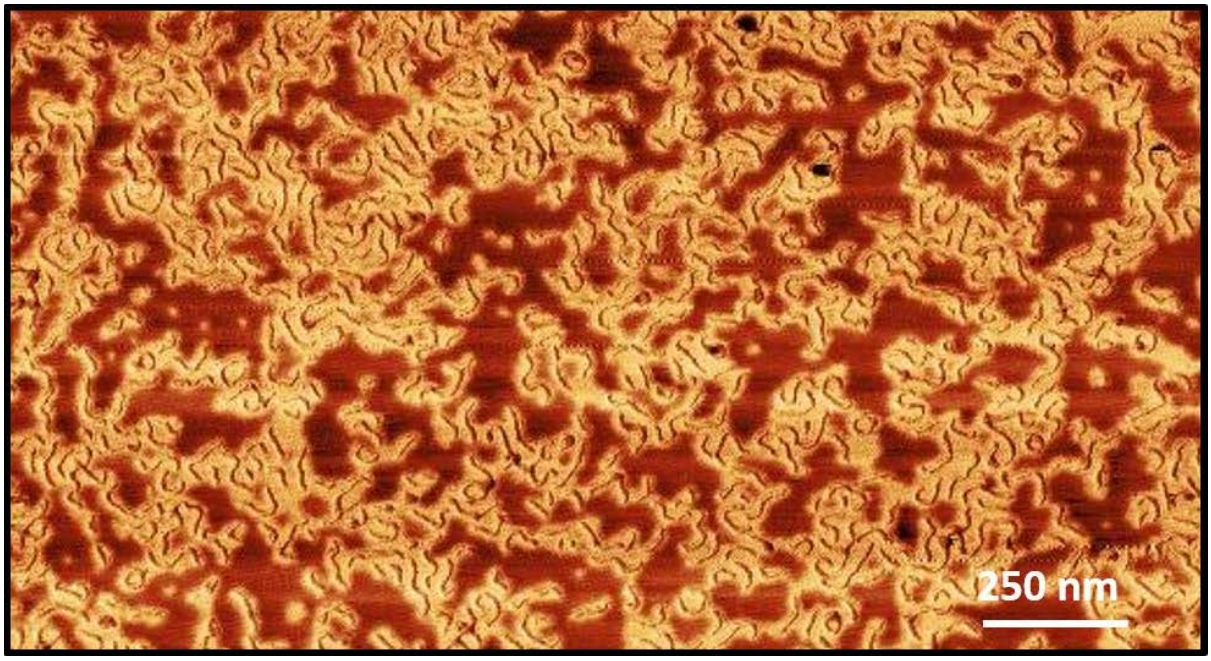

Figure 113. AFM phase micrograph of *c*-[poly(Sty)$_{420}$-*g*-poly(*n*BuA)$_{20}$][6-a].

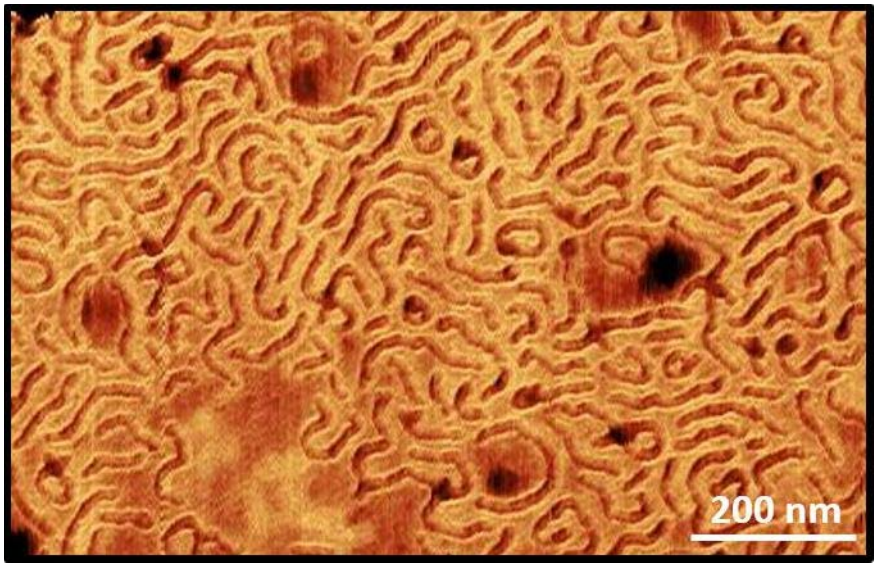

Figure 114. AFM phase micrograph of *c*-[poly(Sty)$_{420}$-*g*-poly(*n*BuA)$_{17}$]$^{6\text{-d}}$.

Figure 115. AFM amplitude micrograph of *c*-[poly(Sty)$_{420}$-*g*-poly(*n*BuA)$_{17}$]$^{6\text{-d}}$.

7. REFERENCES

1 J. M. Berg, J. L. Tymoczko, L. Stryer. Biochemistry, 6th edn; W. H. Freeman: New-York, **2006**.

2 N. Badi, J.-F. Lutz. *Chem. Soc. Rev.* **2009**, *38*, 3383-3390.

3 O. Altintas, C. Barner-Kowollik. *Macromol. Rapid Commun.* **2012**, *33*, 958-971.

4 S. Mavila, O. Eivgi, I. Berkovich, N. G. Lemcoff. *Chem. Rev.* **2016**, *116*, 878-961.

5 J. A. Pomposo. Single-Chain Polymer Nanoparticles; Wiley-VCH: Weinheim, **2017**.

6 M. Gonzalez-Burgos, A. Latorre-Sanchez, J. A. Pomposo. *Chem. Soc. Rev.* **2015**, *44*, 6122-6142.

7 J.-F. Lutz, M. Ouchi, D. R. Liu, M. Sawamoto. *Science* **2013**, *341*, 1238149.

8 F. Sanger, H. Tuppy. *Biochem. J.* **1951**, *49*, 481-490.

9 M. F. Perutz. *Nature* **1962**, *194*, 914-917.

10 J.-F. Lutz, J.-M. Lehn, E. W. Meijer, K. Matyjaszewski. *Nat. Rev. Mater.* **2016**, *1*, 16024

11 J.-F. Lutz. *Macromol. Rapid Commun.* **2017**, *38*, 1700582.

12 G. Guichard, I. Huc. *Chem. Commun.* **2011**, *47*, 5933-5941.

13 J.-F. Lutz. Sequence-Controlled Polymers; Wiley-VCH: Weinheim, **2017**.

14 J.-F. Lutz. *Polym. Chem.* **2010**, *1*, 55-62.

15 E. Schué, A. Kopyshev, J.-F. Lutz, H. G. Börner. *J. Polym. Sci., Part A: Polym. Chem.* **2019**, doi:10.1002/pola.29496.

16 S. S. Sheiko, M. Möller. *Chem. Rev.* **2001**, *101*, 4099-4123.

17 G. Polymeropoulos, G. Zapsas, K. Ntetsikas, P. Bilalis, Y. Gnanou, N. Hadjichristidis. *Macromolecules* **2017**, *50*, 1253-1290.

18 M. Levy. *Polym. Adv. Technol.* **2007**, *18*, 681-684.

19 S. Penczek, J. Pretula, P. Lewinski. *Polymers* **2017**, *9*, 646-663.

20 M. Szwarc. *Nature* **1956**, *178*, 1168-1169.

21 N. Hadjichristidis, M. Pitsikalis, S. Pispas, H. Iatrou. *Chem. Rev.* **2001**, *101*, 3747-3792.

22 S. Aoshima, S. Kanaoka. *Chem. Rev.* **2009**, *109*, 5245-5287.

23 K. Matyjaszewski, T. Davis. Handbook of Radical Polymerization; John Wiley & Sons: New Jersey, **2002**.

24 W. A. Braunecker, K. Matyjaszewski. *Prog. Polym. Sci.* **2007**, *32*, 93-146.

25 C. J. Hawker, A. W. Bosman, E. Harth. *Chem. Rev.* **2001**, *101*, 3661-3688.

26 J.-S. Wang, K. Matyjaszewski. *J. Am. Chem. Soc.* **1995**, *117*, 5614-5615.

27 J. Chiefari, Y. K. B. Chong, F. Ercole, J. Krstina, J. Jeffery, T. P. T. Le, R. T. A. Mayadunne, G. F. Meijs, C. L. Moad, G. Moad, E. Rizzardo, S. H. Thang. *Macromolecules* **1998**, *31*, 5559-5562.

28 K. Matyjaszewski, J. Spanswick. *Mater. Today* **2005**, *8*, 26-33.

29 M. Destarac. *Macromol. React. Eng.* **2010**, *4*, 165-179.

30 K. Matyjaszewski, N. V. Tsarevsky. *Nat. Chem.* **2009**, *1*, 276-288.

31 K. Matyjaszewski. *Science* **2011**, *333*, 1104-1105.

32 H. G. Börner, D. Duran, K. Matyjaszewski, M. da Silva, S. S. Sheiko. *Macromolecules* **2002**, *35*, 3387-3394.

33 K. A. Davis, K. Matyjaszewski, In Statistical, Gradient, Block and Graft Copolymers by Controlled/Living Radical Polymerizations. Advances in Polymer Science; Springer, Berlin, Heidelberg, **2002**.

34 F. S. Bates, M. A. Hillmyer, T. P. Lodge, C. M. Bates, K. T. Delaney, G. H. Fredrickson. *Science* **2012**, *336*, 434-440.

35 S. Zhang, X. Cheng, J. Wang, Z. Zhang, W. Zhang, X. Zhu. *Polym. Chem.* **2018**, *9*, 5155-5163.

36 Y. Tezuka. Topological polymer chemistry: Progress of cyclic polymers in syntheses, properties and functions; World Scientific: Singapor, **2013**.

37 B. Voit. *J. Polym. Sci., Part A: Polym. Chem.* **2005**, *43*, 2679-2699.

38 K. L. Beers, S. G. Gaynor, K. Matyjaszweski. *Macromolecules* **1998**, *31*, 9413-9415.

39 H. G. Börner, K. Beers, K. Matyjaszewski. *Macromolecules* **2001**, *34*, 4375-4383.

40 J. Mayumi, A. Nakagawa, K. Matsuhisa, H. Takahashi, H. Takahashi, M. Iijima. *Polym. J.* **2008**, *40*, 1-9.

41 A. W. York, S. E. Kirkland, C. L. McCormick. *Adv. Drug Delivery Rev.* **2008**, *60*, 1018-1036.

42 S. M. Lindner, M. Thelakkat. *Macromolecules* **2004**, *37*, 8832-8835.

43 Y. Matsuo, R. Konno, T. Ishizone, R. Goseki, A. Hirao. *Polymers* **2013**, *5*, 1012-1040.

44 M. Szwarc, M. Levy, R. Milkovich. *J. Am. Chem. Soc.* **1956**, *78*, 2656-2657.

45 N. Ekizoglou, N. Hadjichristidis. *J. Polym. Sci., Part A: Polym. Chem.* **2002**, *40*, 2166-2170.

46 M. Abubekerov, J. Wei, K. R. Swartz, Z. Xie, Q. Pei, P. L. Diaconescu. *Chem. Sci.* **2018**, *9*, 2168-2178.

47 A. H. Soeriyadi, C. Boyer, F. Nystrom, P. B. Zetterlund, M. R. Whittaker. *J. Am. Chem. Soc.* **2011**, *133*, 11128-11131.

48 J. Vandenbergh, T. de Moraes Ogawa, T. Junkers. *J. Polym. Sci., Part A: Polym. Chem.* **2013**, *51*, 2366-2374.

49 N. G. Engelis, A. Anastasaki, R. Whitfield, G. R. Jones, E. Liarou, V. Nikolaou, G. Nurumbetov, D. M. Haddleton. *Macromolecules* **2018**, *51*, 336-342.

50 G. Gody, T. Maschmeyer, P. B. Zetterlund, S. Perrier. *Nat. Commun.* **2013**, *4*, 2505.

51 F. Meng, Z. Zhong, J. Feijen. *Biomacromolecules* **2009**, *10*, 197-209.

52 Z. Zhang, T. Y. Zeng, L. Xia, C. Y. Hong, D. C. Wu, Y. Z. You. *Nat. Commun.* **2018**, *9*, 2577.

53 C. T. J. Branden. Introduction to Protein Structure; Garland Publishing: New York, **1998**.

54 J. M. Berg, J. L. Tymockzo, G. J. J. Gatto, L. Stryer. Biochemistry, 8th rev. Edn.; W. H. Freeman: New York, **2015**.

55 A. J. Berdis. *Chem. Rev.*, *109*, 2862–2879.

56 D. M. Rosenbaum, D. R. Liu. *J. Am. Chem. Soc.* **2003**, *125*, 13924-13925.

57 J. A. Piccirilli, T. Krauch, S. E. Moroney, S. A. Benner. *Nature* **1990**, *343*, 33-37.

58 J. C. M. van Hest, D. A. Tirrell. *Chem. Commun.* **2001**, 1897-1904.

59 B. Lewandowski, G. De Bo, J. W. Ward, M. Papmeyer, S. Kuschel, M. J. Aldegunde, P. M. E.Gramlich, D. Heckmann, S. M. Goldup, D. M. D'Souza, A. E. Fernandes, D. A. Leigh. *Science* **2013**, *339*, 189-193.

60 N. V. Tsarevsky, B. S. Sumerlin, K. Matyjaszewski. *Macromolecules* **2005**, *38*, 3558-3561.

61 Y. Chen, Z. Guan. *J. Am. Chem. Soc.* **2010**, *132*, 4577-4579.

62 T. B. Yu, J. Z. Bai, Z. Guan. *Angew. Chem. Int. Ed.* **2009**, *48*, 1097-1101.

63 J. C. Sworen, J. A. Smith, J. M. Berg, K. B. Wagener. *J. Am. Chem. Soc.* **2004**, *126*, 11238-11246.

64 M.-A. Berthet, Z. Zarafshani, S. Pfeifer, J.-F. Lutz. *Macromolecules* **2010**, *43*, 44-50.

65 F. Driessen, F. E. Du Prez, P. Espeel. *ACS Macro Lett.* **2015**, *4*, 616-619.

66 R. M. Stayshich, T. Y. Meyer. *J. Am. Chem. Soc.* **2010**, *132*, 10920-10934.

67 T. Yokozawa, Y. Ohta. *Chem. Rev.* **2016**, *116*, 1950-1968.

68 D. J. Gravert, K. D. Janda. *Chem. Rev.* **1997**, *97*, 489−509.

69 R. B. Merrifield. *Angew. Chem. Int. Ed.* **1985**, *24*, 799-810.

70 M. Erdélyi, A. Gogoll. *Synthesis* **2002**, *11*, 1592–1596.

71 S. P. Douglas, D. M. Whitfield, J. J. Krepinsky. *J. Am. Chem. Soc.* **1991**, *113*, 5095-5097.

72 M. H. Caruthers. *Science* **1985**, *230*, 281-285.

73 A. Meszynska, N. Badi, H. G. Börner, J.-F. Lutz. *Chem. Commun.* **2012**, *48*, 3887-3889.

74 S. Pfeifer, Z. Zarafshani, N. Badi, J.-F. Lutz. *J. Am. Chem. Soc.* **2009**, *131*, 9195-9197.

75 H. Kunz. *Angew. Chem. Int. Ed.* **1987**, *26*, 294-308.

76 T. T. Trinh, C. Laure, J.-F. Lutz. *Macromol. Chem. Phys.* **2015**, *216*, 1498-1506.

77 K. Rose, J. Vizzavona. *J. Am. Chem. Soc.* **1999**, *121*, 7034-7038.

78 L. Hartmann, E. Krause, M. Antonietti, H. G. Börner. *Biomacromolecules* **2006**, *7*, 1239-1244.

79 R. L. Malenfant, J. M. J. Fréchet. *Chem. Commun.* **1998**, 2657-2658.

80 S. C. Solleder, M. A. R. Meier. *Angew. Chem. Int. Ed.* **2014**, *53*, 711-714.

81 S. C. Solleder, K. S. Wetzel, M. A. R. Meier. *Polym. Chem.* **2015**, *6*, 3201-3204.

82 R. N. Zuckermann, J. M. Kerr, S. B. H. Kent, W. H. Moos. *J. Am. Chem. Soc.* **1992**, *114*, 10646-10647.

83 A. M. Rosales, R. A. Segalman, R. N. Zuckermann. *Soft Matter* **2013**, *9*, 8400-8414.

84 P. Espeel, L. L. Carrette, K. Bury, S. Capenberghs, J. C. Martins, F. E. Du Prez, A. Madder. *Angew. Chem. Int. Ed.* **2013**, *52*, 13261-13264.

85 S. Martens, J. Van den Begin, A. Madder, F. E. Du Prez, P. Espeel. *J. Am. Chem. Soc.* **2016**, *138*, 14182-14185.

86 S. Martens, A. Landuyt, P. Espeel, B. Devreese, P. Dawyndt, F. Du Prez. *Nat. Commun.* **2018**, *9*, 4451.

87 G. Odian. Principles of Polymerization, Fourth Edition; John Wiley & Sons: Hoboken, **2004**.

88 J. De Neve, J. J. Haven, L. Maes, T. Junkers. *Polym. Chem.* **2018**, *9*, 4692-4705.

89 M. Minoda, M. Sawamoto, T. Higashimura. *Macromolecules* **1990**, *23*, 4889-4895.

90 S. Houshyar, D. J. Keddie, G. Moad, R. J. Mulder, S. Saubern, J. Tsanaktsidis. *Polym. Chem.* **2012**, *3*, 1879–1889

91 J. Xu, C. Fu, S. Shanmugam, C. J. Hawker, G. Moad, C. Boyer. *Angew. Chem. Int. Ed.* **2017**, *56*, 8376-8383.

92 J. Vandenbergh, G. Reekmans, P. Adriaensens, T. Junkers. *Chem. Commun.* **2013**, *49*, 10358-10360.

93 B. Alberts, A. Johnson, J. Lewis, M. Raff, K. Roberts, P. Walter. Molecular biology of the cell. 4th edition; Garland Science: New-York, **2002**.

94 R. McHale, J. P. Patterson, P. B. Zetterlund, R. K. O'Reilly. *Nat. Chem.* **2012**, *4*, 491-497.

95 S. Ida, T. Terashima, M. Ouchi, M. Sawamoto. *J. Am. Chem. Soc.* **2009**, *131*, 10808-10809.

96 S. Ida, M. Ouchi, M. Sawamoto. *J. Am. Chem. Soc.* **2010**, *132*, 14748-14750.

97 D. Pasini, D. Takeuchi. *Chem. Rev.* **2018**, *118*, 8983-9057.

98 Y. Hibi, S. Tokuoka, T. Terashima, M. Ouchi, M. Sawamoto. *Polym. Chem.* **2011**, *2*, 341-347.

99 Y. Hibi, M. Ouchi, M. Sawamoto. *Angew. Chem. Int. Ed.* **2011**, *50*, 7434-7437.

100 M. Ouchi, M. Nakano, T. Nakanishi, M. Sawamoto. *Angew. Chem. Int. Ed.* **2016**, *55*, 14584-14589.

101 N. Ten Brummelhuis. *Polym. Chem.* **2015**, *6*, 654-667.

102 T.-L. Choi, I. M. Rutenberg, R. H. Grubbs. *Angew. Chem. Int. Ed.* **2002**, *41*, 3839-3841.

103 H. Yuki, Y. Okamoto. *Polym. J.* **1970**, *1*, 13-18.

104 J.-F. Lutz, B. Kirci, K. Matyjaszewski. *Macromolecules* **2003**, *36*, 3136-3145.

105 F. R. Mayo, F. M. Lewis, C. Walling. *J. Am. Chem. Soc.* **1948**, *70*, 1529-1533.

106 J. M. G. Cowie, In Alternating Copolymers. Speciality Polymers.; Springer: Boston, MA, **1985**.

107 D. Benoit, C. J. Hawker, E. E. Huang, Z. Lin, T. P. Russell. *Macromolecules* **2000**, *33*, 1505-1507.

108 S. Pfeifer, J.-F. Lutz. *J. Am. Chem. Soc.* **2007**, *129*, 9542-9543.

109 J.-F. Lutz, B. V. Schmidt, S. Pfeifer. *Macromol. Rapid Commun.* **2011**, *32*, 127-135.

110 G.-Q. Chen, Z.-Q. Wu, J.-R. Wu, Z.-C. Li, F.-M. Li. *Macromolecules* **2000**, *33*, 232-234.

111 M. Zamfir, J.-F. Lutz. *Nat. Commun.* **2012**, *3*, 1138.

112 D. Moatsou, C. F. Hansell, R. K. O'Reilly. *Chem. Sci.* **2014**, *5*, 2246-2250.

113 J. D. Rule, J. S. Moore. *Macromolecules* **2002**, *35*, 7878-7882.

114 V. Lapinte, J.-C. Brosse, L. Fontaine. *Macromol. Chem. Phys.* **2004**, *205*, 824-833.

115 N. Baradel, O. Gok, M. Zamfir, A. Sanyal, J.-F. Lutz. *Chem. Commun.* **2013**, *49*, 7280-7282.

116 N. Baradel, S. Fort, S. Halila, N. Badi, J.-F. Lutz. *Angew. Chem. Int. Ed.* **2013**, *52*, 2335-2339.

117 J.-F. Lutz. *Macromolecules* **2015**, *48*, 4759-4767.

118 G. M. Church, Y. Gao, S. Kosuri. *Science* **2012**, *337*, 1628–1628.

119 J. M. Berg, J. L. Tymoczko, L. Stryer. Biochemistry, 5th edition; W. H. Freeman: New York, **2002**.

120 L. Pauling, R. B. Corey, H. R. Branson. *Proc. Natl. Acad. Sci. U. S. A.* **1951**, *37*, 205–211.

121 L. Pauling, R. B. Corey. *Proc. Natl. Acad. Sci. U. S. A.* **1951**, *37*, 729–740.

122 K. Henzler-Wildman, D. Kern. *Nature* **2007**, *450*, 964-972.

123 C. B. Anfinsen. *Science* **1973**, *181*, 223–230.

124 D. Mecerreyes, V. Lee, C. J. Hawker, J. L. Hedrick, A. Wursch, W. Volksen, T. Magbitang, E. Huang, R. D. Miller. *Adv. Mater.* **2001**, *13*, 204-208.

125 J. Rubio-Cervilla, E. Gonzalez, J. A. Pomposo. *Nanomaterials* **2017**, *7*.

126 A. R. de Luzuriaga, N. Ormategui, H. J. Grande, I. Odriozola, J. A. Pomposo, I. Loinaz. *Macromol. Rapid Commun.* **2008**, *29*, 1156-1160.

127 N. Ormategui, I. García, D. Padro, G. Cabañero, H. J. Grande, I. Loinaz. *Soft Matter* **2012**, *8*, 734-740.

128 D. Chao, X. Jia, B. Tuten, C. Wang, E. B. Berda. *Chem. Commun.* **2013**, *49*, 4178-4180.

129 A. E. Cherian, F. C. Sun, S. S. Sheiko, G. W. Coates. *J. Am. Chem. Soc.* **2007**, *129*, 11350-11351.

130 Y. Bai, H. Xing, G. A. Vincil, J. Lee, E. J. Henderson, Y. Lu, N. G. Lemcoff, S. C. Zimmerman. *Chem. Sci.* **2014**, *5*, 2862-2868.

131 J. B. Beck, K. L. Killops, T. Kang, K. Sivanandan, A. Bayles, M. E. Mackay, K. L. Wooley, C. J. Hawker. *Macromolecules* **2009**, *42*, 5629-5635.

132 E. H. H. Wong, S. J. Lam, E. Nam, G. G. Qiao. *ACS Macro Lett.* **2014**, *3*, 524-528.

133 S. K. Hamilton, E. Harth. *ACS Nano* **2009**, *3*, 402-410.

134 O. Altintas, C. Barner-Kowollik. *Macromol. Rapid Commun.* **2016**, *37*, 29-46.

135 G. M. t. Huurne, A. R. A. Palmans, E. W. Meijer. *CCS Chem.* **2019**, *1*, 64-82.

136 A. Sanchez-Sanchez, A. Arbe, J. Colmenero, J. A. Pomposo. *ACS Macro Lett.* **2014**, *3*, 439-443.

137 J. Jeong, Y.-J. Lee, B. Kim, B. Kim, K.-S. Jung, H.-j. Paik. *Polym. Chem.* **2015**, *6*, 3392-3397.

138 J. Willenbacher, O. Altintas, P. W. Roesky, C. Barner-Kowollik. *Macromol. Rapid Commun.* **2014**, *35*, 45-51.

139 Y. Inoue, P. Kuad, Y. Okumura, Y. Takashima, H. Yamaguchi, A. Harada. *J. Am. Chem. Soc.* **2007**, *129*, 6396-6397.

140 E. A. Appel, J. Dyson, J. del Barrio, Z. Walsh, O. A. Scherman. *Angew. Chem. Int. Ed.* **2012**, *51*, 4185-4189.

141 T. Terashima, T. Sugita, K. Fukae, M. Sawamoto. *Macromolecules* **2014**, *47*, 589-600.

142 M. Seo, S. Y. Kim, B. J. Beck, J. M. J. Paulusse, C. J. Hawker, S. Y. Kim. *Macromolecules* **2008**, *41*, 6413-6418.

143 M. A. J. Gillissen, I. K. Voets, E. W. Meijer, A. R. A. Palmans. *Polym. Chem.* **2012**, *3*, 3166–3174.

144 O. Altintas, T. Rudolph, C. Barner-Kowollik. *J. Polym. Sci., Part A: Polym. Chem.* **2011**, *49*, 2566-2576.

145 O. Altintas, P. Gerstel, N. Dingenouts, C. Barner-Kowollik. *Chem. Commun.* **2010**, *46*, 6291-6293.

146 E. B. Berda, E. J. Foster, E. W. Meijer. *Macromolecules* **2010**, *43*, 1430-1437.

147 T. Mes, R. van der Weegen, A. R. Palmans, E. W. Meijer. *Angew. Chem. Int. Ed.* **2011**, *50*, 5085-5089.

148 A. Sanchez-Sanchez, J. A. Pomposo. *Part. Part. Syst. Charact.* **2014**, *31*, 11-23.

149 A. W. Jackson, D. A. Fulton. *Polym. Chem.* **2013**, *4*, 31-45.

150 A. P. P. Kröger, J. M. J. Paulusse. *J. Controlled Release* **2018**, *286*, 326-347.

151 R. Braslau, F. Rivera, C. Tansakul. *React. Funct. Polym.* **2013**, *73*, 624-633.

152 M. V. S. N. Maddipatla, D. Wehrung, C. Tang, W. Fan, M. O. Oyewumi, T. Miyoshi, A. Joy. *Macromolecules* **2013**, *46*, 5133-5140.

153 B. S. Murray, D. A. Fulton. *Macromolecules* **2011**, *44*, 7242-7252.

154 D. E. Whitaker, C. S. Mahon, D. A. Fulton. *Angew. Chem. Int. Ed.* **2013**, *52*, 956-959.

155 L. Buruaga, J. A. Pomposo. *Polymers* **2011**, *3*, 1673-1683.

156 A. Sanchez-Sanchez, D. A. Fulton, J. A. Pomposo. *Chem. Commun.* **2014**, *50*, 1871-1874.

157 B. T. Tuten, D. Chao, C. K. Lyon, E. B. Berda. *Polym. Chem.* **2012**, *3*, 3068–3071.

158 H. Xu, W. Cao, X. Zhang. *Acc. Chem. Res.* **2013**, *46*, 1647-1658.

159 J. Xia, T. Li, C. Lu, H. Xu. *Macromolecules* **2018**, *51*, 7435-7455.

160 D. Yue, G. Cheng, Y. He, Y. Nie, Q. Jiang, X. Cai, Z. Gu. *J. Mater. Chem. B* **2014**, *2*, 7210-7221.

161 H. J. Reich, R. J. Hondal. *ACS Chem. Biol.* **2016**, *11*, 821-841.

162 P. Han, S. Li, W. Cao, Y. Li, Z. Sun, Z. Wang, H. Xu. *J. Mater. Chem. B* **2013**, *1*, 740-743.

163 N. Ma, Y. Li, H. Xu, Z. Wang, X. Zhang. *J. Am. Chem. Soc.* **2010**, *132*, 442-443.

164 S. Ji, W. Cao, Y. Yu, H. Xu. *Adv. Mater.* **2015**, *27*, 7740-7745.

165 X. Pan, F. Driessen, X. Zhu, F. E. Du Prez. *ACS Macro Lett.* **2017**, *6*, 89-92.

166 Y. Fu, J. Chen, H. Xu, C. Van Oosterwijck, X. Zhang, W. Dehaen, M. Smet. *Macromol. Rapid. Commun.* **2012**, *33*, 798-804.

167 Z. Cai, W. Lu, F. Gao, X. Pan, J. Zhu, Z. Zhang, X. Zhu. *Macromol. Rapid Commun.* **2016**, *37*, 865-871.

168 C. K. Lyon, A. Prasher, A. M. Hanlon, B. T. Tuten, C. A. Tooley, P. G. Frank, E. B. Berda. *Polym. Chem.* **2015**, *6*, 181-197.

169 A. M. Hanlon, C. K. Lyon, E. B. Berda. *Macromolecules* **2015**, *49*, 2-14.

170 T. S. Fischer, D. Schulze-Sunninghausen, B. Luy, O. Altintas, C. Barner-Kowollik. *Angew. Chem. Int. Ed.* **2016**, *55*, 11276-11280.

171 A. J. Moreno, F. Lo Verso, A. Sanchez-Sanchez, A. Arbe, J. Colmenero, J. A. Pomposo. *Macromolecules* **2013**, *46*, 9748-9759.

172 N. Hosono, M. A. Gillissen, Y. Li, S. S. Sheiko, A. R. Palmans, E. W. Meijer. *J. Am. Chem. Soc.* **2013**, *135*, 501-510.

173 C. M. Dobson. *Nature* **2003**, *426*, 884-890.

174 D. J. Hill, M. J. Mio, R. B. Prince, T. S. Hughes, J. S. Moore. *Chem. Rev.* **2001**, *101*, 3893-4012.

175 B. V. Schmidt, N. Fechler, J. Falkenhagen, J.-F. Lutz. *Nat. Chem.* **2011**, *3*, 234-238.

176 O. Shishkan, M. Zamfir, M. A. Gauthier, H. G. Börner, J.-F. Lutz. *Chem. Commun.* **2014**, *50*, 1570-1572.

177 Y. Kim, J. Pyun, J. M. Frechet, C. J. Hawker, C. W. Frank. *Langmuir* **2005**, *21*, 10444-10458.

178 C. T. Adkins, H. Muchalski, E. Harth. *Macromolecules* **2009**, *42*, 5786-5792.

179 R. K. Roy, J. F. Lutz. *J. Am. Chem. Soc.* **2014**, *136*, 12888-12891.

180 V. A. Davankov, M. M. Ilyin, M. P. Tsyurupa, G. I. Timofeeva, L. V. Dubrovina. *Macromolecules* **1996**, *29*, 8398-8403.

181 E. Harth, B. V. Horn, V. Y. Lee, D. S. Germack, C. P. Gonzales, R. D. Miller, C. J. Hawker. *J. Am. Chem. Soc.* **2002**, *124*, 8653-8660.

182 P. Frank, A. Prasher, B. Tuten, D. Chao, E. Berda. *Appl. Petrochem. Res.* **2014**, *5*, 9-17.

183 D. M. Stevens, S. Tempelaar, A. P. Dove, E. Harth. *ACS Macro Lett.* **2012**, *1*, 915-918.

184 O. Altintas, J. Willenbacher, K. N. R. Wuest, K. K. Oehlenschlaeger, P. Krolla-Sidenstein, H. Gliemann, C. Barner-Kowollik. *Macromolecules* **2013**, *46*, 8092-8101.

185 H. W. van Roekel, P. J. Stals, M. A. Gillissen, P. A. Hilbers, A. J. Markvoort, T. F. de Greef. *Chem. Commun.* **2013**, *49*, 3122-3124.

186 M. Huo, N. Wang, T. Fang, M. Sun, Y. Wei, J. Yuan. *Polymer* **2015**, *66*, A11-A21.

187 T. Terashima, T. Mes, T. F. De Greef, M. A. Gillissen, P. Besenius, A. R. Palmans, E. W. Meijer. *J. Am. Chem. Soc.* **2011**, *133*, 4742-4745.

188 M. Artar, E. R. J. Souren, T. Terashima, E. W. Meijer, A. R. A. Palmans. *ACS Macro Lett.* **2015**, *4*, 1099-1103.

189 X.-Y. Tu, M.-Z. Liu, H. Wei. *J. Polym. Sci., Part A: Polym. Chem.* **2016**, *54*, 1447-1458.

190 Z. Jia, M. J. Monteiro. *J. Polym. Sci., Part A: Polym. Chem.* **2012**, *50*, 2085-2097.

191 Andrew J. Boydston, Y. Xia, J. A. Kornfield, I. A. Gorodetskaya, R. H. Grubbs. *J. Am. Chem. Soc.* **2008**, *130*, 12775-12782.

192 H. R. Kricheldorf, S.-R. Lee. *Macromolecules* **1995**, *28*, 6718-6725.

193 M. Ryner, A. Finne, A.-C. Albertsson, H. R. Kricheldorf. *Macromolecules* **2001**, *34*, 7281-7287.

194 H. R. Kricheldorf, A. Stricker. *Macromolecules* **2000**, *33*, 696-701.

195 A. J. Boydston, T. W. Holcombe, D. A. Unruh, J. M. J. Fréchet, R. H. Grubbs. *J. Am. Chem. Soc.* **2009**, *131*, 5388–5389.

196 C. W. Bielawski, D. Benitez, R. H. Grubbs. *Science* **2002**, *297*, 2041-2044.

197 M. M. Stamenović, P. Espeel, E. Baba, T. Yamamoto, Y. Tezuka, F. E. Du Prez. *Polym. Chem.* **2013**, *4*, 184-193.

198 B. A. Laurent, S. M. Grayson. *J. Am. Chem. Soc.* **2011**, *133*, 13421-13429.

199 D. Lu, Z. Jia, M. J. Monteiro. *Polym. Chem.* **2013**, *4*, 2080–2089.

200 J. Xu, J. Ye, S. Liu. *Macromolecules* **2007**, *40*, 9103-9110.

201 X.-P. Qiu, F. Tanaka, F. M. Winnik. *Macromolecules* **2007**, *40*, 7069-7071.

202 M. D. Hossain, J. C. Reid, D. Lu, Z. Jia, D. J. Searles, M. J. Monteiro. *Biomacromolecules* **2018**, *19*, 616-625.

203 M. Schappacher, A. Deffieux. *Science* **2008**, *319*, 1512-1515.

204 Y. Xia, A. J. Boydston, R. H. Grubbs. *Angew. Chem. Int. Ed.* **2011**, *50*, 5882-5885.

205 D. E. Lonsdale, M. J. Monteiro. *J. Polym. Sci., Part A: Polym. Chem.* **2011**, *49*, 4603-4612.

206 B. A. Laurent, S. M. Grayson. *Chem. Soc. Rev.* **2009**, *38*, 2202-2213.

207 S. Perrier. *Nat. Chem.* **2011**, *3*, 194-196.

208 S. Srichan, D. Chan-Seng, J.-F. Lutz. *ACS Macro Lett.* **2012**, *1*, 589-592.

209 S. J. Flemer. *Molecules* **2011**, *16*, 3232-3251.

210 D. Plano, Y. Baquedano, D. Moreno-Mateos, M. Font, A. Jimenez-Ruiz, J. A. Palop, C. Sanmartin. *Eur. J. Med. Chem.* **2011**, *46*, 3315-3323.

211 B. J. Bhuyan, G. Mugesh. *Org. Biomol. Chem.* **2011**, *9*, 1356-1365.

212 N. Matuszak, G. G. Muccioli, G. Labar, D. M. Lambert. *J. Med. Chem.* **2009**, *52*, 7410-7420.

213 S. Grimaldi, J.-P. Finet, F. Le Moigne, A. Zeghdaoui, P. Tordo, D. Benoit, M. Fontanille, Y. Gnanou. *Macromolecules* **2000**, *33*, 1141-1147.

214 A. Isidro-Llobet, M. Àlvarez, F. Albericio. *Chem. Rev.* **2009**, *109*, 2455-2504.

215 T. Tamura, T. Oikawa, A. Ohtaka, N. Fujii, N. Esaki, K. Soda. *Anal. Biochem.* **1993**, *208*, 151-154.

216 K. M. Harris, S. Flemer, Jr., R. J. Hondal. *J. Pept. Sci.* **2007**, *13*, 81-93.

217 G. Casi, G. Roelfes, D. Hilvert. *Chembiochem* **2008**, *9*, 1623-1631.

218 O. Flögel, G. Casi, D. Hilvert, D. Seebach. *Helv. Chim. Acta* **2007**, *90*, 1651-1666.

219 T. Koide, H. Itoh, A. Otaka, H. Yasui, M. Kuroda, N. Esaki, K. Soda, N. Fujii. *Chem. Pharm. Bull.* **1993**, *41*, 502-506.

220 M. D. Gieselman, L. Xie, W. A. van der Donk. *Org. Lett.* **2001**, *3*, 1331-1334.

221 A. L. Schroll, R. J. Hondal, S. Flemer, Jr. *J. Pept. Sci.* **2012**, *18*, 155-162.

222 H. R. Kricheldorf. *J. Polym. Sci. A* **2010**, *48*, 251-284.

223 C. Wang, X. An, M. Pang, Z. Zhang, X. Zhu, J. Zhu, F. E. Du Prez, X. Pan. *Polym. Chem.* **2018**, *9*, 4044-4051.

224 S. S. Sheiko, S. A. Prokhorova, K. L. Beers, K. Matyjaszewski, I. I. Potemkin, A. R. Khokhlov, M. Möller. *Macromolecules* **2001**, *34*, 8354-8360.

225 S. S. Sheiko, B. S. Sumerlin, K. Matyjaszewski. *Prog. Polym. Sci.* **2008**, *33*, 759-785.

226 M. Zhang, A. H. E. Müller. *J. Polym. Sci., Part A: Polym. Chem.* **2005**, *43*, 3461-3481.

227 N. V. Tsarevsky, K. Matyjaszewski. *Macromolecules* **2002**, *35*, 9009-9014.

228 J. Qiu, B. Charleux, K. Matyjaszewski. *Polimery (Warsaw, Pol.)* **2001**, *46*, 453-460.

229 S. Ji, W. Cao, Y. Yu, H. Xu. *Angew. Chem. Int. Ed.* **2014**, *53*, 6781-6785.

230 W. Tang, Y. Kwak, W. Braunecker, N. V. Tsarevsky, M. L. Coote, K. Matyjaszewski. *J. Am. Chem. Soc.* **2008**, *130*, 10702-10713.

231 H. Gao, K. Matyjaszewski. *J. Am. Chem. Soc.* **2007**, *129*, 6633-6639.

232 H. Durmaz, A. Dag, N. Cerit, O. Sirkecioglu, G. Hizal, U. Tunca. *J. Polym. Sci., Part A: Polym. Chem.* **2010**, *48*, 5982-5991.

233 Q. Fu, W. Lin, J. Huang. *Macromolecules* **2008**, *41*, 2381-2387.

234 Y. Li, Y. Zhang, D. Yang, Y. Li, J. Hu, C. Feng, S. Zhai, G. Lu, X. Huang. *Macromolecules* **2010**, *43*, 262-270.

235 I. Gadwal, J. Rao, J. Baettig, A. Khan. *Macromolecules* **2014**, *47*, 35-40.

236 S. Cesana, A. Kurek, M. A. Baur, J. Auernheimer, O. Nuyken. *Macromol. Rapid Commun.* **2007**, *28*, 608-615.

237 G. Le Fer, J. Babinot, D. L. Versace, V. Langlois, E. Renard. *Macromol. Rapid Commun.* **2012**, *33*, 2041-2045.

238 L. Xiao, Y. Chen, K. Zhang. *Macromolecules* **2016**, *49*, 4452-4461.

239 S. Billiet, K. De Bruycker, F. Driessen, H. Goossens, V. Van Speybroeck, J. M. Winne, F. E. Du Prez. *Nat. Chem.* **2014**, *6*, 815-821.

240 K. De Bruycker, S. Billiet, H. A. Houck, S. Chattopadhyay, J. M. Winne, F. E. Du Prez. *Chem. Rev.* **2016**, *116*, 3919-3974.

241 P. G. M. Wuts, T. W. Greene. Greene's Protective Groups in Organic Chemistry, 5th Edn; Wiley: New Jersey, **2014**.

242 N. V. Tsarevsky, B. S. Sumerlin. Fundamentals of Controlled/Living Radical Polymerization; The Royal Society of Chemistry: Oxford, **2013**.

243 J. Ruehl, A. Nilsen, S. Born, P. Thoniyot, L.-P. Xu, S. Chen, R. Braslau. *Polymer* **2007**, *48*, 2564-2571.

244 J. Nicolas, B. Charleux, O. Guerret, S. Magnet. *Macromolecules* **2005**, *38*, 9963-9973.

245 P. Deslongchamps. Stereoelectronic Effects in Organic Chemistry: Oxford, **1983**.

246 A. J. Bennet, Q.-P. Wang, H. Slebocka-Tilk, V. Somayaji, R. S. Brown. *J. Am. Chem. Soc.* **1990**, *112*, 6383-6385.

247 J. Vinas, N. Chagneux, D. Gigmes, T. Trimaille, A. Favier, D. Bertin. *Polymer* **2008**, *49*, 3639-3647.

248 S. Robin, O. Guerret, J.-L. Couturier, Y. Gnanou. *Macromolecules* **2002**, *35*, 2481-2486.

249 G. L. Ellman. *Arch. Biochem. Biophys.* **1959**, *82*, 70−77.

250 B. Mandal, B. Basu. *RSC Adv.* **2014**, *4*, 13854-13881.

251 G. Capozzi, G. Modena. The Chemistry of the Thiol Group; Wiley: London, **1974**.

252 B. S. Mamathambika, J. C. Bardwell. *Annu. Rev. Cell Dev. Biol.* **2008**, *24*, 211-235.

253 K. Pulka-Ziach. *J. Pept. Sci.* **2018**, e3096.

254 T. J. Wallace, N. Jocobson, A. Schriesheim. *Nature* **1964**, *201*, 609-610.

255 J. L. García Ruano, A. Parra, J. Alemán. *Green Chem.* **2008**, *10*, 706-711.

256 D. Cho, K. Masuoka, K. Koguchi, T. Asari, D. Kawaguchi, A. Takano, Y. Matsushita. *Polym. J.* **2005**, *37*, 506–511.

257 Y. Inoue, T. Matsugi, N. Kashiwa, K. Matyjaszewski. *Macromolecules* **2004**, *37*, 3651-3658.

258 H.-J. Paik, S. G. Gaynor, K. Matyjaszewski. *Macromol. Rapid Commun.* **1998**, *19*, 47-52.

259 S. C. Hong, T. Pakula, K. Matyjaszewski. *Macromol. Chem. Phys.* **2001**, *202*, 3392-3402.

260 J. R. Schaefgen, P. J. Flory. *J. Am. Chem. Soc.* **1948**, *70*, 2709-2718.

261 S. S. Sheiko, F. C. Sun, A. Randall, D. Shirvanyants, M. Rubinstein, H. I. Lee, K. Matyjaszewski. *Nature* **2006**, *440*, 191-194.

262 I. P. a. S. S. Sheiko, A. N. a. K. Matyjaszewski. *Macromolecules* **2009**, *42*, 1805-1807.

263 J. M. Chalker, S. B. Gunnoo, O. Boutureira, S. C. Gerstberger, M. Fernández-González, G. J. L. Bernardes, L. Griffin, H. Hailu, C. J. Schofield, B. G. Davis. *Chem. Sci.* **2011**, *2*, 1666–1676.

264 T. J. Wallace, J. J. Mahon. *J. Org. Chem.* **1695**, *30*, 1502–1506.

265 B. Balta, G. Monard, M. F. Ruiz-Lòpez, M. Antoine, A. Gand, S. Boschi-Muller, G. Branlant. *J. Phys. Chem. A* **2006**, *110*, 7628-7636.

266 V. Gupta, K. S. Carroll. *Biochim. Biophys. Acta* **2014**, *1840*, 847-875.

267 Y. W. Kim, J. T. Park, J. H. Koh, B. R. Min, J. H. Kim. *Polym. Adv. Technol.* **2008**, *19*, 944-946.

268 H. F. Gilbert. *Adv. Enzymol. Relat. Areas Mol. Biol.* **1990**, *63*, 69–172.

269 M. Putzu, F. Grater, M. Elstner, T. Kubar. *Phys. Chem. Chem. Phys.* **2018**, *20*, 16222-16230.

270 W.-F. Su, In Principles of Polymer Design and Synthesis; Springer Berlin Heidelberg: Berlin, Heidelberg, **2013**, pp 9-26.

271 M. P. Taylor. *J. Chem. Phys.* **2004**, *121*, 10757-10765.

272 Y. Zhu, N. S. Hosmane. *ChemistryOpen* **2015**, *4*, 408-417.

273 Zhang K., T. G. N. *React. Funct. Polym.* **2014**, *80*, 40–47.

274 H. Otsuka, S. Nagano, Y. Kobashi, T. Maeda, A. Takahara. *Chem. Commun.* **2010**, *46*, 1150-1152.

275 T. G. Back, Z. Moussa. *J. Am. Chem. Soc.* **2003**, *125*, 13455-13460.

276 T. Little, J. Meara, F. Ruan, M. Nguyen, M. Qabar. *Synth. Commun.* **2002**, *32*, 1741-1749.

277 E. L. Ruggles, P. B. Deker, R. J. Hondal. *Tetrahedron* **2009**, *65*, 1257-1267.

HUMBOLDT-UNIVERSITÄT ZU BERLIN

Declaration of originatlity/ Eidesstattliche erklärung

Hiermit erkläre ich, dass ich die vorliegende Arbeit zum Thema "Oxidative intramolecular crosslinking in sequence-controlled polymers: Approaches toward more complex designs and folding analysis" selbstständig und unter ausschließlicher Verwendung der angegeben Literatur und Hilfsmittel erstellt habe. Die Arbeit ist bisher an keiner anderen Hochschule eingereicht worden.

I hereby declare that this work "Oxidative intramolecular crosslinking in sequence-controlled polymers: Approaches toward more complex designs and folding analysis" is my own work and that only the denoted resources were used. In this or similar form this thesis work has not been submitted for the award of any other degree.

Berlin, 17 December 2019

Ort, Datum

Unterschrift Antragsteller